Dennis Derickson

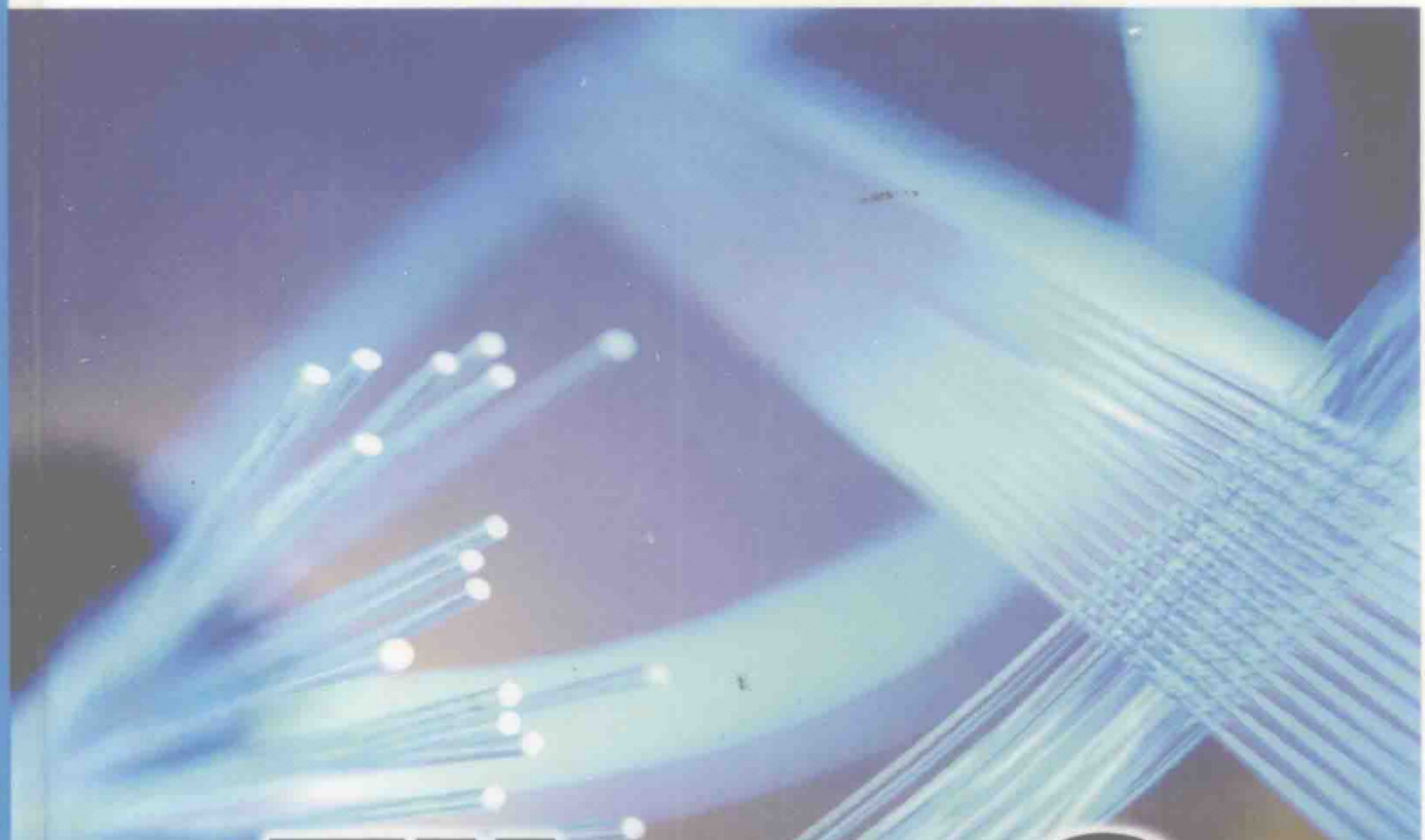

Fiber Optic
Test and Measurement

- Test digital fiber systems to SONET/SDH international standards
- Accurately characterize the behavior of Wavelength Division Multiplexing (WDM) fiber systems
- Test two-port optical devices for insertion loss, reflectivity of components, chromatic and polarization mode dispersion, and the behavior of Erbium-doped fiber amplifiers (EDFAs).

Communications

Dennis Derickson

Fiber Optic Test and Measurement

about the author

DENNIS DERICKSON Agilent Technologies engineers and scientists at three different locations in California and Germany collaborated to produce this work. DENNIS DERICKSON (editor) was one of the founding members of Agilent's fiber optic test and measurement group in Santa Rosa, CA.

THE COMPLETE, PRACTICAL GUIDE TO TESTING FIBER OPTIC COMMUNICATION COMPONENTS AND SYSTEMS.

Fiber optic networks are evolving rapidly—and so is the technology used to design, measure, and test them. *Fiber Optic Test and Measurement* is the first authoritative, complete guide to measuring both current optical networks and those on the horizon. It reflects the collective experience of Agilent Technologies' world-class lightwave test and measurement organization, and presents extensive information that has had limited circulation to date.

Learn how to characterize all three basic components of a fiber optic communication system: the optical transmitter, fiber medium, and optical receiver. Review each fundamental area of fiber optic measurement, including:

- Optical power measurements using several types of photodetectors
- Spectral measurements using diffraction gratings, Michelson interferometers, and both heterodyne and homodyne spectrum analysis
- Polarization measurements—increasingly important in high data rate networks that utilize optical amplifiers
- Modulation measurements via frequency and time domain analysis

The book's unprecedented coverage of advanced fiber technology will be invaluable to professionals implementing or maintaining new optical networks.

This practical guide will help technicians, engineers, and scientists accurately measure and test fiber optic systems, without becoming experts in fiber optic theory. It will be equally useful for experienced fiber optic professionals and those new to the field. application notes that provide a real-world view of IP telephony.

Prentice Hall
Upper Saddle River, NJ 07458
www.phptr.com

ISBN 0-13-534330-5
90000
9 780135 343302

Fiber Optic Test and Measurement

Dennis Derickson, Editor

Christian Hentschel
Joachim Vobis
Loren Stokes
Paul Hernday
Val McOmber
Douglas M. Baney
Wayne V. Sorin
Josef Beller
Christopher M. Miller
Stephen W. Hinch

Prentice Hall PTR
Upper Saddle River, New Jersey 07458

Library of Congress Cataloging-in-Publication Data
Derickson, Dennis.
Fiber optic test and measurement / Dennis Derickson.
p. cm.
Includes index.
ISBN 0–13–534330–5
1. Optical communications—Testing. 2. Optical fibers—Testing.
I. Title.
TK5103.59.D47 1998
621.382'75'0287—dc21 97–20323
CIP

Acquisitions editor: Bernard M. Goodwin
Cover designer: Wanda España
Cover design director: Jerry Votta
Manufacturing manager: Alexis R. Heydt
Marketing manager: Miles Williams
Compositor/Production services: Pine Tree Composition, Inc.

Upper Saddle River, New Jersey 07458

Prentice Hall books are widely used by corporations and government agencies for training, marketing, and resale.

The publisher offers discounts on this book when ordered in bulk quantities. For more information contact:

Corporate Sales Department
Phone: 800–382–3419
Fax: 201–236–7141
E-mail: corpsales@prenhall.com

Or write:

Prentice Hall PTR
Corp. Sales Dept.
One Lake Street
Upper Saddle River, New Jersey 07458

Printed in the United States of America
10 9

ISBN 0-13-534330-5

PRENTICE-HALL INTERNATIONAL (UK) LIMITED, *LONDON*
PRENTICE-HALL OF AUSTRALIA PTY. LIMITED, *SYDNEY*
PRENTICE-HALL CANADA INC., *TORONTO*
PRENTICE-HALL HISPANOAMERICANA, S.A., *MEXICO*
PRENTICE-HALL OF INDIA PRIVATE LIMITED, *NEW DELHI*
PRENTICE-HALL OF JAPAN, INC., *TOKYO*
PEARSON EDUCATION ASIA PTE. LTD., *SINGAPORE*
EDITORA PRENTICE-HALL DO BRASIL, LTDA., *RIO DE JANEIRO*

Preface

There are many excellent books in the area of fiber-optic communication systems. This book tackles one important subset of this broad field: fiber optic test and measurement techniques. It focuses specifically on the measurement and testing of fiber-optic communication links and the components that make up the link. This book also demonstrates methods to characterize the interactions between these components that have dramatic effects on system performance. The area of lightwave measurement technology is rapidly evolving as is the entire fiber optics industry. It is difficult to keep up with the myriad of measurement demands generated in both the telecommunications and data communications area. The contents of this book provide a detailed coverage of measurement principles that are needed to design and maintain fiber optic systems now and in the future.

It became clear to the authors of this book that no single source of information is available in the broad subject area of lightwave test and measurement for fiber optic systems. The authors are with the lightwave test and measurement divisions at Hewlett-Packard. This book combines the collective experience of the lightwave staff at Hewlett-Packard together in a single source. The material in this book has been developed from application notes, seminars, conference presentations, journal publications, Ph.D. theses, and unpublished works from the last ten years. Much of this material has not had wide circulation to date.

The book will be useful for technicians, engineers, and scientists involved in the fiber optics industry or who want to become familiar with it. The book is designed to address the needs of people new to the field and to those intimately familiar with it. Chapter

1 describes the operation of a fiber optic link and its components. It then briefly describes the most common measurement needs of the fiber optic link and components with measurement block diagrams and example results. The chapter will be particularly valuable for the reader who wants a basic introduction but is not ready to dive into the more detailed coverage given in the following chapters. The basic concepts of the measurements will be presented with a minimum of mathematical detail. The main chapters of the book are designed so that the first section of each chapter provides an overview. Graphical aids are used whenever possible to help in understanding. Later sections of each chapter are geared to cover the material in greater depth for more advanced readers.

Chapters 2 to 6 cover the fundamental areas of fiber optic measurements:

a. Optical power measurements (Chapter 2);
b. Spectral measurements (Chapter 3 to 5);
c. Polarization measurements (Chapter 6).

The measurement of power is fundamental to most every lightwave measurement. Chapter 2 covers methods of power measurement and associated accuracy concerns. The area of optical spectral measurements is quite broad and is divided into three chapters. Chapter 3 covers the most common method using a diffraction-grating based optical spectrum analyzer. Chapter 4 covers the area of wavelength meters. Wavelength meters are the electrical analogue of frequency counters because they allow very accurate measurements of laser wavelength. Chapter 5 covers the area of very high wavelength-resolution spectral measurements.

The coverage of polarization in fiber optic systems (Chapter 6) is an area that historically has been underemphasized. This situation has changed since data rates have increased and optical amplifiers have been installed into fiber optic systems.

Chapters 7 and 8 focus on the measurement of the modulation on lightwave signals. In Chapter 7, the emphasis is on frequency-domain analysis of intensity modulation. The measurement of laser modulation bandwidth, distortion, and intensity noise are covered. Chapter 8 discusses time-domain measurements of the modulation. Here subjects such as eye-diagram analysis, temporal signal jitter, and bit-error-ratio measurements are covered.

Chapters 9 to 13 cover measurement topics that are common to two-port optical devices. Two-port optical devices include optical fiber, optical amplifiers, filters, couplers, isolators, and any other device where light enters and leaves. Chapter 9 covers the techniques used to measure insertion loss. Chapter 10 and 11 cover methods of measuring the reflectivity of components. Chapter 12 covers the measurement of chromatic and polarization mode dispersion. Finally, Chapter 13 covers erbium-doped fiber amplifier (EDFA) testing.

Contents

CHAPTER

1

Introduction to Fiber Optic Systems and Measurements

Dennis Derickson

1.1 INTRODUCTION

This book explores test and measurement techniques for fiber optic systems. Its primary area of concern is the fiber optic link and its related components: the optical transmitter, the fiber medium, two-port optical components such as filters and isolators, and the optical receiver.

The field of fiber optic test has become more complex as fiber optic systems have evolved. The pioneers in fiber optic research must be credited with hard work and perseverance. First they developed the basic technology of low-loss fiber, produced reliable lasers, fabricated photodetectors, and demonstrated modest bandwidth link capabilities. Because the technology was not yet commercialized, they also had to develop the test and measurement technology required to sustain the research. With deployment of fiber optic systems in the late-1970s, commercial fiber optic measurement equipment became available. The test needs for these first fiber optic systems were modest. A loss test set consisting of a source and a power meter was used to check for the presence of signals or the loss in a fiber component. An optical time-domain reflectometer could be used to find the location of a break in an optical fiber.

What are the changes in the industry that caused fiber optic communications and the associated measurement technology to become more sophisticated?

Wavelength now matters. Early fiber optic systems did not have to be especially concerned with the spectral content of the laser sources. The center wavelength range for a laser to be qualified was often over a 1260 to 1340 nm window. Today's telecommunication systems can incorporate multiple wavelength channels spaced at 100 GHz (0.8 nm) increments that are co-propagating on a single fiber. These multiple wavelength systems

are referred to as wavelength division multiplexed (WDM) systems. Each of the channels must be stable in wavelength and power. Simple, accurate, and inexpensive instruments to test the power, signal to noise ratio, and wavelength of each channel are now needed.

The data rates used in fiber have dramatically increased. The commercial state of the art for high-speed telecommunication systems has pushed beyond the previous 2.5 Gb/s rate to 10 Gb/s. Researchers are demonstrating 40 Gb/s technology and beyond. The push toward 10 Gb/s was not an easy one for fiber optic systems. The width of the optical spectrum from laser sources must be carefully analyzed and controlled. The chromatic dispersion and polarization mode dispersion of installed fiber must be checked for compatibility with high data rates. The bandwidth response of packaged optical transmitters, receivers, and associated components had to be optimized.

Optical amplifiers are now basic building blocks of fiber optic networks. The development of erbium-doped fiber amplifiers (EDFAs) has caused a significant change in the design of fiber optic links. An optical amplifier is used to directly boost the optical signal to compensate for loss in the optical fiber. Previous systems used repeaters to regenerate the digital signals when the signal-to-noise ratio was degraded by fiber loss. Repeaters convert the optical signal to an electrical signal, reproduce the digital pattern and retransmit the signal back onto the fiber with an optical transmitter. The economics of optical amplifiers are so compelling that working repeaters are often removed and replaced with amplifiers. Optical amplifiers have motivated the switch from 1300 nm to the lower loss 1550 nm wavelength in optical fiber. Optical amplifiers are an enabling technology that allows WDM systems to be practical over long spans. Each wavelength channel is simultaneously amplified within a single amplifier. The use of optical amplifiers also allows the use of optical components that have significant loss such as wavelength multiplexers and demultiplexers.

Short link-length data communications systems are displacing copper cables. Data communication is moving towards fiber as the dominant transmission medium. Early fiber-optic data communications systems used surface-emitting light-emitting diodes (LEDs) with data rates in the 10 to 622 Mb/s range. Vertical cavity surface-emitting lasers now allow data communication rates over 1.5 Gb/s at very low cost. The range of applications for data communications is expanding. Fiber optic links are now cost competitive with even very short copper-cable links. Fiber optics are used to interconnect arrays of computer workstations and hard disk drives. The local area network backbone for many businesses uses fiber optic links with very high bandwidths.

The complexity of fiber optic systems continues to grow. Researchers are now working to give fiber optics a more pervasive role in telecommunications. Previously, the role of a fiber optic cable was to provide a low-loss link between point A and point B. Future systems will utilize optical methods to route the path of a signal through a telecommunication network. Passive optical network concepts would allow a signal to stay in the optical domain over the majority of the network path. Optical routers allow the signals to be directed to the correct destinations. Multiple wavelength systems are a key enabler allowing these advanced functions to be implemented.

It is necessary to understand some of the basic features of a fiber-optic communication link before launching into a chapter-by-chapter analysis of fiber optic test and mea-

surement requirements. It is the goal of this chapter to provide some basic background in fiber optic systems and measurement techniques that will introduce readers to the measurement-specific chapters that will follow. There are many textbooks[1–3] that provide a much more detailed presentation that are highly recommended reading. Palais[1] recommends that only 7 out of his 12 chapters be covered in a one-semester college course. This Chapter 1 gives a condensed summary of the operational principles of fiber optic links that should take only a few hours to read. It also introduces some of the measurement issues associated with fiber-optic link design, manufacture, installation, and maintenance. The level of discussion in this introduction is intentionally very qualitative. Hopefully those who are not familiar with some of the measurement issues will gain an introduction and appreciation before studying the measurement-specific chapters that follow.

What is coming next in this chapter? A general fiber optic link is described. Important measurements methods for fiber-optic link characterization are then described. The link is then broken up into its individual components for description and measurement analysis: the optical transmitter, the fiber medium and optical components, and the optical receiver. Finally, a chapter-by-chapter description of the book's contents is given.

1.2 FIBER OPTIC LINKS: THE BASICS

The fiber optic link exists to provide the lowest-loss connection between two points. Fiber optic links provide the lowest cost and highest performance solution for everything but the shortest link lengths. Fiber optic links are capable of transmitting digital- and analog-formatted signals. Section 1.2.1 will discuss the basic features of digital communication links. Section 1.2.2 will describe WDM systems where more than one signal is present on the fiber optic cable. Section 1.2.3 will describe analog communication systems and associated testing requirements. After this short introduction to fiber optic links, Section 1.3 will discuss some of the basic measurements for end-to-end characterization of the link.

1.2.1 Digital Communication Links

Figure 1.1 shows a diagram of a digital fiber-optic link. Signal waveforms are shown at several key points along the signal path. These waveforms illustrate some of the fundamental characteristics of a fiber optic link. After reading this chapter, it will be useful to return to this figure to see how well the basic measurement concepts of a fiber optic system are illustrated in a single figure. Let us now discuss the link operation as the signal flow proceeds from the electrical input to the electrical output.

In this example, the input electrical data stream to the optical transmitter is a non-return to zero (NRZ) digital pattern of 0, 1, 0, 0, 1, 1. The electrical signal is converted to an optical signal with the electrical-to-optical (E/O) converter, the optical transmitter. The optical transmitter is essentially a current-to-power converter. In a perfect E/O converter every electron injected into the source should produce a single output photon. Semiconductor laser (light amplified by stimulated emission of radiation) diodes are the predomi-

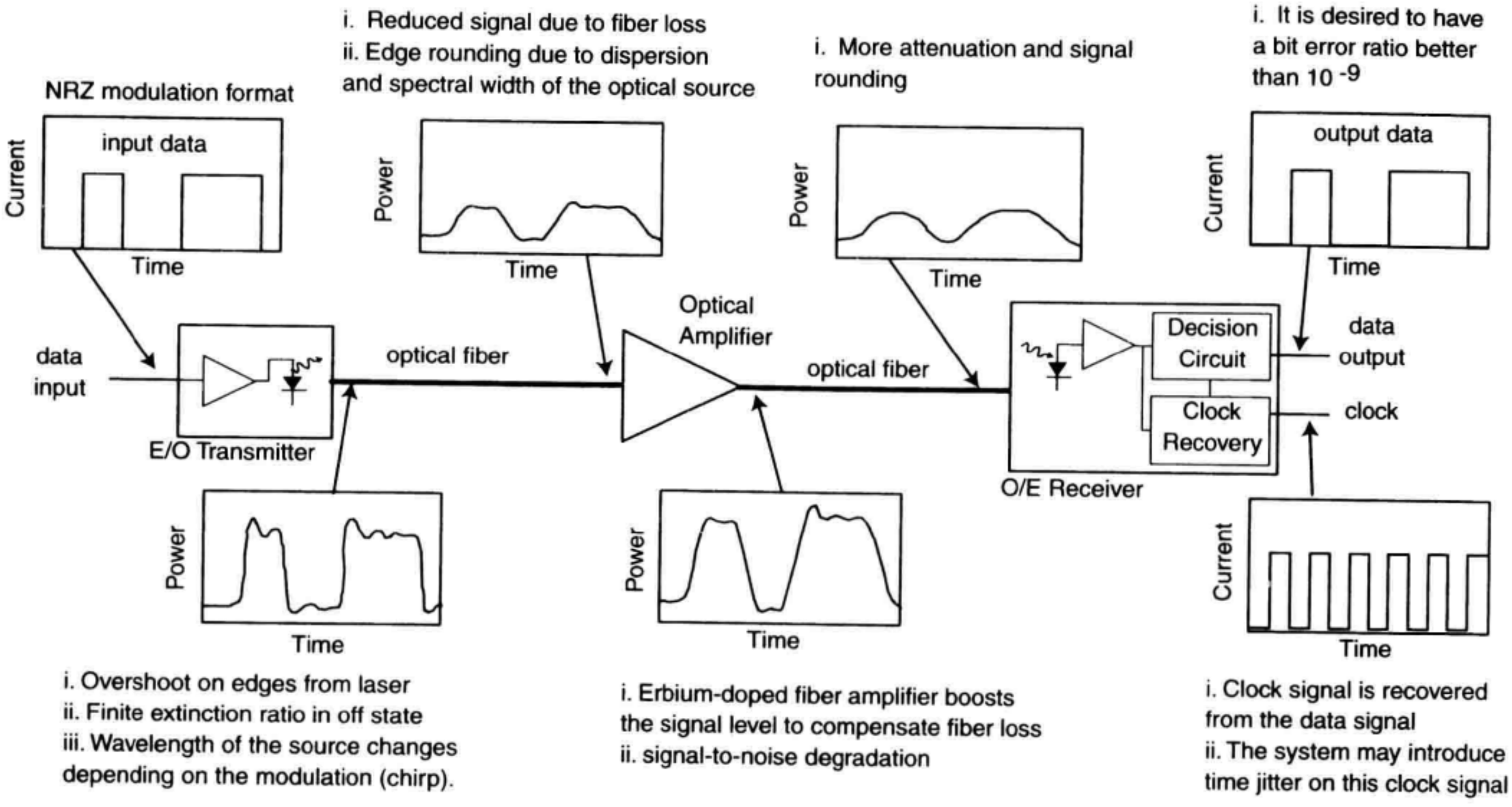

Figure 1.1 A digital fiber-optic communication link.

nant sources for long-distance, high-speed digital systems. Lasers provide high optical power, narrow spectral width, and modulation rates beyond 10 Gb/s. LEDs are common lightwave sources for shorter distances and lower data rates. Section 1.6 compares the available fiber-optic transmitter types.

International standards such as Synchronous Optical Network (SONET) and Synchronous Digital Hierarchy (SDH)[4–6] specify data rates and formats used for digital modulation in telecommunication systems. Data rates from 51.84 Mb/s to 9.95 Gb/s are specified in the SONET/SDH standards. Each of these high-speed channels contains lower data rate signals that have been time-interleaved using a method called time division multiplexing (TDM). A different set of standards exist for data communication fiber-optic links. Gigabit ethernet and fibre channel[7,8] are examples of high speed data communication interface specifications. Fibre channel systems are becoming very popular for computer peripheral applications with up to 1.063 Gb/s data rates. Fiber distributed data interface (FDDI) is another standard used for local area networks.[9]

Figure 1.1 shows that the output of the optical transmitter is not a perfect replica of the input electrical signal. A significant test and measurement challenge is to characterize the waveform and signal-to-noise degradation present in E/O converters. The laser transmitter in this example has significant overshoot during the transition from the zero to one state. This ringing of the laser output power is caused by interactions between the round-trip time of photons in the laser and the speed at which the optical gain can be changed by a step change in current.[10] The characteristic frequency of the ringing is referred to as the relaxation oscillation frequency. It has a typical value between 2 to 30 GHz depending on laser design parameters.

Figure 1.1 shows how the edges of the digital waveform become more rounded after propagation through the fiber optic cable. This waveform spreading leads to distance limitations in an optical fiber link. The spectral width of an optical source is a major consideration for waveform spreading. Excess laser bandwidth is important due to chromatic dispersion in optical fibers. The different wavelengths contained in the optical signal travel at different velocities due to chromatic dispersion. After propagating through long fiber lengths, adjacent data bits start to overlap leading to intersymbol interference and errors. Fabry-Perot lasers and LEDs are optical source examples that have wide spectral width. The spectral width of these sources may limit their usefulness for long fiber-optic links.

Even narrow spectral-width sources have concerns. Distributed feedback (DFB) lasers are the dominant source for high-performance telecommunication applications. During the modulation transition between the one and zero power levels, the wavelength of DFBs is pulled away from its nominal operating value. This wavelength shift is commonly referred to as "chirp." Chirp causes the spectral width of the laser to be much wider than is necessary to transmit the information. A 2.5 Gb/s digitally modulated signal should occupy an optical bandwidth of less than 10 GHz to accommodate the information. A chirped laser could have an optical bandwidth of 30 GHz or more.

The optical transmitter establishes the wavelength of the fiber optic link. The choice of laser wavelength is driven by the loss characteristics of optical fiber cables. This leads us into a discussion of the characteristics of optical fiber.

1.3 DIGITAL COMMUNICATION LINKS

1.3.1 Optical Fiber

The premier feature of optical fiber is its extremely low loss. This has made it the dominant transmission medium for long link lengths. Section 1.4 describes fiber optic cable operation in more detail. An overview is given here.

Loss characteristics. The loss versus wavelength of optical fiber is shown in Figure 1.2a for many different types of fibers. The loss characteristics of fiber determines where optical communication is practical. At 1550 nm, singlemode optical fiber has an attenuation of 0.2 dB/km. This allows fiber optic signals to be propagated through very long lengths of fiber without regeneration. A fiber optic link at a 2.5 Gb/s rate can tolerate a 25 dB signal loss before system noise becomes a problem. This means that a distance of 125 km could be spanned with such a link. This is roughly 1000 times lower loss than a coaxial cable at 2.5 Gb/s. This low insertion loss is the driving force behind the fiber optic revolution.

Figure 1.2 also illustrates the wavelengths used in fiber optic systems. Axes are given in wavelength frequency and wavenumber. These variables are related by the following equations.

$$\text{frequency} = \frac{c}{\lambda_{vac}} \tag{1.1}$$

$$\text{wavenumber} = \frac{1}{\lambda_{vac}} \tag{1.2}$$

Here λ_{vac} is the wavelength of light in a vacuum and c is the speed of light in a vacuum. Fiber optic transmitters emit in the wavelength range between 630 nm (476 THz) and 1650 nm (182 THz). As a reference, the visible portion of the optical spectrum lies in the range of 400 to 700 nm.

Digital fiber-optic links are categorized by their end applications. Telecommunication systems use the 1300 and 1550 nm windows for lowest loss in the fiber. Since a telecommunication system must cover a very large distance, loss in the fiber is of high importance. Attenuation values as low as 0.2 dB/km are available at 1550 nm using singlemode fiber. Erbium-doped fiber amplifiers (discussed in Chapter 13 later) are also available at 1550 nm, making this the highest performance wavelength available. Erbium-doped amplifiers require optical pump lasers at either 980 nm or 1480 nm. 1650 nm is an important wavelength that is used to monitor the loss characteristics of a fiber while live traffic is being carried.

Data communication systems use multimode glass-fiber at either 780 to 850 nm, 980 nm or 1300 nm bands. Since shorter distances are being covered, higher loss can be tolerated. The 780 to 850 nm wavelength range has developed because of the availability of inexpensive optical fiber components and for historical reasons. These systems generally use data rates up to 1 Gb/s over links that are less than a few km. Plastic fiber-optic links are used with 650 nm sources. The data rate is typically less than 100 Mb/s with a

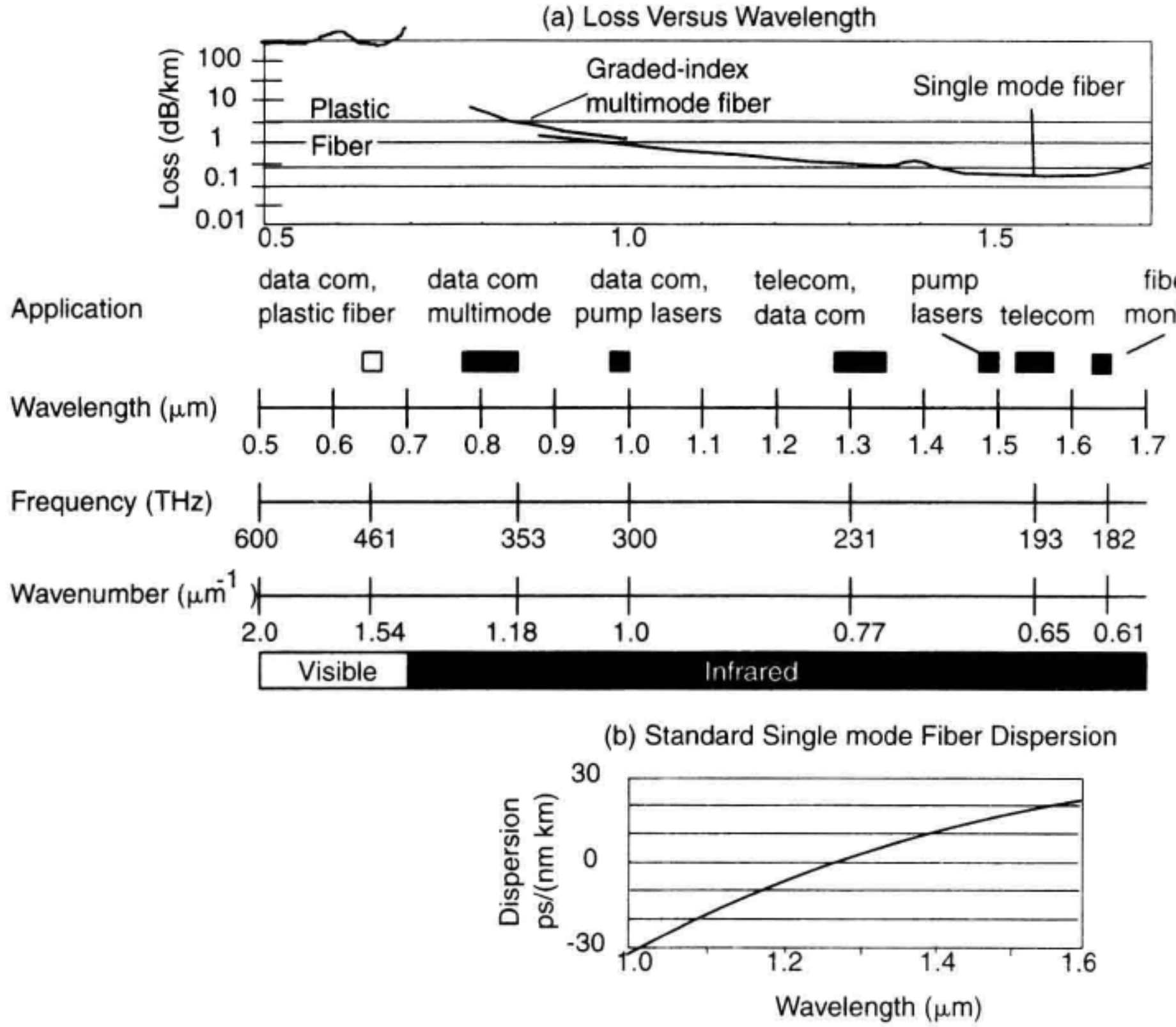

Figure 1.2 (a) Loss in optical fiber waveguides and important wavelengths for fiber optic communications. (b) Chromatic dispersion of standard singlemode fiber.

range of tens of meters limited by the higher loss of plastic fiber and dispersion, which leads us to the next section.

Chromatic dispersion in singlemode fibers. The loss characteristics of optical fiber often limit the distance that a signal can propagate. This is not always the case. In singlemode fibers, chromatic dispersion can limit the distance over which fiber optic signals can propagate. Chromatic dispersion describes the fact that the speed of signal propagation in the fiber depends on the wavelength of the light. Figure 1.1 illustrates the detrimental effects of fiber dispersion. Notice that as the signal propagates through a long length of fiber, the edges of the waveform start to become more rounded. Eventually, the adjacent bits start to overlap in time causing the digital waveform to have poor readability. Pulse spreading causes adjacent digital bits to interfere with each other. The amount of signal rounding depends on the amount of chromatic dispersion in the cable and the spectral width of the laser transmitter. Chapter 12 describes how to make measurements

of chromatic dispersion. Chapters 3 to 5 discuss methods of characterizing the spectral width of sources.

Figure 1.2b gives some example data for the chromatic dispersion of a singlemode fiber-optic cable. For much of the installed singlemode fiber in the world, the dispersion is minimized near 1310 nm. This fiber will be referred to as "standard fiber." In standard fiber, the wavelength of lowest loss is not the wavelength of lowest dispersion. Dispersion-shifted fiber (DSF) was developed so that the lowest loss wavelength and the lowest dispersion wavelengths would coincide at 1550 nm. WDM systems do not work well near zero dispersion wavelengths. This has led to WDM-optimized fibers where the zero dispersion wavelength is shifted slightly away from the low-loss 1550 nm wavelength.

Polarization mode dispersion (PMD) in singlemode fibers. If insertion loss or chromatic dispersion do not limit link length, it is possible that polarization mode dispersion will ultimately limit link lengths. Polarization mode dispersion arises because the velocity of propagation depends on the polarization state of the lightwave signal. The PMD of a fiber optic cable is not constant over time, making it difficult to compensate for. This effect will ultimately limit the highest achievable data rates for a single-wavelength fiber-optic system. Chapter 12 covers PMD measurements.

Modal dispersion in multimode fiber. Multimode fiber suffers from a more severe type of dispersion—modal dispersion. Modal dispersion is caused by light rays taking different length paths down the same fiber. This results in the same intersymbol interference problems discussed with chromatic dispersion.

1.3.2 Optical Amplifiers and/or Optical Repeaters

After propagating through a length of fiber, the signal-to-noise ratio degrades or the distortion becomes great enough that the signal needs to be reconditioned. Fiber optic systems often use optoelectronic repeaters to detect the signal, and regenerate, retime, and then retransmit the signal onto the fiber with another optical transmitter.

Fiber optic systems also use optical amplifiers to boost the signal midspan if long-link distances is required. Optical amplifiers can compensate for fiber loss at the expense of adding a small amount of noise and distortion to the signal. Erbium-doped fiber amplifiers (EDFAs) are the predominant optical amplifier technology.[11] These amplifiers have revolutionized the way fiber optic systems are designed. EDFAs offer low noise contribution (3 to 4 dB noise figure), high gain (to 40 dB), and high output-power capability (approximately 50 mW of output power) near 1550 nm. Undersea telecommunication systems with hundreds of cascaded optical amplifiers have proven that long link-length optically amplified systems are practical.[12] The TPC-5 link across the Pacific Ocean successfully uses 260 cascaded optical amplifiers to cover an 8600 km span.

1.3.3 O/E Converters

The optical signal is then converted back into the electrical domain with an O/E converter. The O/E converter is an optical power to electrical current converter. Ideally, each received photon would be converted to an electron. p-i-n diode detectors are commonly

used. They can have extremely high bandwidth, but the sensitivity of high-speed photoreceivers is often limited by the noise contribution of the electronics following the detector. Avalanche photodetectors (APDs) are used for high-sensitivity systems. APDs can produce several electrons for each received photon. This electronic gain in the APD allows the sensitivity of the system to be set by the APD noise characteristics and not by the noise of the following electronics. This results in higher sensitivity, especially at high data rates.

In addition to O/E conversion, the optical receiver must recreate the input data stream and clock signal. Since the received signal power can vary, the receiver must have an automatic gain control stage or limiting amplifier. It is important to accurately extract the clock from the data with very good timing accuracy. The clock signal is used to trigger the decision circuit that decides if a 1 or a 0 has been received.

1.4 WAVELENGTH DIVISION MULTIPLEXED SYSTEMS

1.4.1 Wavelength Division Multiplexed Systems

Figure 1.1 shows how a single wavelength digital waveform is sent through a fiber optic link. Increasing the data rate of a single wavelength channel is one strategy to increase the throughput on optical fibers. The data rate for a single optical channel will eventually reach its limits due to chromatic dispersion and/or polarization mode dispersion. An important strategy to further increase the available bandwidth is to add multiple wavelength channels. Multiple wavelength systems are referred to as being wavelength division multiplexed (WDM). Early WDM systems used a wide wavelength spacing. It was common to increase the bandwidth of a 1310 nm link by adding a 1550 nm channel. The installation of WDM systems is often driven by economic reasons. It is less expensive to update the terminal equipment to WDM capability than to install new fiber optic cables. The introduction of the Erbium-doped fiber amplifier has moved nearly all WDM activity to the 1530 to 1565 nm wavelength window. More recent WDM installations are referred to as dense WDM (DWDM) systems due to the narrow spacing between optical channels.

Figure 1.3 shows the diagram of a DWDM fiber optic link. Lasers are combined in a wavelength multiplexer to a single fiber. International standards organizations are defining standard wavelength channels for DWDM systems.[13] A common standard is a DWDM laser wavelength spacing of 100 GHz between channels. Systems use 4, 8, 16, or 32 channels located on the 100 GHz channel grid shown in Table 1.1.

Wavelength multiplexers are used to combine and separate the wavelength channels onto a single fiber with low loss. EDFA booster amplifiers are used to counteract the insertion loss of the wavelength multiplexers at the transmitter and the receiver. A single EDFA can amplify all of the wavelength channels simultaneously.

With the introduction of WDM systems, new roles emerged for the use of fiber optics in telecommunication systems. Previously, when a set of signals needed routing to a

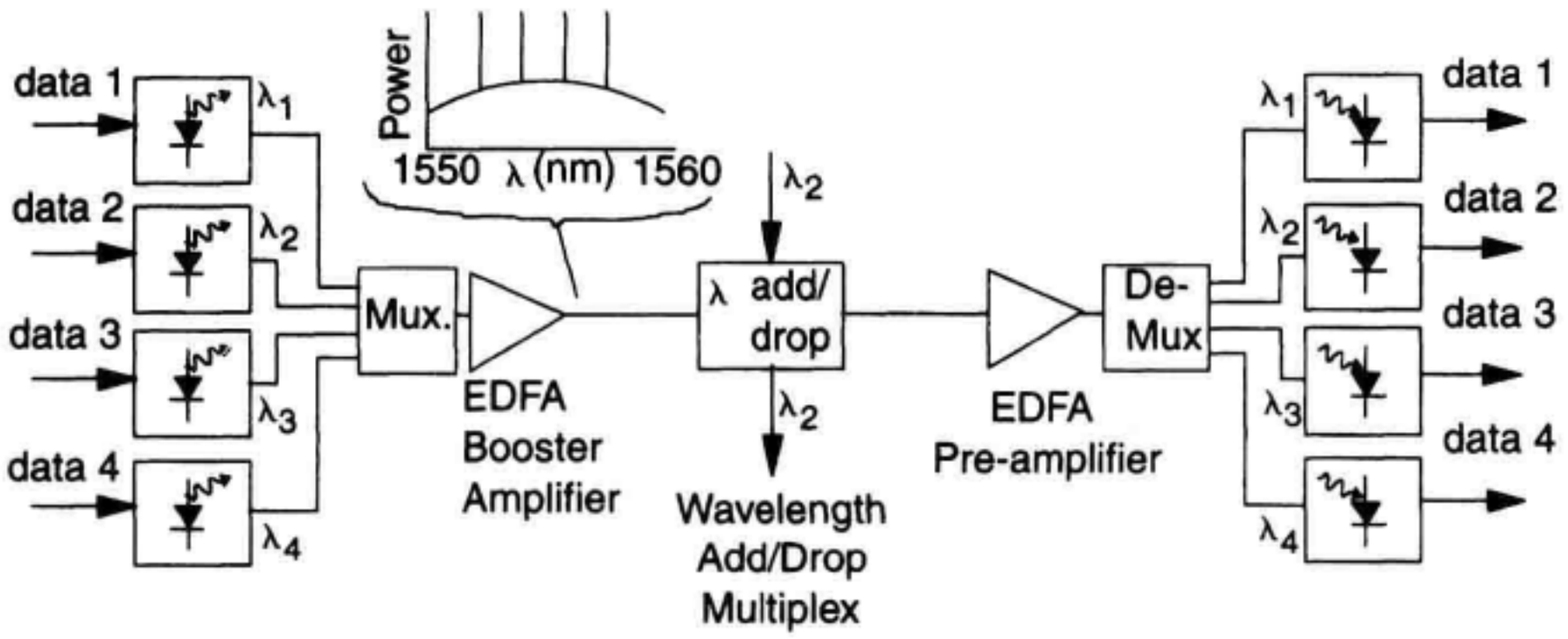

Figure 1.3 A wavelength division multiplexed (WDM) fiber optic link.

particular location, the optical signal was detected and then routed electronically. The coming trend is to allow the optics to do some of the routing functions. The ability to add and drop certain wavelength channels from a fiber while sending on other channels undisturbed is an example of optical routing capability.

At the receiver, an EDFA is used to compensate for the loss of the demultiplexer filters and to increase receiver sensitivity. The demultiplexer sorts the wavelengths out to the individual receivers for detection.

The switch from single wavelength to multiple wavelength systems has introduced measurement challenges:

1. In single wavelength systems, the absolute wavelength of a laser and associated components was not critical. Laser wavelengths now need to be measured with less than 0.01 nm accuracy. Studies on aging of semiconductor lasers require wavelength resolutions of 0.001 nm.
2. The loss versus wavelength of optical components has taken on new importance. The wavelength demultiplexor at the receiver must reject the signal from adjacent channels. This requires accurate, high-dynamic range measurement capability. Cross talk between channels can also be introduced through fiber nonlinearities that can cause power from one channel to be converted to another channel. Fiber nonlinearities are discussed in Appendix B.
3. The monitoring of wavelength, channel power, and signal-to-noise ratio is required for network management. Single wavelength systems require power measurements at various points in the network to find fault conditions. Simple power measurement is not sufficient in WDM systems. Spectral monitors are now necessary to sort out performance of each channel.

Table 1.1 ITU-T Defined WDM Wavelength Channels

Frequency (THz)	Wavelength (nm)
195.6	1532.7
195.5	1533.5
195.4	1534.9
195.3	1535.0
195.2	1535.8
195.1	1536.6
195.0	1537.4
194.9	1538.2
194.8	1539.0
194.7	1539.8
194.6	1540.6
194.5	1541.3
194.4	1542.1
194.3	1542.9
194.2	1543.7
194.1	1544.5
194.0	1545.3
193.9	1546.1
193.8	1546.9
193.7	1547.7
193.6	1548.5
193.5	1549.3
193.4	1550.1
193.3	1550.9
193.2	1551.7
193.1	1552.5
193.0	1553.3
192.9	1554.1
192.8	1554.9
192.7	1555.7
192.6	1556.6
192.5	1557.4
192.4	1558.2
192.3	1559.0
192.2	1559.8
192.1	1560.6

1.5 ANALOG LINKS

1.5.1 Analog Links

There are many systems that transmit analog signals over the fiber optic link. Figure 1.4 shows a typical diagram of an analog fiber-optic link and a measurement system. The goal of an analog link is to reproduce an identical version of the input signal at the output. A small amount of noise and signal distortion can appear at the output due to fiber optic contributions. It is a significant design challenge to keep the degradation levels low.

One very important application of analog fiber-optic links is in cable-TV video distribution. Cable TV systems use analog signals that directly connect to the television receivers. Older cable TV systems use long cascades of electronic amplifiers that result in noise build-up and poor reception near the fringes of the system coverage. Analog fiber-optic links are used to decrease the number of electronic repeaters between the system head end and the subscriber. A star configuration of fiber optic cables feeds the signal to local neighborhoods. The signal is then converted back to analog electronics and distributed to the subscribers over coaxial cable. The analog fiber-optic links in this application must have very low intermodulation and harmonic distortion levels to insure the quality of reception at the consumer. Laser transmitters and receivers developed for cable TV systems must be linear. Important fiber optic transmitter and receiver parameters such as the composite second-order and composite triple-beat distortions are described in Darcie et al.[14] The laser transmitter must be tested with a complex input signal that can contain dozens of video and data channels. Optical reflections in analog systems can cause laser frequency variations to be coupled into an increase in system noise (see Appendix A). Chapter 7 in this book addresses many of the measurement categories important for these applications.

Analog links are also used for low-loss distribution of microwave signals. An example application is antenna remoting and distribution of signals for phased array radars.[15]

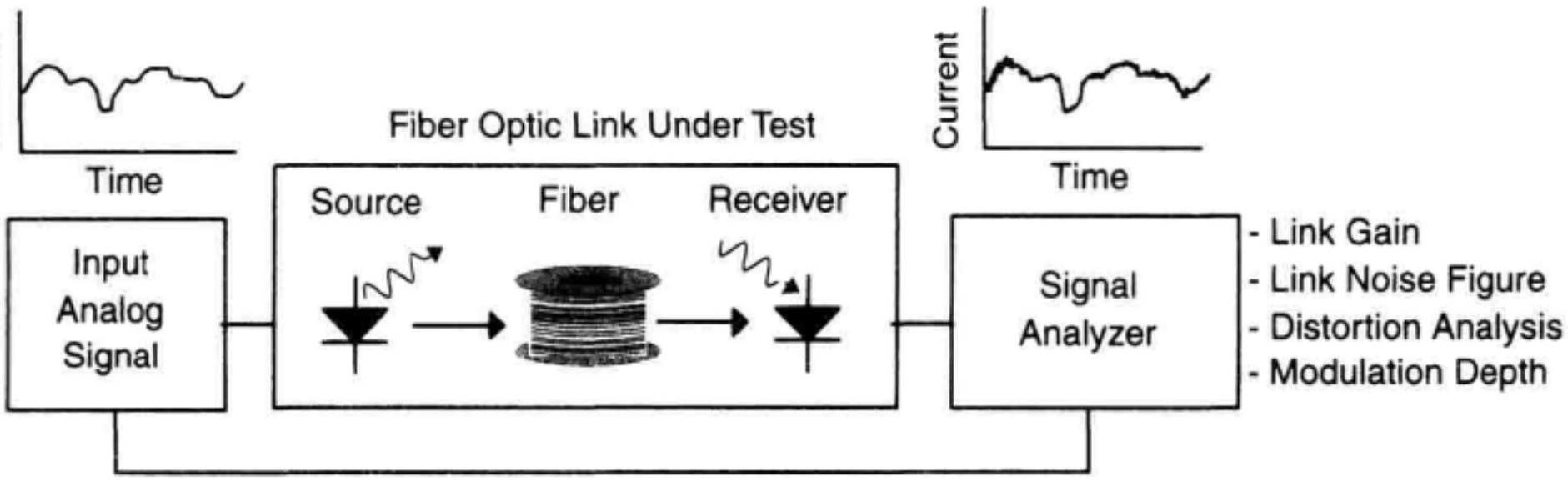

Figure 1.4 An analog fiber-optic link.

1.6 CHARACTERIZATION OF DIGITAL FIBER-OPTIC LINKS

Section 1.2 introduced some of the basic features of fiber optic links. It must be emphasized again that the primary purpose of a fiber optic link is to provide a low-loss data connection between two points. This section will outline techniques used to verify that acceptable end-to-end performance is achieved.

1.6.1 Bit Error Ratio

The most important parameter of a digital system is the rate at which errors occur in the system. A common evaluation method is the bit error ratio test as shown in Figure 1.5. A custom digital pattern is injected into the system. It is important to use a data pattern that simulates data sequences most likely to cause system errors. A pseudo-random binary sequence (PRBS) is often used to simulate a wide range of bit patterns. The PRBS sequence is a "random" sequence of bits that repeats itself after a set number of bits. A common pattern is $2^{23}-1$ bits in length. The output of the link under test is compared to the known input with an error detector. The error detector records the number of errors and then ratios this to the number of bits transmitted. A bit error ratio of 10^{-9} is often considered the minimum acceptable bit error ratio for telecommunication applications. Data communications have more stringent requirements where 10^{-13} is often considered the minimum. A common measurement is to test the bit error ratio as a function of loss in the optical fiber. Chapter 8 describes bit error ratio measurements in detail.

1.6.2 Waveform Analysis

Bit error ratio measurements provide a pass/fail criteria for the system and can often identify particular bits that are in error. It is then necessary to troubleshoot a digital link to find the cause of the error or to find the margin in performance that the system provides. Digital waveforms at the input and output of the system can be viewed with high-speed oscilloscopes to identify and troubleshoot problem bit patterns as is shown in Figure 1.6. The pattern generator used in bit error ratio analysis can be coordinated with the oscilloscope to view the particular pattern that caused an error. Chapter 8 discusses methods of digital waveform analysis.

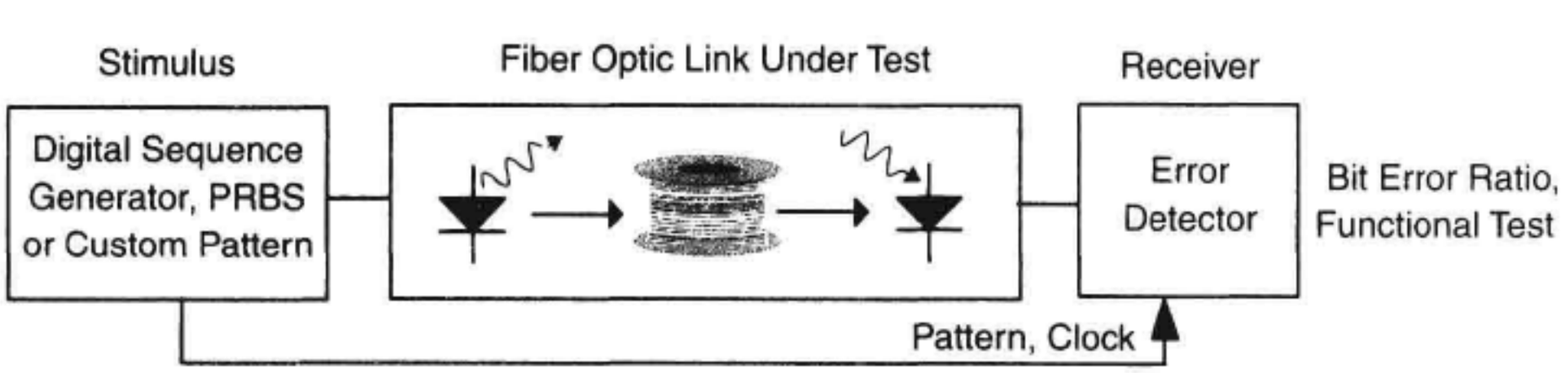

Figure 1.5 Bit error ratio measurements and functional test.

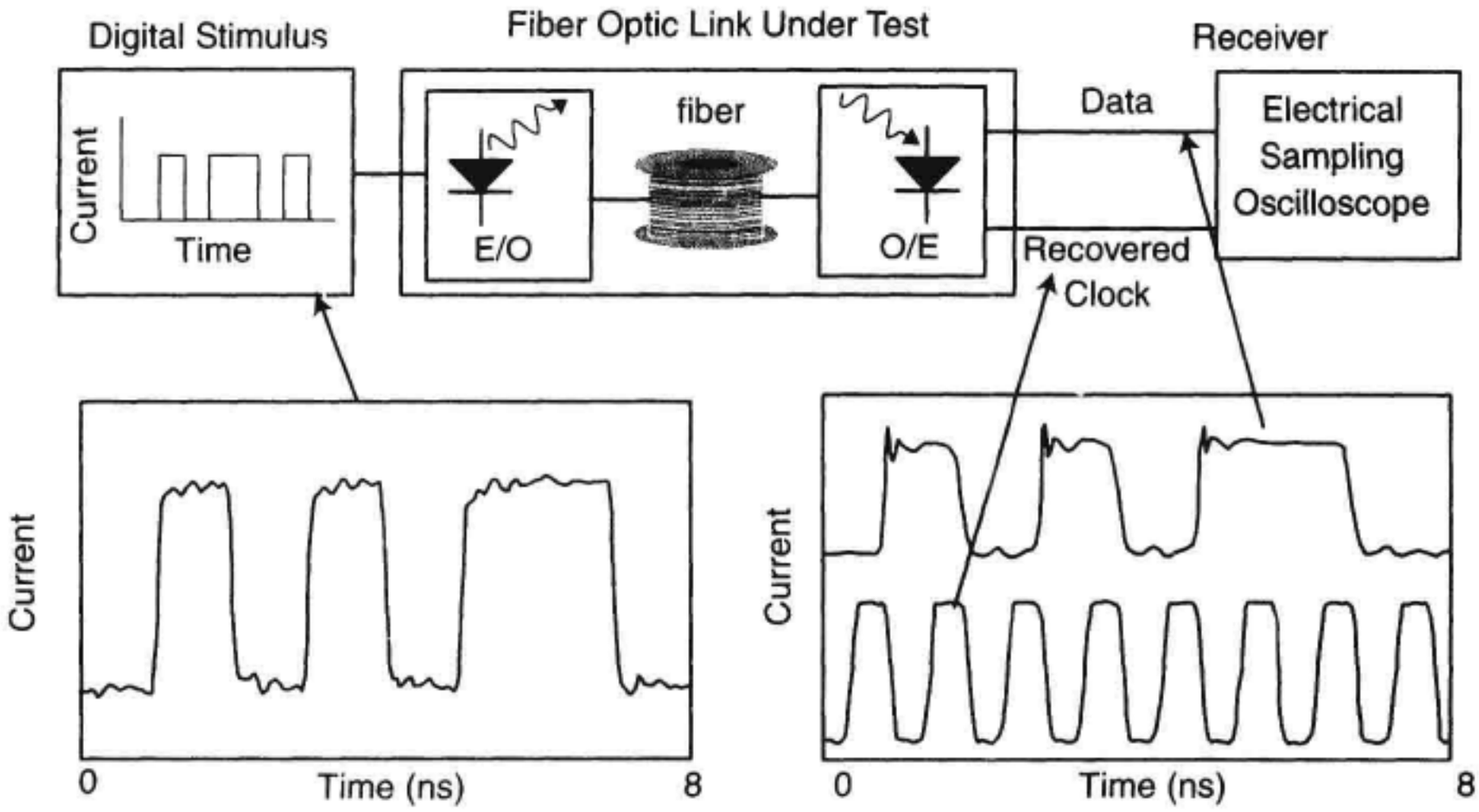

Figure 1.6 Waveform analysis of a fiber optic link.

1.6.3 Link Jitter

Another link evaluation is clock jitter measurement as shown in Figure 1.7. Control of jitter is important to insure that many fiber optic links can be successfully cascaded together.[16,17] A perfect clock waveform would have a uniform bit period (unit interval) over all time. The fiber optic system can add variability to the unit interval period which is referred to as jitter. Three types of jitter measurements are performed: absolute jitter, jitter transfer, and jitter tolerance. Absolute jitter measurements look at the jitter produced at the link output with a low-jitter clock signal at the input. Jitter transfer characterizes the amount of jitter produced at the output of the device under test compared to the amount of jitter at its input as a function of frequency. An example of a jitter transfer measurement is given in Figure 1.7b. The plot shows jitter modulation frequencies where the jitter at the output is increased compared to the jitter at the input (unacceptable). Standards such as SONET and SDH have specified levels of jitter transfer that can be tolerated as a function of the jitter modulation frequency.[4]

Jitter tolerance measurements find the highest level of jitter at the input of a system that can still produce acceptable output bit error ratio. Results of these measurements indicate how well links can be cascaded together without producing timing-related errors. Jitter tests are described in detail in Chapter 8.

1.6.4 Summary

Fiber-optic link measurements determine if the system meets its end design goals. In order for a link to meet its design goals, all of the components contained within the link must be characterized and specified to guarantee system performance. The following sections of Chapter 1 describe the characteristics of each component along with an analysis

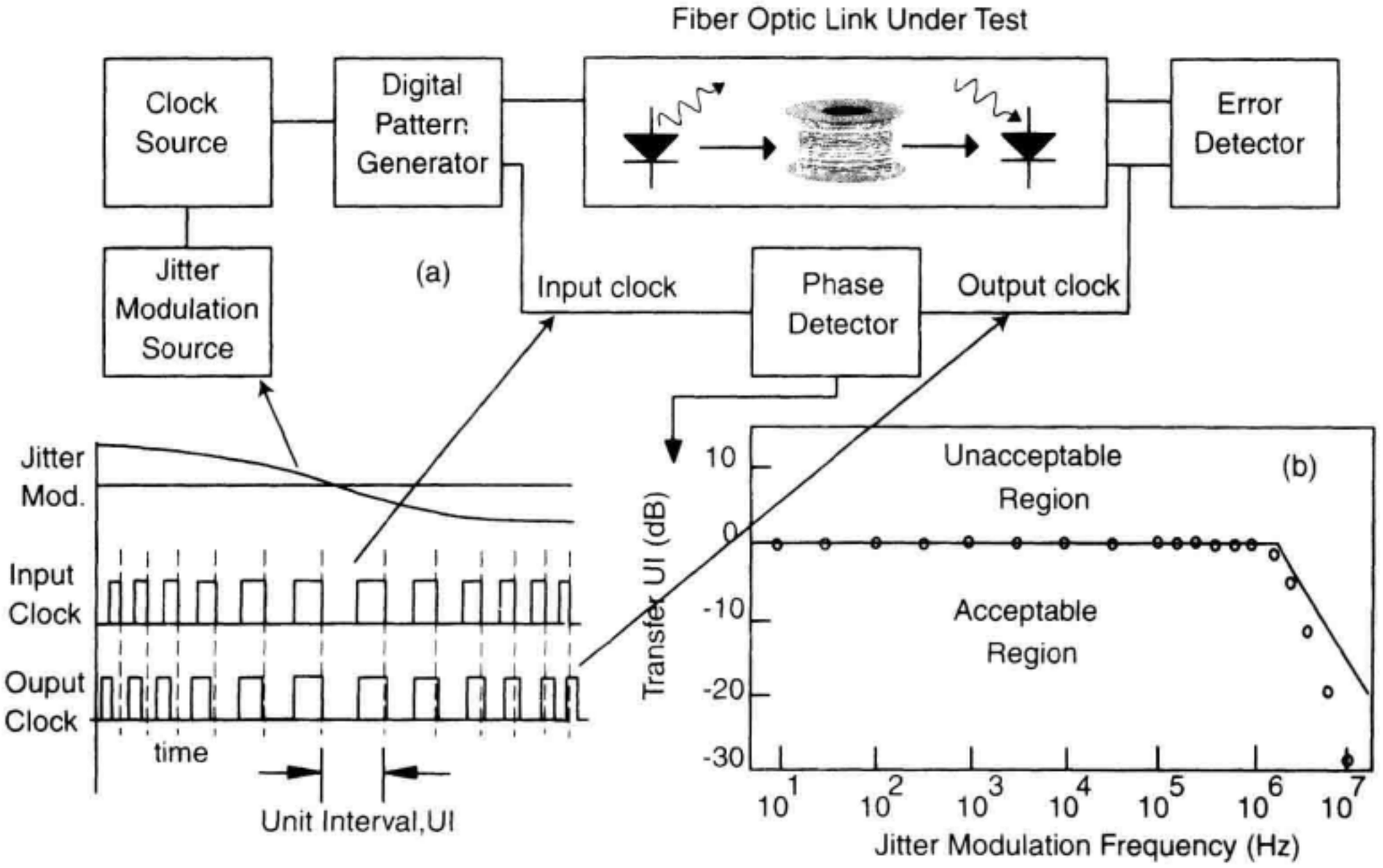

Figure 1.7 (a) System to characterize link jitter. (b) A jitter transfer function measurement example.

of the testing needs for these components. The discussion starts with optical fibers and amplifiers. The discussion then continues with optical transmitters and receivers. In each section, a brief description of each component type is made. This is then followed by a description of the testing requirements on each component. References are then made to sections of the book where more detail can be found on the measurement methods.

1.7 OPTICAL FIBERS AND TWO-PORT OPTICAL COMPONENTS

Figure 1.8 illustrates the basic features of an optical fiber. Figure 1.8a shows the end view of the fiber and the corresponding index of refraction profile. The central part of the fiber is called the core and the outer portion is called the cladding. The fiber is most often made from silica (SiO_2) glass. The center core of the fiber is doped to produce a slight increase in the index of refraction and a corresponding decrease in signal velocity. A common core dopant is Ge. The index of refraction difference between the core and cladding is very small, typically around 0.01.

The optical signal is confined to the core due to the principle of total internal reflection. In total internal reflection, a ray of light incident on the core-to-cladding boundary will be 100% reflected back toward the core as long as a critical angle is not exceeded. This confined reflection of light rays is illustrated in the fiber side-view drawing in Figure

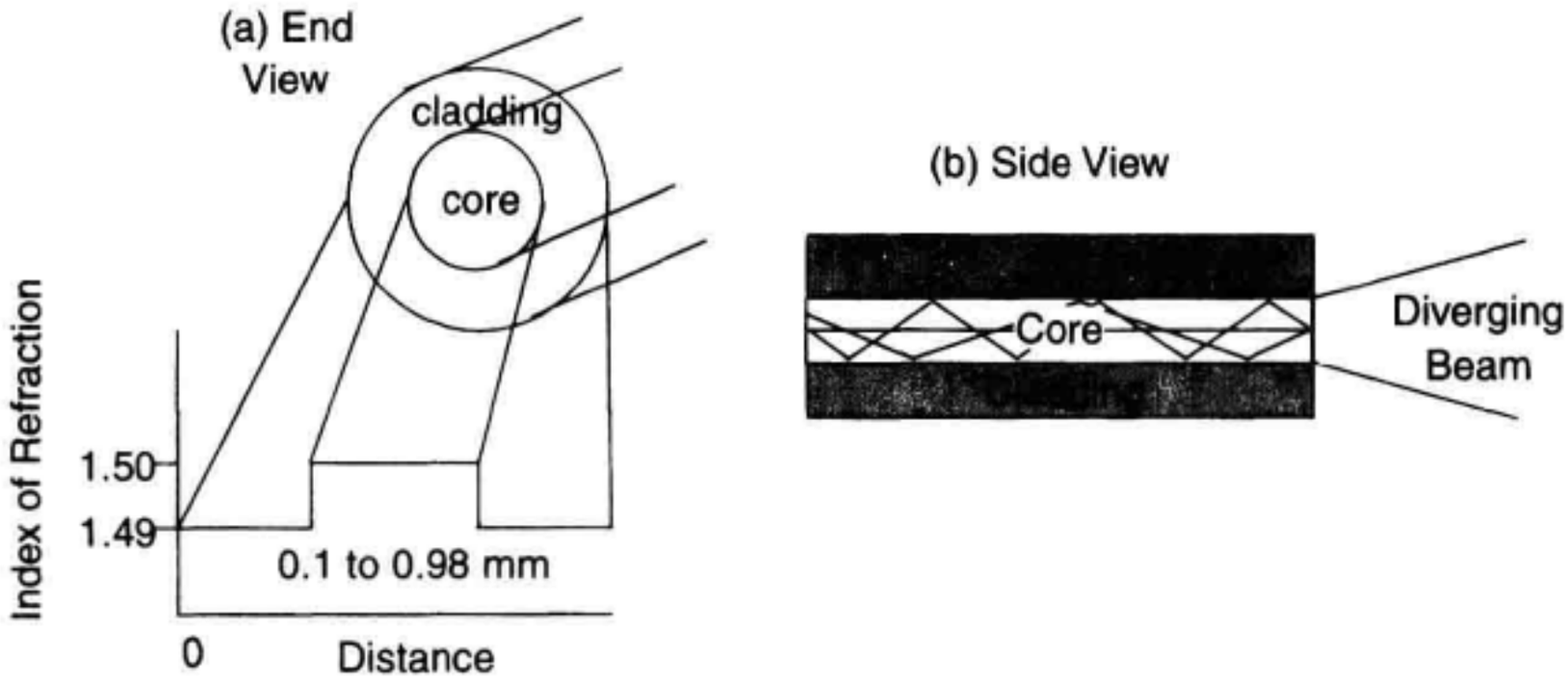

Figure 1.8 (a) End view of a step-index multimode fiber. (b) Side view of the fiber.

1.8b. For an index of refraction difference of 0.01, the critical angle is a shallow 6.6 degrees.

Multimode and singlemode fiber. There are two important classes of fiber used in links: singlemode and multimode fiber. Singlemode fiber is associated with high bandwidth telecommunication applications where long link length is required. Multimode fiber is associated with data communication systems, lower data rates, and short link lengths.

Singlemode and multimode terminologies refer to the profile of light found in the end view of the fiber and the paths that light takes along the fiber length. Figure 1.8b shows a side view of a multimode fiber and three example rays that propagate through the fiber. One ray could take a path following the center of the fiber. Another ray could take a path that bounces off of the cladding. These two example rays have a very different path length through the fiber. In a singlemode fiber, the size of the core is reduced until only one path (mode) is allowed to propagate through the fiber.

1.7.1 Step-Index Multimode Fiber

Figure 1.8 illustrates a step-index multimode fiber. When specifying a fiber type, the dimensions and the modal character of the fiber are specified. A common step-index fiber has a core diameter of 100 μm and a cladding diameter of 140 μm. The index of refraction is abruptly stepped from the core to the cladding. This multimode fiber would be referred to as 100/140 SI MM fiber. The first two dimensions are the core and cladding diameters, the SI refers to step index and MM refers to multimode. Multimode fibers have the advantage of ease of use and cost of associated components when compared to singlemode fiber. The larger fiber-optic core dimensions make fiber coupling to transmitters and receivers less stringent. It also becomes easier for operators to prepare optical connectors.

980/1000 SI MM plastic fibers are used in very low-cost and short link-length applications. The primary advantage of these fibers is that they are easy to install and maintain. Very simple tools can be used to add connectors. Plastic fibers use a low-loss win-

dow at 650 nm. Here fiber loss is 0.2 dB/m, almost 1,000 times greater than the loss minimum for glass optical fibers.

1.7.2 Graded-Index Multimode Fiber

Figure 1.9 illustrates the operation of a graded-index multimode fiber. In graded-index fiber, the refractive index changes gradually between the core and the cladding. Multimode fibers for data communication at 850 nm and 1300 nm use either a 50 μm or 62.5 μm core diameter. Common graded index fibers are 50/125 GI MM and 62.5/125 GI MM types with 62.5/125 being more common. The outer diameter of the glass fiber is 125 μm. Additional coatings are added over the glass cladding to protect the fiber resulting in an increase in the diameter to 250 μm.

Multimode Fiber Dispersion. A consequence of multimode fiber designs is that an optical pulse will quickly spread out in time due to the multiple paths available for the signal. The signal spreading limits the maximum link length or maximum data rate that the fiber can accommodate. Modal dispersion is a measure of this multipath signal distortion. Figure 1.9c shows how an input data sequence can be spread out in time causing adjacent bits to overlap. Errors will occur if the data is allowed to spread too widely. Multimode dispersion is characterized by a pulse-broadening parameter. It is stated in terms of the ps of pulse broadening per unit of fiber length. It can also be related to a bandwidth-distance product. For a 500 MHz-km product (a typical value for multimode fiber), you could make a 622 MHz link over a 1 km length or a 155.5 MHz link over 4 km length with equal pulse broadening penalty.

Multimode Fiber Speckle Pattern. If a multimode fiber is illuminated with a narrow spectral-width optical source, a dark and light "speckle pattern" is formed in the end view as shown in Figure 1.9a. The dark and light patterns form because light from different optical paths add constructively or destructively. If a multimode fiber cable is

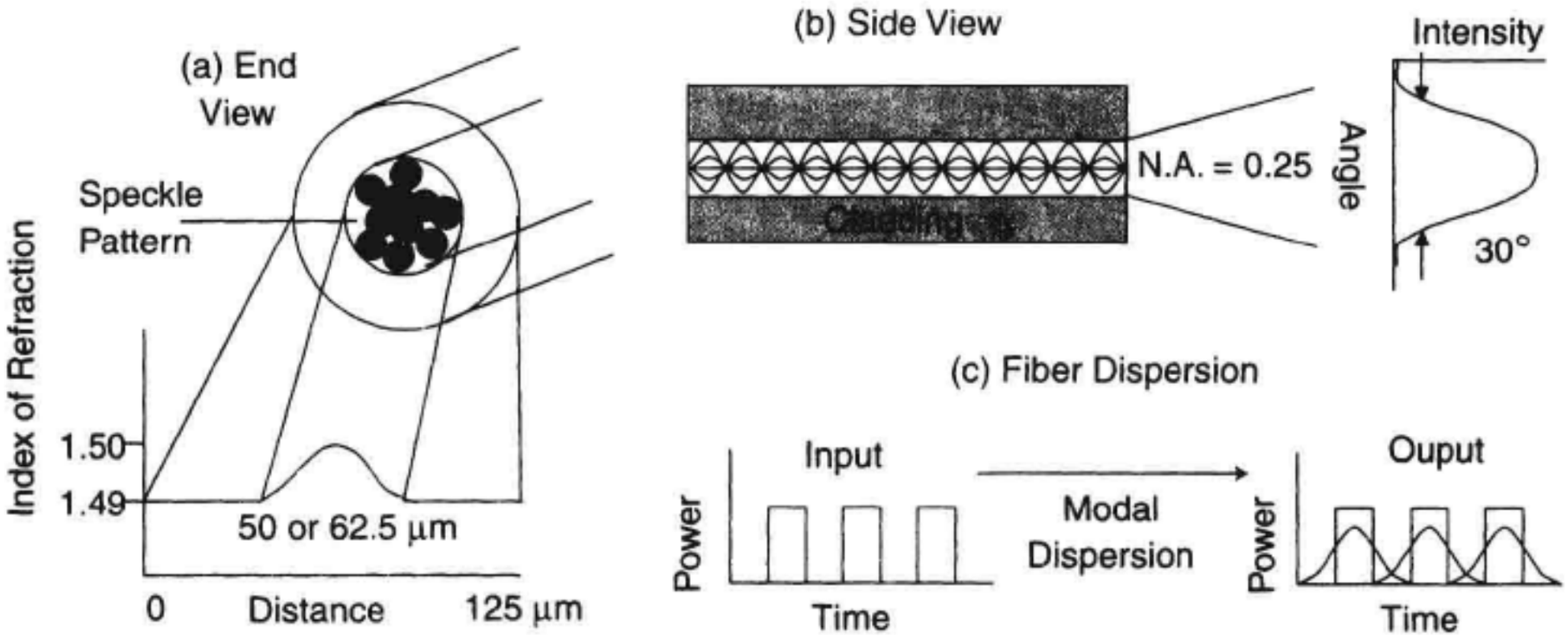

Figure 1.9 (a) End view of a graded-index multimode fiber. (b) Side view of the fiber. (c) The effects of modal dispersion.

Table 1.2 Comparison of Multimode Fiber Characteristics

Multimode Fiber	Core (μm)	Cladding (μm)	Numerical Aperture	Attenuation dB/km	Pulse Broadening
62.5/125 GI	62.5	125	0.27	0.7 @ 1300 nm	500–1200 MHz-km
50/125 GI	50	125	0.21	0.5 @ 1300 nm	500–1500 MHz-km
100/140 SI	100	140	0.2–0.3	5 @ 850 nm	20 MHz-km (22 nm/km)
980/1000 SI plastic	980	1000	0.5	0.2 dB/m @ 660 nm	(110 ns/km)

wiggled, the speckle-pattern distribution will change. This change in speckle pattern can lead to mode selective loss if optical components in the system have loss dependent on the exact cross-section modal structure. If a wide spectral width source excites a multimode fiber, the speckle pattern becomes less defined. This mode selective loss property of multimode fiber data communication systems encourages the use of lightwave sources with moderately broad spectral widths.

Divergence Angle. Light diverges from fibers in a cone-shaped radiation pattern. The steepness of the cone depends on the difference in refractive index between the core and the cladding and the diameter of the waveguide. In general, multimode fibers have a fairly steep divergence angle. Figure 1.9b shows the far-field power versus angle that is found in a 50/125 GI MM fiber.

Table 1.2 compares the characteristics of multimode fibers.

1.7.3 Singlemode Fiber

Singlemode fiber provides the lowest loss and lowest dispersion optical waveguide. Figure 1.10 illustrates a singlemode fiber. The diameter of the core in a standard singlemode fiber used in telecommunication applications is approximately 9 μm. The outer diameter

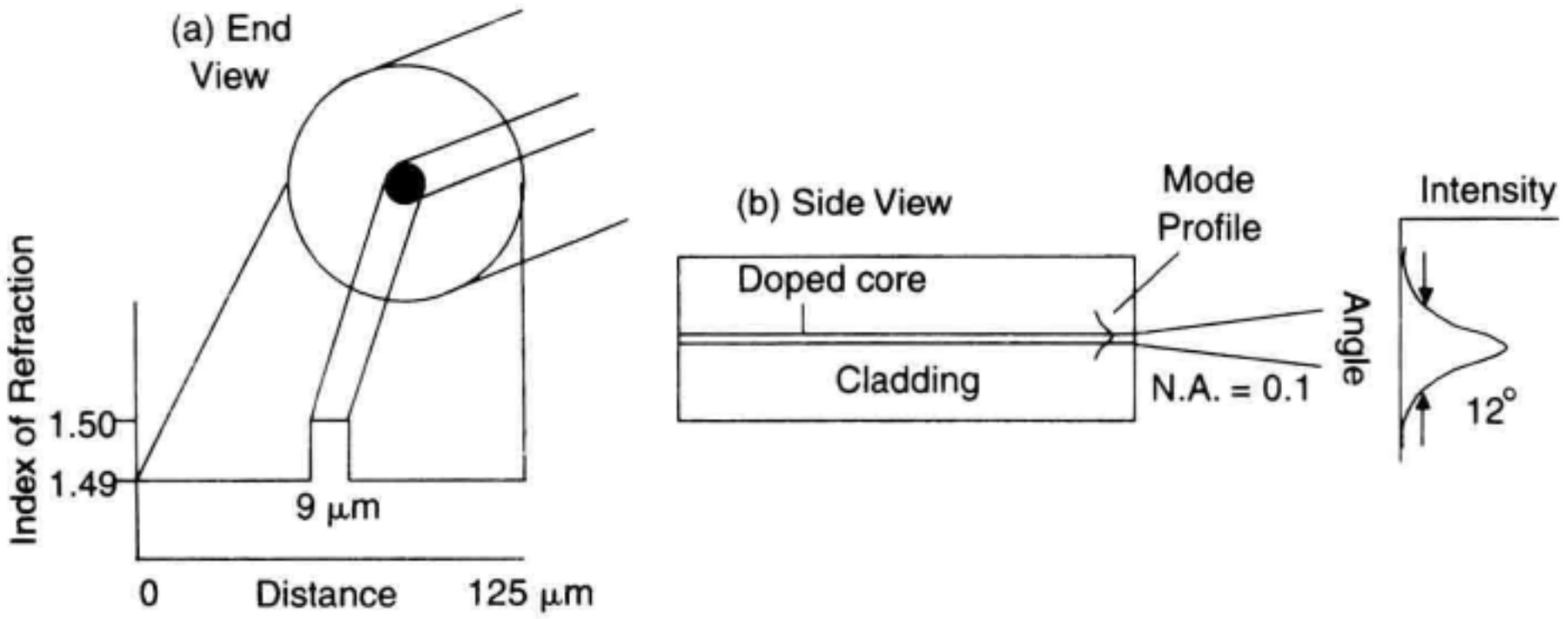

Figure 1.10 (a) End view of a singlemode fiber. (b) Side view of the fiber.

of singlemode fiber is 125 μm. This fiber would be referred to as 9/125 SI SM where SM refers to singlemode.

A singlemode fiber has a single lobed cross-section. This single lobe is associated with a single path that the light can take along the core of the fiber. When light exits the core, it begins to diverge with a cone-shaped radiation pattern. For singlemode fiber, the angle of the cone is about 12 degrees. The divergence angle is often quoted in terms of the numerical aperture (NA). The NA is defined to be the sin of half of the divergence angle. The NA of singlemode fiber is sin (12/2) = 0.1. Singlemode fiber can also be produced at shorter wavelengths (into the visible spectrum) by reducing the diameter of the core region and changing the doping profile. As an example, singlemode fiber for a red wavelength (632 nm) has a 3 μm core diameter.

Chromatic Dispersion. Since only a single path for light exists in singlemode fiber, the modal dispersion of multimode fiber is not present. Chromatic dispersion dominates in singlemode fibers. The glass fiber has a propagation velocity that is wavelength dependent. Standard singlemode fiber has its minimum total dispersion at 1310 nm. Dispersion is often quoted in terms of the dispersion parameter, D, which has units of ps/(nm km). Multiplying the dispersion parameter by the spectral width of the optical transmitter and by the link distance gives an indication of how much pulse broadening will occur. As an example, standard singlemode fiber has a dispersion parameter of 20 ps/(nm km) at 1550 nm. A high performance DFB laser has a spectral width of 0.2 nm when modulated. If the signal were propagated over a 50 km length, each bit would be spread by 200 ps. At the SONET standard rate of OC-48 (2.5 Gb/s), the bit period is 400 ps. The dispersion in this link example would result in a large degradation in link performance.

There are several types of singlemode optical fiber used for the telecommunications wavelengths between 1300 nm and 1550 nm. Five important fiber types are listed below. Table 1.3 lists some of the important characteristics of these singlemode fibers.

- **Standard singlemode fiber:** This fiber has its dispersion minimum at 1310 nm. This is the most common fiber in use today.
- **Dispersion-shifted singlemode fiber:** This fiber has its dispersion minimum shifted to 1550 nm. This allows fiber to have low loss and low dispersion at the

Table 1.3 Singlemode Fiber Parameters

	Attenuation		Chromatic Dispersion	
Fiber Type	***1310 nm***	***1550 nm***	***1310 nm***	***1550 nm***
9/125 Conventional	0.35	0.25	0	17
9/125 Dispersion shifted	0.35	0.25	−15	0
9/125 WDM optimized	0.35	0.25	−12	3

same wavelength. Much larger data rates and link lengths are available in this fiber. This fiber was deployed in the late-1980s and early-1990s.

- **WDM-optimized fiber:** This fiber offers low, but nonzero chromatic dispersion at 1550 nm. It is being used in newly installed systems that will use WDM communication techniques. The introduction of a finite amount of dispersion minimizes channel cross-talk due to nonlinearities in fibers. Nonlinearities in optical fibers are discussed in Appendix B. This fiber started deployment in the mid-1990s.
- **Polarization maintaining (PM) fiber:** This fiber is optimized so that the polarization of a signal does not change with distance. PM fiber is often used for short distance interconnections between optical components that have polarization dependencies. An example is a laser connected to an external modulator that is polarization dependent. Chapter 6 discusses measurements associated with polarization-maintaining fiber.
- **Erbium-doped singlemode fiber.** Erbium added to the core of singlemode fiber allows for the formation of an optical amplifier near 1550 nm. The erbium atoms must be excited with an optical pumping signal in order to provide amplification. Section 1.4.3 and Chapter 13 discuss EDFAs in more detail.

1.7.4 Optical Fiber Amplifiers and Two-Port Optical Components

EDFAs are such important optical components that they deserve special mention. A description of EDFAs will also illustrate some of the passive optical components used in fiber optic systems. Figure 1.11 shows a diagram of a typical EDFA and supporting optical components. A pump laser at either 980 nm or 1480 is coupled into the erbium-doped fiber through a WDM coupler. This coupler allows the pump to be coupled with minimum loss while at the same time providing a low-loss path for signals at the amplification wavelength. The 980 nm and 1480 nm wavelengths are chosen because erbium atoms absorb energy well at these wavelengths. If enough optical pump energy is absorbed, the erbium doping provides optical gain in the region between 1530 and 1570 nm. The gain in the amplifier is equal in either direction through the doped fiber. An isolator is used to suppress gain in one direction.

The pumping configuration of the amplifier determines many of the optical amplifier parameters. The optical pump is often inserted both at the input and the output. The highest output power is achieved with a pump at the output. The lowest noise amplifier

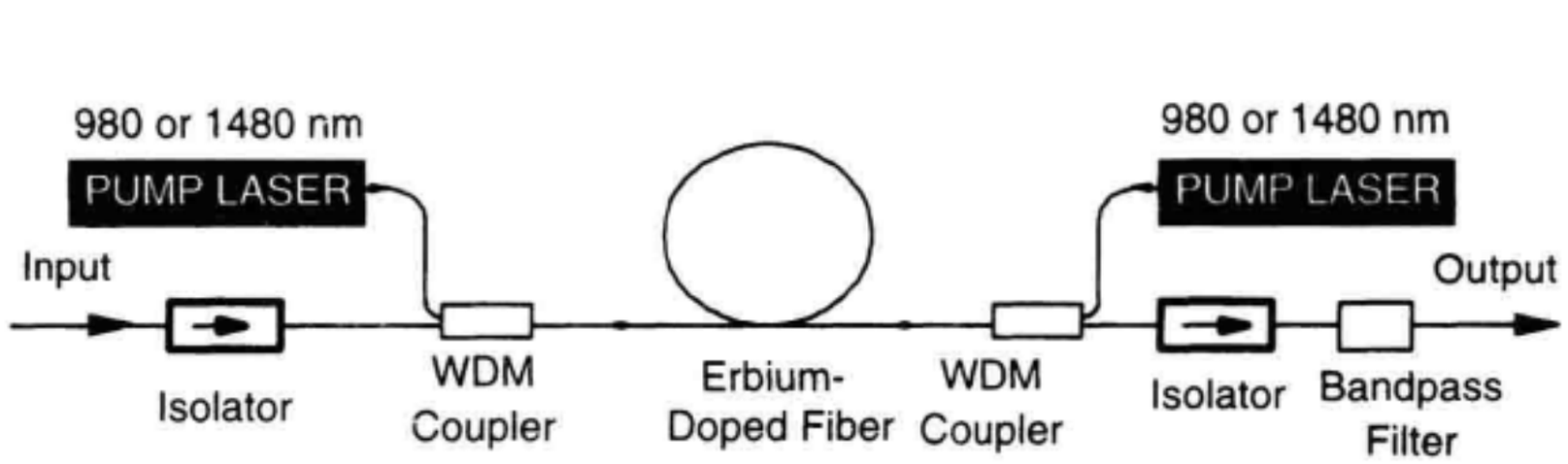

Figure 1.11 Erbium-doped fiber amplifier (EDFA) block diagram.

occurs with a pump at the input if low-loss components are used. 980 nm pumps provide the lowest noise-contribution amplifiers.

A high-gain EDFA produces a large amount of noise power at its output. Randomly generated light in the amplifier is boosted to high levels at the amplifier output. This noise is referred to as amplified spontaneous emission (ASE). The noise is produced over a broad range of wavelengths corresponding to the gain bandwidth of the amplifier. An optical bandpass filter is often used in conjunction with the amplifier so that the amount of amplified noise is reduced to a narrow window around the desired signal wavelength. The ASE from optical amplifiers can be a useful measurement tool as is described in Chapter 9.

The EDFA is used to allow longer fiber-optic link lengths without resorting to regeneration. The utility is actually more far-reaching. WDM technology is greatly aided by the addition of amplifiers. The optical amplifier can be used to compensate for losses in filters and other optical components. More complex amplifier configurations have two-gain stages with functional elements such as add-drop multiplexers placed between the stages. This allows high-loss optical components to be inserted into the system without an overall system performance degradation. Chapter 13 gives a good introduction to the basics of EDFAs and methods for their characterization.

1.8 MEASUREMENT OF OPTICAL FIBER AND TWO-PORT OPTICAL COMPONENTS

In 1.4, a description of two-port optical components was given. This section outlines the types of measurements performed on these components. Figures 1.12 to 1.16 illustrate measurement categories. This book will not discuss measurement of some of the physical properties of fiber such as pull-strength, fiber concentricity, or core parameters. For this coverage, refer to References 2, 18, and 19.

1.8.1 Insertion Loss

Figure 1.12a shows a typical measurement set-up and result for an insertion loss measurement. To make an insertion loss measurement, both a source and receiver are necessary.

For the source, either a wavelength tunable laser or a broadband source is used. The tunable laser provides a high power, narrow spectral width signal. Broadband sources produce a signal over a wider wavelength range than the tunable laser source but at a much lower power per unit wavelength.

The receiver is either an optical power meter or an optical spectrum analyzer (OSA). The power meter is a calibrated optical to electrical converter. It does not provide wavelength information. The OSA has a tunable bandpass filter ahead of the power meter. The OSA is capable of measuring power and wavelength.

One insertion loss measurement method uses a tunable laser as the source and an optical power meter (OPM) as the receiver. This method features large measurement range and fine wavelength resolution in most measurements. Tunable lasers have wave-

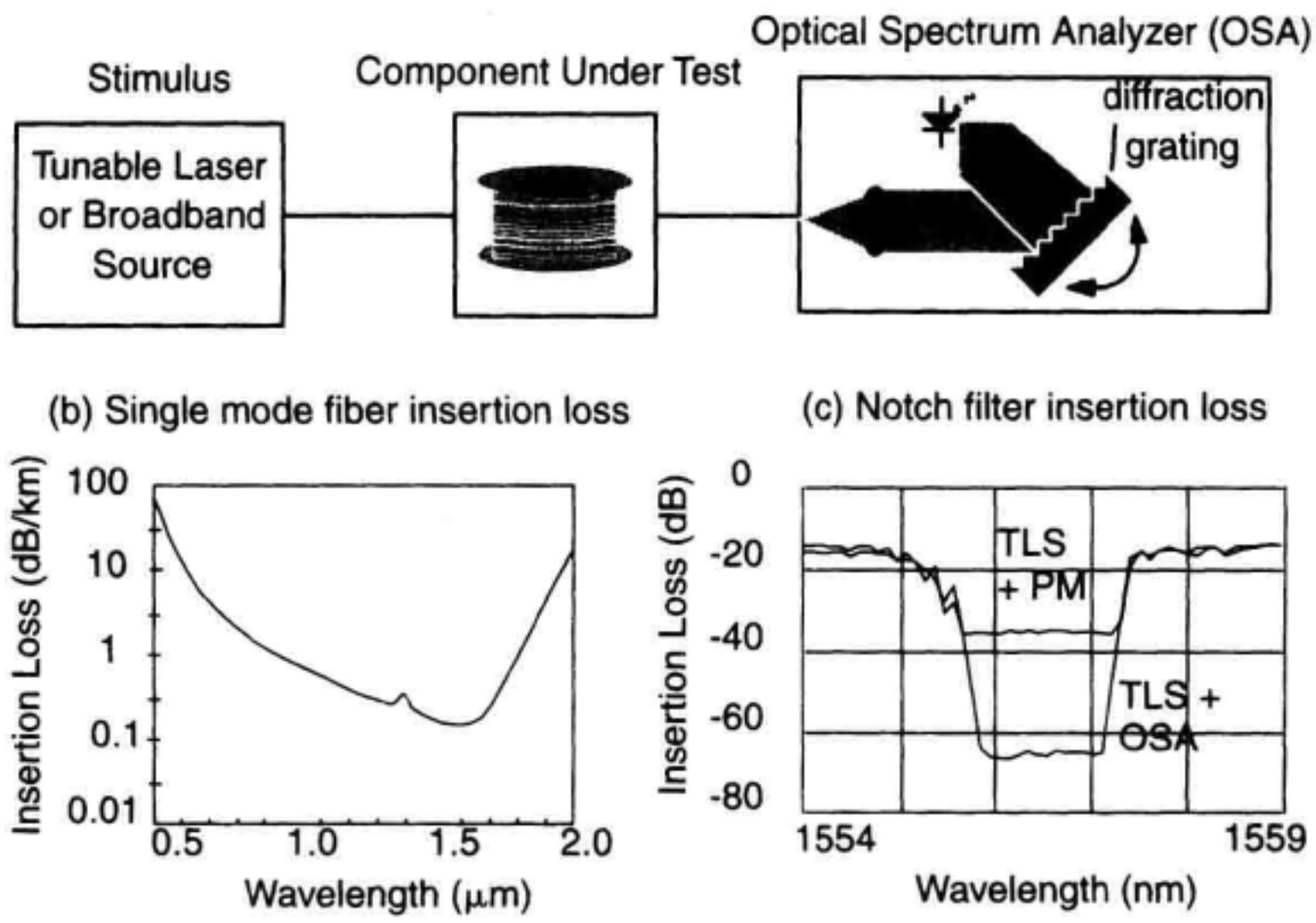

Figure 1.12 (a) Insertion loss measurement of two-port optical devices. (b) Measurement of singlemode fiber loss with a white light source and optical spectrum analyzer (OSA). (c) Measurement of a notch filter with tunable laser source (TLS) and a power meter (PM) or an OSA.

length tuning ranges of less than 200 nm. Detection of broadband noise from the tunable source is a major limitation of this measurement case.

Broadband emission sources can be used with an OSA to cover a broader wavelength range. Tungsten lamp emitters can cover the entire fiber-optic communication wavelength range in a single source. Optical amplifiers can provide broadband emission over narrower wavelength ranges, but with much higher power. The broadband source/OSA solution offers wide wavelength range coverage, moderate measurement range, and fast measurement speed. Figure 1.12b shows an example measurement of the loss of a singlemode fiber. A tungsten lamp source is used to cover this wide wavelength range. The tungsten lamp source has the disadvantage of having a very low power level per unit of optical bandwidth.

The highest performance solution is to use a tunable laser as the source and an OSA as the receiver. The use of a tunable laser provides the highest possible resolution due to the narrow spectral width of the source. The OSA provides additional filtering to reject some of the broadband noise emission that unintentionally emits from tunable lasers. Figure 1.12c shows the measurement of a notch filter with a tunable laser source and either a OPM or an OSA as a receiver. Measurements on deep-notch filters is one of the most difficult insertion loss measurements. Chapter 9 covers insertion loss measurement methods in detail.

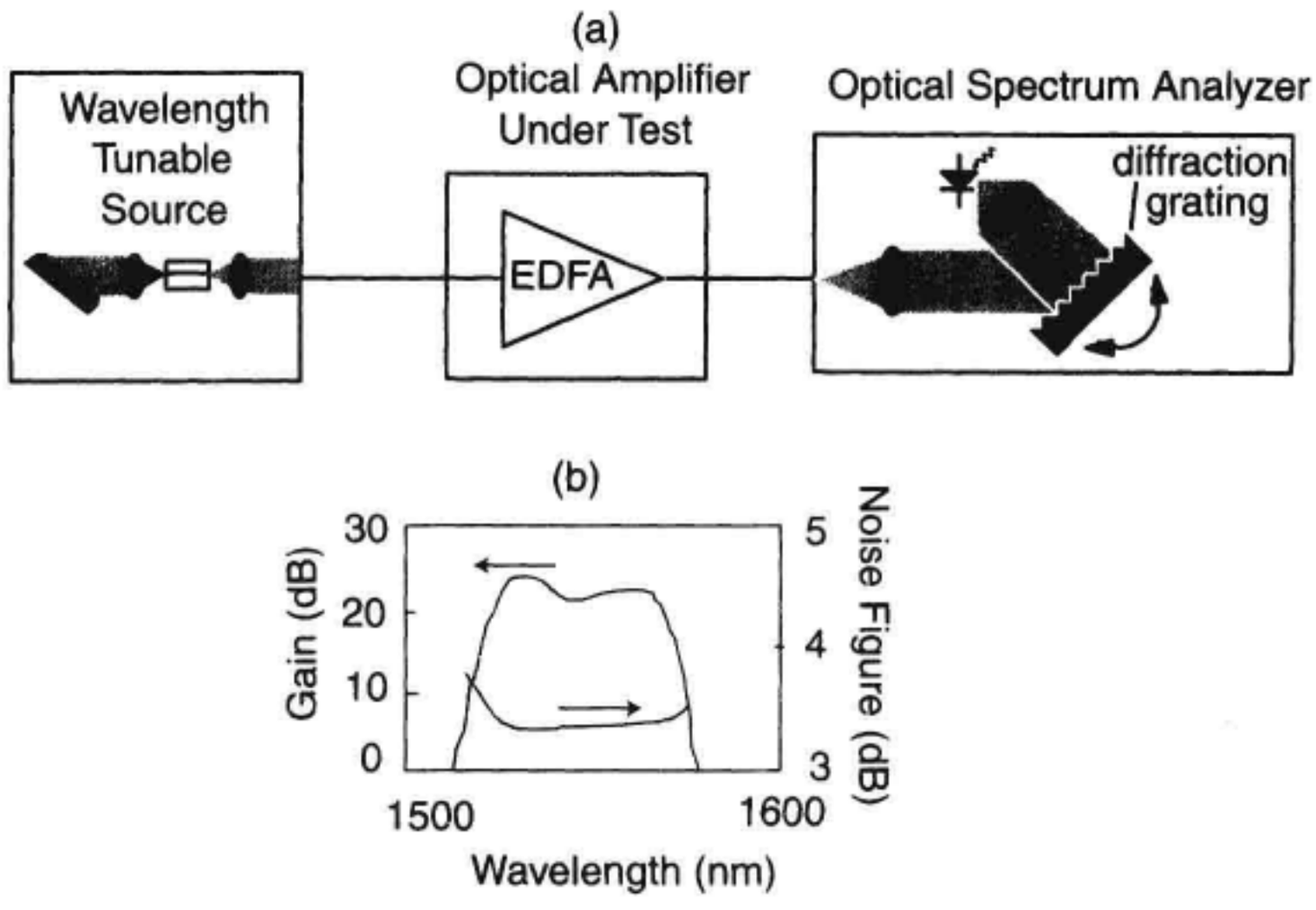

Figure 1.13 (a) Optical amplifier gain and noise figure measurements. (b) Gain and noise figure versus wavelength for an EDFA.

1.8.2 Amplifier Gain and Noise Figure Measurement

For active optical devices, both amplifier gain and amplifier noise contributions must be characterized. Figure 1.13 shows a test configuration used to measure gain and noise figure of optical amplifiers. Figure 1.13b shows a typical result from such a measurement.

Gain measurements are often done in large signal conditions when the amplifier is experiencing gain saturation. This requires the use of a high-power excitation source.

Characterization of the noise contribution can be done with optical domain or electrical domain measurements. Optical techniques measure the level of the ASE coming from the amplifier. Electrical techniques use a photodetector and an electrical spectrum analyzer to characterize the total amount of detected noise produced by the system. Care must be taken in the measurement of the amplifier noise. The noise generated by the optical amplifier must be distinguished from the amplified noise generated from the source at the input to the amplifier.

For WDM systems, the amplifier may need to be characterized using the same signal-loading conditions as will be seen in the actual application. Several new WDM amplifier characterization techniques have been demonstrated that reduce the number of sources necessary for amplifier characterization. Chapter 13 covers the characterization of optical amplifiers.

1.8.3 Chromatic Dispersion

Chromatic dispersion measurements characterize how the velocity of propagation in fiber or components changes with wavelength. This measurement of chromatic dispersion is accomplished by analyzing the group delay through the fiber as a function of wavelength

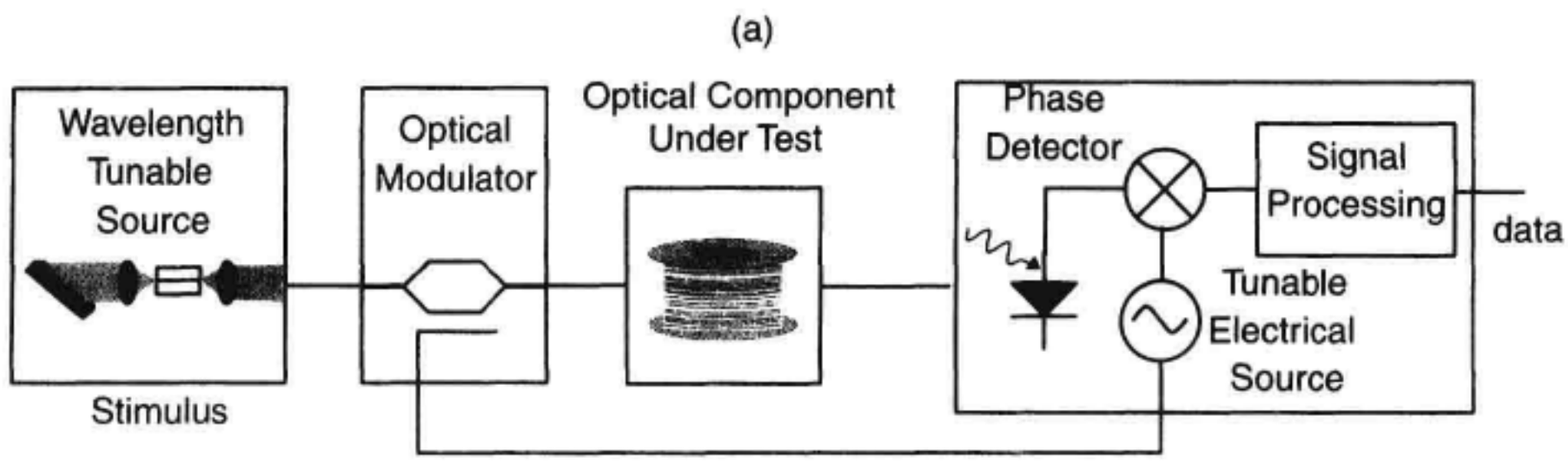

Figure 1.14 (a) Chromatic dispersion measurement of two-port optical devices. (b) Relative group delay versus wavelength. (c) Dispersion parameter versus wavelength.

as is shown in Figure 1.14a. A wavelength tunable optical source is intensity modulated as the stimulus for the device under test. The phase of the detected modulation signal is compared to that of the transmitted modulation. The wavelength of the tunable source is then incremented and the phase comparison is made again. By calculating how the phase delay changes with wavelength, the group delay of the fiber is measured. Figure 1.14b shows data for relative group delay versus wavelength for 1550 nm dispersion-shifted singlemode fiber. The group delay data is used to calculate the dispersion parameter results shown in Figure 1.14c.

The accurate characterization of the minimum fiber dispersion wavelength, λ_o, is important in the design of high-speed TDM and WDM communication systems. WDM systems do not operate well if there is extremely low dispersion. Fiber nonlinearities such as four-wave mixing cause the WDM channels to cross-couple leading to degradation in bit error performance. Undersea fiber installations use dispersion management techniques to reduce nonlinear effects and still achieve low average dispersion. A dispersion-managed fiber system has low dispersion on average with segments of positive and negative dispersion connected together.

High-speed TDM systems often suffer from chromatic dispersion limitations, especially at data rates of 10 Gb/s and above. Dispersion compensation components such as chirped Bragg grating filters and dispersion compensation fibers require accurate measurement of dispersion. Chapter 12 covers measurement of chromatic dispersion in detail.

1.8.4 Polarization-Related Measurements

The polarization state of a lightwave signal can have a significant effect on the performance of a lightwave system. Polarization of the lightwave signal refers to the orientation of the electric field in space. It is important to understand how the insertion loss and group delay of a two-port optical component vary as a function of the input signal polarization. The concept of polarization and how it affects lightwave systems is discussed in detail in Chapter 6.

The polarization state of the lightwave signal can vary significantly along the length of the fiber. A linearly polarized signal that is introduced into a fiber will evolve through elliptical and linearly polarized states as it propagates down the fiber. This is due to the fact that the velocity of propagation in a fiber can be dependent on the polarization of the input light source.

Figure 1.15 illustrates a measurement technique to characterize the polarization transfer function of optical fiber and optical fiber components. The key equipment piece is a polarization analyzer. The polarization analyzer is able to measure the polarization state that is incident on it. The polarization state of a signal can be represented by a Jones polarization-state vector. The Jones state vector contains two complex numbers that quantify the amplitude and phase of the vertical and horizontal components of the optical field. The goal of this measurement is to characterize the polarization-transforming properties of the optical fiber. The polarization transfer function is represented by the Jones transfer matrix illustrated in Figure 1.15. This two-by-two complex matrix will predict the output polarization state for any input polarization state. The Jones matrix is experimentally measured by applying three well-known polarization states at the input to the component under test and then characterizing the resulting output polarization state in the polarization analyzer. The Jones matrix can be used to find the worst-case

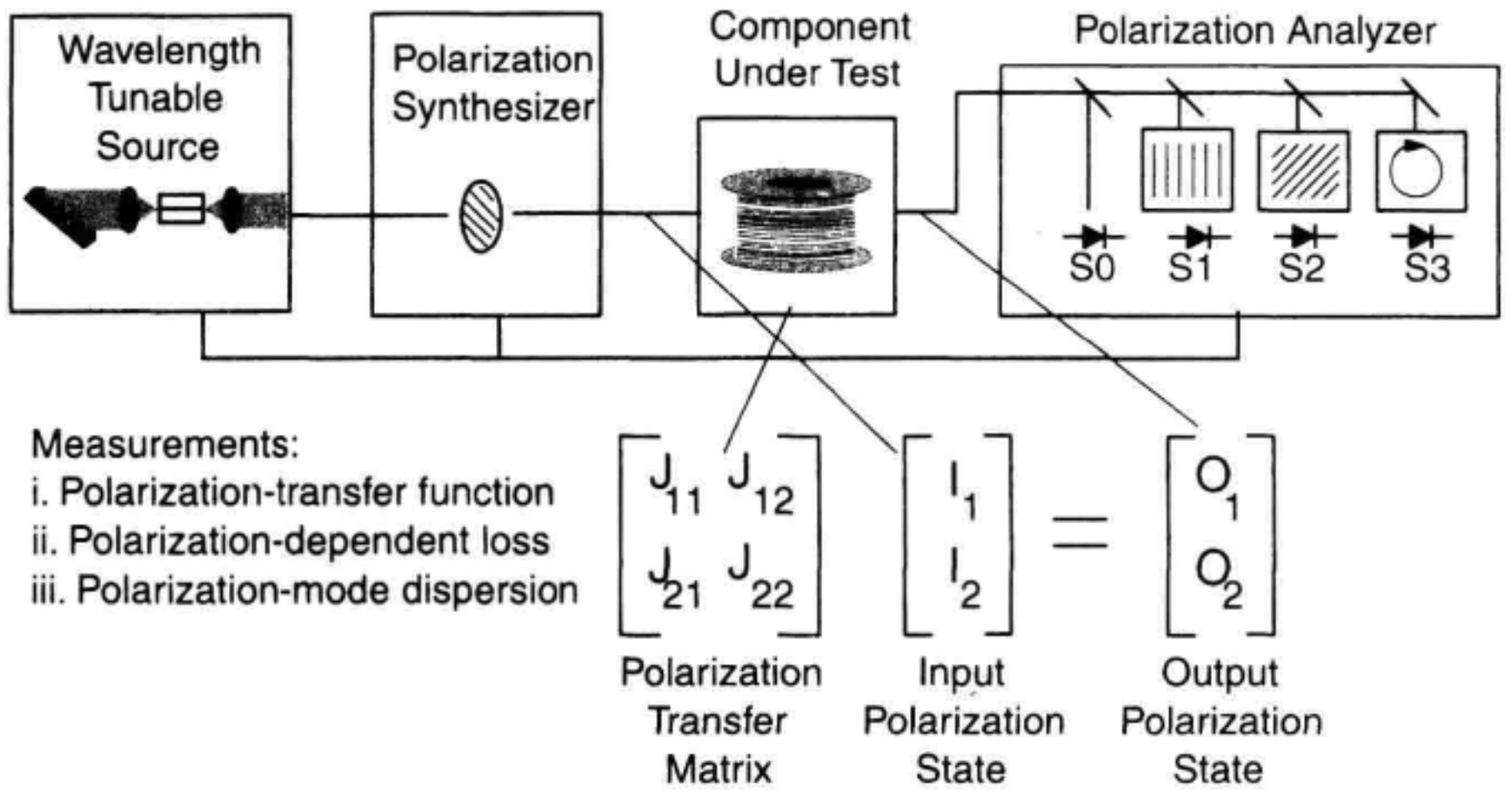

Figure 1.15 Polarization transfer function measurements.

polarization-dependent loss (PDL) and polarization-mode dispersion (PMD) of the device under test.

PMD is a term used to describe the fact that the group delay is polarization dependent. PMD, in addition to chromatic dispersion, can cause adjacent digital bits to interfere. PMD can limit the highest bit rate that is achievable in a fiber optic system. Chapter 12 covers characterization methods for PMD.

PDL is another polarization-related effect in two-port optical devices. PDL occurs when the loss through a device depends on the input state of polarization. Small flexures in an optical fiber can dramatically change the polarization transfer function of a fiber. A component with PDL will convert these polarization fluctuations into system loss changes. It is therefore desirable to reduce PDL in system components. There are several methods of PDL measurement covered in this book. One method shown in Chapter 6 uses the Jones polarization transfer function to predict the highest- and lowest-loss case. Chapter 9 discusses methods that use a variant of the measurement set-up of Figure 1.12. By adding a polarization synthesizer to the insertion-loss measurement, the lowest- and highest-loss polarization input states can be found experimentally.

1.8.5 Reflection Measurements

When fiber optic cables are deployed, it is important to monitor insertion-loss performance as well as to look for major faults such as a fiber breaks. Optical time-domain reflectometry (OTDR) is the primary tool for these applications. Figure 1.16 shows an OTDR measurement block diagram. OTDRs inject a pulsed signal onto the fiber optic cable. A small amount of the pulsed signal is continuously reflected back in the opposite direction by irregularities in the optical fiber structure. This reflected signal is referred to as Raleigh backscatter. The magnitude of the Raleigh backscattered signal is surprisingly large. A pulse that occupies 1 m of optical fiber will return a signal 73 dB lower than the incident signal. By measuring the amount of backscatter signal versus time, the loss versus distance of the fiber optic cable is measured. If a fiber optic break occurs, the backscatter will stop and the break location is detected. Chapter 11 describes OTDR measurements in detail. For traditional OTDRs, accuracy of several meters is sufficient for finding faults. In optical components, a much higher distance resolution is necessary.

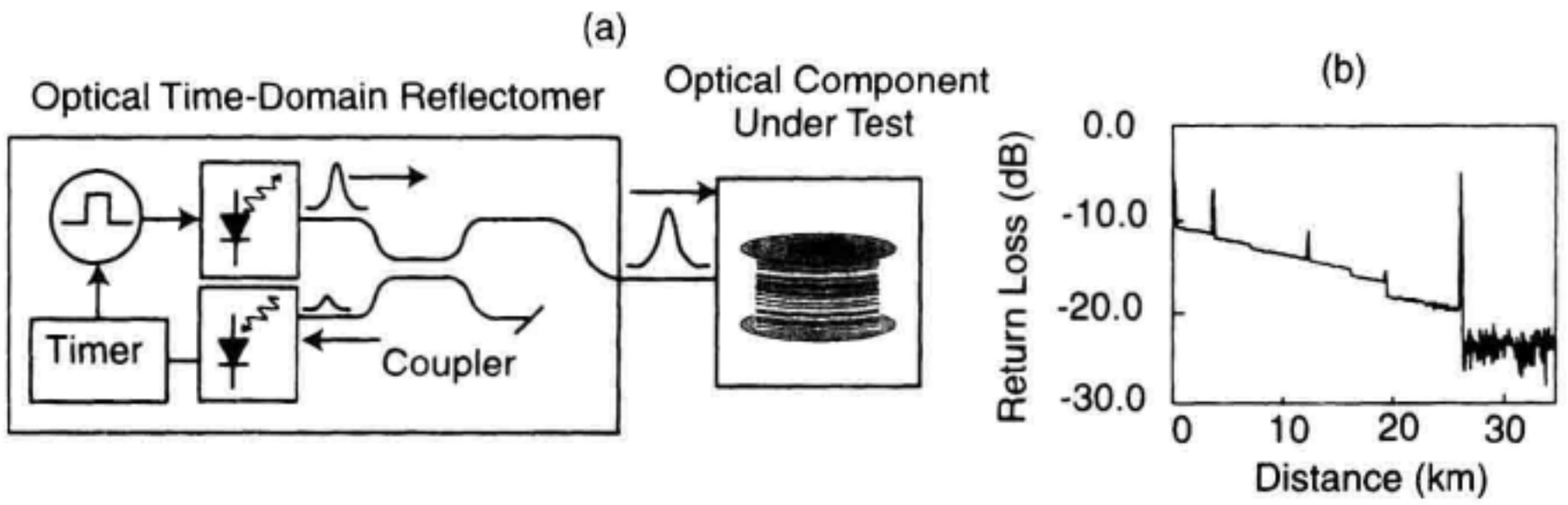

Figure 1.16 (a) Optical time-domain reflectometer (OTDR). (b) Example OTDR display.

Chapter 10 describes some of the techniques that are used for high resolution OTDRs. High resolution OTDRs are capable of detecting reflections with 10 μm resolution.

1.9 OPTICAL TRANSMITTERS

Optical sources are one of the most researched areas in fiber optic communications. The characteristics of the source often determine the maximum length of a fiber link and the data rate that is achievable. This section will describe the types of optical transmitters used in telecommunications and data communications applications. Section 1.12 will describe the measurements that are made on optical transmitters.

1.9.1 Fabry-Perot Lasers

The Fabry-Perot (FP) laser diode is the most widely used source for lightwave telecommunication systems. This popularity is due to the simplicity of fabrication and low cost. FP lasers perform best when used with low chromatic-dispersion fibers due to their substantial spectral width.

Figure 1.17a illustrates a sectional view of an FP laser parallel to the direction of light emission. The laser has two parts: a semiconductor optical amplifier to provide gain and mirrors to form a resonator around the amplifier. The semiconductor optical amplifier is formed by applying current to a lower-bandgap active layer surrounded by higher-bandgap materials. The surrounding higher-bandgap materials confine electrons and holes into a small volume. The applied current excites electrons from the low energy valence band state to the higher energy conduction band state. As the high-energy electrons lose

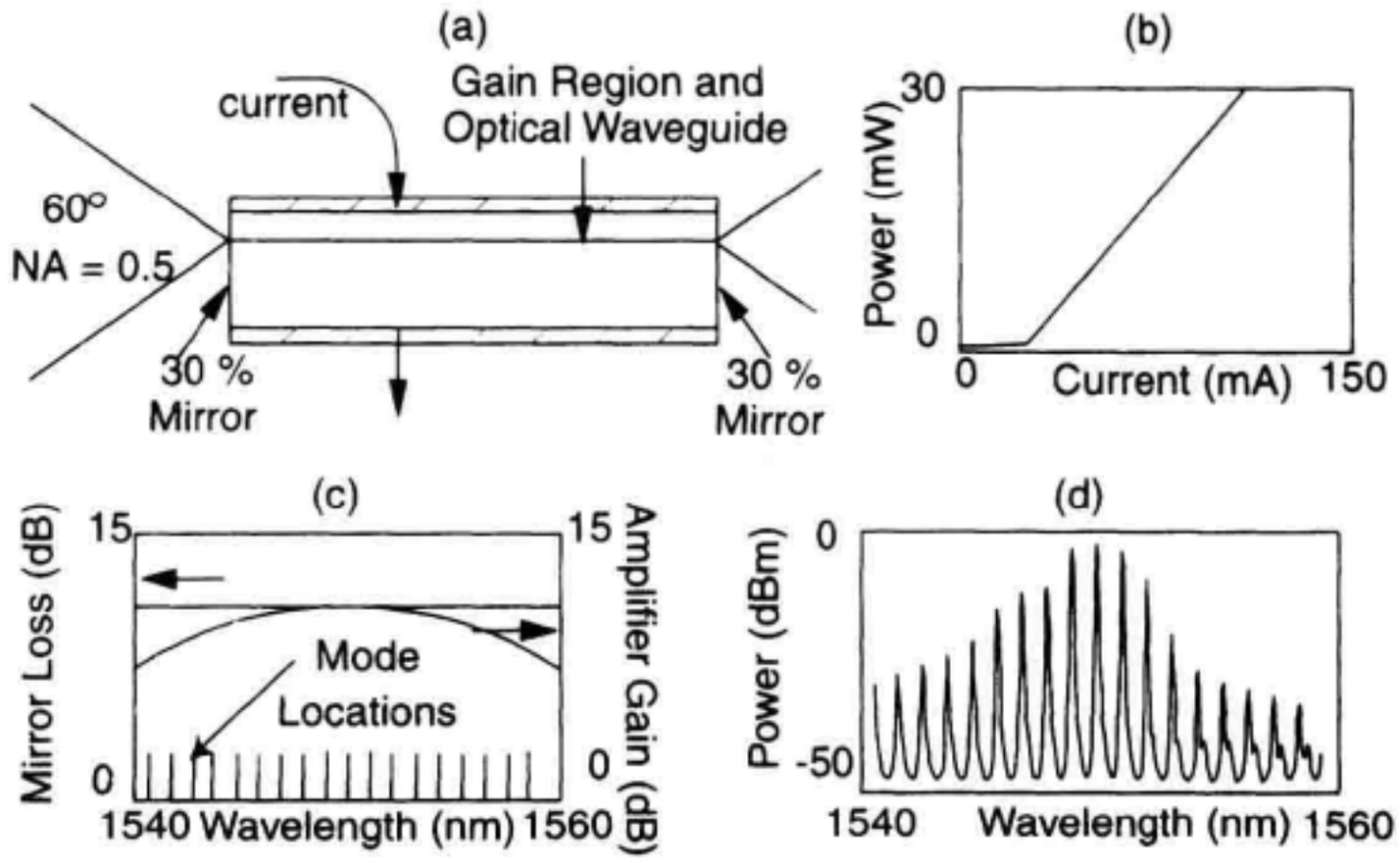

Figure 1.17 (a) Cross-section of a Fabry-Perot (FP) laser diode. (b) Light versus current characteristic. (c) Amplifier gain, mirror loss, and longitudinal mode location. (d) Power versus wavelength for the FP laser.

energy, they give off light. The low-bandgap and high-bandgap layers form an optical waveguide to direct the light that is produced. The active region composition is designed to emit at the desired wavelength. For lasers emitting in the 1100 to 1700 nm region, compounds of In, Ga, As, and P are grown on top of InP substrates. For the 780 to 980 nm range, compounds of In, Al, Ga, and As are grown on top of GaAs substrates. The semiconductor crystal is cleaved to form a mirror. The air-to-semiconductor interface at the cleavage plane provides 30% reflectivity and 70% transmission. Light emits from the laser with a steep-angle cone-shaped radiation pattern.

Figure 1.17b shows the optical output power versus current that is measured from an FP laser. As the current increases, the optical amplifier gain increases. When the amplifier gain equals the mirror loss, the lasing threshold is reached. The laser breaks into oscillation above threshold current. The slope of the power versus current curve above threshold indicates how efficient the laser converts injected electrons into emitted photons. FP lasers are capable of producing many mW of output power. FP lasers for EDFA-pump applications are designed to produce 100 mW into a singlemode fiber. FP lasers can be modulated to very high rates by varying the current to the laser diode.

Fig. 1.17c plots some of the FP-laser parameters that define its operation. The gain versus wavelength, the mirror reflectivity versus wavelength, and the location in wavelength of the longitudinal modes of the laser are shown when pumped above threshold. The optical amplifier needs a net gain of 11 ($11 = 1/0.3 \times 1/0.3$) at threshold to overcome the loss in the two 30% reflectivity mirrors. The distance between the two mirrors determines the spacing between the possible lasing wavelengths as is illustrated by the tick marks in Figure 1.17c. These wavelengths are called the longitudinal modes of the laser. The longitudinal mode spacing (in Hz) is the velocity divided by twice the length of the cavity. A typical FP laser is 300 μm long, has an index of refraction of 3.3, and therefore has a longitudinal mode spacing of 150 GHz. A 150 GHz spacing in frequency corresponds to a 1.25 nm spacing in wavelength at 1550 nm. The mirror reflectivity is independent of wavelength in an FP-laser design. The gain versus wavelength function of the optical amplifier determines the spectral shape of the laser.

Figure 1.17d shows the power versus wavelength that occurs in a typical FP laser. FP lasers operate with significant power in many longitudinal modes. The power distribution between these longitudinal modes is constantly shifting, resulting in extra low frequency intensity variations called mode-partition noise. The relatively wide spectral width of FP lasers limits their usefulness for long-distance communication.

1.9.2 Distributed Feedback Lasers (DFBs)

The DFB laser was designed to overcome the spectral shortcomings of the FP laser.[20] Figure 1.18a shows the structure of a DFB laser. It is very similar to an FP laser with the addition of a Bragg reflector structure located near the light-emitting active region. The Bragg reflector grating provides a periodic change in the index of refraction in the waveguide. Each period of the grating reflects a small amount of light back in the opposite direction. The Bragg grating forms an efficient mirror at the wavelength where the grating period is one-half of the wavelength of light in the semiconductor material. At 1550 nm,

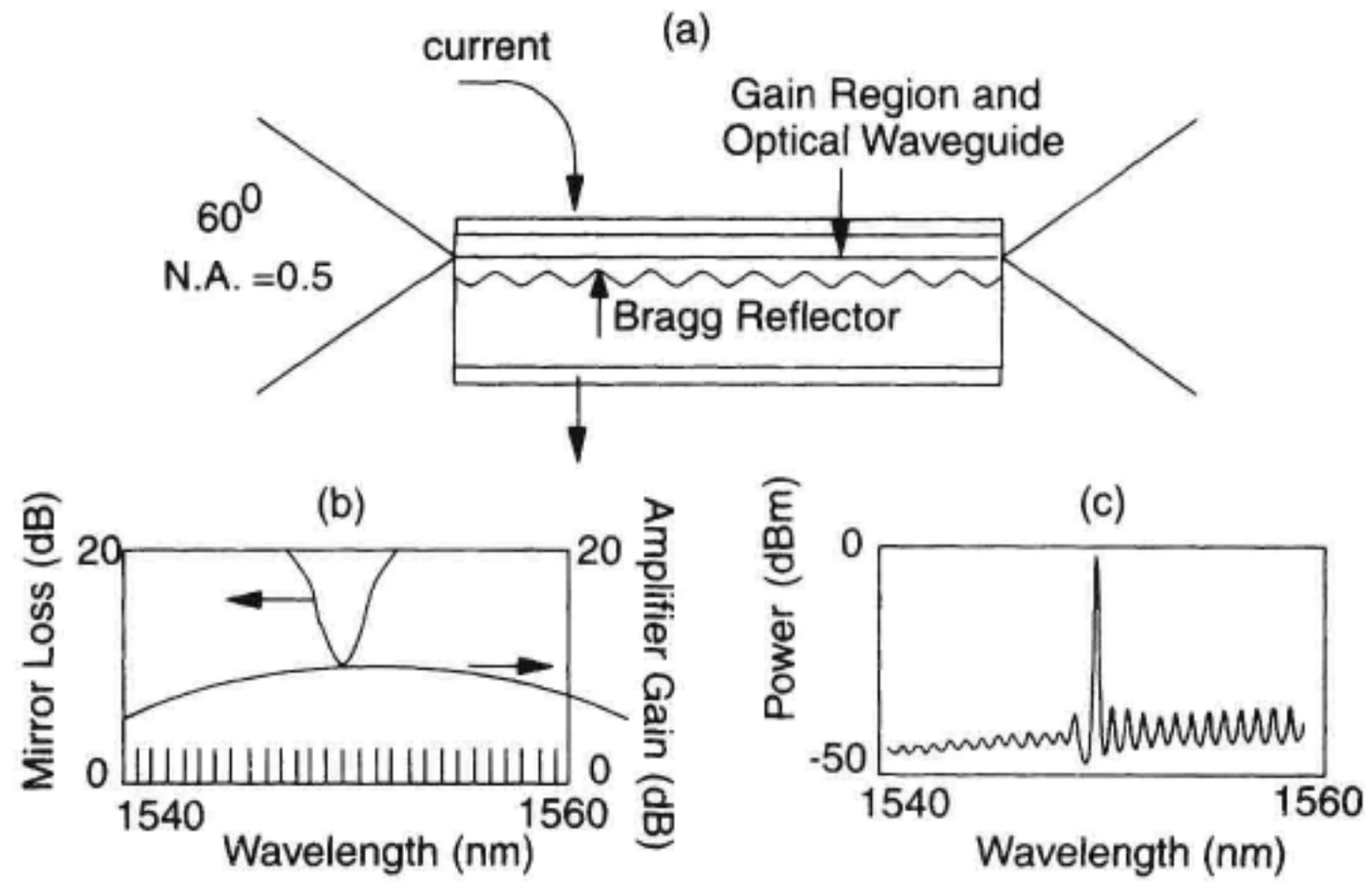

Figure 1.18 (a) Cross-section of a distributed feedback (DFB) laser. (b) Bragg grating reflectivity, amplifier gain, and longitudinal mode location. (c) Power versus wavelength for the DFB laser.

the Bragg grating period is 116 nm. The small dimensions of the grating make the device fabrication technology more critical than an FP laser. Extra wafer processing steps are necessary to etch the Bragg grating into the semiconductor material and to grow new material on top. This results in a more expensive laser diode.

The effect of the Bragg grating on the mirror reflectivity shape is shown in Figure 1.18b. The Bragg grating reflection passband is only a few nanometers wide. As the current is increased in this laser, only a narrow wavelength range can reach the threshold condition. This frequency-dependent mirror reflectivity forces all of the laser power to emit in a single longitudinal mode. Figure 1.18c shows the single longitudinal mode spectral shape of a DFB laser. DFB lasers are the industry standard for use in long-distance fiber-optic links.

1.9.3 Vertical Cavity Surface-Emitting Laser (VCSEL)

The vertical cavity surface-emitting laser (VCSEL) was originally developed as a low-cost alternative to FP and DFB lasers.[21] The first commercial application of these lasers is in the area of high-speed data communication links replacing LEDs. Vertical cavity lasers emit perpendicular to the top plane of a semiconductor wafer. The VCSEL uses a multilayer dielectric mirror that is grown directly on the semiconductor surface as shown in Figure 1.19a. This mirror consists of alternations of high and low index of refraction layers to form a Bragg reflector. The distinguishing feature of this structure is its extremely short optical amplifier length (on the order of 100 nm). This length is compared to the 300 μm length typical of an FP or DFB laser. This short amplifier length limits the available gain from the amplifier to a very small value. Figure 1.19b shows the gain, mirror reflectivity, and mode locations of the VCSEL design. The mirror reflectivity is very high so

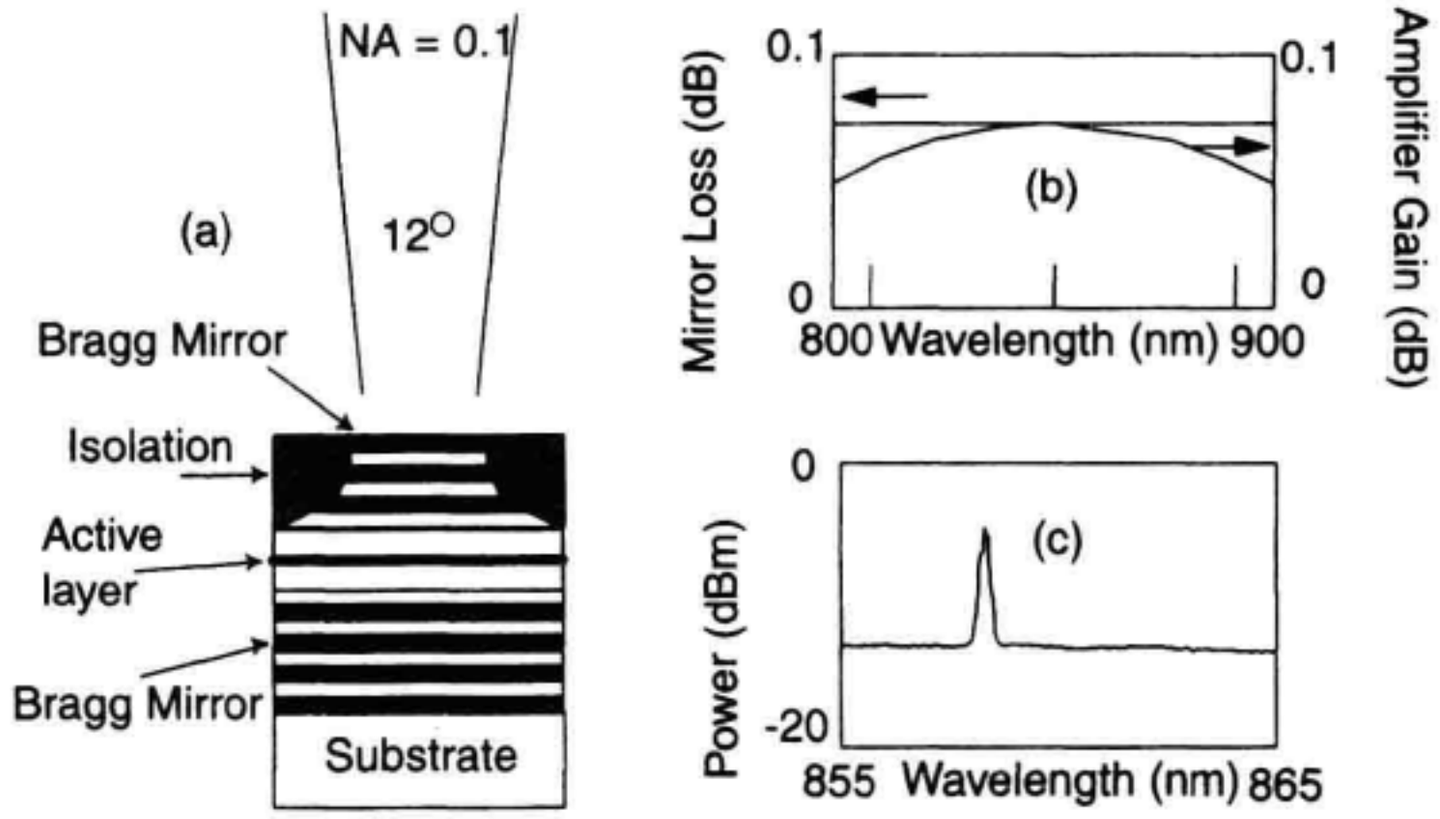

Figure 1.19 (a) Cross-sectional view of a vertical cavity surface emitting laser (VCSEL). (b) Mirror reflectivity, amplifier gain, and longitudinal mode location. (c) Optical spectrum of a VCSEL.

that the low-gain optical amplifier can achieve threshold. Only a single longitudinal mode is available for lasing because of the small distance between mirrors. For a 1 μm cavity length, the longitudinal mode spacing would be 45 THz. As can be seen in Figure 1.19c, there is no sign of closely spaced longitudinal modes as is seen in the DFB laser of Figure 1.18c.

In data communication applications, the diameter of the laser is chosen to be large enough to support multiple modes in the plane perpendicular to the lasing direction. This causes the central lasing peak to spectrally broaden. The wider spectral width is often designed into VCSELs to avoid mode-selective loss in multimode fiber applications. The major advantage of the VCSEL design is the ease of fabrication, simplified on-wafer testing, and simple packaging resulting in lowered costs. The VCSEL has higher output power and higher modulation rates than surface-emitting LEDs for data communications. To date, this type of laser is commercially available in the 780 to 980 nm wavelength range. The 1300 nm and 1550 nm versions are still in the laboratory stage.

Sources with External Modulators: Narrow Spectral Width Under Modulation. It is important to have a narrow spectral width source while modulation is applied to a laser. Wide spectral width sources in conjunction with chromatic dispersion leads to intersymbol interference in optical fibers. Although DFB lasers have a single lasing wavelength, they are not a perfect source for fiber optic systems. If a high-speed current modulation is applied to a DFB laser, the laser's center wavelength is pulled up and down in wavelength during the modulation. This laser wavelength pulling is referred to as chirp. Chirp causes substantial broadening of the modulated laser linewidth. Chapter 5 covers measurement techniques for modulated laser linewidth.

The solution to reducing chirp and modulated spectral width to small values is to separate the functions of lasing and of modulation. This is accomplished with DFB lasers

followed by external modulators. The next two sections describe two important types of external modulator lasers.

1.9.4 DFB With Electrooptic Modulator

Figure 1.20a shows a Mach-Zehnder (MZ) modulator[22] that follows a DFB laser. The MZ modulator consists of an integrated optical waveguide on a material that can exhibit the electrooptic effect. Electrooptic materials have an index of refraction that can be changed with the application of voltage.

MZ modulators operate using interferometry techniques. The optical signal is branched into two separate paths and is then recombined at the output. The two paths of the interferometer are nearly, but not exactly, the same length. When light from the two paths is combined at the output, the two signals will have slightly different phases. If the two signals are exactly in phase, the light will combine in the output waveguide with low loss. If the two combining signals are 180 degrees out of phase, the light will not propagate in the output waveguide resulting in light radiation from the waveguide to the surrounding substrate. The electrooptic effect makes the velocity of propagation in each arm of the interferometer dependent on a voltage applied to an electrode. Figure 1.20b shows the transmission versus voltage for a MZ interferometer. Depending on the modulation voltage, the light will propagate with high or low loss at the output combining waveguide. The modulator is normally biased in the half-on, half-off state which is called quadrature.

Well designed MZ modulators do not contribute to spectral broadening of the DFB laser signal. An important design consideration for MZ modulators is the V_π of the modulator as shown in Figure 1.20b. It is desirable to keep V_π as low as possible to reduce the modulator drive requirements. MZ modulators have demonstrated modulation bandwidths above 50 GHz. Both $LiNbO_3$ and GaAs material systems have been used for modulator fabrication. The main disadvantage of external modulators is cost and ease of use. MZ modulators must have a specific input polarization state to function properly. The polar-

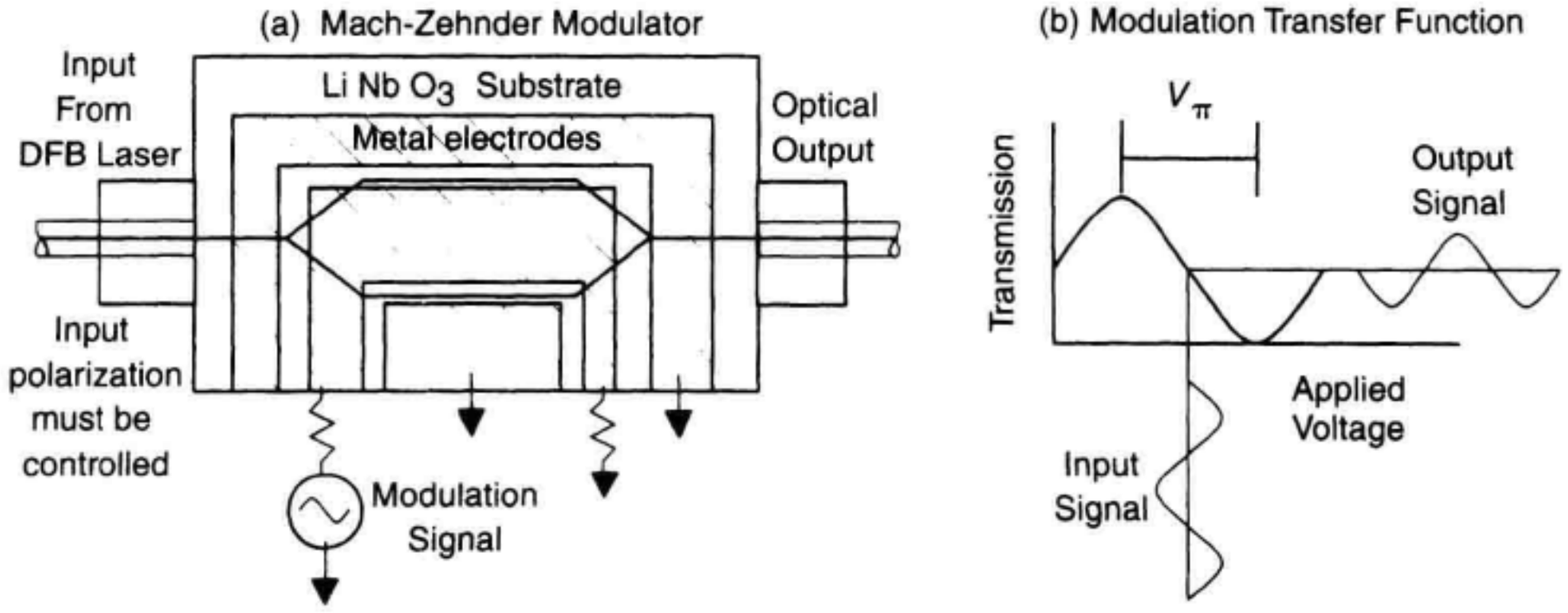

Figure 1.20 (a) Mach-Zehnder (MZ) interferometer modulator. (b) Modulation transfer function for a Mach-Zehnder interferometer.

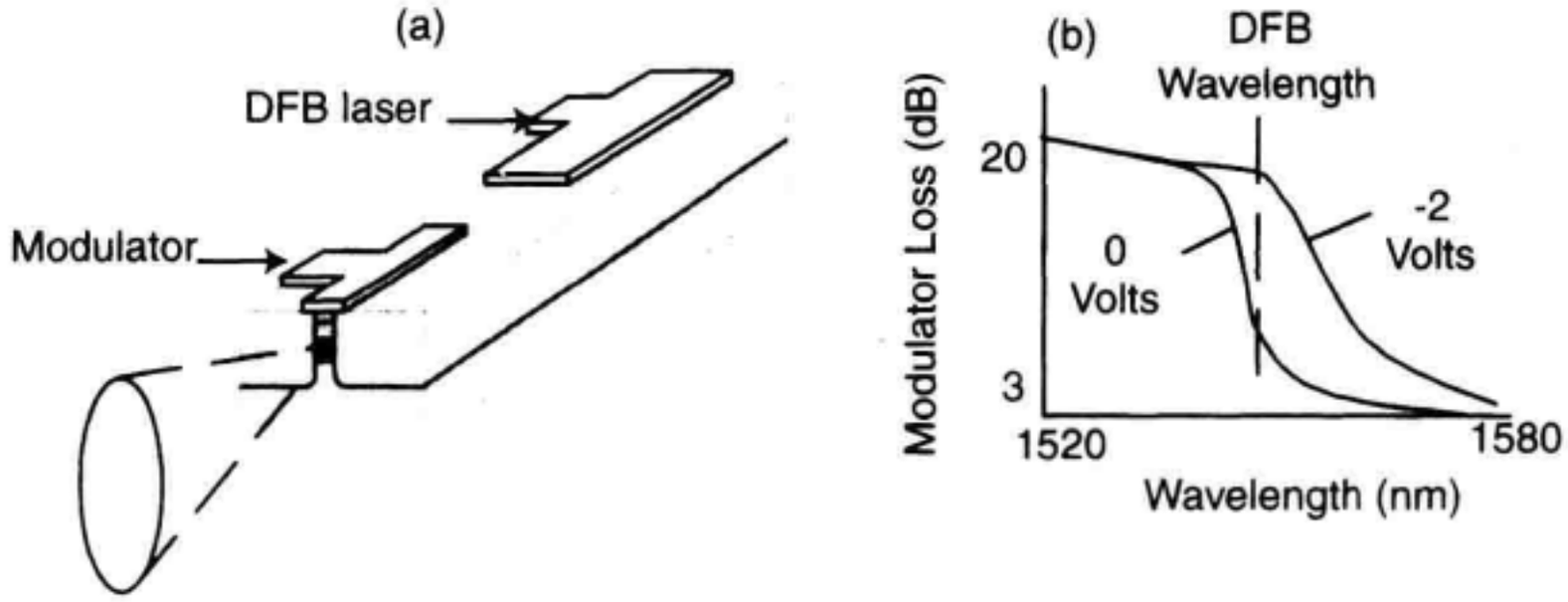

Figure 1.21 (a) DFB laser followed by an integrated electroabsorption external modulator. (b) Transmission characteristics of the electroabsorption modulator as a function of reverse-bias voltage.

ization state must be controlled between the DFB and the modulator. DFB lasers with MZ modulators are the highest performance solution for long link lengths. MZ modulators are also used in high-performance analog communication links.

1.9.5 DFB With Integrated Electroabsorption Modulator

A DFB laser with an integrated electroabsorption modulator (DFB/EA) is shown in Figure 1.21a. The electroabsorption principle of operation is illustrated in Figure 1.21b. This modulator uses the effect that the band gap of a semiconductor can be adjusted in wavelength as a function of reverse-bias voltage. The DFB's lasing wavelength is placed at the absorption edge. The modulator's absorption edge is adjusted to a high-loss or low-loss condition depending on the modulation voltage. The electroabsorption modulator causes a slight broadening of the input DFB spectral width but is adequate for most long-distance applications. The slight broadening is due to the fact that the loss and the delay in the modulator are coupled. The major advantage of electroabsorption modulators is that they are integrated on the same chip as the DFB laser. This allows the cost of external modulation to approach the cost of a DFB laser alone. Clever fabrication techniques using selective area epitaxy have simplified the fabrication of two separate active-region compositions on to the same substrate. This type of laser has the potential to become the dominant solution for long-distance digital links due to its lower cost.

1.10 LEDS

LED sources are important for short-distance fiber-optic links in data and telecommunication applications typically using multimode fiber. LED sources are low cost and have adequate performance for many applications. The two most common wavelengths for multimode data communication systems are 850 nm and 1300 nm.

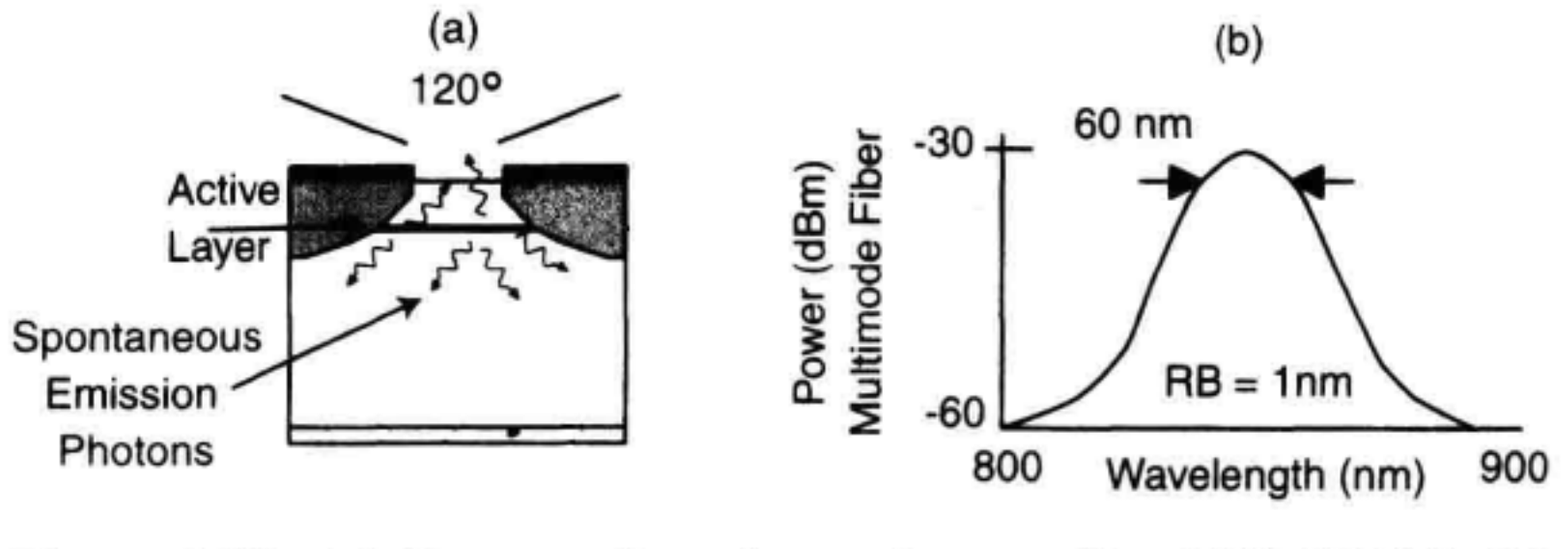

Figure 1.22 (a) Cross-section of a surface-emitting LED (SLED). (b) Power versus wavelength for the SLED as coupled into a 50/125 graded-index multimode fiber. The optical spectrum analyzer bandwidth is 1 nm.

1.10.1 Surface-Emitting LEDs

The most common multimode source is the surface-emitting LED (SLED) shown in Figure 1.22a. The SLED has low-bandgap semiconductor materials sandwiched between high-bandgap materials as is found in semiconductor lasers. The major difference in an LED is that there are no mirrors to provide feedback. Current is passed through the active region to create hole and electron pairs in the low-bandgap active region. The electrons from the conduction band lose energy spontaneously and emit photons in all directions. A fraction of the generated light is coupled into the multimode fiber. Figure 1.22b shows the spectral characteristics of the SLED as coupled into a 50/125 GI multimode fiber. The spectral width is over 60 nm. Compare this with the 0.1 nm spectral width of a DFB laser. The wide SLED spectral width limits its usefulness for very long link lengths. The broad spectral content of an SLED is an advantage in reducing speckle-related mode-selective loss in multimode fiber systems. The advantage of the SLED is its reliability and low cost. The power from surface emitting SLEDs is usually much less than 1 mW coupled into a multimode fiber. The bandwidth of surface emitting LEDs is limited by the carrier lifetime in the active region. Data rates up to 622 Mb/s have been achieved with these devices.[2.23]

1.10.2 Edge-Emitting LED

Figure 1.23a shows a diagram of an edge-emitting LED (EELED). The EELED is very similar to an FP laser without mirrors. This EELED configuration shows two segments. One segment is forward biased to produce gain in a semiconductor optical amplifier. The other segment is reverse biased to produce an optical absorber. The absorber prevents the optical amplifier from becoming an FP laser. The output of the semiconductor optical amplifier is also antireflection-coated to further prevent a mirror from forming. The EELED optical amplifier produces ASE. Spontaneously emitted light at the input of the amplifier produces ASE at the amplifier output. The spectral shape of the EELED is shown in Figure 1.23b when coupled into singlemode fiber. The spectral width of the EELED is 60 nm in this example centered at 1550 nm. The spectral shape of the EELED is similar to the

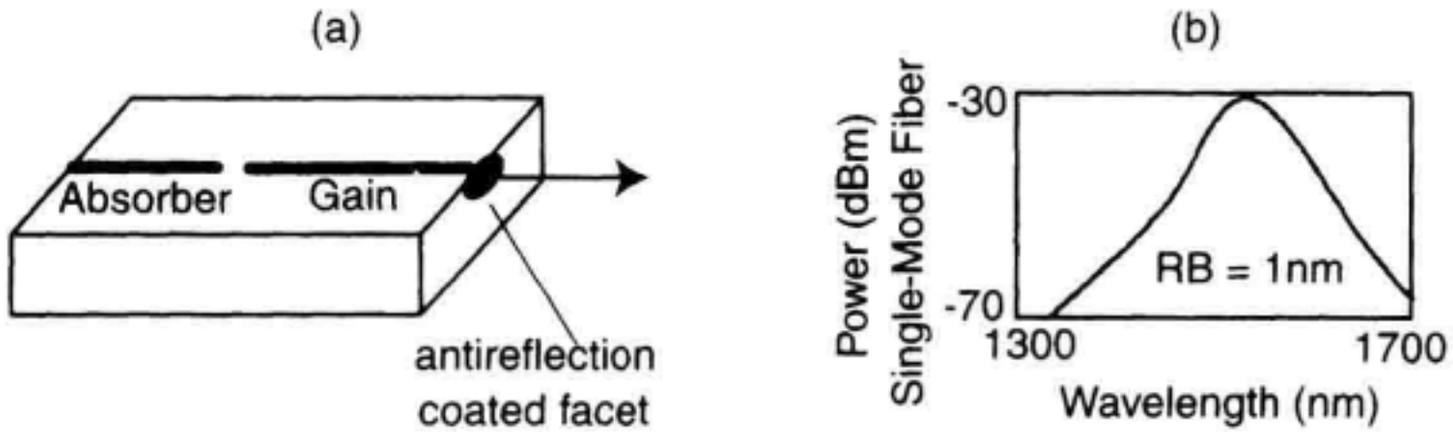

Figure 1.23 (a) Side-view of an edge-emitting LED (EELED). (b) Power versus wavelength for the EELED as coupled into a 9/125 μm singlemode fiber. The OSA bandwidth is 1 nm.

gain versus wavelength function of the optical amplifier. EELEDs are capable of producing several mW of power. EELEDs are limited in their modulation speed by carrier lifetime in the active region to a few hundred MHz. Chapter 9 describes the use of EELEDs in detail along with measurement applications.

1.10.3 Comparison of Optical Sources

Table 1.4 shows a comparison of the characteristics of the lightwave sources that were introduced in this section. The large range of source characteristics reflect the diversity of applications for fiber optic links.

1.11 OPTICAL RECEIVERS

The optical receiver detects the lightwave signal and then conditions the resulting electrical signal to the appropriate levels with receiving electronics. Figure 1.1 showed a diagram of a digital optical receiver. Photodetectors are used for optical to electrical conversion. A variable gain amplifier or limiting amplifier is used to get a specified signal level to a decision circuit. The clock must also be extracted from the incoming signal. The simplest clock extraction circuit is a bandpass filter and a frequency doubling circuit. More advanced phase-locked loop circuits are often used for clock extraction. The clock signal is then used to trigger a sampling circuit that decides the digital value of the incoming data. A good coverage of optical receiver design is given in Miller and Kaminov.[2] Sections 1.11.1 and 1.11.2 describe the operation of p-i-n and avalanche photodetectors in more detail.

1.11.1 p-i-n Photodetectors

Figure 1.24a shows a diagram of a p-i-n photodetector. The p-i-n designations refer to the doping of the top three layers of the detector structure. The i, or intrinsic layer, is chosen to be a low-bandgap material that absorbs incoming photons. The bandgap of this layer determines the longest wavelength light that can be absorbed. The p-i-n doping structure

Table 1.4 Comparison of Lightwave Sources

Source Type	Application	Associated Fiber Type	Data Rate	CW Spectral Width	Modulated Linewidth, Chirp	Power into Fiber mW
Fabry-Perot laser	datacom, telecom	singlemode/ multimode	to 10 Gb/s	5 nm multiple line	medium	2–100 S.M.
DFB laser	telecom, analog	singlemode	to 10 Gb/s	10 MHz single line	good	2–20 S.M.
DFB with electro-absorbtion	telecom	singlemode	to 10 Gb/s	10 MHz single line	excellent	0.2 S.M.
DFB with Mach-Zehnder	telecom, analog	singlemode	> 10 Gb/s	10 MHz single line	highest performance	0.2 S.M.
Vertical cavity laser	datacom	multimode	to 5 Gb/s	1 GHz for multiple mode	medium for multiple mode	0.1 M.M.
Surface-emitting LED	datacom	multimode	622 Mb/s	10 THz broadband	broadband source	0.1 M.M.
Edge-emitting LED	datacom	singlemode/ multimode	155 Mb/s	5 THz broadband	broadband source	0.1 S.M.

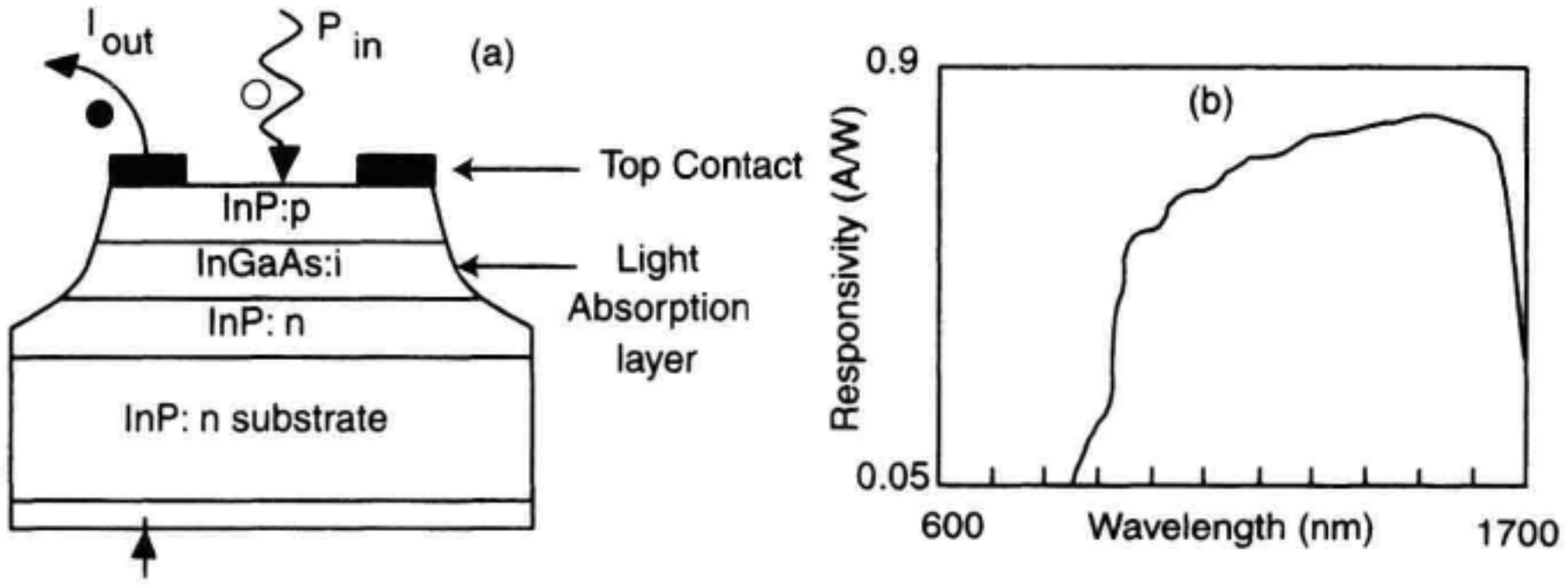

Figure 1.24 (a) p-i-n photodetector diagram. (b) Responsivity versus wavelength for a InGaAs/InP detector.

causes a very high electric field to be developed across the intrinsic layer. Once a photon is absorbed, a hole and electron are created in the layer. The electric field sweeps these two charged particles out to be collected in an external electrical circuit. Thus a p-i-n detector is a photon to electron converter. The amount of current produced per unit of input power is called the detector responsivity.

A common material for the p-i-n photodetector is an InGaAs undoped layer surrounded by doped p and n InP material. An example of absorption versus wavelength function for an InGaAs/InP p-i-n detector is shown in Figure 1.24b. Well designed p-i-n detectors can convert over 90% of the incoming photons to electrons. These detectors are capable of responding to signals that are modulated to very high rates. The capacitance and the transit time to sweep out electrons and holes determine the ultimate bandwidth capability. Detectors have been designed with over 100 GHz of modulation bandwidth.[24] Chapter 2 describes the operation of this type of detector in more detail.

1.11.2 APD Detectors

A diagram of an avalanche photodetector (APD) detector is shown in Figure 1.25.[25,26] The APD was designed to improve the sensitivity compared to a p-i-n-based receiver. The sensitivity issue surrounding p-i-n receivers is that it is often difficult to design a wideband electronic amplifier after the photodetector with a low enough noise contribution. The APD addresses this problem by providing low-noise, high-bandwidth electronic amplification that is designed into the detection process. The APD has a low-bandgap semiconductor absorption region very similar to that of a p-i-n detector. The electrons are then accelerated to very high velocities toward a separate multiplication region. The high-energy electrons collide with the lattice to form new free electrons in an avalanche multiplication process. The ideal low-noise APD multiplies electrons but does not multiply holes in the avalanche process. This condition results in minimum noise contribution from the multiplication process. APD detectors result in receivers that have better sensitivity than p-i-n-based receivers when used in high-speed systems. APDs require a high-bias voltage to produce avalanche conditions. The multiplication process is also temperature-

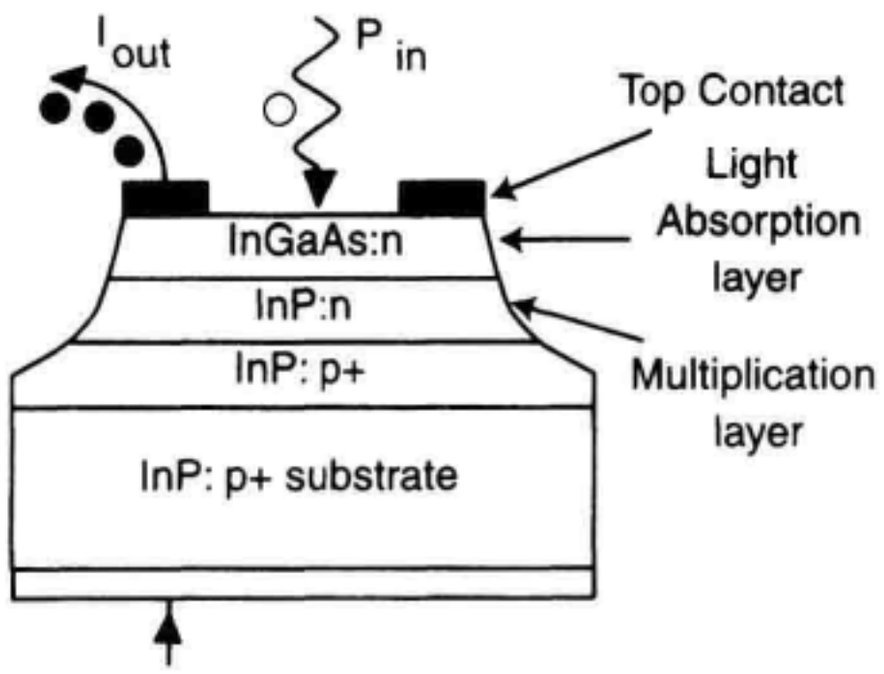

Figure 1.25 Avalanche photodetector diagram with separate absorption and multiplication regions.

dependent making the supporting circuitry more difficult to design. APDs are commonly used in systems up to a rate of 2.5 Gb/s. Higher bandwidth devices are being developed in research laboratories.

1.12 OPTICAL TRANSMITTER AND RECEIVER MEASUREMENTS

Sections 1.9 and 1.11 described the operational principles of sources and receivers for fiber optic systems. Knowledge of component operation is important for understanding the testing requirements for these devices. This section examines some of the measurement areas important for characterizing optical transmitters and receivers. The discussion is organized by measurement areas. Sections 1.12.1 to 1.12.5 describe three fundamental source characterization areas of optical power, polarization, and spectral measurements. Sections 1.12.6 to 1.12.8 cover techniques used to measure the modulation characteristics of lightwave components. Section 1.12.9 describes reflectometry techniques for optical transmitters and receivers.

1.12.1 Power

Power measurement is fundamental to all areas of optical characterization. Figure 1.26 illustrates a basic power-meter instrument diagram. Light from the optical fiber is imaged onto a diode photodetector. The photodetector is used to convert the optical power into a

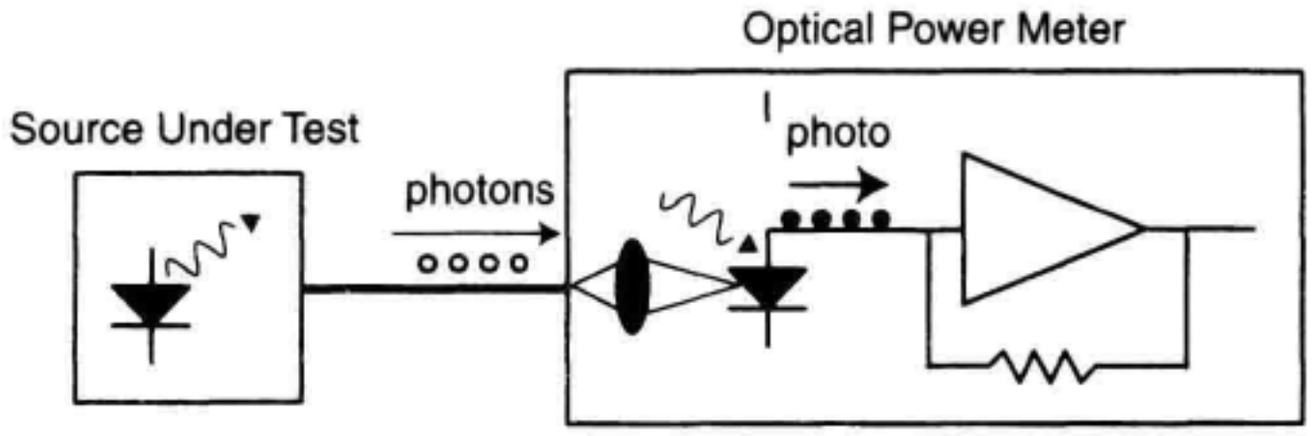

Figure 1.26 Optical power measurement.

proportional electrical current. The conversion efficiency between the input power and the output current of a photodetector is called the responsivity with units of Amps/Watt.

The responsivity of the detector must be calibrated in order to make optical power measurements. Unfortunately, the responsivity is a function of wavelength for all photodetectors. Knowledge of the signal wavelength is required to get accurate power measurements. Fortunately, photodetectors are available with responsivities that are relatively independent of wavelength in the telecommunications fiber-optic wavelength bands. Standards labs have developed thermal-detector heads that measure the temperature rise caused by optical signal absorption. Thermal detectors can be very accurate and are wavelength-independent but suffer from poor sensitivity. Thermal detectors are used to calibrate photodetectors but are not often used outside of standards laboratories.

Photodiode detectors are capable of measuring optical power levels of approximately −110 dBm to +10 dBm. The upper power limit is determined by saturation effects in the photodetector that cause the responsivity to decrease. Higher power levels can be measured using calibrated optical attenuators. The low power level is limited by the averaging time of the measurement and the dark current of the photodetector. The dark current of a photodetector is the amount of current measured in the absence of an optical input signal. Ultimately, the lower power level will be limited by the particle nature of light. For the most sensitive measurements, individual photons of light can be counted. Photon-counting detectors that can count individual photons are difficult to achieve in the infrared range of 1200 to 1700 nm. Sensitivity of optical receivers is covered in detail in Appendix A.

Care must be taken in the design of power meters so that the power measurement is independent of the input polarization state of the signal. Any movement of an optical fiber can alter the polarization state that is incident on the detector.

Another consideration is the reflectivity of the optical head. Large reflections can feedback signal to the optical source potentially altering the power and spectral characteristics of the incoming light. Chapter 2 covers the area of optical power measurements and calibration.

dB Optical and dB Electrical. The decibel (dB) is a commonly used unit for comparing power levels in systems.

$$\text{dB} = 10 \log\left(\frac{\text{Power}_1}{\text{Power}_2}\right) \tag{1.3}$$

The use of dBs is confusing in fiber optic measurements because we often talk about both changes in optical power before photodetection and changes in electrical signal power after photodetection. This is best illustrated by an example. Let's say that a 1 mW optical signal is incident on a photodetector that has a responsivity of 1 A/W. If the power of the optical signal is dropped from 1 mW to 0.5 mW, this represents a 3 dB drop in optical power. What happens to the power in the photodetected electrical signal in this same example? The 1 mW to 0.5 mW optical power change would result in a 1 mA to 0.5 mA electrical current change. The halving in electrical current causes the electrical power to

drop by 6 dB since the electrical power dissipation is proportional to the current squared. Any dB change in optical power will result in a 2 dB change in electrical power. To eliminate confusion in dB, it is customary to refer to the optical power drop in terms of dB optical and the electrical power drop after detection in terms of dB electrical. This distinction of electrical and optical dBs is especially important for the modulation analysis description given in Sections 1.12.6 to 1.12.8.

1.12.2 Polarization

The polarization state of a source is a second fundamental property of the lightwave signal. Polarization refers to the electric field orientation of a lightwave signal. Laser sources are predominantly linear polarized sources. LEDs have no preferred direction of polarization and are predominantly unpolarized. A polarized lightwave signal will go through dramatic changes in its polarization state as it propagates through optical fiber. This change in polarization state in fiber is due to a weak change in the velocity of propagation as a function of polarization state. Stress in the fiber or ovality of the waveguide shape causes this polarization dependence of fiber. Components in fiber-optic communication systems may have polarization-dependent loss, gain, or velocity. A system with a polarized input and a large polarization-dependent loss will perform unpredictably depending on temperature or fiber stress. It is therefore important to understand the polarization characteristics of optical sources.

The goals of a polarization measurement are to determine the fraction of the total light power that is polarized and to determine the orientation of the polarized component. Figure 1.27 illustrates a polarization analyzer instrument that characterizes the polarization state of a lightwave signal. This instrument consists of four power meters with polarization characterizing optical components in front of them. The polarization analyzer measures the Stokes parameters; S_0, S_1, S_2, and S_3. The total power of the signal is the parameter S_0. All of the other Stokes parameters are normalized to S_0. S_1 indicates the power difference between vertical and horizontal polarization components. S_2 indicates the power difference between +45 and –45 degrees linear polarization. S_1 and S_2 are measured with polarizers in front of detectors. S_3 indicates the power difference between right-hand and left-hand circular polarization. S_3 is measured with a waveplate in front of a detector.

Polarization State. The polarization state of a source is conveniently visualized using a Poincaré sphere representation. Figure 1.27 shows a diagram of the Poincaré sphere. The axes of the Poincaré sphere are the Stokes parameters normalized to the total power S_1, S_2, and S_3. The polarization state of a source can then be represented by the three-dimensional coordinates (S_1, S_2, S_3). The value of any of the coordinates is between zero and one. The outer surface of the sphere represents signals that are highly polarized, such as most lasers. The equator of the sphere contains all of the linear polarization states. The poles show circular polarization states. Points between the equator and the poles are elliptically polarized.

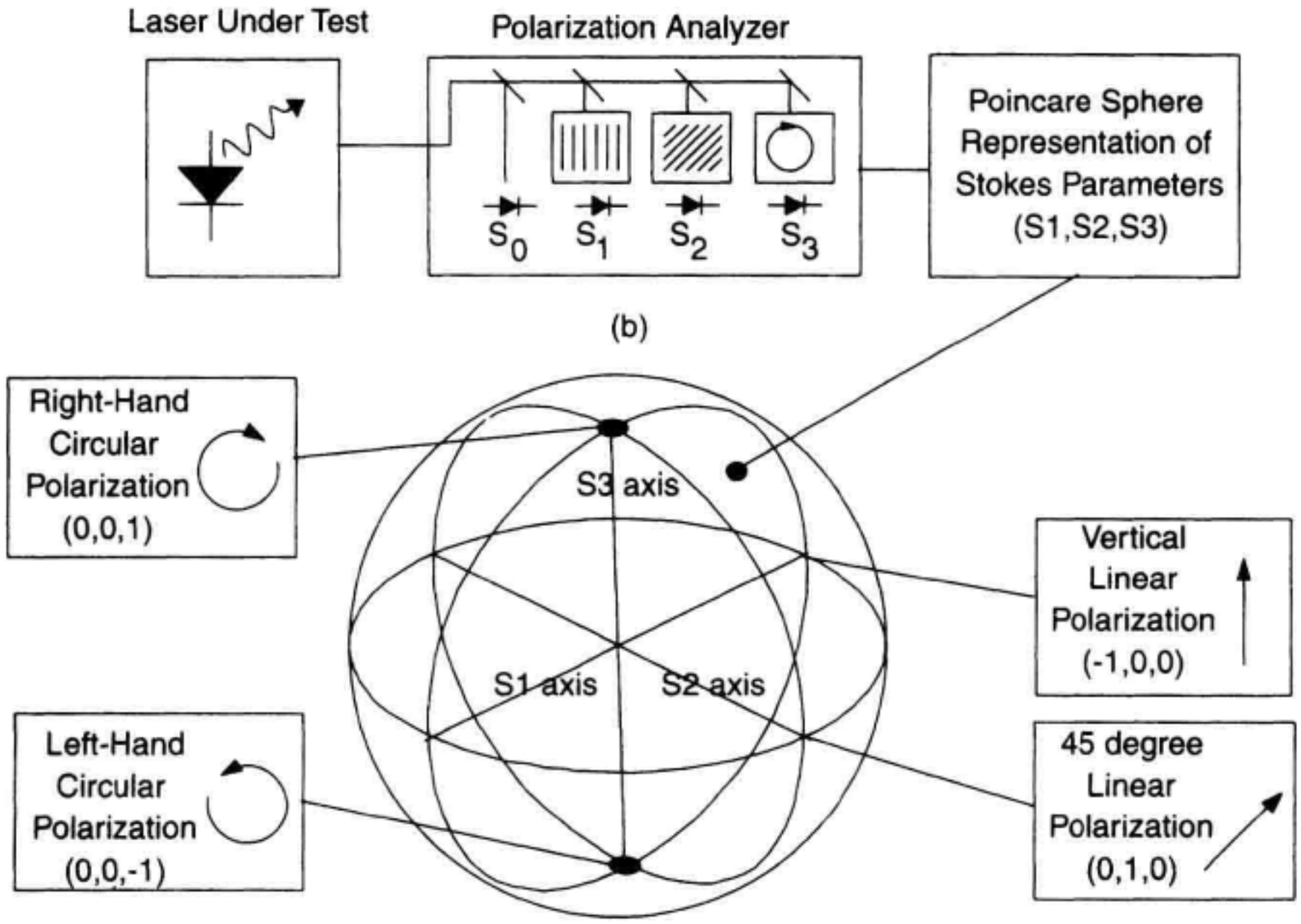

Figure 1.27 (a) Equipment used to measure polarization state. (b) Poincaré sphere representation of polarization state.

Degree of Polarization. The interior of the sphere is used to represent partially polarized light. The center of the sphere is for unpolarized lightwave signals such as those from a light bulb or the sun. The degree of polarization (DOP) is used to indicate the extent of polarization in a source. 100% DOP is found on the outer surface and 0% DOP is found in the center. Most lasers will have a DOP of greater than 95%. Most LEDs have very low degrees of polarization.

The Poincaré sphere provides a convenient tool for visualizing how the polarization of a source changes as it passes through different parts of a lightwave system. Optical fiber is slightly birefringent. Birefringent materials have a velocity that is polarization dependent. A laser that is coupled into an optical fiber may start out with linear polarization. After traveling through a length of optical fiber, the polarization state could be found anywhere on the surface of the Poincaré sphere. Since the polarization of an optical signal is constantly changing along the length of a long optical fiber, it is very important that all optical components have performance that is polarization independent. Parameters such as polarization-dependent loss (PDL) and polarization mode dispersion (PMD) are very important in today's lightwave systems. Chapter 6 is devoted to polarization measurements for fiber optic systems. Chapter 12 covers the PMD measurement area.

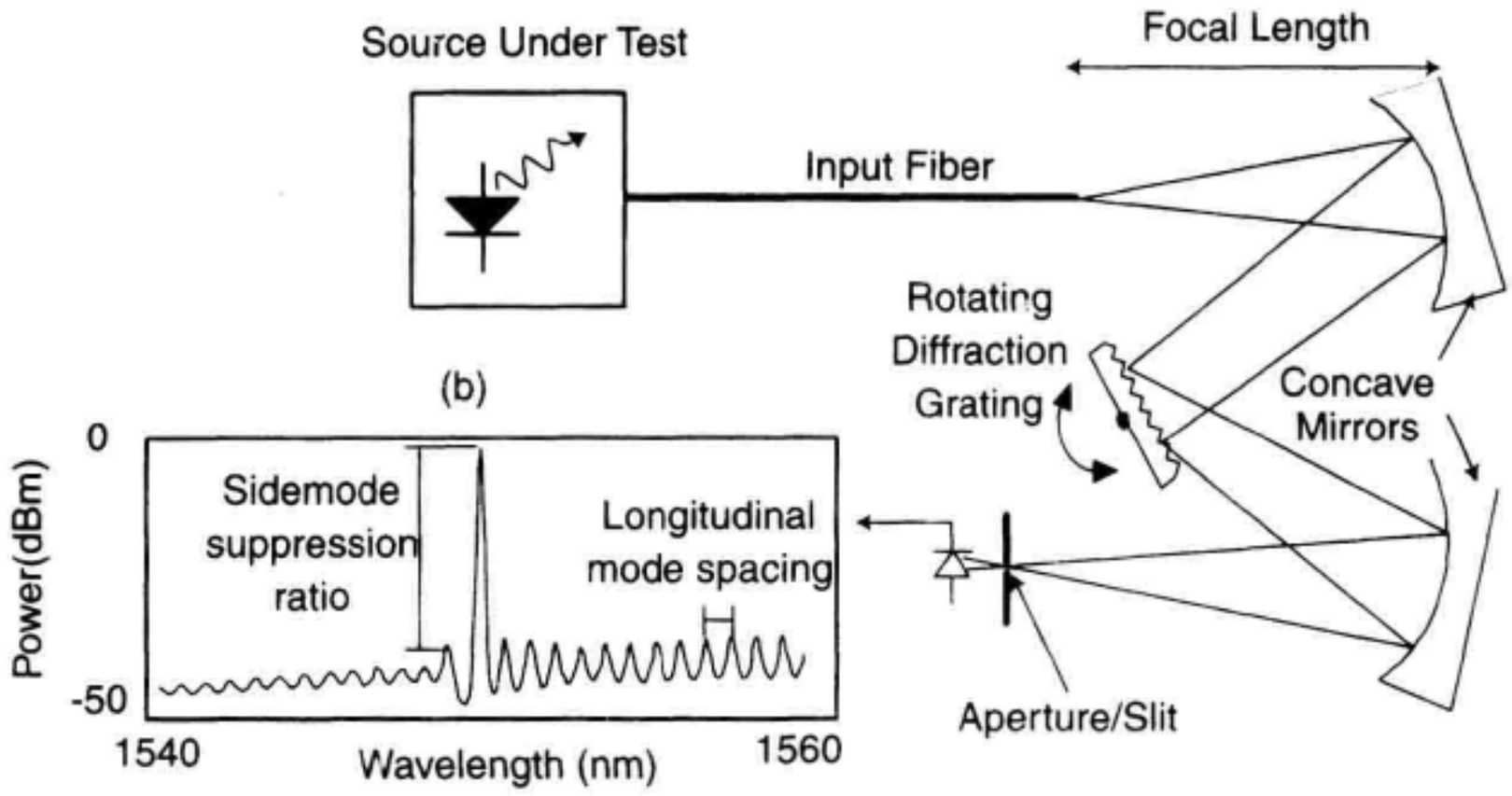

Figure 1.28 (a) Diagram of an OSA. (b) Measurement parameters of a DFB laser.

1.12.3 Optical Spectrum Analysis

The third fundamental property of a signal is its spectral content. An OSA is used to measure the power versus wavelength coming from an optical source. Figure 1.28a shows an OSA that uses a diffraction grating to accomplish wavelength filtering. An OSA consists of a tunable bandpass filter and an optical power meter. Diffraction grating filters are used for most general purpose fiber-optic input OSAs. The light from the input fiber is collimated (light rays made parallel) and applied to the diffraction grating. The diffraction grating has a series of finely spaced reflectors (for example, 1000 reflectors/mm). The diffraction grating separates the input light into different angles depending on wavelength. The light from the grating is then focused onto an output slit. The grating is rotated to select the wavelength that reaches the optical detector. The filter bandwidth for such an instrument is determined by the diameter of the optical beam that is incident on the diffraction grating and on the aperture sizes at the input and output of the optical system. The filter bandwidth of an OSA is limited to the 0.01 to 0.1 nm range due to physical size constraints for a portable instrument.

OSAs that use FP interference filters can also be used. FP filters offer the possibility of very narrow wavelength resolution. The disadvantage is that these filters have a passband that regularly repeats versus wavelength. Chapter 4 covers OSAs using these types of filters.

Figure 1.28b shows a spectral plot for a DFB laser that is being modulated with 2.5 Gb/s digital data. This plot shows that the laser emits in one predominant longitudinal mode. Other modes are suppressed by over 30 dB. The spacing between modes in this diagram is 1.4 nm. The OSA for this measurement must have a very narrow passband and steep skirts. A filter stopband that is at least 50 dB down is needed to accurately measure

the value of the smaller sidelobes. Chapters 3 covers diffraction-grating methods of optical spectrum measurement.

Although high resolution can be obtained with diffraction-grating spectrometers, they do not have sufficient resolution to look at the detailed structure of a laser longitudinal mode. The width of each longitudinal mode in Figure 1.28b is limited by the filter width of the OSA. Section 1.12.5 and Chapter 5 will describe methods that are used to look at the fine detail of the spectrum.

The absolute accuracy of an OSA wavelength measurement is determined by how accurately the diffraction grating can be positioned and by the environmental stability of the monochrometer equipment. If precision wavelength measurement with picometer resolution is required, wavelength meter measurement techniques are used (Section 1.12.4).

1.12.4 Accurate Wavelength Measurement

It is often necessary to know the wavelength of an optical source very accurately. An example application is to measure the wavelength drift of a temperature-stabilized DFB laser versus ambient temperature. Resolution of 0.001 nm would be desired in such an application. The OSA techniques discussed in Chapter 3 are not sufficiently accurate to measure the wavelength of a laser with picometer resolution. Figure 1.29a illustrates a method by which very accurate wavelength measurements can be made. The most common wavelength meter implementation uses a Michelson interferometer configuration. The light from the unknown source is split into two paths that are then recombined at a photodetector. One of the path lengths is variable and the other is fixed in length. As the variable arm is moved, the photodetector current varies due to constructive and destructive interference as is shown in Figure 1.29b. The period of this interference is one half of the wavelength of light in the medium of the interferometer. To accurately measure the wavelength of the unknown signal, a reference laser with a known wavelength is introduced into the interferometer. The wavelength meter compares the interference pattern of

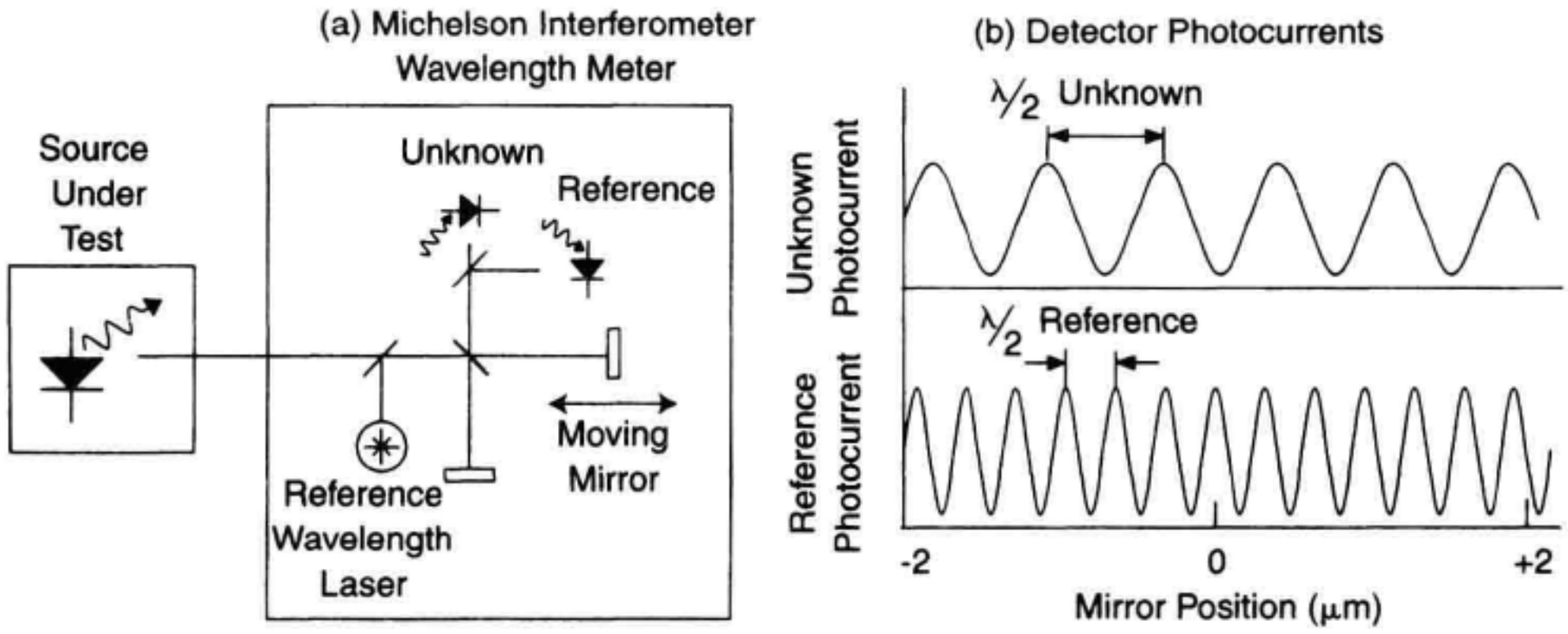

Figure 1.29 (a) Michelson interferometer wavelength measurement. (b) Photocurrent waveforms from the unknown and reference detectors as a function of mirror position.

the known laser to that of the unknown laser to determine the wavelength of the unknown signal. Since the unknown signal and the wavelength reference take the same path through the interferometer, the measurement method is less sensitive to environmental changes. Fourier transforms can be done on the interference photocurrent to determine the full spectral characteristics of the optical source. Wavelength meters have limited dynamic range compared to grating-based OSAs.

Helium-neon (HeNe) lasers emitting at 632.9907 nm are often used as wavelength references. HeNe lasers have a well-known wavelength that is relatively insensitive to temperature. Using HeNe references, wavelength accuracies of less then 1 part per million are possible. A 1550 nm laser can be measured to an accuracy of better than ± 0.0015 nm. Chapter 4 covers accurate wavelength measurement methods.

1.12.5 Linewidth and Chirp Measurement

Neither OSAs nor wavelength meters offer sufficient wavelength resolution to display the details of each longitudinal mode of a laser. The linewidth of an unmodulated DFB laser is most often less than 10 MHz. The width of the laser lines in Figure 1.28b is limited by the finite filter width of the OSA which in this plot is 12 GHz. Resolution improvements of 1000 times are required to study the fine spectral detail of laser sources. Heterodyne and homodyne analysis tools are used to examine the fine structure of optical signals. These analysis methods allow the measurement of modulated and unmodulated spectral shapes of the longitudinal modes in laser transmitters.

Heterodyne. Figure 1.30a illustrates a heterodyne measurement set-up. In heterodyne measurements, the unknown signal is combined with a stable, narrow-linewidth local oscillator (LO) laser. The LO signal is adjusted to be within 50 GHz of the unknown signal to be detected by conventional electronic instrumentation. The LO must have the same polarization as the unknown signal for best conversion efficiency. The unknown signal and the LO mix in the photodetector to produce a difference frequency (IF signal) in the 0 to 50 GHz region. The intermediate frequency (IF) signal is analyzed with an electronic signal analyzer such as a spectrum analyzer.

Figure 1.30b shows the result of a heterodyne measurement of a laser under sinusoidal modulation at 500 MHz. The carrier and the two modulation sidebands are easily resolved with this technique. The major limitation of heterodyne techniques is the availability of very stable LO signals.

Homodyne. Homodyne analysis techniques give more limited information on the optical spectrum, but are much easier to perform. Homodyne techniques are similar to heterodyne analysis except that the LO is a time-delayed version of itself. If an optical signal is delayed in time by more than the inverse of the source spectral width (measured in Hz), the signal becomes phase independent of the original signal, allowing it to be an effective LO. The signal and the delayed version of the signal are combined in a manner similar to that of Figure 1.30a. The intermediate frequency is centered around 0 Hz because both signals have the same center wavelength. Figure 1.30c shows an example of a homodyne measurement of an unmodulated DFB laser. The measured linewidth is 20

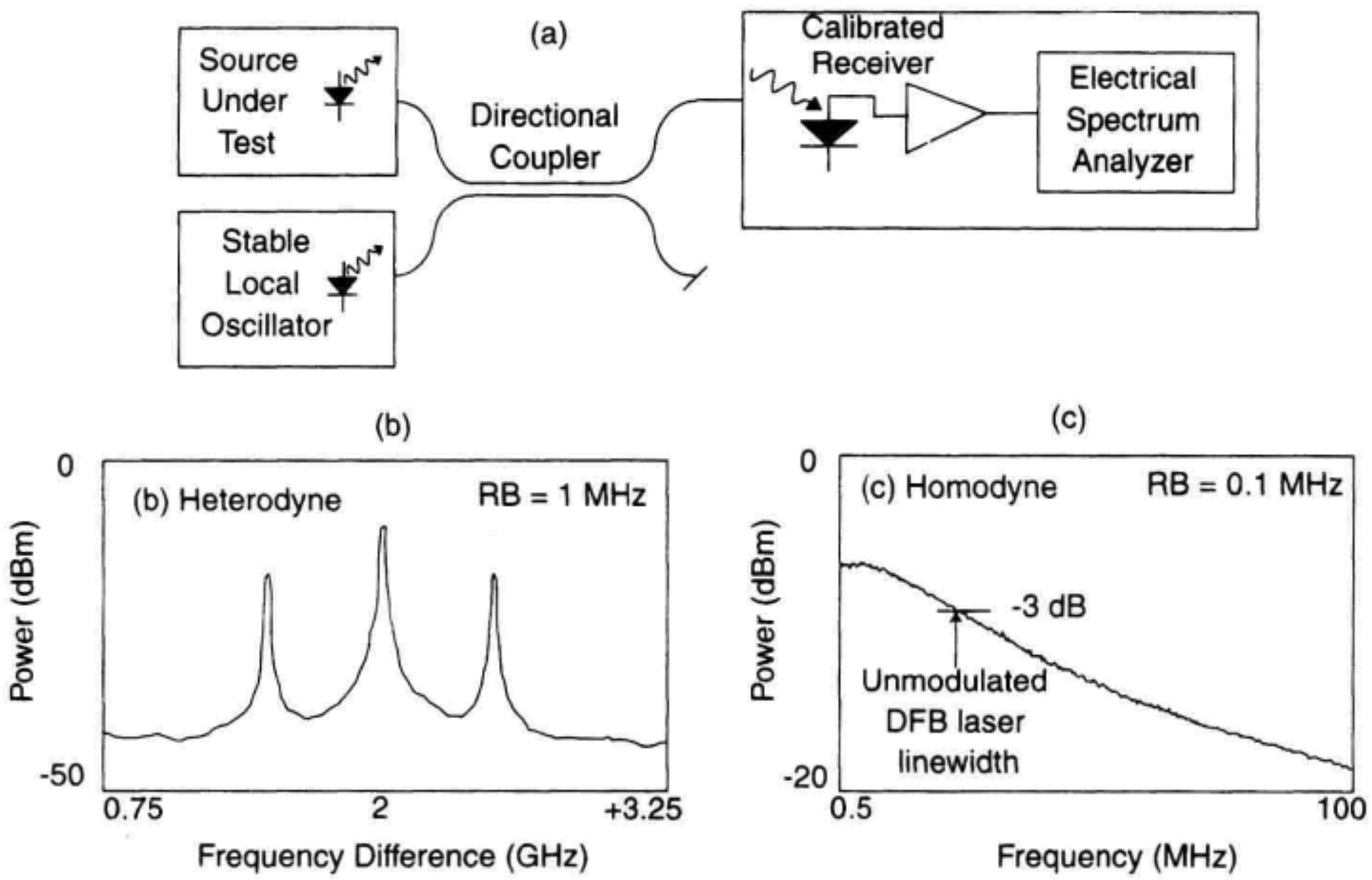

Figure 1.30 (a) Measurement configuration for Heterodyne spectrum analysis. (b) Intensity modulation sidebands for a DFB laser modulated at 1 GHz using Heterodyne measurement techniques. (c) Unmodulated linewidth measurement of a DFB laser using Homodyne techniques.

MHz. A limitation of this technique is that the asymmetries of the optical spectrum can not be seen. Homodyne analysis does not offer any information about the center wavelength of a laser.

Homodyne and Heterodyne techniques are also useful in characterizing laser chirp. Chapter 5 discusses homodyne and heterodyne spectrum analysis techniques.

1.12.6 Modulation Analysis: Frequency Domain

Most lightwave systems use intensity modulation to convey information on to the optical signals. Techniques are necessary to analyze parameters associated with this modulation. This section describes characterization methods that display information as a function of the modulation frequency.

Figure 1.31a shows a diagram of a lightwave signal analyzer. It consists of a photodetector followed by a preamplifier and an electrical spectrum analyzer to display the spectral content of the modulation on the lightwave signal. The modulation frequency response of the optical receiver, amplifier, and the electrical spectrum analyzer must be accurately calibrated as a unit. The display of Figure 1.31b shows the power of the modulation signal as a function of the modulation frequency. Do not confuse this information with the display of an OSA as shown in Figure 1.28b.

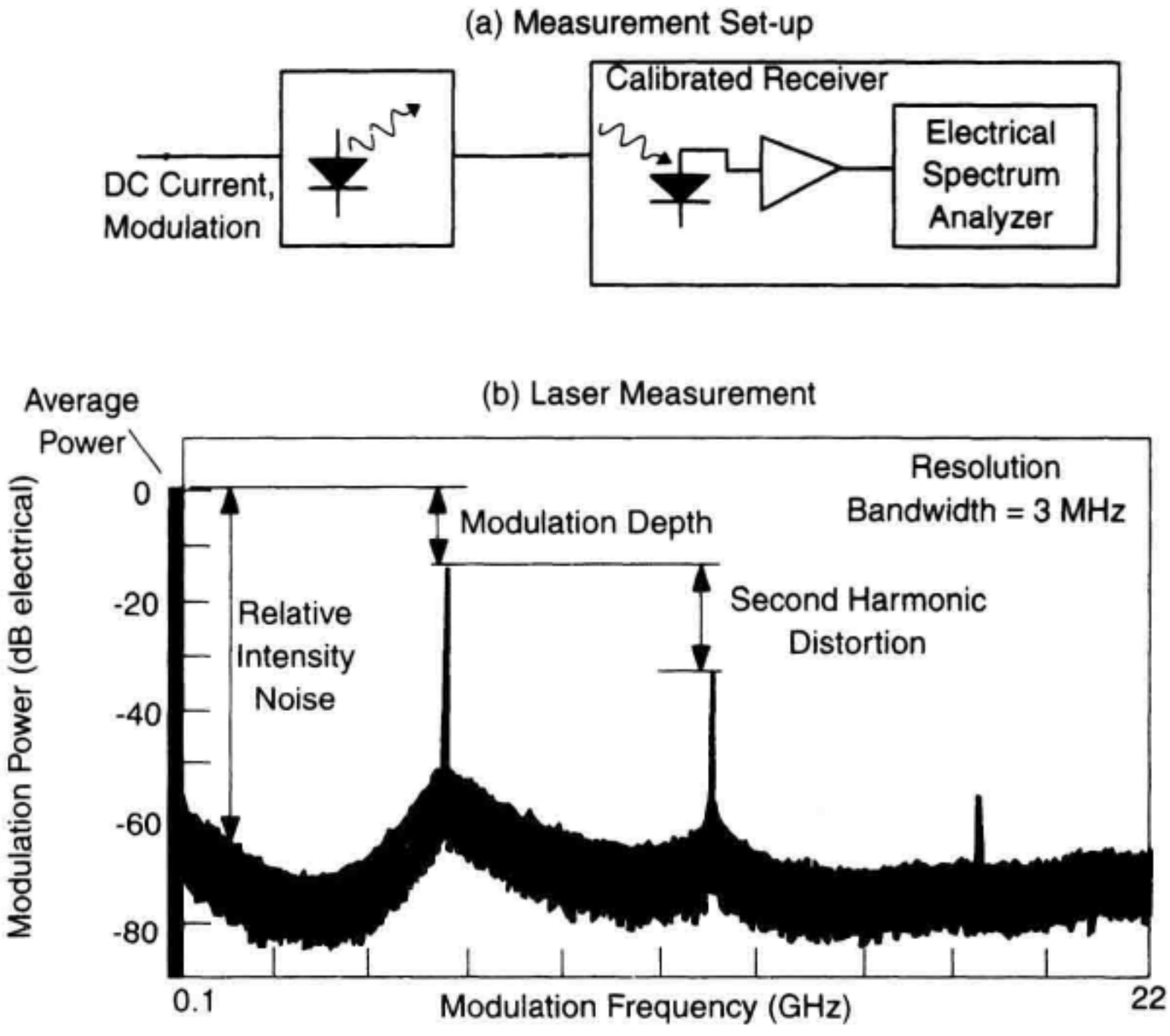

Figure 1.31 (a) Frequency domain analysis of the optical modulation. (b) DFB laser measurement example showing modulation depth, distortion, and intensity noise parameters.

This modulation domain signal analyzer allows the measurement of several characteristics of the modulation:

1. Depth of optical modulation.
2. Intensity noise.
3. Distortion.

Figure 1.31b shows a measurement example of a DFB laser modulated at 6 GHz. The display is presented in dB electrical units. A comparison of the average power and the 6 GHz modulation line indicates that this source has a small depth of modulation. The magnitude of the lines at 12 and 18 GHz compared to the 6 GHz modulation show the second and third harmonic distortion levels of the optical source. Distortion measurements are critical for lasers designed to work in analog cable-TV signal distribution applications. Lasers also add intensity noise to the optical signal. The relative intensity noise (RIN) of a source is characterized by ratioing the noise level at a particular modulation frequency to the average power of the signal. RIN measurements are normalized to a 1 Hz bandwidth. A DFB laser without modulation may have a RIN level of −145 dB/Hz. Chapter 7 covers frequency domain modulation measurements and calibration techniques in detail.

1.12.7 Modulation Analysis: Stimulus-Response Measurement

It is important to know how fast a laser can be intensity modulated or the upper modulation rate limits of an optical receiver. The modulation response of optical receivers, transmitters, and optical links can be measured using the instrumentation shown in Figure 1.32a. An electrical vector network analyzer with calibrated O/E and E/O converters is illustrated. The electrical source of the network analyzer is connected to the optical transmitter. An optical receiver is connected to the input of the electrical network analyzer. The electrical network analyzer compares both the magnitude and phase of the electrical signals entering and leaving the analyzer.

Figure 1.32b shows a measurement of the frequency response of a DFB laser transmitter. Although not shown, the phase response and group delay of the transmitter is also measured. DFB lasers are capable of efficient modulation into the GHz range. The modu-

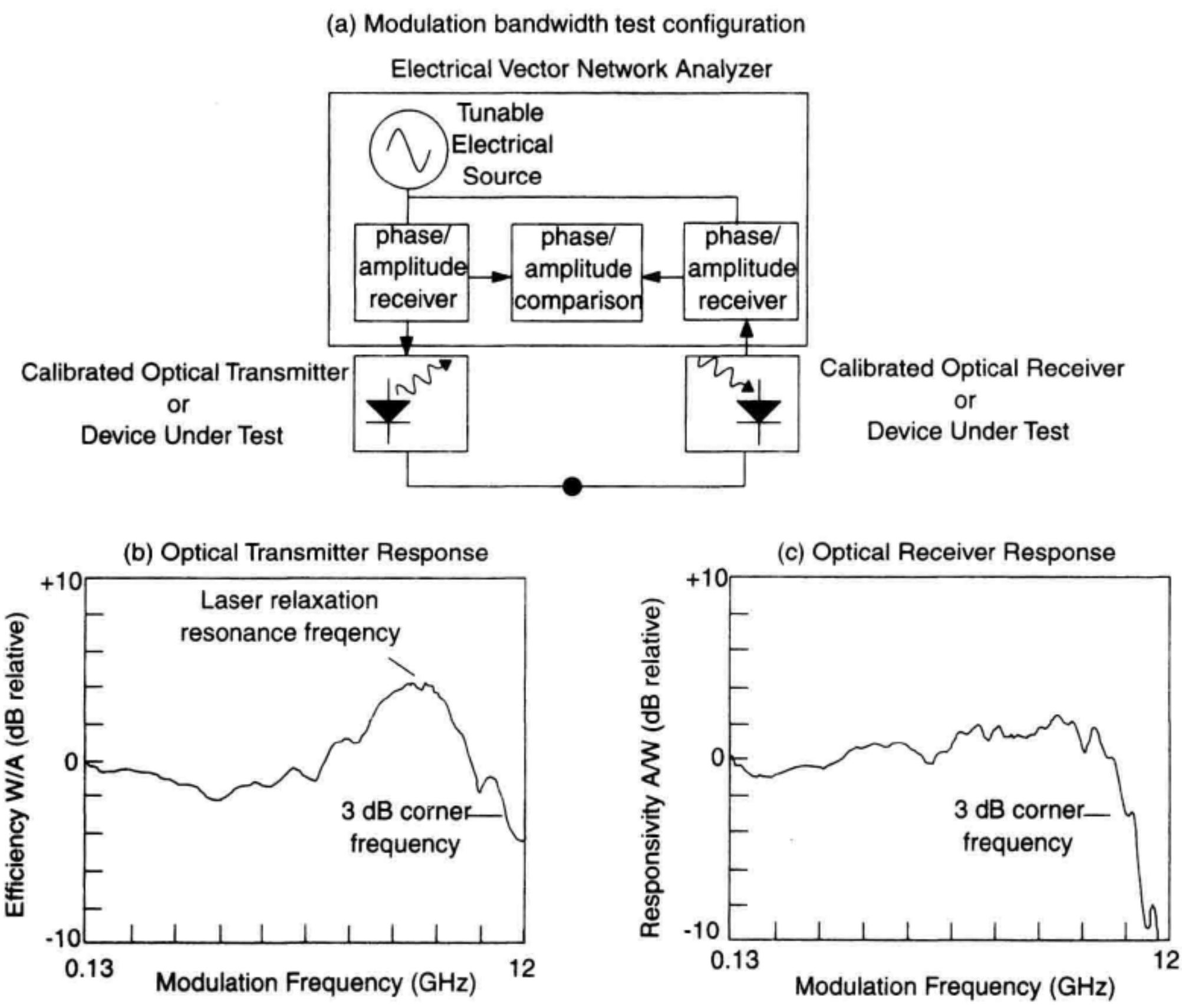

Figure 1.32 (a) Equipment to measure modulation efficiency as a function of modulation frequency. (b) DFB laser modulation response. (c) Optical receiver modulation response.

lation response often has peaking near the upper modulation frequency limits of the laser. This peaking occurs at the laser relaxation oscillation frequency.[10] Figure 1.32c shows a measurement of the modulation response of an optical receiver.

Calibration of the O/E and E/O converters in both magnitude and phase response is one of the major challenges in making such a measurement. Calibration of the magnitude and phase response of the electrical vector network analyzer is well established. Calibration of the O/E response is much more difficult. Let us assume that the device under test is an optical receiver. In order to measure the optical receiver magnitude and phase response, it is necessary to know the magnitude and phase response of the optical transmitter. The calibration of an optical transmitter magnitude and phase response with high accuracy is a considerable challenge. Chapter 7 covers methods of stimulus-response calibrations and related measurement issues.

1.12.8 Modulation Analysis: Time Domain

The majority of fiber optic links use digital modulation techniques. The shape of the modulation waveform as it progresses through a link is of great interest. The optical power versus time can be characterized by detecting the lightwave signal and applying the electrical signal to an oscilloscope as is shown in Figure 1.33a. High speed sampling oscillo-

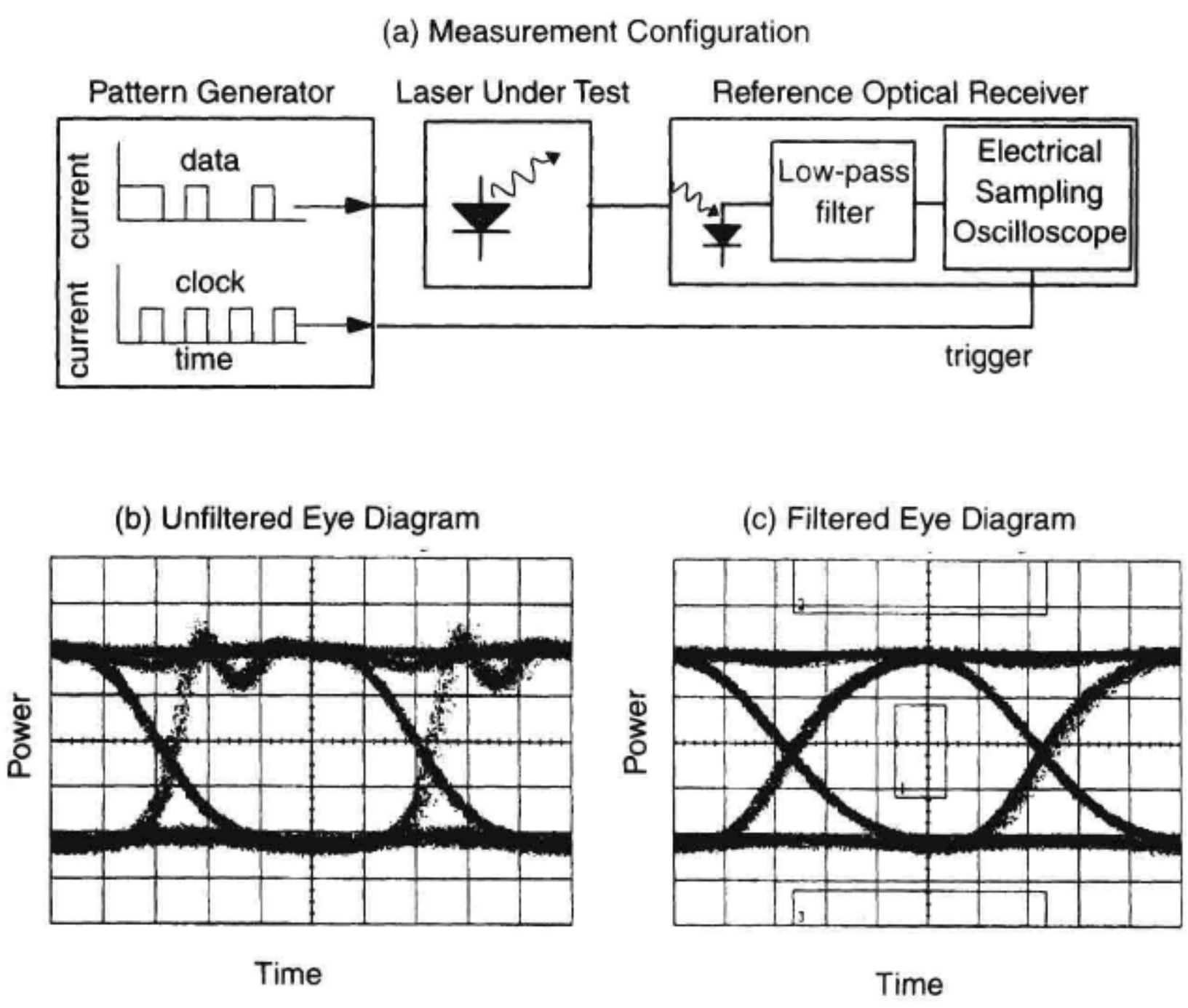

Figure 1.33 (a) Time-domain analysis of the optical modulation. (b) Eye diagram of digitally modulated DFB laser with high bandwidth optical receiver. (c) Eye diagram with SONET reference optical receiver.

scopes are often used due to the gigabit per second data rates involved in both telecommunication and data communication systems.

Figures 1.33b and 1.33c illustrate eye diagram measurements which are often used to characterize the quality of a lightwave signal. The clock waveform is applied to the trigger of the oscilloscope. The laser output is applied to the input of the oscilloscope through a calibrated optical receiver. The display shows all of the digital transitions overlaid in time. This eye-diagram display can be used to troubleshoot links that have poor bit-error ratio performance. Several laser characteristics can lead to poor error-rate performance. Optical sources have significant overshoot and ringing on the waveform transitions. Random- and pattern-dependent transition times cause jitter between the input electrical waveform and the output optical waveform. International standards such as SONET (Synchronous Optical NETwork), SDH (Synchronous Digital Hierarchy), and Fibre Channel specify limits on the amount of waveform distortion and time jitter that are acceptable. Figure 1.34c is an example of an eye-diagram measurement using a standardized receiver as specified by SONET and SDH. SONET/SDH reference receivers specify an optical receiver with a tightly controlled modulation response that is filtered at 3/4 of the bit rate. A mask constructed around the eye diagram is shown in Figure 1.33c. The measurement system can count the number of samples that fall within the mask window region. Chapter 8 covers time-domain measurements of lightwave signals.

1.12.9 Optical Reflection Measurements

It is important to have low reflection levels in fiber optic links. DFB lasers must be isolated from reflections so that the laser doesn't become unstable in wavelength or power. Multiple reflections of optical signals can also cause fluctuations in laser frequency to be converted to intensity noise (see Appendix A).

The total optical return-loss of an optical receiver or transmitter can be measured with the apparatus of Figure 1.34a. An optical source is applied to a device under test through a directional coupler. Light is then reflected back toward the source from the device under test. The reflected signal is separated from the incident signal in the directional coupler. By comparing the forward and reverse signal levels, the total optical return-loss is measured. Figure 1.34b shows the return-loss versus wavelength for a packaged laser using a tunable laser source for excitation. The return-loss is frequency dependent in this optical device because of the many reflective surfaces found in the component. If a total return-loss level is found to be too large, it is important to be able to locate the reflecting surfaces. This requires optical time-domain reflectometry techniques.

Figure 1.35a illustrates a high resolution OTDR measurement based on broadband source interferometry. The spacing between reflections inside optical components requires different OTDR techniques than for fault location in optical fibers as was shown in Figure 1.16. Optical component characterization requires very fine distance resolution in the millimeter to micron range compared to the meter range for fiber reflectometry. This technique uses a Michelson interferometer and a broadband light source to locate reflections with 20 μm accuracy. When a broadband source is used to excite a Michelson interferometer, interference occurs only when the movable mirror to directional coupler dis-

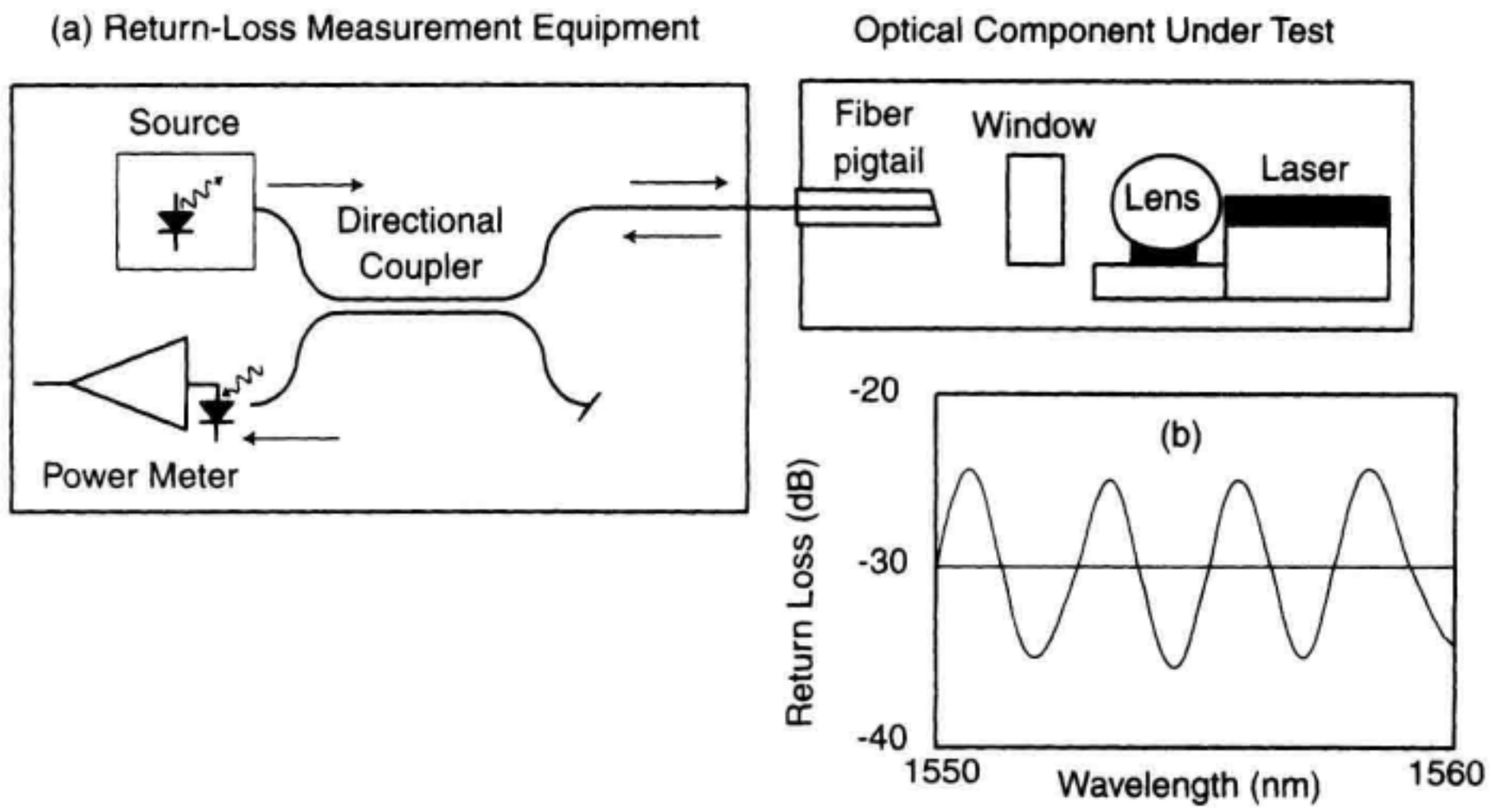

Figure 1.34 (a) Total return-loss measurement setup. (b) Example measurement of reflectivity as a function of wavelength for a packaged laser.

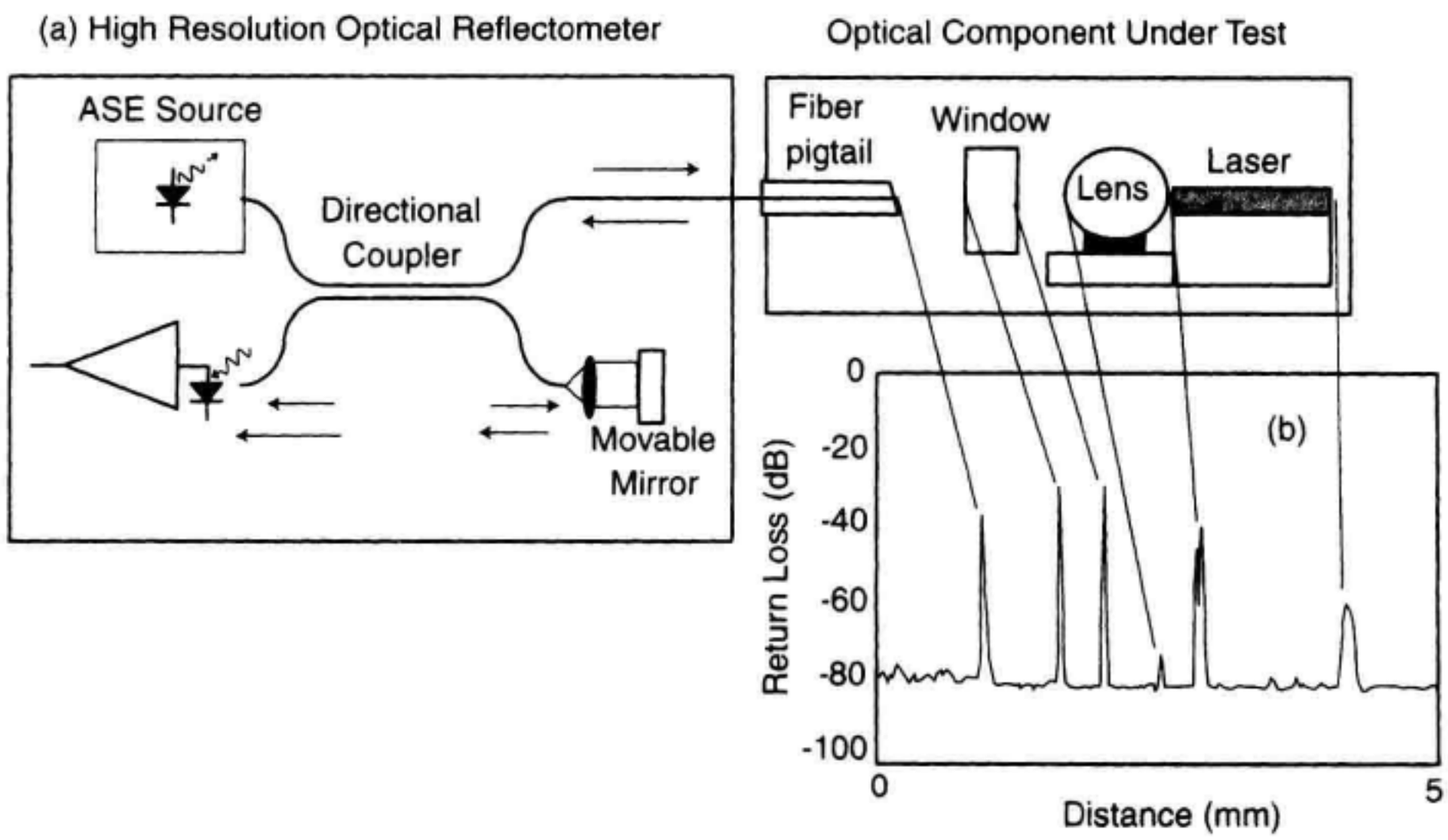

Figure 1.35 (a) High resolution optical reflectometer for measuring return-loss versus distance. (b) Example measurement for a packaged laser showing locations of various reflecting surfaces.

tance equals the distance from the device under test reflection to the directional coupler. The resolution of the measurement is determined by the spectral width of the broadband light source. A 50 nm wide source centered at 1310 nm is capable of 20 μm distance resolution. The example measurement of Figure 1.35b shows that the location of individual reflections inside the packaged component can be easily resolved. Chapter 10 describes total and distance resolved reflection measurements for components such as optical transmitters as well as optical receivers.

1.13 ORGANIZATION OF THE BOOK

Chapter 1. This chapter gives a highly condensed summary of fiber optic links and the measurement techniques used to characterize these links. The level of presentation is intended to be qualitative. The chapter refers readers to various points in the book where more detailed measurement descriptions are given. Here is a chapter by chapter summary of the following portions of the book.

Chapter 2. Power Measurement. Power is one of the fundamental properties of a lightwave signal. The photodetector is the most common device for measuring power. Several different types of detectors are available to cover the fiber optic wavelength bands.

Chapter 3. Optical Spectrum Analysis. The measurement of the wavelength of light is another fundamental lightwave property. This chapter concentrates on the most common measurement technique of using a diffraction grating as an optical filter.

Chapter 4. Accurate Wavelength Measurements. Very accurate measurement of the wavelength of light (1550 ± 0.001 nm, for example) can be made using a Michelson interferometer with a built-in wavelength standard.

Chapter 5. Heterodyne and Homodyne Spectrum Analysis. This chapter discusses the measurement of optical spectrum using homodyne and heterodyne spectrum analysis. These methods allow the spectrum of an optical signal to be resolved with very high resolution.

Chapter 6. Polarization. The polarization of the lightwave signal is another fundamental property. Some sources are unpolarized, other sources of light are 100% polarized. The fiber medium tends to change the polarization state of a signal dramatically as light propagates down the length. Because the state of polarization is ever-changing in many fiber optic systems, the components used in the system must be tolerant to polarization changes. This leads to the importance of polarization-dependent loss and polarization-dependent delay through components.

Chapter 7. Frequency Domain Analysis of Lightwave Modulation. The lightwave signal must be modulated in order for information to be transmitted. The most common lightwave-modulation method is intensity modulation. This chapter will analyze the modulation of the lightwave signal in the frequency domain. Noise and distortion are commonly measured parameters in the frequency domain. This chap-

ter will include the modulation stimulus-response behavior of optical receivers and transmitters.

Chapter 8. Time Domain Analysis of Lightwave Modulation. The most common intensity modulation is on–off digital modulation. This type of modulation is often best studied in the time domain. Oscilloscopes with optical front ends are used to look at the eye diagram in order to set up parameters such as extinction ratio and eye-mask conformance. Jitter measurement in lightwave systems is also covered.

Chapter 9. Insertion Loss Measurements. The measurement of the loss of multiport optical devices is covered. This measurement area has become very important due to the development of WDM systems. There are several methods to resolve loss versus wavelength. One can use a wavelength tunable laser and a power meter, a white light source in conjunction with an OSA or a tunable laser in conjunction with an OSA. Each of these measurement combinations has its strengths and weaknesses.

Chapter 10. Return Loss Measurements. The reflectivity of optical components is an important measurement. Systems are often intolerant of reflections. Total return-loss measurements are covered first. Instruments that allow high-resolution spatially resolved measurement of reflectivity are the primary focus of this chapter.

Chapter 11. Optical Time-Domain Reflectometry. This chapter covers one of the most important measurement areas in fiber optic communications. When a fiber is broken in a system, optical time-domain reflectometers are used to locate the break. Recent developments in the area now have OTDRs used as preventive maintenance tools for the installed fiber base.

Chapter 12. Chromatic Dispersion and Polarization-Mode Dispersion Measurements. Chromatic dispersion measurements of fiber and dispersion compensation devices is important for WDM and high-speed TDM systems. New fibers and components are being developed that allow dispersion management of new and upgraded fiber optic links. Polarization mode dispersion is becoming a primary effect that may limit the ultimate speed from TDM systems.

Chapter 13. Erbium-Doped Fiber Amplifier Measurements. Erbium-doped fiber amplifiers have changed the way new telecommunication systems are designed. Because of this special role, an entire chapter is devoted to EDFA description and characterization. The development of WDM systems has caused the measurements of EDFAs to be more complex.

Appendix A. Limits on Low-Level Optical Measurements: Noise. This section discusses the types of noise and their origins for optical and electronic systems.

Appendix B. Limits on High-level Optical Measurements: Nonlinearities. This section discusses the nonlinear behavior of optical fiber and how it limits the range of measurements.

Appendix C. Connector Care. One of the most common failure modes of fiber-optic test equipment is damage to optical connectors. This chapter will give examples of connector damage and discuss methods to prevent it.

APPENDIX: RELATIONSHIPS BETWEEN WAVELENGTH AND FREQUENCY

Authors in this book will be using both wavelength and frequency to describe optical measurement parameters. It is useful to be familiar with the relationships between these variables. This is especially useful when authors are quoting bandwidths in terms of small wavelength or small frequency deviations.

Wavelength and Frequency are related by the following relationship

$$v = f\lambda \tag{1.4}$$

where v is the velocity of light in the medium, f is the frequency of the signal, and λ is the wavelength in the medium. The velocity when propagating through a material is related to the index of refraction of the material by the following relationship

$$v = \frac{c}{n} \tag{1.5}$$

where c is the speed of light and n is the index of refraction of the material. The speed of light is approximately 299,792,458 m/sec. The wavelength of a signal varies with the index of refraction in the medium.

$$\lambda = \frac{\lambda_o}{n} \tag{1.6}$$

λ_o is referred to as the free-space wavelength, the wavelength that would be measured in a vacuum.

Oftentimes, it is important to look at differences in wavelength, $\Delta\lambda$ or differences in frequency between two signals, Δf. It is important to know how to be able to convert between these two variables:

$$\Delta\lambda = -\frac{v\Delta f}{f^2} = -\frac{\Delta f\lambda^2}{v} \tag{1.7}$$

$$\Delta f = -\frac{v\Delta\lambda}{\lambda^2} = -\frac{f^2\Delta\lambda}{v} \tag{1.8}$$

These equations are very useful since it is often necessary to convert back and forth between these parameters. At the communication band centered at 1300 nm, $\Delta\lambda = 0.1$ nm is equivalent to a Δf of 40 GHz. At the communication band centered at 1550 nm, $\Delta\lambda = 0.1$ nm is equivalent to a Δf of 12 GHz.

REFERENCES

General References on Fiber Optic Communications

1. Palais, Joseph C. *Fiber Optic Communication.* Englewood Cliffs, NJ: Prentice-Hall, 1992.
2. *Fiber Optic Telecommunications II,* edited by Stewart E. Miller and Ivan P. Kaminow, San Diego: Academic Press, 1988.
3. Hentschel, Christian. *Fiber Optics Handbook.* 3rd ed. Boblingen, Germany: Hewlett Packard, 1989.

References on Different Communication Standards

4. Synchronous Optical Network (SONET) Transport Systems: Common Generic Criteria, GR-253-CORE, Bellcore, Piscataway, NJ, Dec. 1994.
5. Digital Hierarchy—Optical Interface Rates and Formats Specifications (SONET), ANSI tl.105–1991, American National Standards Institute, New York, 1992.
6. Optical Interfaces for Equipments and Systems Relating to the Synchronous Digital Hierarchy, ITU G.957, International Telecommunications Union, Geneva, 1990.
7. Benner, Alan F. *Fibre Channel: Gigabit Communications and I/O for Computer Networks.* New York: McGraw-Hill, 1996.
8. Sachs, Martin and Anujan Varma. 1996. Fibre Channel and Related Standards. *IEEE Communications Magazine.* 34, 8: 40–50.
9. Ross, F.E. 1989. An Overview of FDDI: The Fiber Distributed Interface. *IEEE JSAC,* Vol. JSAC-7, 7: 1043–1051.

Wavelength Chirp References

10. Dutta, N.K. and G.P. Agrawal. 1986. *Long Wavelength Semiconductor Lasers.* New York: Van Nostrand Reinhold, 1986.

EDFA References

11. Desivire, E. 1994. *Erbium Doped Fiber Amplifiers: Principles and Applications.* New York: Wiley.
12. *Special Issue on Global Undersea Communication Networks. IEEE Communications Magazine.* 34, 2: Feb. 1996.

WDM References

13. Bellcore GR-2918-Core Document, Generic Criteria for SONET Point to Point Wavelength Division Multiplexed Systems in the 1550 nm Region, Bellcore, Piscataway, NJ, 1996.

Analog Transmission References

14. Darcie, T., et al. 1990. Lightwave Subcarrier CATV Transmission Systems. *IEEE Trans. on Microwave Theory and Techniques.* 38, 5: pp. 524–533.
15. Cox, C.H. 1991. Analog Fiber-Optic Links with Intrinsic Gain. *Microwave Journal,* (Sept.): 90–99.

Jitter References

16. Bures, Kenneth J. 1992. Understanding Timing Recovery and Jitter in Digital Transmission Systems—Part I, *RF Design* (Oct.): 42–53.
17. Trischitta, P. and E. Varma. 1989. *Jitter in Digital Transmission Systems,* Boston: Artech House.

Fiber References

18. Tosco, F., ed., 1990. Fiber Measurements. In *CSELT Fiber Optic Communication Handbook,* Chapter 4, pp. 273–416. "Fiber Measurements," Blue Ridge Summit, PA: McGraw-Hill TAB Books.
19. Marcuse, D. *Principles of Optical Fiber Measurements.* New York: Academic Press, 1981.

Fiber Optic Device References

FP and DFB, VCSEL Lasers

20. Dutta, N.K. and G.P. Agrawal. 1986. *Long Wavelength Semiconductor Lasers.* New York: Van Nostrand Reinhold.
21. Coldren, Larry A. and Scott Corzine. 1995. *Diode Lasers and Photonic Integrated Circuits.* New York: Wiley Interscience.

Mach-Zehnder Modulators

22. Jungerman, Roger, Catherine Johnson, David McQuate, Kari Salomaa, Mark Zurakowski, Robert Bray, Geraldine Conrad, and Donald Cropper. 1990. $LiNbO_s$ modulator for instrumentation applications, *Journal of Lightwave Technology.* 1990. 8, No. 9 (Sept.): 1363–1370.

LED References

23. Saleh, B.A. and M.C. Teich. 1991. *Fundamentals of Photonics.* New York: John Wiley.

Photodetector References

24. Wey, Y.G., K. Giboney, J.E. Bowers, M. Rodwell, P. Silvestre, P. Thiagarajan, and G. Robinson. 1995. 110 GHz InGaAs/InP Double Heterostructure p-i-n Photodetectors, *IEEE Journal of Lightwave Technology* 13, No. 7 (July): 1490–1499.
25. Stillman and Wolfe, *Semiconductors and Semimetals, Vol. 12, Infrared Dectors II,* edited by Williardson and Beer (ed.), Academic Press, 1977.
26. Sloan, Susan. 1994. Photodetectors. In *Photonic Devices and Systems,* ed. Robert G. Hunsperger, 171–246. New York: Marcel Dekker.

CHAPTER

2

Optical Power Measurement

Christian Hentschel

2.1 INTRODUCTION

Optical power measurement is the basis of fiber optic metrology. An optical power detector is found in nearly every lightwave test instrument. Two types of power measurements can be distinguished: absolute and relative power measurement. Relative power measurements are important for the measurement of attenuation, gain, and return loss. (See Chapter 9 for details.) Absolute power measurement is needed in conjunction with optical sources, detectors, and receivers. For example, the absolute power of an optical transmitter or optical amplifier is important for the power margin of a communication system and for eye-safety considerations. The sensitivity of an optical receiver is also specified in units of absolute optical power.

Optical power is generally defined on the basis of electrical power, because electrical power can be precisely measured through current and voltage. Therefore, all optical power measurements should be traceable to electrical power measurements. Most national standards laboratories, such as NIST (U.S.), PTB (Germany) and NPL (U.K.) host substantial activities on this subject.

Two main groups of optical power meters can be identified: power meters with thermal detectors, in which the temperature rise caused by optical radiation is measured, and photodetectors, in which the incident photons generate electron-hole pairs.

Although photodetector-type power meters suffer from a relatively small wavelength coverage and the need for absolute calibration, their astounding sensitivity usually makes them the preferred choice. Nevertheless, power meters with thermal detectors are sometimes preferred in the calibration laboratories because of their wide and flat wavelength characteristics. In addition, thermal detectors can be directly traceable to electrical

Table 2.1 Comparison of thermal power meters and photodetector power meters

Characteristics	Power meters with thermal detectors	Power meters with photodetectors
Wavelength dependence	+ wavelength-independent + wide wavelength range	– wavelength dependent, – wavelength range 2:1
Self-calibration	+ available	– not available (calibration indispensable)
Sensitivity	– very low (typically 10 μW)	+ very high (down to less than 1 pW)
Accuracy	±1% depending on calibration method	±2% depending on calibration method

power measurements. Altogether, there is good reason for the existence of both types of power meters. Table 2.1 compares the two types of power meters.

2.2 POWER METERS WITH THERMAL DETECTORS

Various principles of thermal detectors have been developed. A typical example is shown in Figure 2.1, from Bischoff.[1] This detector uses a method called substitution radiometry, which can be understood as a self-calibration method. In this method, the power meter is first exposed to the optical radiation. Then the radiation is switched off (with a shutter or chopper) and replaced by electrically generated power. This electrical power is controlled

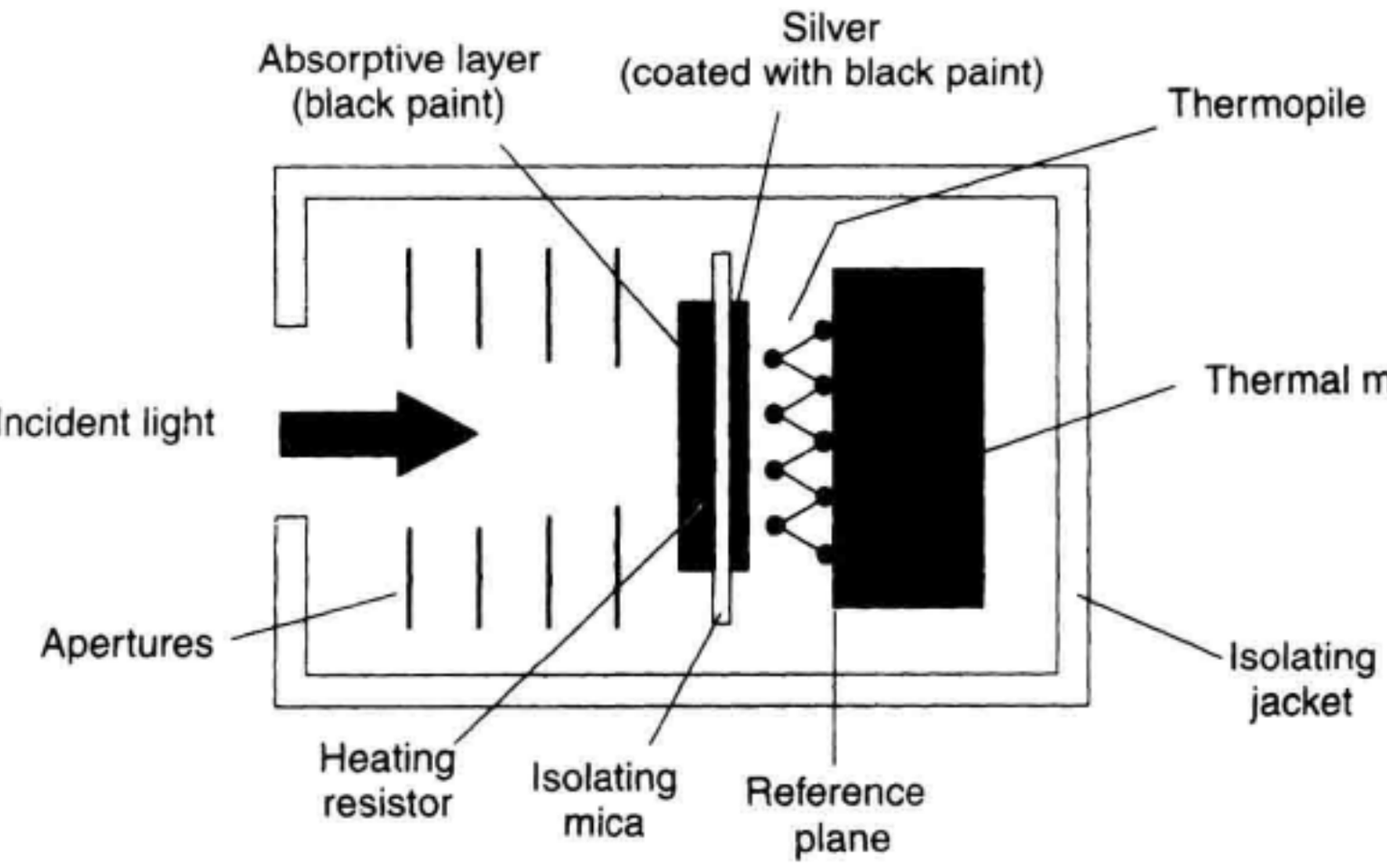

Figure 2.1 Thermal detector with electrical substitution.

so that a time-independent temperature is maintained. Electrical power can be measured very accurately, thereby providing the basis for the accuracy of this method.

In the detector of Figure 2.1, the incident light hits an absorptive layer, for example, one made from black paint. The substitution is accomplished with a heating resistor that is thermally well coupled to the absorptive layer. The back of the heating resistor carries an isolated sheet of silver for the purpose of equalizing any temperature differences. The silver is also coated with black paint. The temperature rise is measured with a thermopile (a series connection of thermocouples) which is brought into close proximity to the silver.

The thermopile produces a voltage proportional to the temperature difference between the absorptive layer and the reference plane, in this case the surface of a relatively large thermal mass. For this application, linearity is irrelevant because the only aim is to achieve equal temperatures for the two types of excitations. The following critical points need to be observed when the goal is highest accuracy:

1. Reference plane on large thermal mass: The thermal mass must be sufficiently large to maintain constant temperature during the relatively long measurement times. Long measurement times are typical because of the long time constants involved.
2. Blocking of background radiation and stray light: The thermal detector not only measures the power of the radiation source, but also changes in room temperature. This effect is reduced by a jacket with thermal isolation. In addition, a series of apertures makes sure that the detector is irradiated by the optical source only.
3. Optimization of heat flow: A negligible thermal resistance between the absorptive layer and the heater would be ideal. The thermal resistance to the jacket—due to convection and radiation—should be as high as possible.
4. High absorptance: Reflected light (both specular and diffuse) does not contribute to the detector's temperature rise and must be corrected for. Therefore, the absorptance should come close to 100%. A reflectance measurement is necessary in any case, as part of the initial calibration.
5. Accurate measurement of the electrical power: The electrical power is measured by current and voltage measurement, where voltage probes near the heating resistor are used to obtain accurate voltage results. A small contribution to the temperature rise is caused by the resistor leads. Bischoff[1] suggests eliminating this effect by an arrangement which includes additional contacts to the resistor and a constant current through the leads, independent of whether the heater is on or not.

More recently, another elegant way of operating this setup was published by the PTB, reference.[2] Instead of sequential exposure to optical radiation and electrical power, the sensor (in this case a thin-film sensor) is continuously heated by electrical power which is slightly larger than the optical power to be measured. The sensor voltage is recorded without the optical power applied. Then the sensor is exposed to the optical power, and a feedback loop reduces the electrical power until the sensor voltage is the same as before (on-line calibration). The desired optical power measurement result is simply the difference of electrical powers between the two steps, without a need of analyzing the sensor voltages.

The biggest problems in using power meters with thermal detectors is their low sensitivity and the correspondent long measurement times. Some improvement is possible on the basis of pyroelectric sensors or thermopiles using semiconductor material. Typical characteristics of thermal power meters are: sensitivity down to 1 μW, uncertainty as low as $\pm 1\%$, spectral range from ultraviolet to far infrared, and time constant of several seconds to minutes depending on the detector size. These characteristics make thermal power meters well suited for calibration purposes. In other fields of fiber optic measurements they are rarely used, however.

A special form of a thermal power meter is the cryoradiometer.[3] This is a thermal detector that is placed into vacuum and cooled to approximately 6 K using liquid helium. Cryoradiometers are the most precise optical power meters due to the following phenomena:

1. At 6 K, the thermal mass (the energy needed to raise the temperature by 1 K) of the absorbing material is drastically reduced. This reduces the time constants and the measurement times accordingly.
2. Heat loss due to radiation is virtually eliminated because the radiated energy is proportional to T^4 (T in K).
3. Heat contributions from the resistor leads can be eliminated by making them superconducting.
4. Convection losses are eliminated by operating the detector in vacuum.

Based on these properties, cryoradiometers are claimed to have power measurement uncertainties as low as $\pm 0.01\%$. Cryoradiometers are usually only found in national calibration laboratories because of the high cost of purchasing and operating this equipment.

2.3 POWER METERS WITH PHOTODETECTORS

A big advantage of photodetectors is that they can measure power levels down to less than 1 pW (–90 dBm). High modulation frequency response is another advantage. On the other hand, a relatively strong wavelength dependence is observed, and the spectral band is usually not more than one octave wide, see Section 2.3.2. In contrast to thermal detectors, there is no self-calibration for photodetectors. Some efforts have gone into self-calibration of photodetectors aimed at a quantum efficiency of one.[4] This technique was abandoned because of insurmountable difficulties. Nevertheless, this detector type is the most important today, because of its great sensitivity, fast measurement time, and ease of use.

Photodetector-type power meters are usually categorized into small-area power meters, to be used only when power from a fiber is to be measured, and large-area power meters for open beam *and* fiber applications.

Figure 2.2 shows a cross-section through a commercial large-area optical sensor head based on a photodetector. Important elements are the antireflective coating on the connector adapter, the pinhole and the angled position of the detector, all to avoid multiple reflections. Temperature stabilization using a thermoelectric cooler ensures stable measurement results. The photodetector is operated at zero-bias voltage in order to eliminate any offset currents.

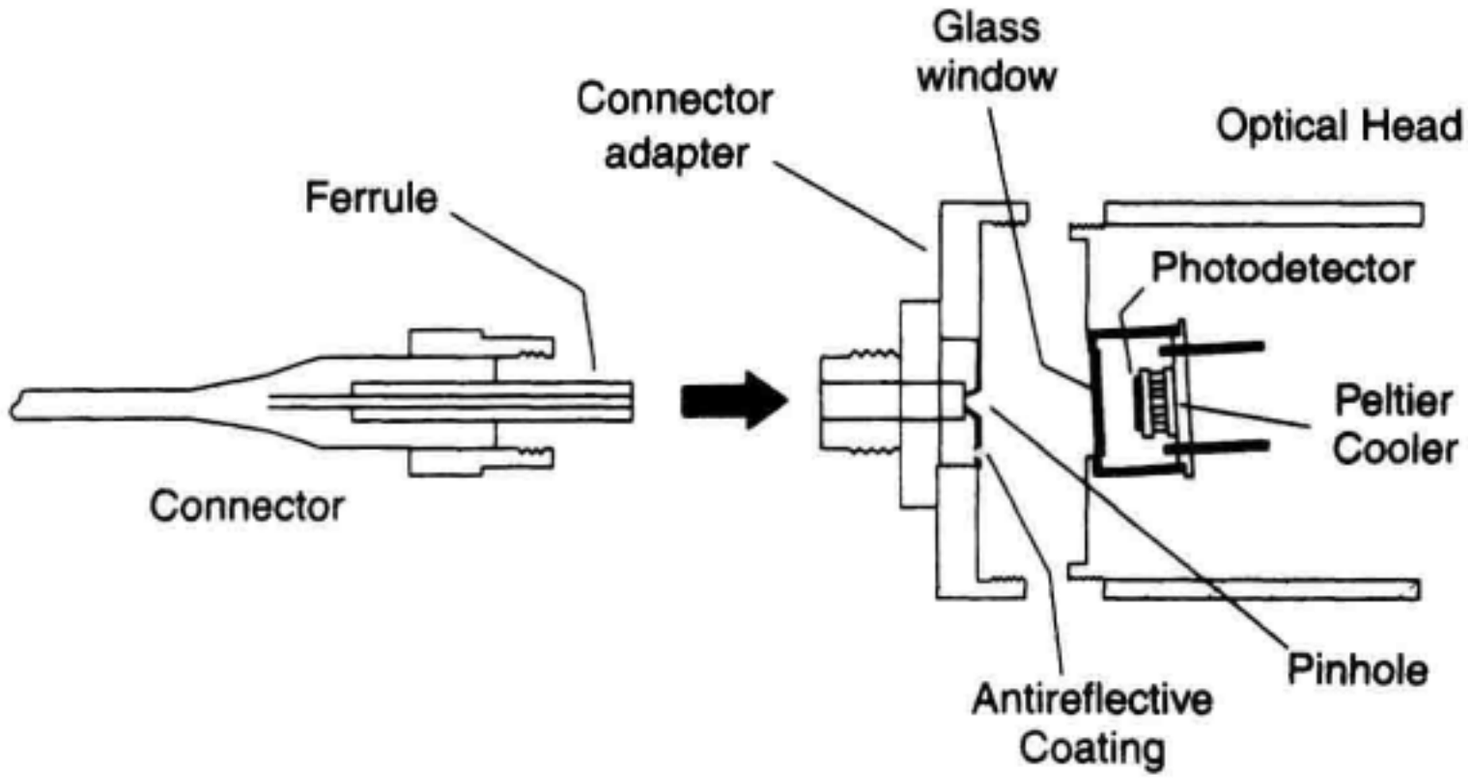

Figure 2.2 Cross-sectional view of a large-area power sensor.

Optical power measurement with photodetector-type power meters often seems as easy as voltage measurements. However, a number of critical points should be checked before a statement on the accuracy can be made. The most important contributions to accurate power measurements are:

Individual correction of wavelength dependence;
Temperature stabilization;
Wide power range with good linearity;
Good spatial homogeneity;
Low polarization dependence;
Low reflections;
Compatibility with different types of fiber.

The following sections discuss these points in more detail.

2.3.1 p-i-n-diode Operation

Figure 2.3 shows a cross-sectional view of a planar InGaAs p-i-n diode as a typical example of a photodetector.

Ideally, each incident photon is absorbed in the intrinsic (i-) layer, and an electron-hole pair is created as long as the photon energy is at least as large as the (material-dependent) bandgap energy. The holes and electrons are swept out of the i-region by the large built-in electric field. This creates the photocurrent. There are two terms which describe the conversion efficiency:

1. Quantum efficiency η, defined as the number of electrons per photon, and
2. Responsivity r, defined as the photocurrent per unit of optical power.

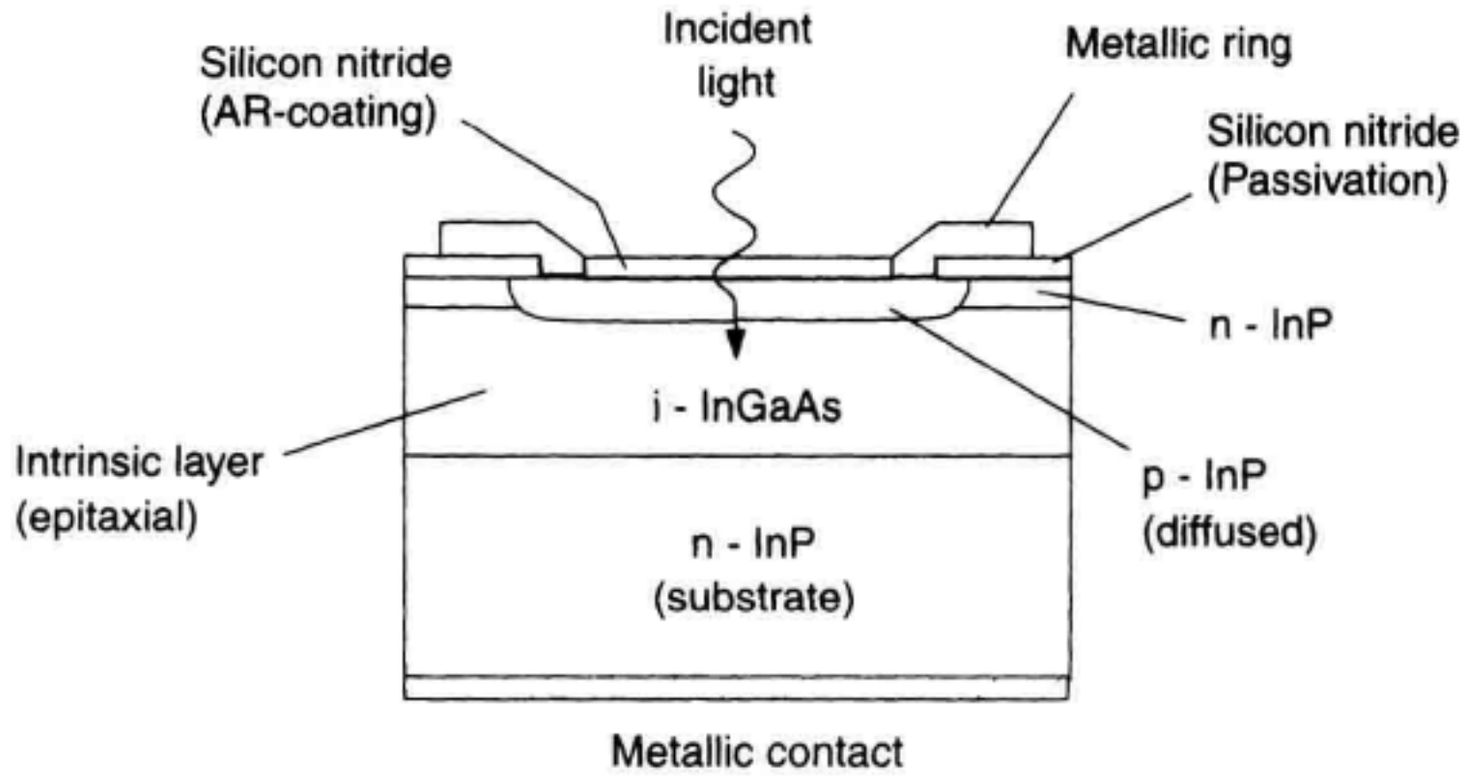

Figure 2.3 Cross-sectional view of an InGaAs photodetector.

In the ideal case of $\eta = 1$, the detector's spectral responsivity is proportional to the wavelength λ. This relation can be derived as follows: the responsivity is defined as the photocurrent, I, per unit of optical power, P:

$$r = \frac{I}{P} \tag{2.1}$$

Let us now calculate the current and optical power which correspond to each photon. Each photon represents the energy E_{ph}:

$$E_{ph} = h\nu = \frac{hc}{\lambda} \tag{2.2}$$

where h = Planck's constant, ν = optical frequency, and c = speed of light in vacuum. Optical power is defined as energy per time span Δt. In our case, the optical power which corresponds to one photon is:

$$P_{ph} = \frac{E_{ph}}{\Delta t} = \frac{hc}{\lambda \Delta t} \tag{2.3}$$

The quantum efficiency η was assumed to be 1. Then the correspondent electrical current is one electron charge q per time span Δt:

$$I_{ph} = \frac{q}{\Delta t} \tag{2.4}$$

Inserting the power and current into Equation 2.1 yields the linear spectral responsivity of an ideal photodetector with $\eta = 1$:

$$r_{(\eta=1)} = \frac{e\lambda}{hc} \tag{2.5}$$

Practical photodetectors deviate from this ideal wavelength dependence in several ways:

1. There is a long wavelength limit (cutoff wavelength) beyond which the photon energy becomes lower than the bandgap energy of the semiconductor material used. The responsivity falls off rapidly after this wavelength. The detector material determines the long wavelength limit, as shown in Figure 2.4.
2. At short wavelengths, some of the photons are absorbed outside of the i-region of the photodetector, and the number of electron-hole pairs is reduced.
3. The responsivity may also be reduced by recombination: when the electrons recombine with the holes before they reach the electrodes, then the photocurrent is reduced: another contribution to $\eta < 1$.
4. Any reflections from the detector surface or from inside the detector reduce the responsivity as well. This is a critical factor because reflections can produce substantial inaccuracies in optical power and insertion loss measurements. Pure InGaAs, for example, has a refractive index of 3.5, leading to a reflectivity of 31%. Antireflective coatings are typically used to reduce the effect. Single-layer, quarter-wavelength coatings are most often used. They reduce the reflectivity down to around 1% within a limited wavelength range. Sometimes, a periodic structure of the responsivity is observed. This indicates optical interference in the diode (see Figure 2.9). Multilayer coatings are applied when low reflectivity over a wider wavelength range is needed.

2.3.2 Spectral Responsivity

Figure 2.4 shows typical responsivity measurement results for three types of photodetectors. All three curves are normalized to a maximum of 1.

Silicon is the appropriate detector for the short-wavelength range between 500 and 1000 nm. For the long wavelength region, both germanium and InGaAs detectors can be

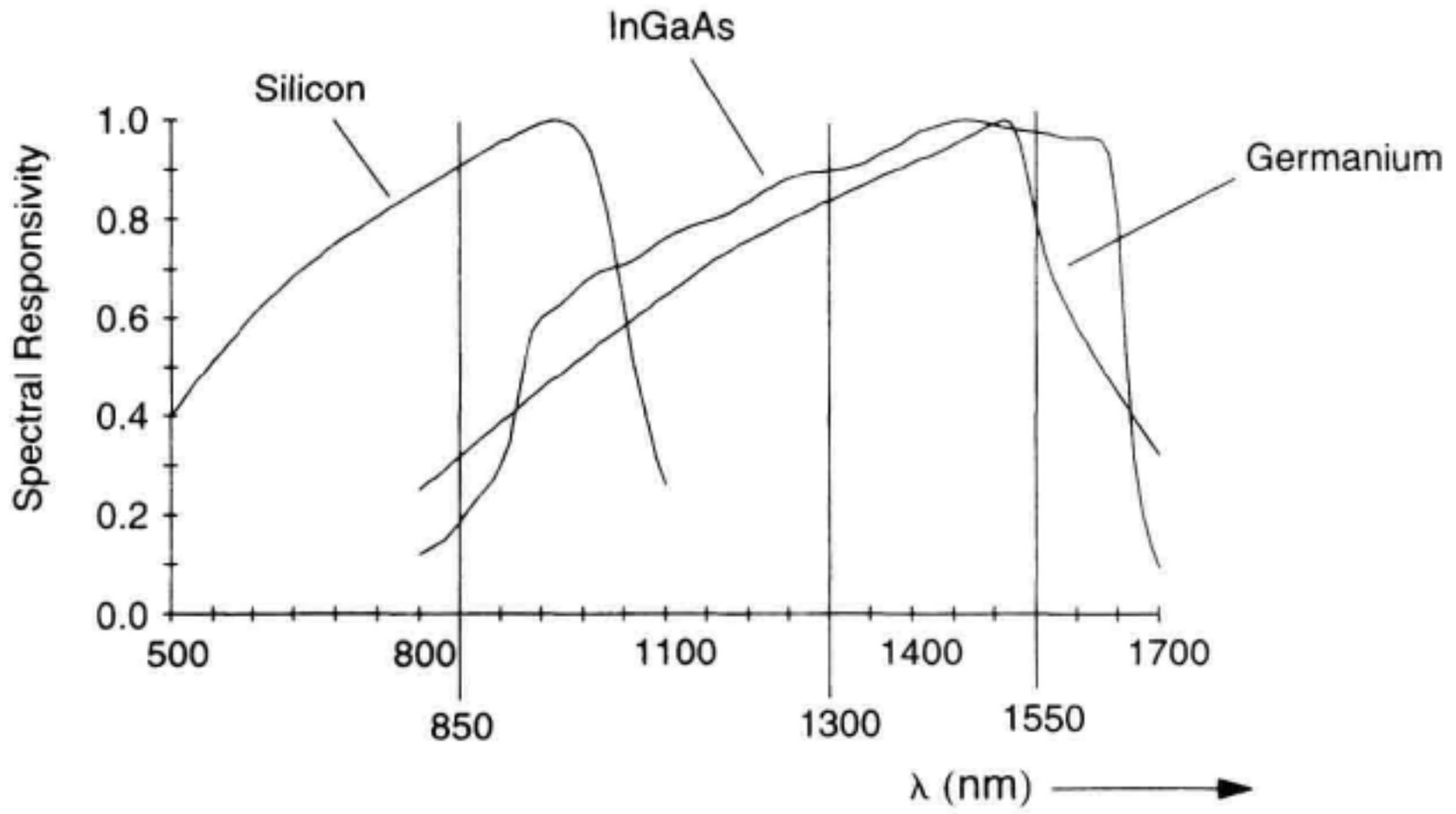

Figure 2.4 Spectral responsivities of three different detector types (all curves normalized to 1).

used. Germanium is presently the lower cost solution. It can be recommended when the sources to be measured are spectrally narrow and the wavelength is well known. This is particularly important around 1550 nm: in this region, a germanium detector produces a 1% error when the power meter's wavelength setting is incorrect by 1 nm.

In contrast, InGaAs detectors are essentially flat around 1550 nm (better than 0.1%/nm wavelength error). This makes them well-suited for optical amplifier (EDFA) applications, as the flat portion of the curve corresponds well to the usable gain region of EDFAs (1525 to 1570 nm). However, InGaAs is a more expensive technology.

2.3.3 Temperature Stabilization

Temperature-stabilized detectors can be expected to generate reproducible measurement results. Figure 2.5 shows that the responsivity of a germanium detector exhibits a relatively small temperature dependence for most of the wavelength range. In contrast, there is a substantial change beyond the cutoff wavelength, for example, at 1550 nm. This change can be most easily described as a shift of cutoff wavelength, in this case approximately 1 nm/K. Nearly the same wavelength shift, 1 nm/K, can be observed in InGaAs detectors at wavelengths around 1650 nm.

2.3.4 Spatial Homogeneity

The responsivity of photodetectors can vary across the detector surface. Figure 2.6 shows an example of the relative responsivity of an InGaAs photodetector of 5 mm diameter at 1550 nm. Wide variations in the homogeneity of commercial detectors—from perfect to marginal (as in Figure 2.6)—are usually observed.

Inhomogeneous photodetector surfaces create measurement uncertainties because the position and diameter of the incident beam cannot be perfectly controlled. This is especially true for multimode fibers, where speckle-pattern effects will cause the power distribution in the fiber cross-section to fluctuate.

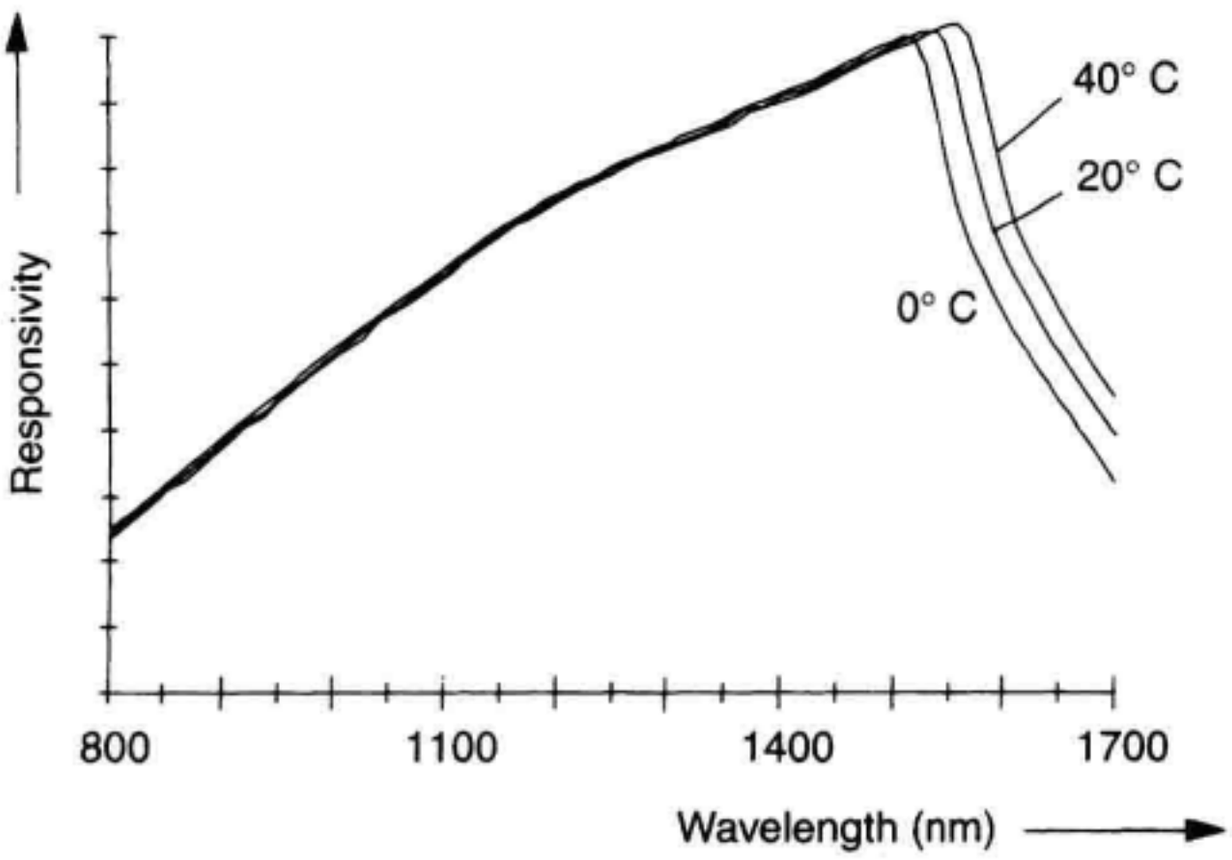

Figure 2.5 Spectral responsivity of a germanium detector at different temperatures.

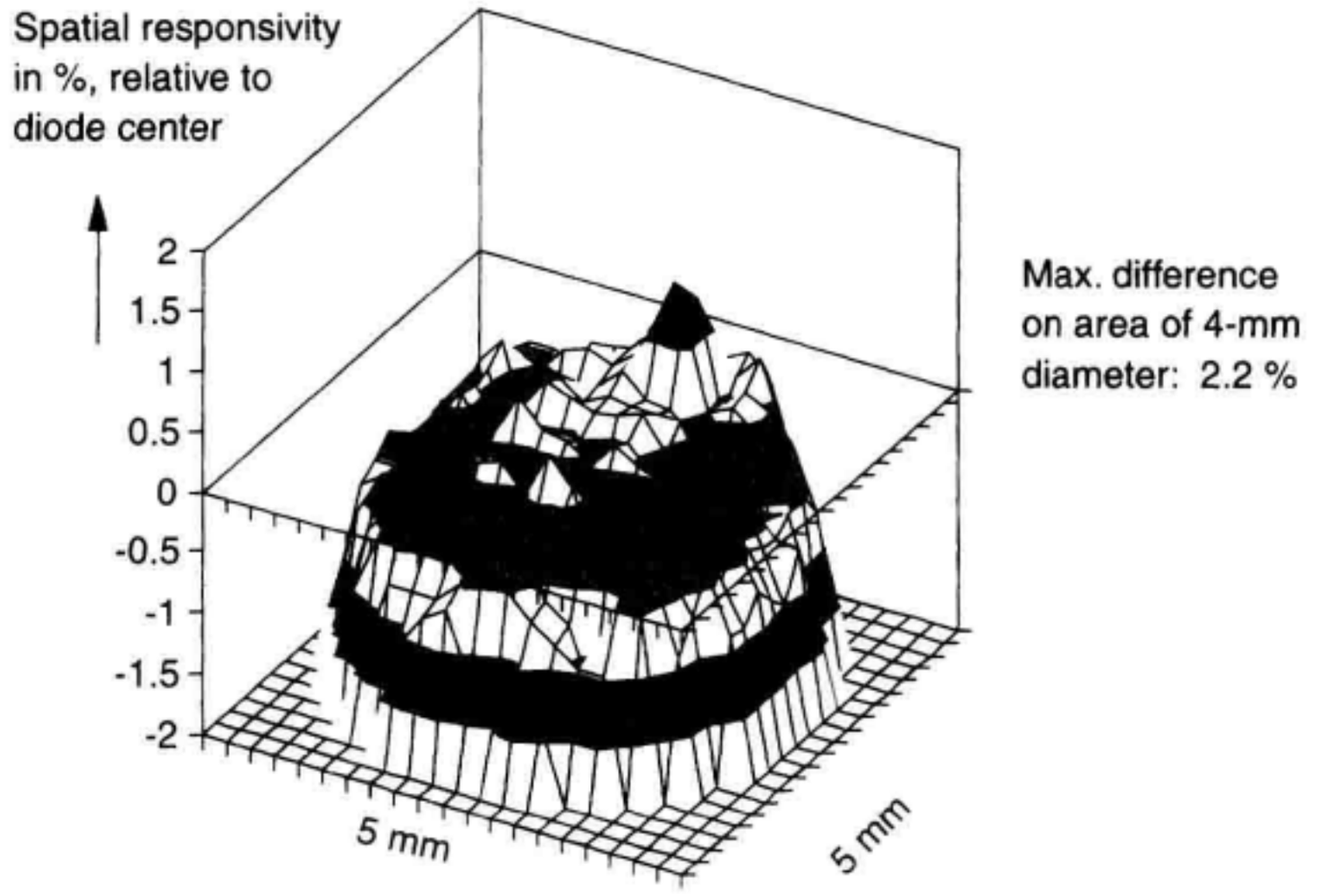

Figure 2.6 Spatial homogeneity of an InGaAs detector, measured at 1550 nm.

2.3.5 Power Range and Nonlinearity

Ideally, optical power meters display correct measurement results over many decades of optical power. However, this capability is often impaired by the meter's nonlinearity. Measurement linearity is important for accurate insertion loss (or gain) measurements. In an optical power meter, nonlinearity contributors can be classified into:

1. The photodetector nonlinearity: Photodetectors are usually thought to be very linear over six or more decades of optical power. However, there are three effects which may cause limitations:
   a. noise at low power levels;
   b. supralinearity at medium power levels;
   c. saturation at high power levels.
2. The electronic nonlinearity which can be split into:
   a. the in-range nonlinearity of the analog amplifier that follows the photodetector, for example offset at low power levels and amplifier saturation at high power levels;
   b. the ranging discontinuity observed by switching from one power range to another, caused by nonmatching amplifier gains.

The nonlinearity is defined as:

$$N(P) = \frac{r(P) - r(P_0)}{r(P_0)} \tag{2.6}$$

where $r(P)$ is the power meter's responsivity at an arbitrary power level, and $r(P_0)$ is the responsivity at the reference level (usually 10 μW). The nonlinearity is usually wavelength-dependent, due to the wavelength-dependent photodetector characteristics. Notice that a different, but equivalent, definition of the nonlinearity is given in Section 2.6.

Figure 2.7 illustrates the nonlinearity effects listed above.

The choice of reference level influences the nonlinearities (by definition, the nonlinearity is zero at the reference level). However, the choice of reference level has no influence on the accuracy of insertion-loss measurements. It can be shown that the loss measurement error due to nonlinearity is the *difference* between the nonlinearities at the two relevant power levels. This difference is independent from the reference level.

The low end of the power range is usually limited by the detector's shot noise due to dark current. The dark current depends on the active area and on the semiconductor material. When comparing detectors of the same diameter, InGaAs detectors have up to 100 times lower dark currents than germanium detectors.

One might expect that the dark current is eliminated by operating the detector at zero-bias voltage. This is correct for the diode-external current only. Internally, the dark current is compensated by an equally large diffusion current, where both currents produce shot noise. Accordingly, the shot noise current at zero input power is given by:[5]

$$<i_n^2> \; = 2\,q\,B_n \Sigma I = 2qB_n \times 2I_{\text{dark}} \;\; [A^2] \tag{2.7}$$

where q = electron charge, ΣI = total current, I_{dark} = dark current, and B_n = noise equivalent bandwidth. Time averaging is indicated by brackets $< >$. Note that the shot noise is frequency-independent.

Under light exposure, the photocurrent adds to the total current and produces additional shot noise:

$$<i_n^2> \; = 2\,e\,B_n \Sigma I = 2eB_n(2I_{\text{dark}} + rP_{\text{opt}}) \tag{2.8}$$

where r = responsivity and P_{opt} = received optical power.

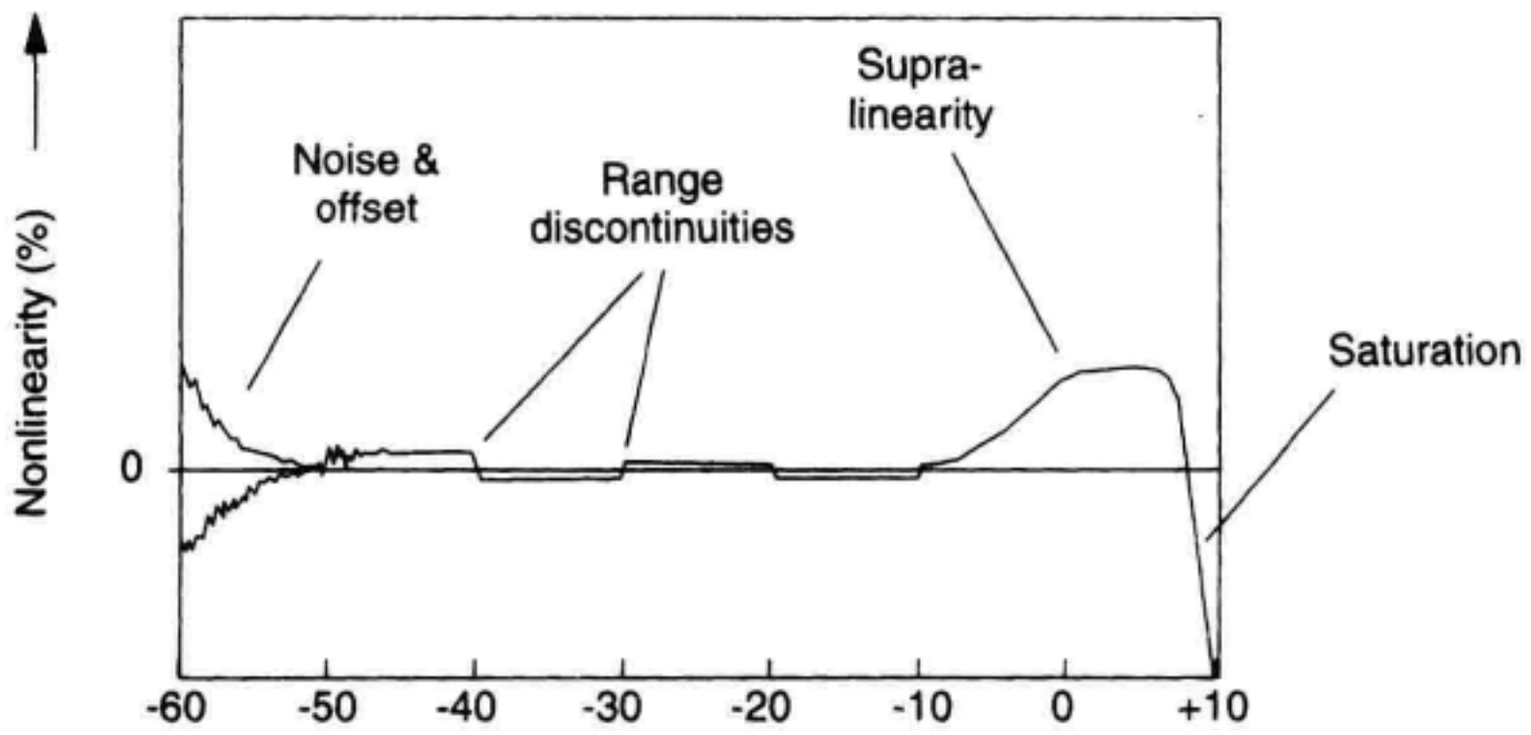

Figure 2.7 Possible nonlinearity effects of an optical power meter.

To relate this to power meter noise, the shot noise can be expressed as noise-equivalent power NEP (this is an RMS value):

$$\text{NEP} = \frac{1}{r}\sqrt{[i_n^2]} = \frac{1}{r}\sqrt{2eB_n(2I_{\text{dark}} + rP_{\text{opt}})}\left[\frac{W}{\sqrt{Hz}}\right] \tag{2.9}$$

A signal-to-noise ratio, *SNR*, can be calculated using:

$$\text{SNR} = \frac{P_{\text{opt}}}{\text{NEP}} \tag{2.10}$$

Figure 2.8 shows an example of the power dependence of the SNR. It was calculated using a dark current of 1.5 μA (a typical value for a germanium detector of 5 mm diameter at 25C) and a noise equivalent bandwidth of 100 Hz. At low power levels, the SNR increases by 10 dB for every 10 dB increase in optical power. At higher power levels, where the photocurrent becomes larger than the dark current, the SNR increases by only 5 dB for every 10 dB power increase. This is because the noise level increases with the optical power.

The lowest SNRs exist at low power levels. An improvement is possible by reducing the dark current: either by cooling or by reducing the detector's active area (the dark current is proportional to the active area). A longer averaging time also reduces the noise problem. Variable averaging time should be implemented in a modern power meter.

Range discontinuities are caused by the necessity to switch the gain of the electronic amplifier, depending on the input power level. Otherwise, a power range of more than six decades could not be realized. A range discontinuity means that the power meter does not display exactly the same power level when switching between power ranges. These effects should be substantially lower than 1% in a good power meter.

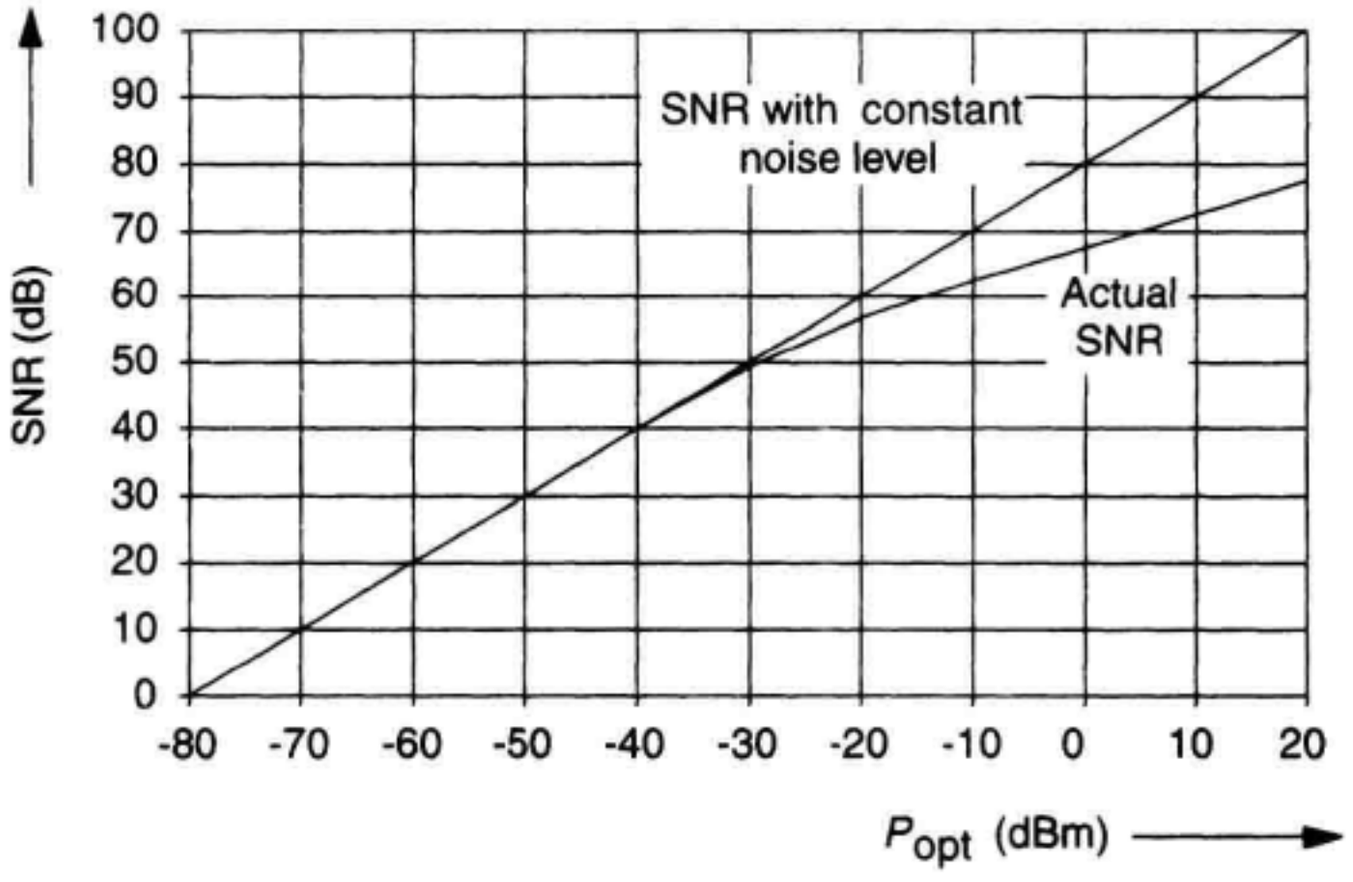

Figure 2.8 Power dependence of the signal-to-noise ratio (example).

A less-known nonlinearity effect is *supralinearity,* an increase in responsivity typically starting at power levels of around 100 μW. To our knowledge, this effect has not been carefully studied. A possible explanation is "traps" in the semiconductor material causing increased recombination at low power levels. When the power reaches higher levels, then these traps become saturated, the recombination decreases, and the responsivity increases. The correspondent nonlinearity can reach several percent. The strongest supralinearity effects are usually observed at the borders of the usable wavelength range of the specific detector. See Stock[6] for more details.

On the high power end, the responsivity drops due to *saturation,* caused by a reduction of the electric field across the pn-junction along with recombination in the active region. This effect starts at input powers of typically a few milliwatts. For many years, such power levels corresponded well to the output power levels of commercial laser diodes. With the advent of optical amplifiers, this situation has changed dramatically: Today's pump lasers produce optical powers in the 100 mW region, and optical amplifiers capable of more than 1 W output power are commercially available. Neutral-density filtering or power splitting can be used to shift the power scale to higher levels. Section 2.4.2 covers the area of high-power measurement.

2.3.6 Polarization Dependence

Crystalline structures in the semiconductor material and in the photodetector's coating or mechanical stress in the detector are the usual causes for polarization dependence in optical detectors. Also, detectors are often tilted against the beam axis to reduce multiple reflections. Tilting always causes additional polarization dependence. The polarization dependencies of modern large-area photodetectors range from a few 0.001 dB peak-to-peak for selected straight detectors to 0.05 dB peak-to-peak in unselected angled detectors. A relatively strong wavelength dependence of the polarization characteristics can also be observed and is usually caused by the quality of the antireflective coating. Beyond the cutoff wavelength, the detector material becomes transparent which tends to increase the polarization dependence as well.

2.3.7 Optical Reflectivity and Interference Effects

Without antireflective coatings, optical detectors exhibit reflectivities up to 30% (see section 2.3.1). Such detectors cause multiple reflection- and optical-interference problems in absolute power- and insertion-loss measurements. This is the reason why all commercial detectors feature antireflective coating, for example, silica on silicon detectors and silicon nitride on InGaAs detectors (see Figure 2.3).

Figure 2.9 shows the measured reflectance of an InGaAs photodetector with a single-layer antireflective coating made from silicon nitride with a thickness of a quarter wavelength. Silicon nitride has a refractive index $n = 1.95$ and acts as an impedance transformer matching the refractive index of InP ($n = 3.2$) with air ($n = 1$). The quarter-wave layer is responsible for the overall minimum around 1250 nm for this specific diode. While ideally there should be a gentle minimum, the measurement shows some additional ripple. This is caused by the upper InP-layer (see Figure 2.3) which forms an additional

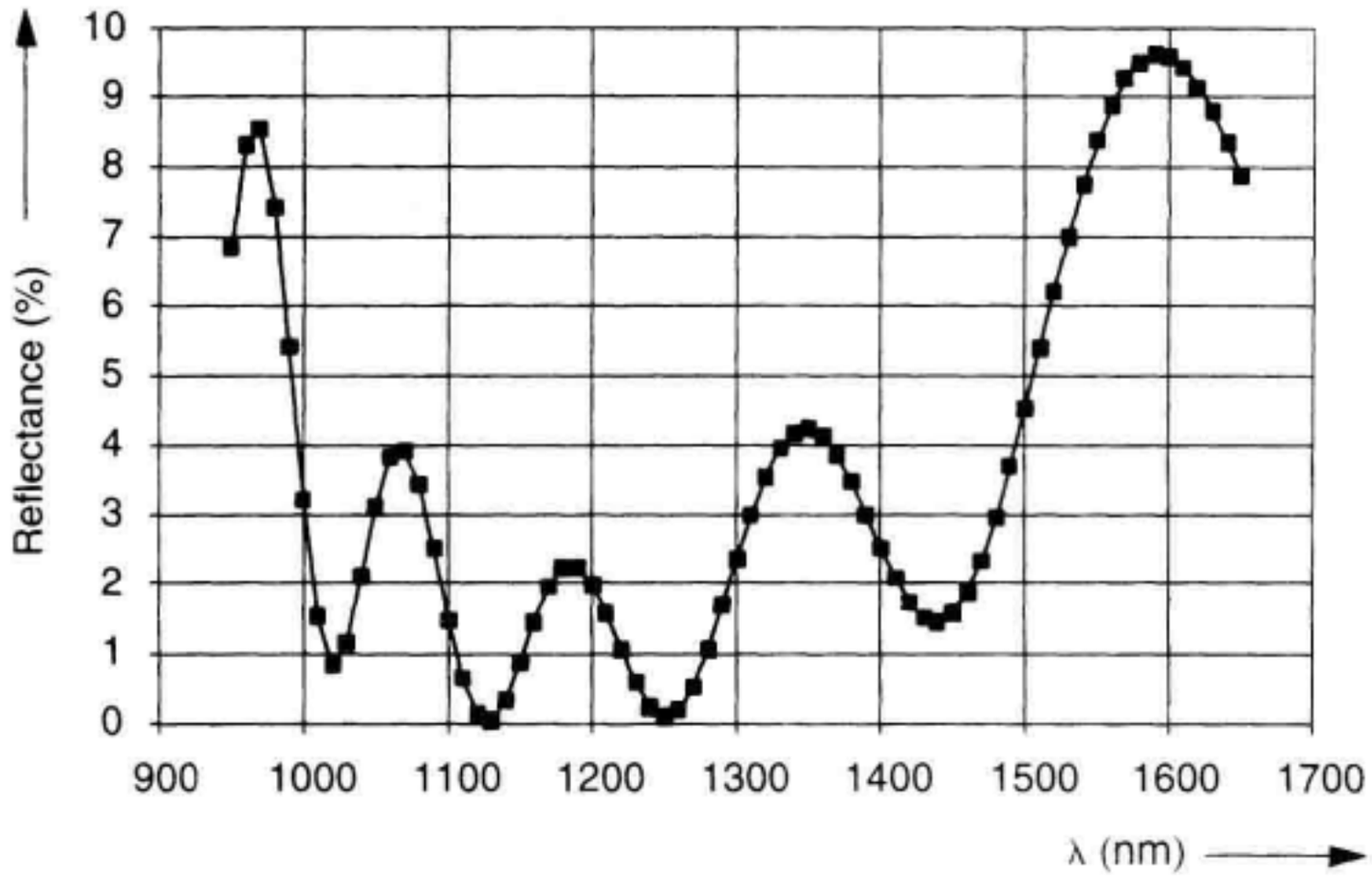

Figure 2.9 Typical reflection pattern of an InGaAs detector with AR coating.

resonator due to the fact that InP has a refractive index of 3.2, in contrast to the refractive index of 3.52 for the intrinsic InGaAs layer.

The result is a wavelength-dependent reflectance between 1% and 10%. Another typical characteristic is that the reflectance varies substantially from detector to detector: It is obvious that a slight thickness change of the InP layer shifts the pattern to a different wavelength.

Reflections and optical interference can also be created by the glass cap which usually covers the detector can. The glass can itself act as a resonator if it is sufficiently flat. Therefore, glass caps with perfect optical quality are to be avoided.

Figure 2.2 demonstrates that reflections from the detector surface *or* the glass cap go back to the connector adapter and the connector. From there, doubly reflected light can strike the detector again. These effects were first mentioned in Gallawa and Li.[7] If the detector is sufficiently large, then the unwanted power fraction on the detector is the product of the photodetector reflectance and the reflectance of the optical interface. To reduce these problems, the adapter of Figure 2.2 is coated with an antireflective coating on the inside, and a pinhole shields the highly reflective connector end.

2.3.8 Compatibility with Different Fibers

A wide range of optical fibers are used in fiber optic communication. There is usually no problem measuring the power from a standard singlemode fiber with its small numerical aperture of 0.1. In contrast, it can be very difficult to measure the output power from a thin-core singlemode fiber with a high numerical aperture of 0.4 (used in optical amplifiers). In some cases, the fiber end may even be angled to reduce optical reflection problems. Then the effective numerical aperture increases even further.

Compatibility with Singlemode Fibers. The far-field power density (irradiance) from a singlemode fiber, $H(z)$, is usually described by a gaussian beam:

$$H(z) = H_0 \exp - \frac{2r^2}{w(z)^2} \tag{2.11}$$

where z = distance from the source on the beam axis (see Figure 2.10), w = radius of the beam waist at which the power has dropped to $1/e^2$, at the distance z, and r = radial distance from the optical axis.

The numerical aperture of the fiber is defined by the 5% angle of the far field. If the detector diameter coincides with the circle created by the numerical aperture, then the detector misses 5% of the total beam power. The corresponding 95% detector radius is:

$$r_{\text{det}} = z\frac{NA}{\sqrt{1 - NA^2}} \cong zNA \tag{2.12}$$

Generally, when the power density at the detector radius has decayed to $x\%$, then there is $x\%$ of the total power outside the detector. This is a property of the gaussian beam. The coupling efficiency is given by:

$$\eta = 1 - \exp\left[-\frac{2r_{\text{det}}{}^2}{w^2}\right] \tag{2.13}$$

It is advisable to replace w, the $1/e^2$ beam radius, by the 5% beam radius which corresponds to the fiber's numerical aperture. The gaussian beam profile yields:

$$w = 0.817r_{5\%} = 0.817\ zNA \tag{2.14}$$

Then the coupling efficiency can be expressed on the basis of the numerical aperture:

$$\eta = 1 - \exp\left[-\left(\frac{1.71r_{\text{det}}}{zNA}\right)^2\right] \tag{2.15}$$

Example: If the detector radius is 2.5 mm, the distance between the fiber end and the detector is 8 mm (as in the power meter of Figure 2.2), and the numerical aperture of the singlemode fiber is 0.3, then the coupling efficiency is 96%, indicating the aperture limitation of this power meter configuration.

Compatibility with Angled Fiber Ends. Special care must be taken to capture light from angled fiber ends. Angled fiber ends are aimed at reducing reflections. Figure 2.10 shows a singlemode fiber, both with straight and angled fiber end. Let us assume that, in the case of the straight fiber end, the detector captures the beam fully, and that in the angled case the detector misses a part of the beam.

In both cases, the numerical aperture of the fiber is defined by the 5%-angle γ of the far field. In the angled case, the tilt of the beam axis, β, can be calculated using Shell's law:

$$\beta = \arcsin(n \sin \alpha) \cong (n - 1)\alpha \tag{2.16}$$

The effective numerical aperture for the angled case is:

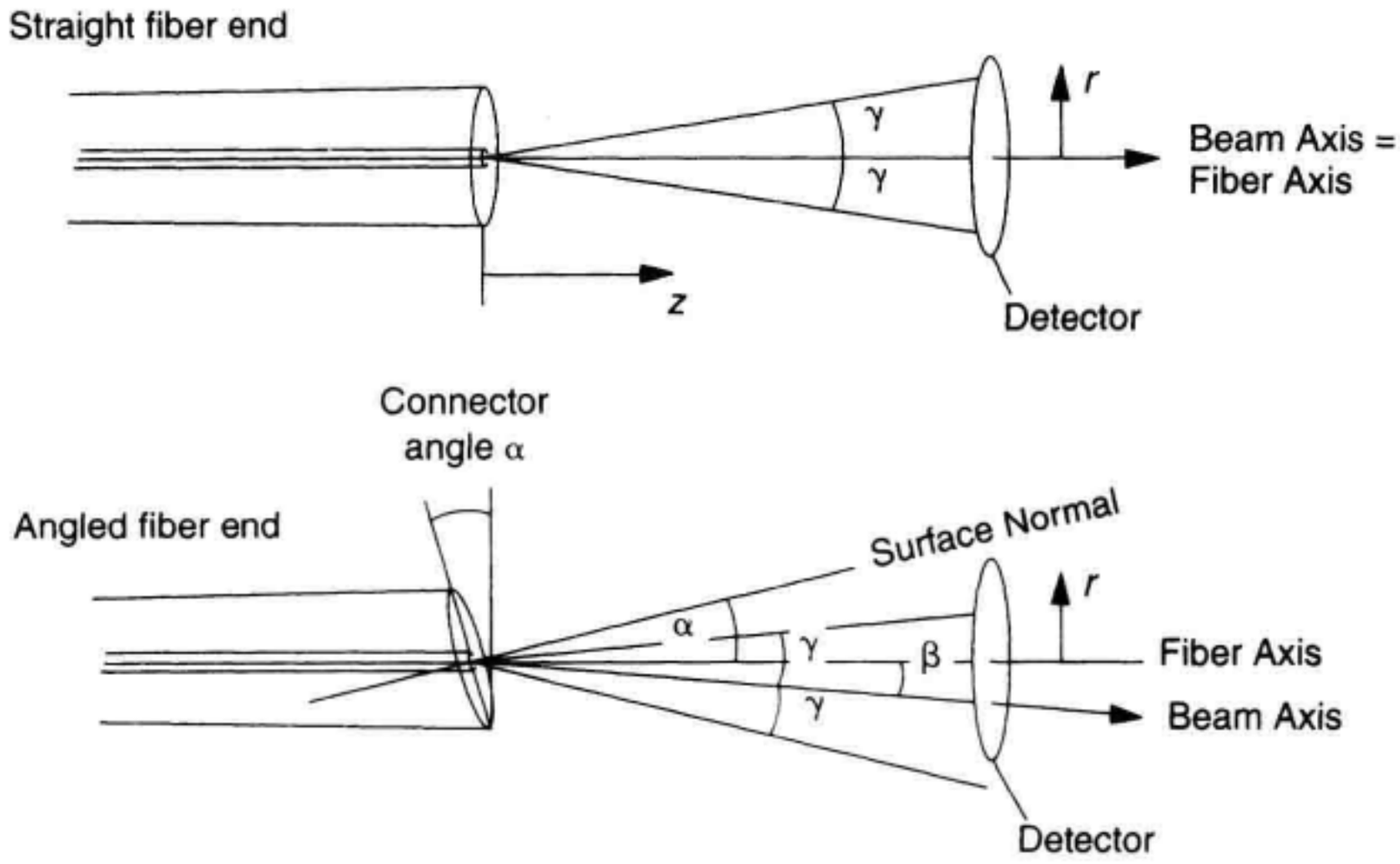

Figure 2.10 Power measurements from straight and angled fiber end.

$$\mathrm{NA}_{\mathrm{eff}} = \sin(\gamma + \beta) \tag{2.17}$$

in comparison to simply NA = sin γ for the straight case. A shorter distance to the detector would be needed to capture the beam fully. Other possibilities are:

1. Tilting the fiber, so that the beam axis is realigned to hit the center of the detector; or
2. Using a lens to reduce the effective beam diameter (see Figure 2.11).

Compatibility with Fibers of High NA. Some of the fibers used in conjunction with optical amplifiers are thin-core, high-numerical-aperture fibers. Numerical apertures up to 0.4 and even 0.5 are not unusual. Such numerical apertures can also occur with multimode fibers. Ideally, a power meter should present the same responsivity to all parts of the beam. In situations with high numerical aperture, this requirement is hard to meet. For a given photodetector diameter, often 5 mm, there are three possibilities:

1. Decreasing the distance between fiber end and photodetector. This solution may cause reflection problems because the fiber tends to capture more of the power that is reflected from the detector surface. Another problem can be caused by the fact that the photodetector's responsivity is lower for those parts of the beam that hit the detector at larger angles.
2. Using a lens with high numerical aperture in order to collimate the beam. This solution can also create problems because light emitted at larger angles will be more strongly reflected off the lens than the on-axis beams. Figure 2.11 shows the power meter of Figure 2.2 with a lens inserted into the beam path; this assembly captures

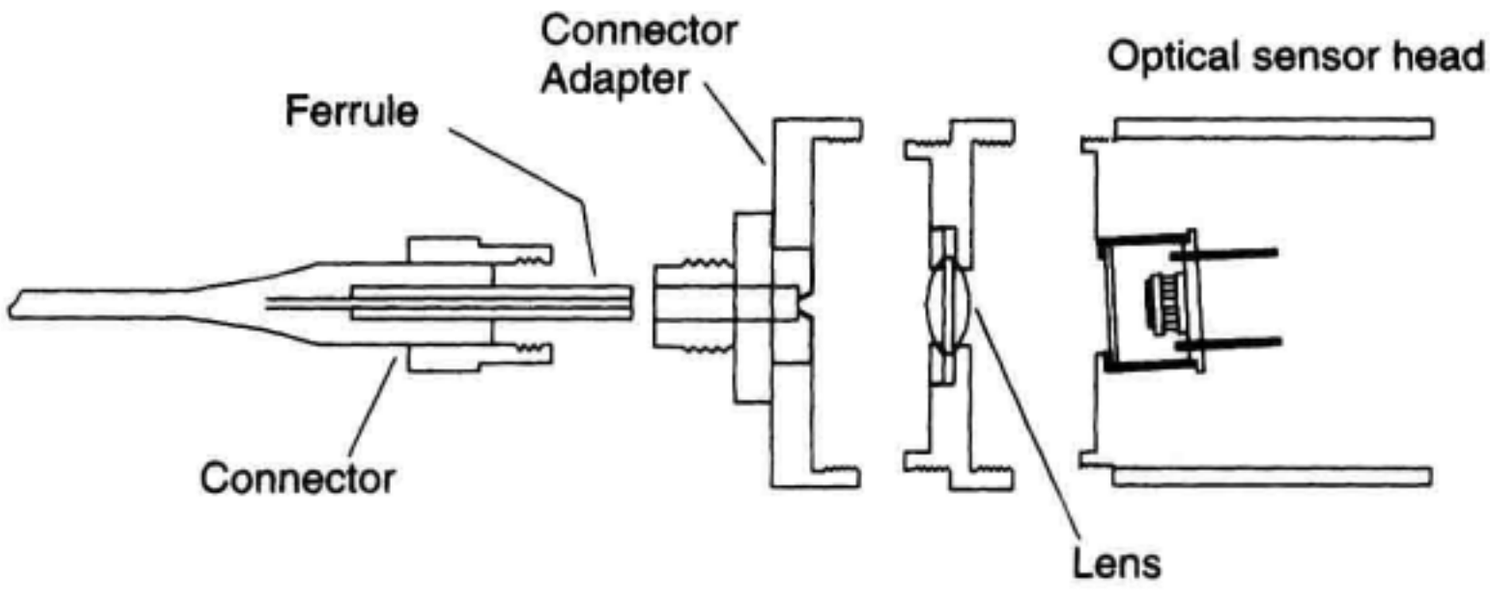

Figure 2.11 Using a lens to capture beams of higher numerical aperture.

approximately 98% of the total power for numerical apertures of 0.3. Tilting the detector becomes an important detail of this solution because otherwise the reflected power would be imaged back into the fiber. The insertion loss of the lens can be calibrated out as discussed below.

3. Using an integrating sphere in combination with the photodetector. Ideally, an integrating sphere should perfectly scatter all incident light so that the power measurement result becomes independent on the fiber's numerical aperture. To accomplish this, the detector should not be exposed to either direct beams from the source or to beams after only one reflection (see Figure 2.12). Even under those conditions, measurements have shown that commercial integrating spheres also have some angle-dependent responsivities depending on their construction. Particularly beams forming large angles (high numerical aperture) against the connector axis go through different attenuations than the near-axis beams.

In addition, some of the materials used to scatter the beam inside the integrating sphere tend to absorb moisture, so that the scattering characteristics change with the relative humidity. Integrating spheres are capable of high-power measurement, because the optical

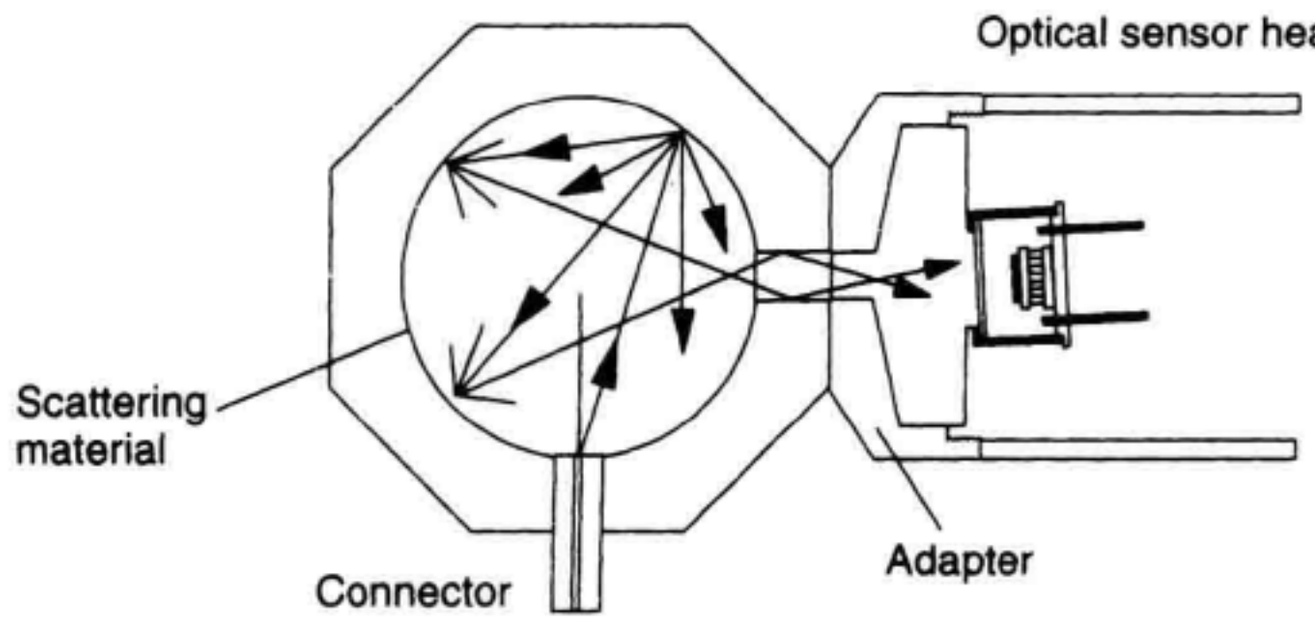

Figure 2.12 Optical power measurement with integrating sphere.

power is attenuated by 30 dB or more before it reaches the detector, and because the absorption takes place over a relatively large area.

Compatibility with Multimode Fibers. Multimode fibers, particularly graded-index multimode fibers, generate irregular far-field patterns (speckle patterns) which are caused by optical interference between the different fiber modes. This is only a problem when the source is a laser diode; the spectral width of an LED is too large to create optical interference. Speckle patterns go through rapid changes when the fiber is moved, because changing the path lengths of the individual modes by only fractions of the wavelength creates a different speckle pattern.

Along with these rapid changes, speckle patterns usually create additional uncertainties because the photocurrent is a convolution of the speckle pattern with the detector's spatial homogeneity (see Section 2.3.4).

The numerical aperture of multimode fibers ranges from 0.2 to 0.5 depending on the core diameter and refractive-index profile. Therefore, the problems of multimode fibers are essentially the same as for thin-core singlemode fibers.

2.4 ABSOLUTE POWER MEASUREMENT

Absolute optical power, in mW or dBm (decibels relative to 1 mW) is a key parameter for all optical sources. Figure 2.13 shows an example of an absolute power measurement in which the power from a pigtailed laser diode is measured. This is a typical production test, to ensure the appropriate system margin or that the laser meets the specified performance.

While this measurement seems simple, there are a number of questions to be answered before the measurement result can be claimed to be accurate. It is obvious that most of these questions are related to the performance of the power meter used, and that there may be substantial differences in measurement results when different types of power meters are used. See the discussion on the uncertainty of absolute power measurement in Section 2.4.3.

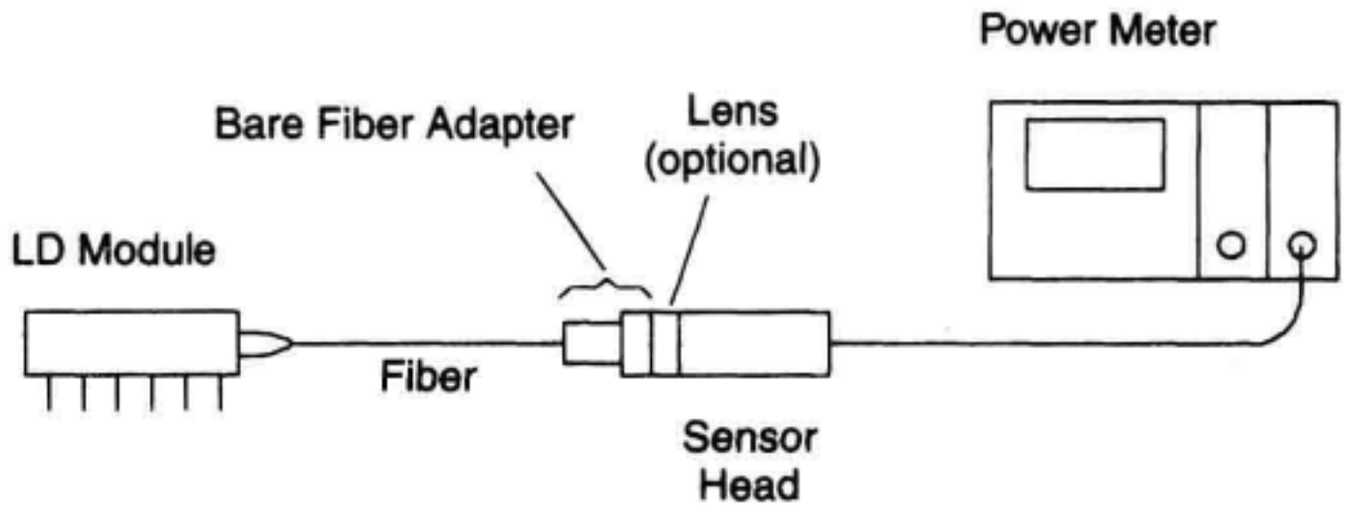

Figure 2.13 Power measurement of a pigtailed laser diode.

Before the discussion of the uncertainties, two specific examples of absolute power measurement are analyzed in more detail below: LED measurement and high-power measurement.

2.4.1 LED-Power Measurement

In contrast to the power from narrow-linewidth laser diodes, LED power is sometimes difficult to measure because of the LED's wide spectral width and the fact that the photodetector's responsivity changes within this spectral range. However, a correction is possible when the detector's spectral responsivity and the LED's spectral power density are known. Figure 2.14 depicts the situation for the example of a 1550 nm LED and a germanium detector.

The symbols in Figure 2.14 are as follows:

λ_0 = arbitrarily chosen wavelength (preferably the LED peak wavelength) for which the power meter is corrected;
$r_{rel}K(\lambda)$ = responsivity relative to λ_0, where $r_{rel}(\lambda_0) = 1$;
p_0 = spectral power density of the LED at the wavelength λ_0, in watts/nm;
$f(\lambda)$ = factor describing the LED's spectral emission, where $f(\lambda_0) = 1$.
On this basis, the correct LED power is:

$$P = p_0 \int f(\lambda)\delta\lambda \tag{2.18}$$

In contrast, the uncorrected measurement result is:

$$P_m = p_0 \int f(\lambda) r_{rel}(\lambda) d\lambda \tag{2.19}$$

Accordingly, a correction factor can be calculated to be:

$$K = \frac{P}{P_m} = \frac{\int f(\lambda)d\lambda}{\int f(\lambda) r_{rel}(\lambda)d\lambda} \tag{2.20}$$

Analyzing this equation shows that there is no error if the LED spectrum is symmetrical *and* the detector's responsivity is linearly changing with respect to wavelength. However, this is not generally the case.

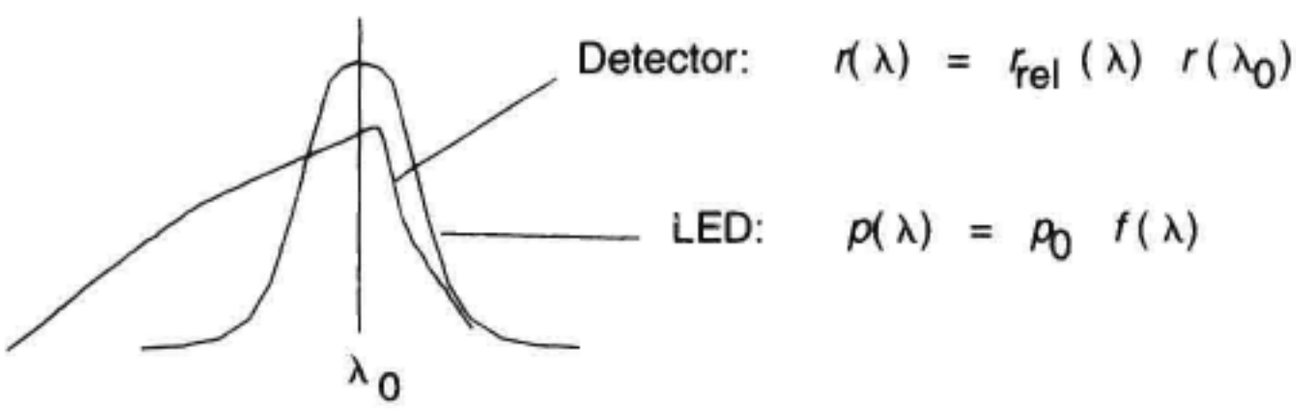

Figure 2.14 Modeling an LED and a photodetector.

The following measurement procedure is suggested:

1. Determine the LED's center wavelength, for example, from its data sheet.
2. Set the power meter to the LED's wavelength λ_0 and measure the LED power.
3. If the LED spectrum is essentially symmetrical and the photodetector's responsivity is nearly linear within the LED's spectral band, use the measured power as the result.

   If one of these conditions is not met, then calculate the correction factor as in Equation 2.20 and multiply the measured power with the correction factor to obtain the correct power.

2.4.2 High-Power Measurement

Optical power meters based on photodetectors can measure maximum power levels of a few milliwatts. Beyond this power level, the photodetector goes into saturation. For many years, such power levels were sufficient, because they corresponded well to the output power levels of commercial laser diodes.

The advent of optical amplifiers changed this situation. The complication starts with the pump lasers, which produce 100 mW or more. The amplifiers' output powers must be measured as well. Except for preamplifiers, designed to generate a few milliwatts at the most, all optical amplifiers generate power levels exceeding the measurement range of conventional power meters. Today, the highest powers from EDFAs exceed 1 watt. Since the output power is a key parameter, the question is: How can such large power levels be measured with good accuracy?

Figure 2.15 shows a commercial high-power optical head with a 5 mm InGaAs detector and a window made from absorbing glass, to reduce the incident optical power to a suitable level. It can measure up to 500 mW. In order to prevent local overheating of the absorber at power levels exceeding 100 mW, it is recommended to create a spot diameter of not less than 3 mm on the detector (measured at the 5% points). At the given distance of 8 mm between the fiber end and the detector, a 3 mm spot is obtained when the numer-

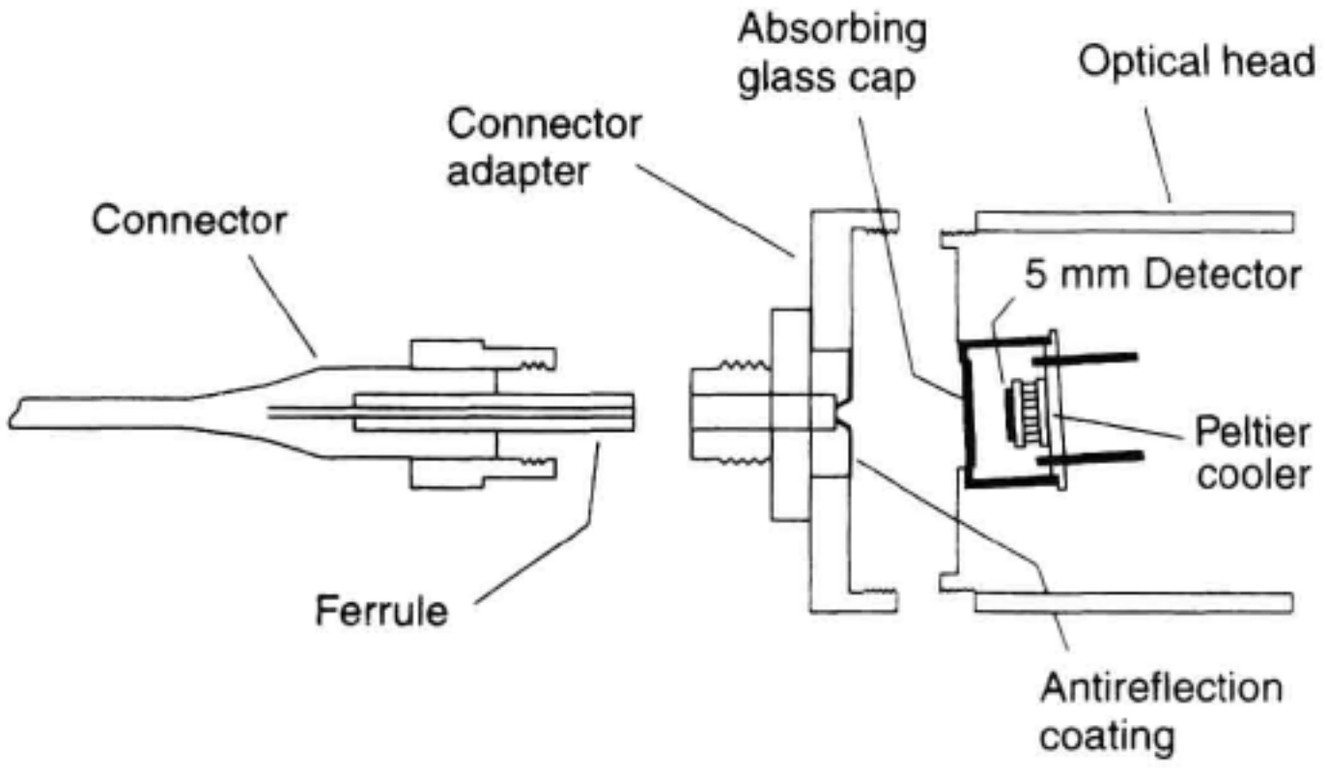

Figure 2.15 High-power measurement with absorber in front of the detector.

ical aperture of the fiber is 0.2. In this case, the coupling ratio is 100%. A beam with a numerical aperture of 0.3 will create a spot diameter of 4.5 mm and a coupling ratio of 96%. A standard singlemode fiber with a numerical aperture of 0.1 yields a spot diameter of only 1.5 mm; in this case a simple spacer between the adapter and the optical head can be used to create a spot diameter of 3 mm.

Alternative solutions for high-power measurement are:

1. Inserting a mesh-type filter consisting of thin wires between the fiber end and the detector. This solution has wide wavelength range and high-power capability, because increased wire temperature will not influence the attenuation.
2. Inserting a scattering filter, for example, a ceramic disc between the fiber end and the detector. This technique also has wide wavelength range and high-power capability. In addition, scattering introduces depolarization, thereby reducing the polarization dependence of the optical head. A polarization dependence of 0.003 dB p-p can be achieved in conjunction with an FP laser diode, and 0.015 dB p-p for a single-line laser, for example, a DFB laser or an external-cavity laser (ECL). A disadvantage is the fact that different beam geometries (fiber types) will cause different attenuations, because this technique splits power away from the detector.
3. Splitting some power away before the measurement, for example, with the help of a fiber coupler. This solution is limited to certain fiber types because the coupler fibers must be of the same type as the fiber to be measured.
4. Inserting an integrating sphere between the fiber end and the detector; see the discussion in Section 2.3.8. This is usually an expensive solution, where some angle dependence and dependence on relative humidity may have to be taken into account.

Several of these techniques can be combined, too. Notice that a collimating lens may have to be inserted before these filters to ensure that beam diameter remains smaller than the detector diameter.

Common to all of the above techniques is the need for calibrating the filter attenuation. Figure 2.16 shows the calibration setup. An optical attenuator may have to be inserted between the source and the detector to ensure stable output power.

The calibration is a simple two-step procedure which can be performed by the user (for the specific fiber and wavelength used): Set a power level that can be handled by the unattenuated sensor, measure the power, P_1, attach the filter and measure the power again, P_2. The desired filter attenuation is the ratio of the two power levels.

2.4.3 Uncertainties in Absolute-Power Measurement

The following partial uncertainties should be considered in absolute-power measurements. As usual, root-sum-squaring can be used to calculate the total uncertainty.

1. Random uncertainty, for example, due to the power instability of the source: Power instabilities could be inherent to the source or caused by external reflections travel-

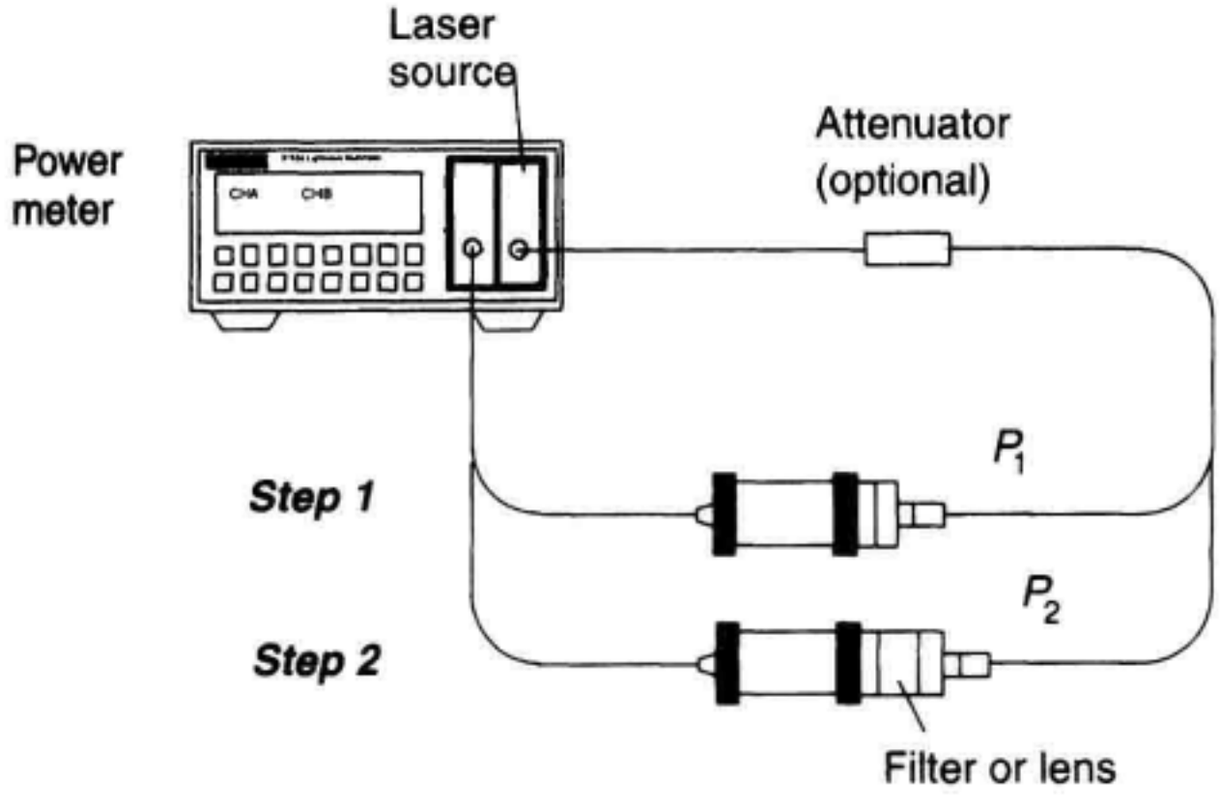

Figure 2.16 Calibrating filtered- or lensed-detectors.

ing back to the source. Most laser sources are sensitive to reflections. This uncertainty depends strongly on the specific situation. It can range from less than 0.1% to several percent.

2. Systematic uncertainty due to power-meter calibration: It is assumed that the power meter is regularly recalibrated following the manufacturer's recommendations and that the wavelength correction is set to the wavelength of the source. The absolute uncertainty and the conditions for which this uncertainty applies should be obtained from the power meter's data sheet (for example, power range, numerical aperture of the fiber, connectors, and wavelength). Absolute uncertainties are ±2% in the best case.

If the actual measurement conditions coincide with the specified conditions, then the uncertainty analysis ends here. If not, then consider the following:

3. Systematic uncertainty due to wavelength: The wavelength of the source (center wavelength) should be accurately known. Otherwise, the partial uncertainty will be the wavelength uncertainty multiplied by the power meter's responsivity versus wavelength slope (%/nm) at that wavelength.
4. Systematic uncertainty due to the spectral width of the source: In the measurement of laser diodes, this uncertainty will usually be negligible. In LED measurement, there will be no error if the spectrum is symmetrical about the center wavelength and the power meter's responsivity is linear within the wavelength range of interest. Otherwise a correction factor or an uncertainty can be calculated on the basis of Section 2.4.1.
5. Systematic uncertainty due to beam geometry: In the best case, the beam is centered on the detector and the beam diameter is about $^2/_3$ of the detector diameter. If this is not the case, then an appropriate uncertainty may have to be calculated. Particularly,

problems can be expected when the fiber end is angled and the beam partly misses the detector. See the discussion in Section 2.3.8.

6. Systematic uncertainty due to power level: Optical power meters have extremely wide power ranges of up to 100 dB. Uncertainties due to power level can be expected when the actual power approaches the noise level, or when it exceeds the high end of the specified power range. These subjects are discussed in Sections 2.3.5 and 2.4.2.
7. Systematic (and random) uncertainty due to reflections: Commercial power meters are often calibrated with an open beam, for example, from a white light source filtered by a monochromator. In the actual measurement with a fiber, the fiber is held by a connector and connector adapter. In this case, doubly reflected power may strike the detector, causing an increase of the power reading. Read the discussion in Section 2.3.7. Reflections can also cause power stability problems, such as problems described in (1) of this list.

2.5 RESPONSIVITY CALIBRATION

The most important criterion in conjunction with accurate measurement of absolute power is calibration. Generally, all power meters are calibrated through comparison: A test meter and a power measurement standard are exposed to a suitable radiation source, either sequentially or in parallel. If a calibration in fine-wavelength steps over a wide wavelength range is desired, then the source should be a halogen white-light source which is spectrally filtered with a monochromator. A power level of approximately 10 μW and a spectral width of up to 5 nm are desirable. Figure 2.17 shows a typical monochromator-type calibration setup.

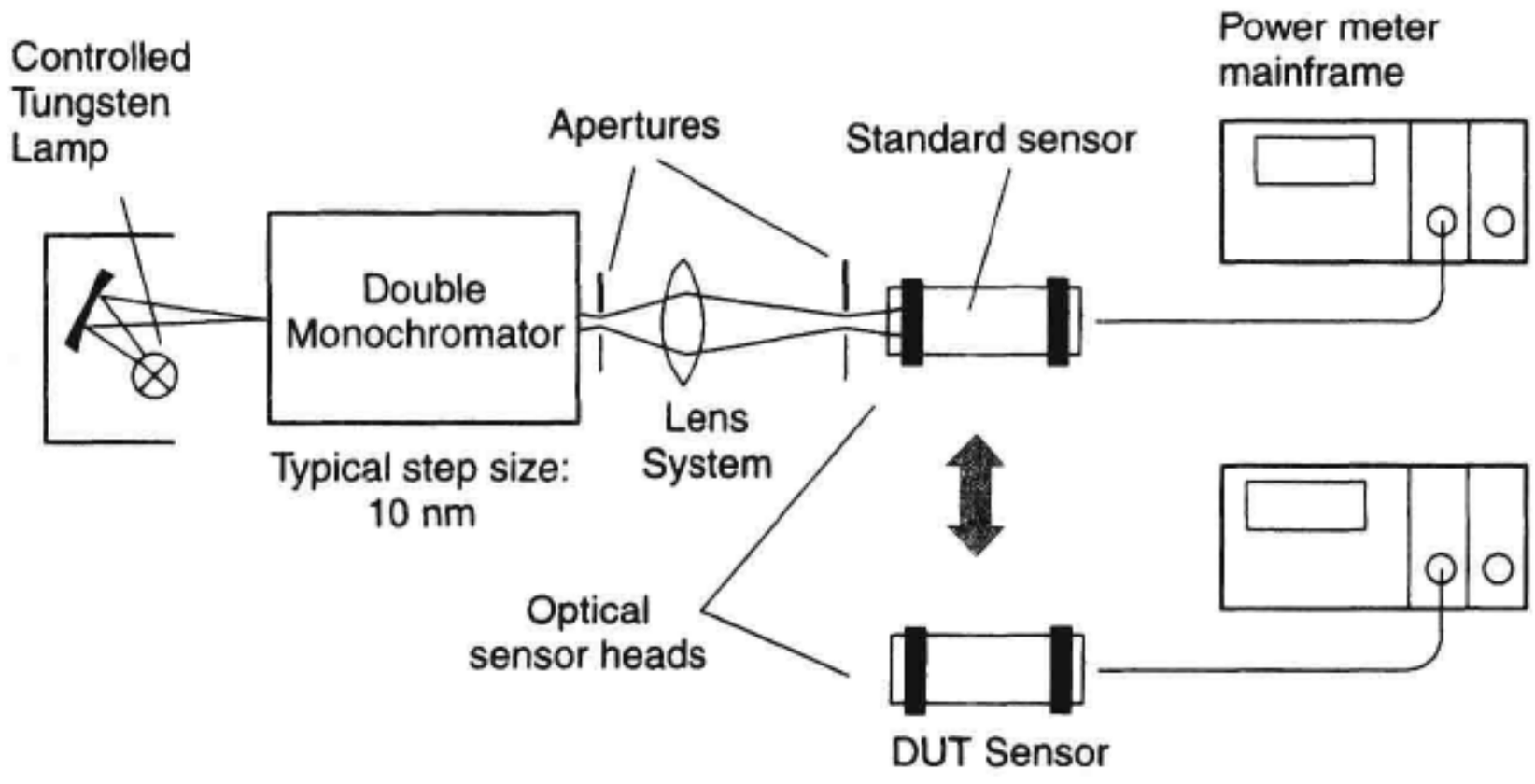

Figure 2.17 Responsivity calibration with monochromator source.

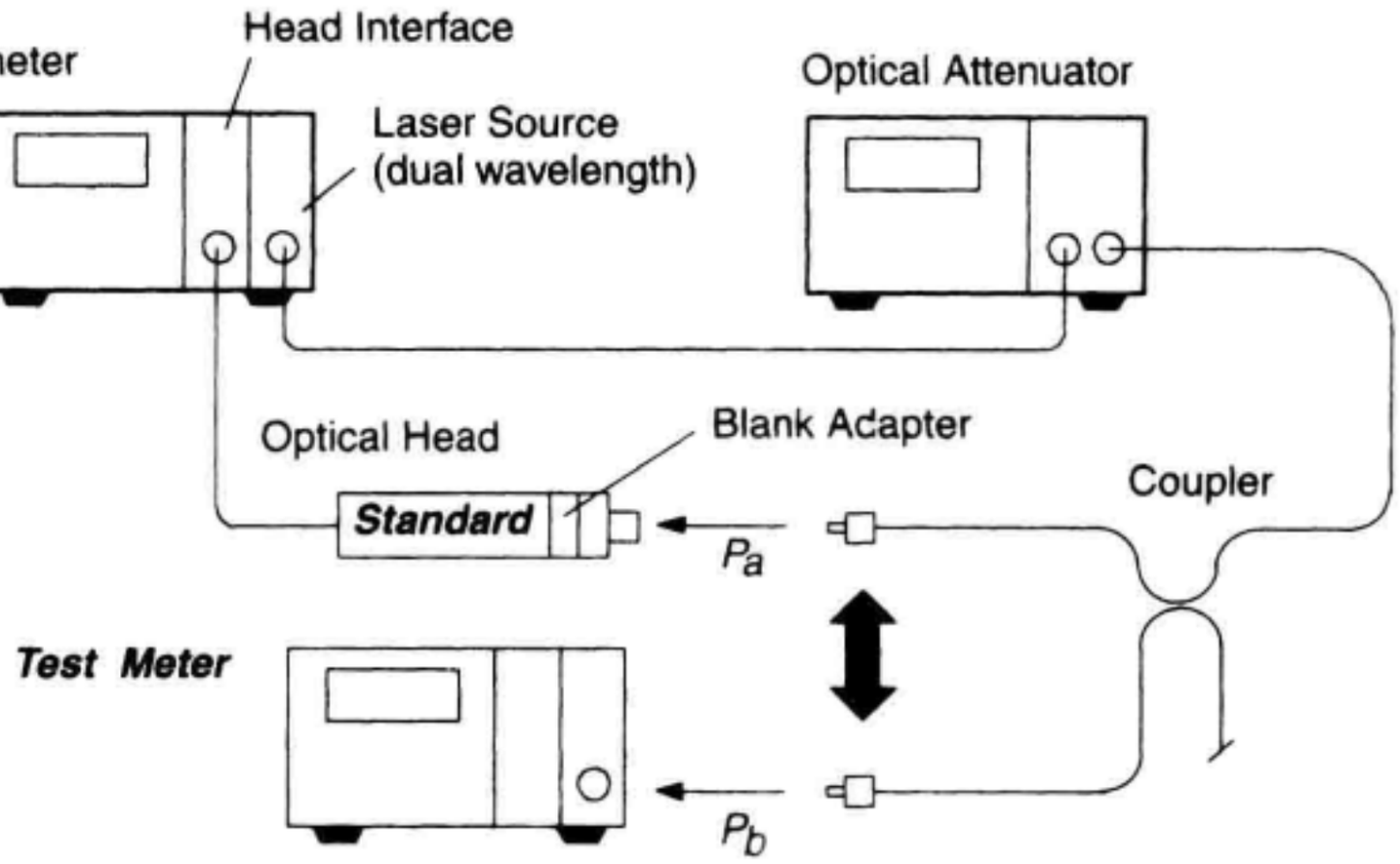

Figure 2.18 Alternative calibration setup using fixed wavelength sources.

Two types of standard sensors are commonly used: thermal detectors and photodetector sensors. Both need regular calibration within an unbroken chain to a national standards laboratory; see Section 2.5.1.

A monochromator-based calibration setup is expensive and difficult to operate and maintain. A more affordable setup is shown in Figure 2.18. A dual-wavelength source (FP laser) generates precisely known wavelengths around 1300 and 1550 nm. The attenuator is used to isolate the source and to set the appropriate power level. The coupler is used to split the power and to provide power monitoring. A specially calibrated optical head is used as the standard. A blank adapter serves as a spacer, to enlarge the spot diameter on the detector to approximately 2.4 mm (at the 5% points).

If dual-wavelength calibration is insufficient, for example, because absolute power measurements over wavelength is required, then a tunable laser source can be used as well. However, some care is recommended to avoid optical inference caused by the narrow linewidth of the tunable laser.

Switching the two coupler arms between the standard and the test meter (DUT) can be used to determine both the split ratio and the correction factor. See Figure 2.19, in which the symbol P is used for the correct power levels from the standards, and D is used for the displayed power of the DUT.

Equations 2.21 and 2.22 show how the coupling ratio and the correction factor can be calculated. Notice that a drift of the source power between the two steps has no influence on either result.

$$\text{Coupling ratio: } c = \frac{P_1}{kD_1} = \frac{kD_2}{P_2} \tag{2.21}$$

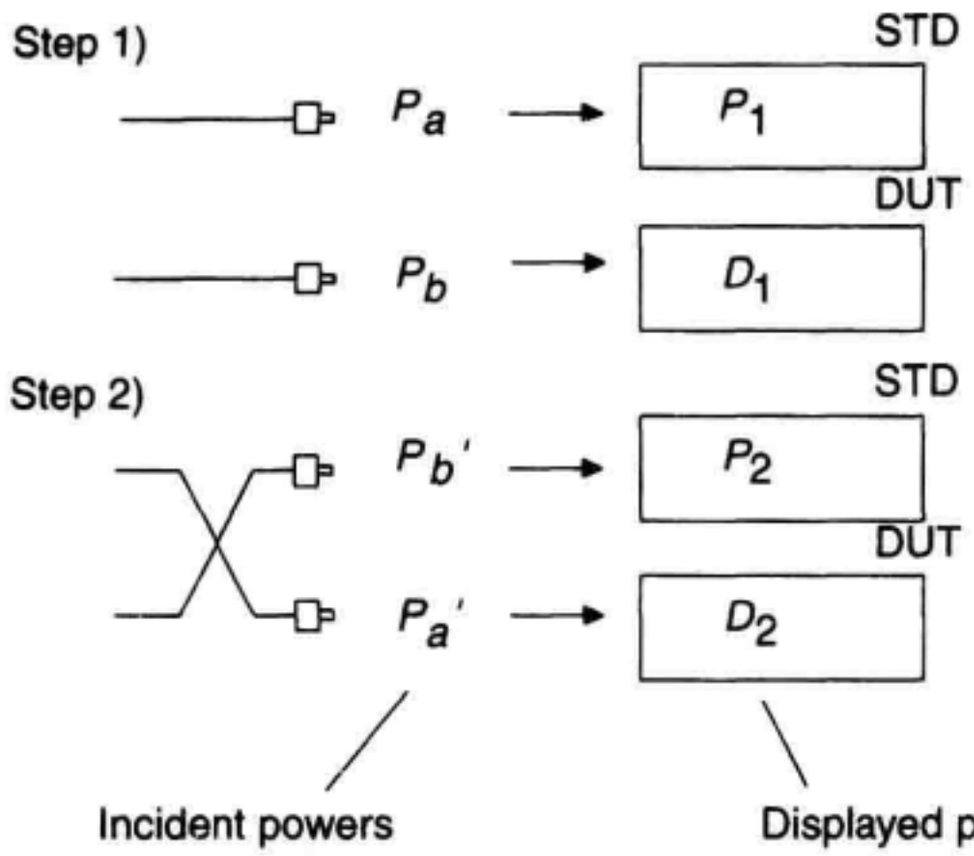

Figure 2.19 Measurement results obtained during calibration.

$$\text{Correction factor: } k = \sqrt{\frac{P_1 P_2}{D_1 D_2}} \tag{2.22}$$

The correction factor can either be used to correct the test meter or, without correction, as a test result for the calibration certificate.

2.5.1 Traceability and Uncertainty in Responsivity Calibrations

An unbroken chain of comparison to the national laboratory is considered a proof of traceability. Further credibility is usually given by the fact that the national laboratories compare their power scales on a more or less regular basis.[8] Figure 2.20 shows a typical traceability chain for a commercial optical power meter, together with the equipment used

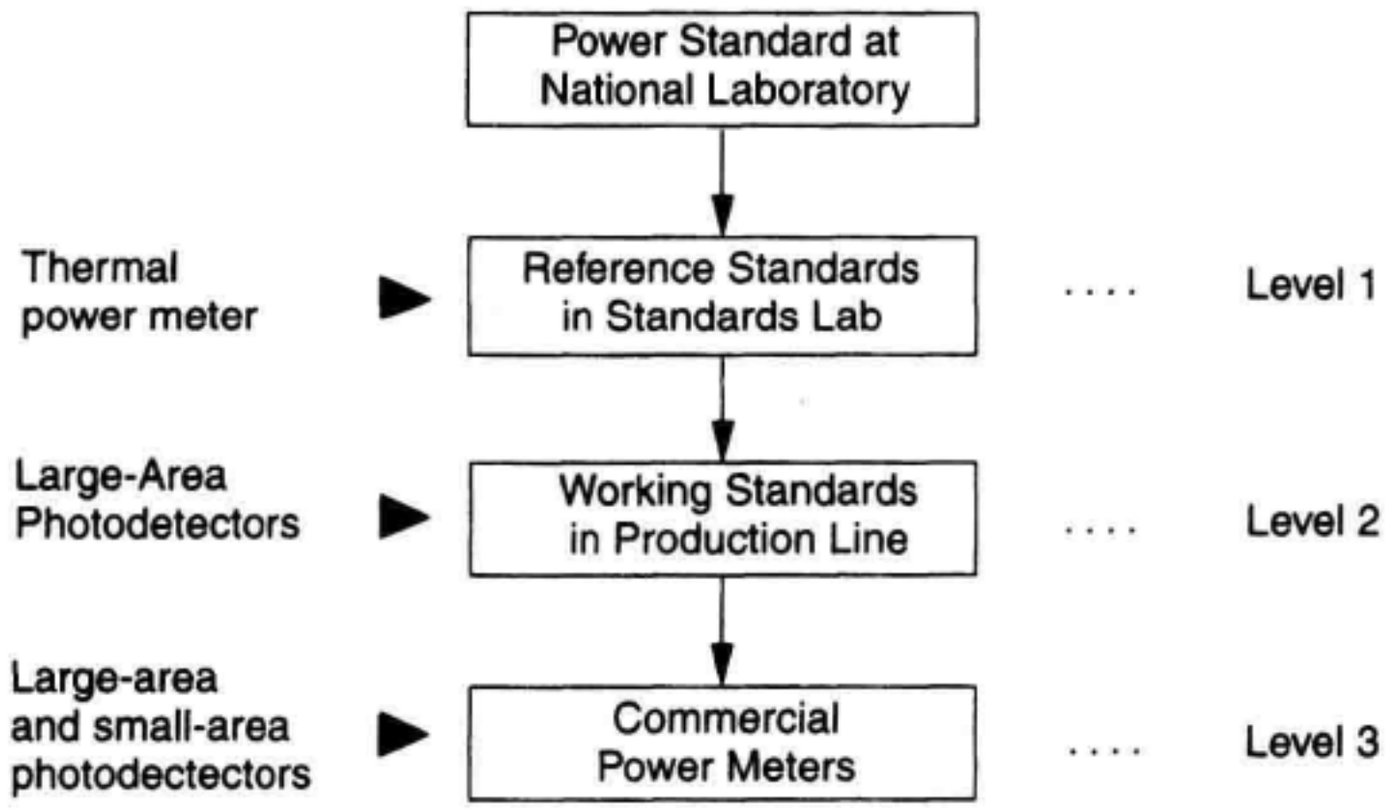

Figure 2.20 Example of a traceability chain.

at each of the levels. Each of these comparisons (indicated by arrows) must be repeated in regular intervals.

For the calculation of the measurement uncertainty of the test meter (the end of the chain), it is important to know the calibration conditions for each of the steps, for example, the measurement instrumentation, the power levels, the wavelengths, and the beam diameters. Only then can the uncertainties for each step and, finally, for the test meter be calculated. Calibration of optical power meters is thoroughly discussed in References 9 and 10. According to Reference 9, each calibration step is accompanied by classes of uncertainties. The term "parent meter" is always used for the higher-level power meter (the standard). For each calibration step, the uncertainty "classes" are as follows:

1. The parent meter's uncertainty at reference conditions: This is the uncertainty of the standard power meter for a specific set of conditions, either as stated by the national laboratory, or as calculated along with its own calibration.
2. The transfer-related uncertainties of the parent meter: This category of uncertainties is due to differences between the calibration conditions and the "use" conditions of the parent meter causing changes of measurement results of the parent meter. This uncertainty should be accumulated, by root-sum-squaring, from the following effects: aging of the working standard and changes in the wavelength, temperature, reflection conditions, power level (nonlinearity), beam geometry, and spectral width of the source.
3. The transfer-related uncertainties of the test meter: This category of uncertainties is due to tolerance bands of test conditions causing changes of test meter results. This uncertainty is strongly influenced by a) how well the test conditions are known, and b) what the stated test conditions (for example, on the calibration certificate) are. It should be accumulated from the following effects and their tolerance bands, all of which are assumed to have an influence on the test meter results: the wavelength, the temperature, the reflection conditions, the power level, the beam geometry, the spectral width of the source, and the state of polarization.
4. The random uncertainty of the transfer process: This uncertainty expresses changes of the correction factor obtained in consecutive measurements with the same instruments.

Again, these are the uncertainties for *one* calibration step, to be accumulated to the test meter's "uncertainty at reference conditions." In a traceability chain of, for example, three higher-level instruments, three calibration steps are necessary. Then three recursive uncertainty calculations have to be carried out. On this basis, the calibration uncertainties achieved today for commercial power meters are ±2% in the best case.

The "uncertainty at operating conditions" should be accumulated, by root-sum-squaring, the uncertainty at reference conditions and the additional uncertainty caused by using the instrument at conditions which are different from the calibration conditions; Section 2.4.3, list items 3 to 7.

2.6 LINEARITY CALIBRATION

Power-meter linearity calibration is necessary because of two reasons: first, to extend the calibration of absolute power to the whole power range, and, even more important, to prepare the basis for high-accuracy loss and gain measurements (see Chapter 9). In these measurements, the optical power may have to cover a wide range of six or more decades.

The linearity is expected to be almost wavelength-independent. Therefore, it is sufficient to calibrate at only one or two wavelengths within the detector's spectral responsivity region.

As discussed in Section 2.3.5, photodetectors provide excellent linearity from the noise level to approximately 1 mW. This leads to the fact that often the specifiable linearity is not limited by the linearity of the instrument, but by the performance of the linearity calibration setup. Two calibration methods are discussed below. An overview of the available techniques is presented in Yan and co-workers.[11]

2.6.1 Linearity Calibration Based on Comparison

The easiest way to perform a linearity calibration is to measure an arbitrary attenuation with both the test meter and a standard meter (for example, a meter calibrated by a national laboratory) and to compare the two attenuation results. A possible measurement setup is shown in Figure 2.21.

The first attenuator is used to set the power level, to generate additional fixed attenuations (for example, 10 dB) and to split the power (a power-splitter is built into this specific attenuator model). The second attenuator is used to increase the measurement range: for very high power levels, the second attenuator reduces the power level to the usable range for the standard sensor; for very low power levels, the two sensors can be switched

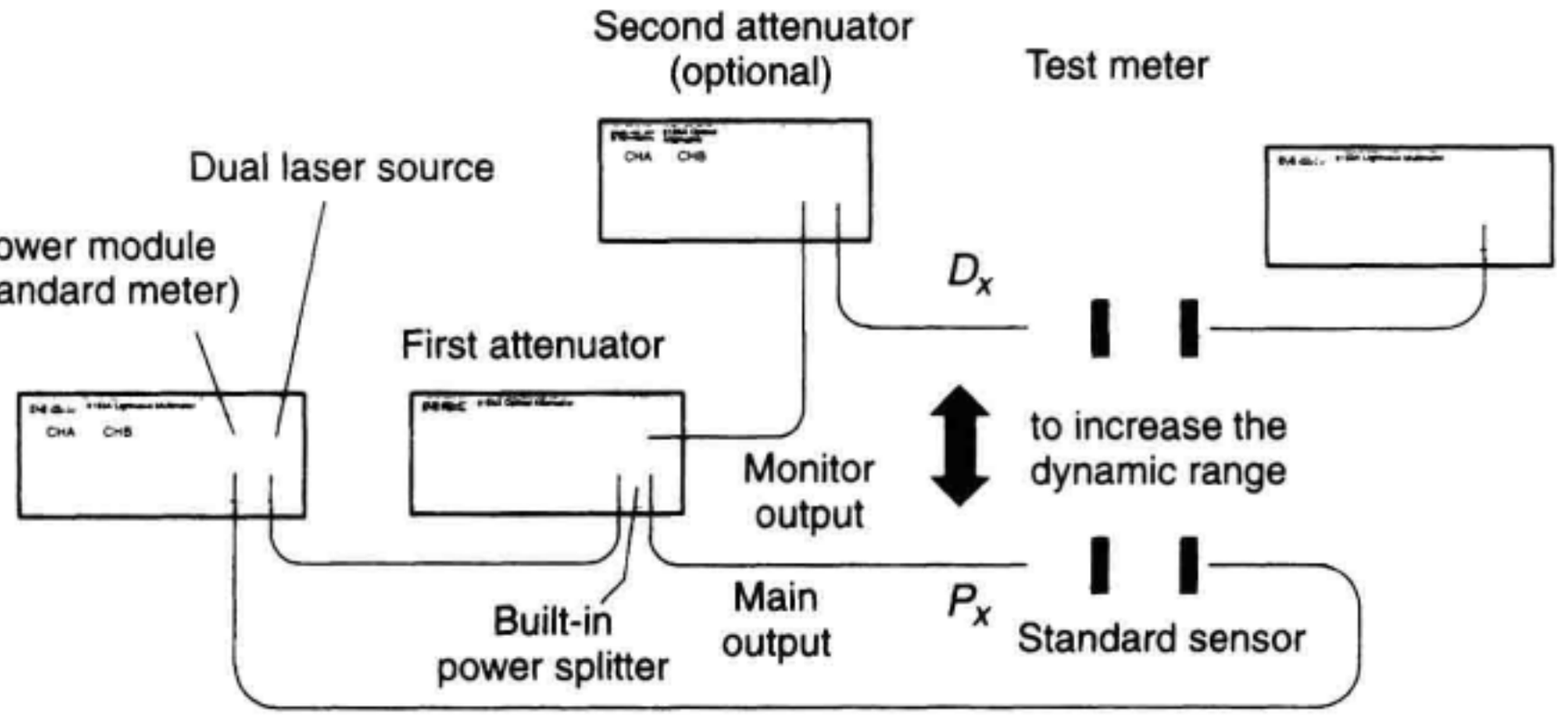

Figure 2.21 Linearity calibration based on comparison with a standard sensor.

and the second attenuator produces the low power levels. Any difference between the two measured attenuations indicates nonlinearity.

The nonlinearity of an optical power meter is internationally defined so that it represents directly the correspondent error in a loss measurement.[9]

$$N(D_x) = \frac{A_m - A}{A} = \frac{D_x/D_0}{P_x/P_0} - 1 \tag{2.23}$$

where A is the true power ratio, A_m is the measured power ratio, D_x/D_0 is the displayed power ratio (of the test meter) and P_x/P_0 are the true power ratio (of the standard meter). See Figure 2.22.

The calibration procedure is as follows:

1. Set the desired reference power on the test meter, D_0 (for example, 10 μW). Record the powers P_0 (standard meter) and D_0.
2. Increase (decrease) the attentuation of the first attenuator (for example, by 10 dB), and record the powers, P_1 (P_2, ,) and D_1 (D_2, ,).
3. Calculate the nonlinearity for the power D_1 (D_2 , ,) using Equation 2.23. In these calculations, the reference level is changing from step to step, which is why these nonlinearities are termed "partial."
4. Increase the attenuation further by repeating steps 2. and 3., until the low (high) end of the power range is reached. It is advisable to measure the nonlinearity due to range discontinuities by simply changing the power range and recording the measurement results in both ranges.
5. Decrease the attenuation to obtain the power levels above P_0 and to obtain the correspondent nonlinearity results, by repeating steps 2. and 3.

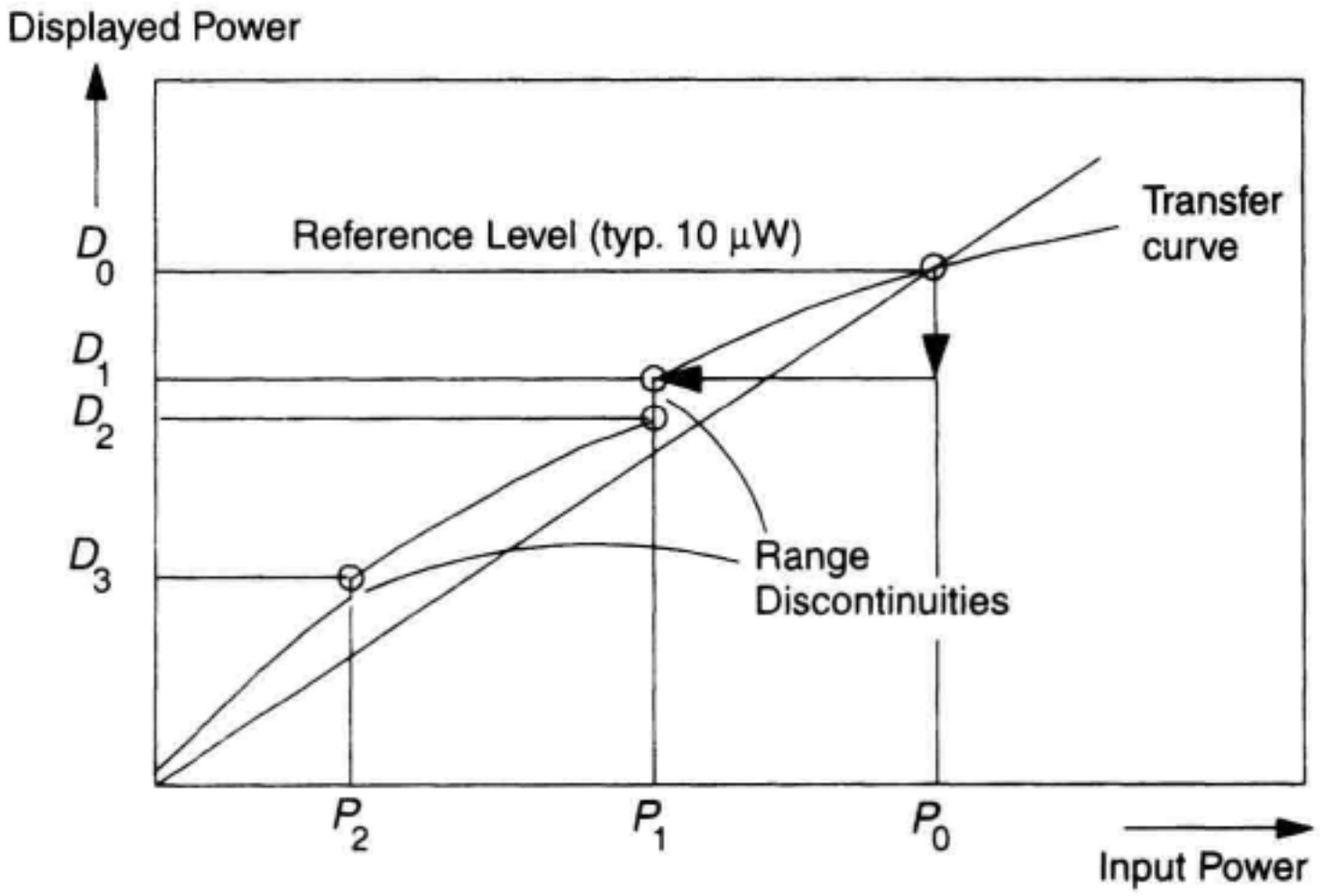

Figure 2.22 Power levels used in linearity calibration.

Finally, the nonlinearity data must be re-calculated on the basis of *one* fixed power level, e.g., 10 μW. This can be accomplished by accumulating the partial nonlinearities. See reference[10] for further details. The results are nonlinearity data for a number of power levels above and below the reference level D_0. By definition, the nonlinearity is zero at D_0.

Notice that the standard meter can operate in a much smaller power range than the test meter. For example, a linearity calibration over 70 dB is possible with a 20 dB calibrated range of the standard meter. This is possible by repetitive adjustment of the power at the standard meter using the second attenuator.

Uncertainty. Calibrations should aim at the lowest uncertainties. Accordingly, the uncertainties must be well understood. As usual, we distinguish between "systematic" and "random" uncertainties. The following potential uncertainties should be considered.

"Systematic" uncertainties. This type of uncertainty represents repeatable errors in the measurement data. The most important systematic uncertainty is the (calibrated) nonlinearity of the linearity standard.

Linearity standards are often calibrated using a self-calibrating technique (see Section 2.6.2). The calibration result should include nonlinearity data and their uncertainty. The nonlinearity, if any, can be corrected for. The uncertainty will reflect the performance of the calibration setup and of the meter under test. It will also depend on the power range over which the calibration was carried out.

"Random" uncertainties. There are two possibilities in the determination of the random uncertainties: Either you evaluate the individual contributions to the random uncertainty, or you evaluate them experimentally as one ensemble. For completeness, random uncertainties can be reduced by averaging.

1. Random uncertainty "source stability": Laser sources tend to drift. Also, back-reflections towards the source may cause power instability. Any attenuation between the source and the power meters will help. Fortunately, the method is more or less insensitive to power changes because *both* power meters will see the same change.
2. Random uncertainty "Optical interference": Optical interference problems (power fluctuation) may occur if both conditions a. and b. are met.
   a. The product of the reflectances in the setup is sufficiently large, and
   b. the coherence lengths of the lasers are in the same order of magnitude as (or longer than) the distance between reflection points.
3. Random uncertainty "polarization dependence": There are several components in the setup which can produce power changes due to their polarization dependence: the optical attenuators, the coupler and the power meter itself. It is highly recommended that all fibers be fixed by taping them to the table. This will ensure stable polarization states and power results.

Total Uncertainty. It is recommended to calculate first the standard uncertainty representing *one* attenuation step by root-sum-squaring all relevant partial uncertainties

(systematic and random) in the form of standard deviations. Then the *total* uncertainty, on the basis of a 95% confidence level, is given by:

$$U = \pm 2\sigma_{\text{single step}}\sqrt{n} \tag{2.24}$$

where $\sigma_{\text{single step}}$ is the standard uncertainty for a single attenuation step and n is the number of steps where counting starts from the reference level. The factor of 2 converts the standard uncertainty to an uncertainty with 95% confidence level.

This calibration method suffers from the fact that a linearity standard is necessary, and that each of the single-step uncertainties includes the uncertainty of the standard; therefore, the uncertainty will rarely be less than ±0.1% for a 10 dB step. These problems are avoided by the superposition method.

2.6.2 Linearity Calibration Based on Superposition

An alternative linearity calibration method is based on power superposition. This is a self-calibrating method which does not need a standard meter. Therefore, a traceability to a national standards laboratory is not mandatory. This principle was first mentioned in Sanders.[12]

A possible measurement setup is shown in Figure 2.23.

In the beginning, the two attenuators are both set to high attenuation and so that each beam separately gives rise to the same powers at the DUT: $D_a \cong D_b$. Each attenuator is equipped with a shutter. The shutter of the respective other attenuator remains closed. Then the two beams are combined by opening both shutters at the same time. This reading should now be the sum of the two preceding individual readings:

$$D_c = D_a + D_b\,(\cong 2D_a) \tag{2.25}$$

Any deviation indicates nonlinearity. Accordingly, the nonlinearity for the first power D_c is:

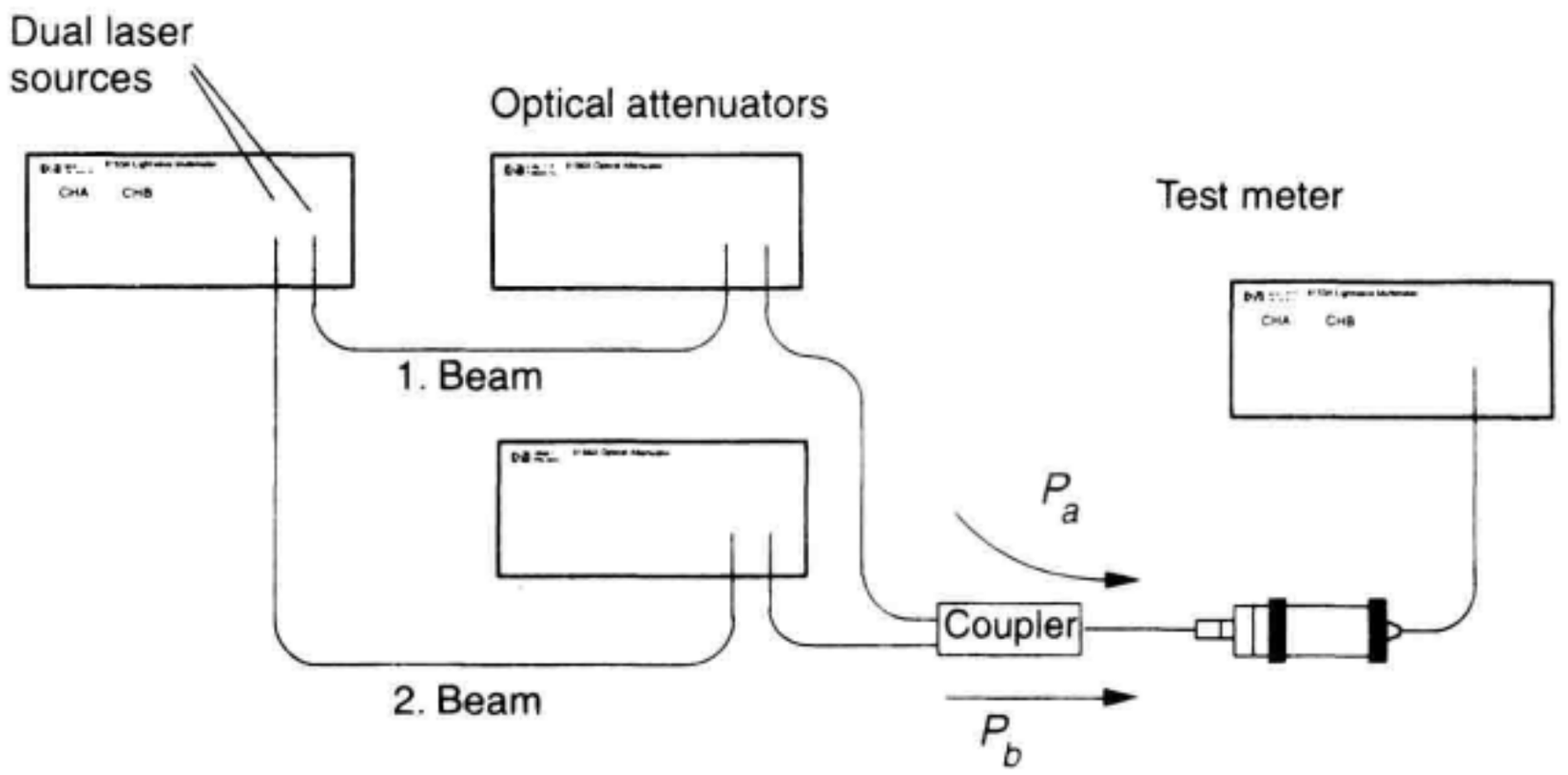

Figure 2.23 Nonlinearity calibration using the superposition method.

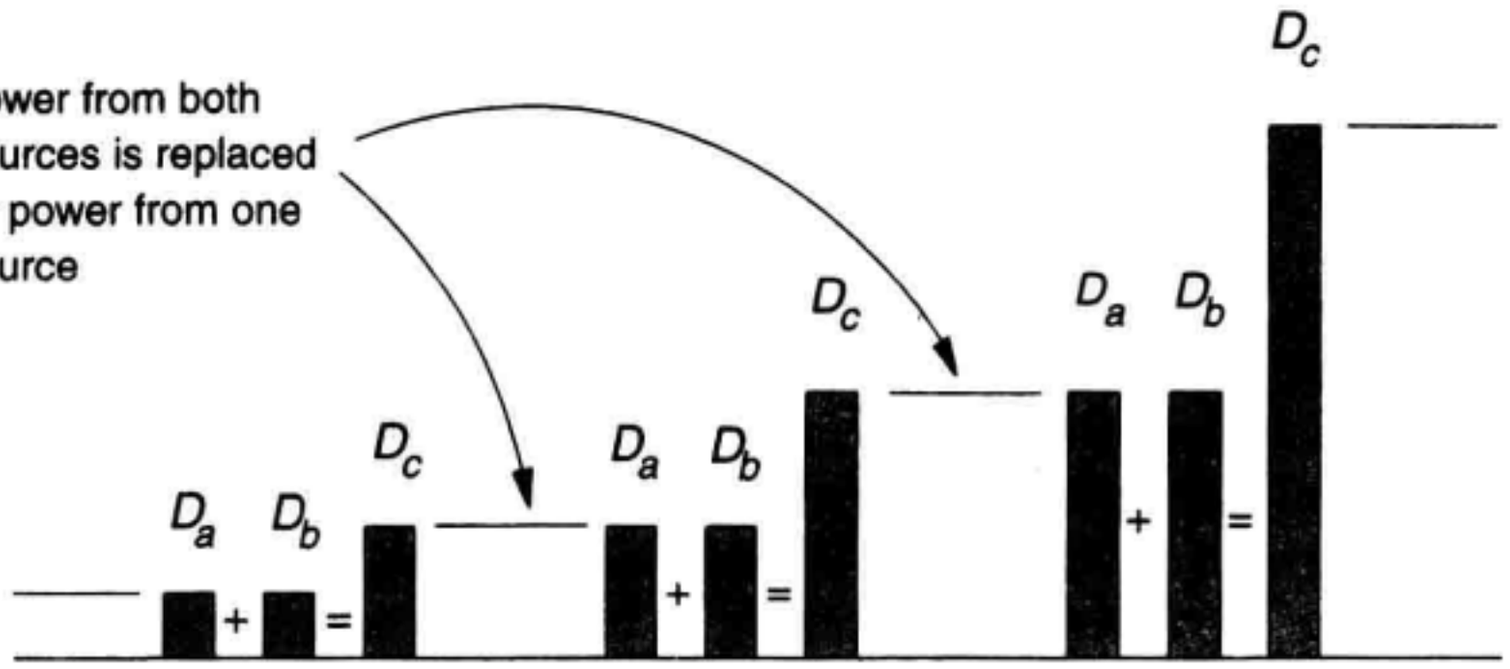

Figure 2.24 Power superposition used in linearity calibration.

$$N_1 = \frac{D_c}{D_a + D_b} - 1 \tag{2.26}$$

The next cycle starts by generating the combined power separately with each of the attenuators, before combining them again. This is indicated in Figure 2.24. Notice that the result of Equation 2.26 should be considered as a partial nonlinearity because it uses a changing power level as the reference. At the end of the measurement, the partial nonlinearities for all steps will be determined.

Finally, the *total* nonlinearity can be calculated, in other words, the nonlinearity with respect to a fixed reference level. Start by choosing a reference level, for example, 10 μW, at which the total nonlinearity is zero by definition. Then use the following equation for power levels lower than the reference level:

$$N_{\text{total}}(D_n) = -\sum_{i=-1}^{n} N_i \tag{2.27}$$

where $n = -1, -2$, etc. indicates the power level number below the reference point and N_i is the partial nonlinearity for the i^{th} *step* ($i = 0$ for the step between the reference power and the next-higher power). For power levels higher than the reference level, the total nonlinearity is:

$$N_{\text{total}}(D_n) = -\sum_{i=0}^{n-1} N_i \tag{2.28}$$

where $n = 1, 2$, etc. The final result is a list of total nonlinearities for the whole power range in 3 dB steps (because the power is doubled in each step).

Uncertainty. The uncertainty goals for this type of measurement should be better than ±0.1% for a 10 dB power range. This is an aggressive goal. Accordingly, the mea-

surement uncertainties must be well understood. In the following, only the differences between the uncertainties of the comparison method, Section 2.6.1, and this method are discussed.

"Systematic" uncertainties. The big advantage of this method is that there is no linearity standard, and consequently no uncertainty due to the linearity standard.

A small systematic uncertainty may be caused by multiple reflections. There is one main reflection in the setup: the fiber end that stimulates the optical power meter. It usually represents a reflectance $R_a = 3.5\%$ (equivalent to -14.7 dB). If the reflected wave, on its way back to the source, hits a second reflection point with reflectance R_b, then the incident power level is increased to:

$$P_{\text{total}} = (1 + R_a B_b) P_{\text{inc}} \quad \text{[watts]} \tag{2.29}$$

This problem is insignificant if the second reflectance is sufficiently small (for example, $R_b \leq 10^{-4}$, equivalent to -40 dB) and remains constant. However, R_b may change due to activating the optical shutters.

"Random" uncertainties. The random uncertainties of this method are essentially the same as the random uncertainties of the comparison method.

Total uncertainty. Again, it is recommended to calculate first the standard uncertainty representing *one* 3 dB step by root-sum-squaring all relevant partial uncertainties (systematic and random) in the form of standard deviations. Then the *total* uncertainty, on the basis of a 95%-confidence level, is given by:

$$U = \pm 2\sigma_{3dB}\sqrt{n} \tag{2.30}$$

where $\sigma_{3\,dB}$ is the standard uncertainty for one 3 dB step and n is the number of 3 dB steps counted from the reference level. State-of-the-art uncertainties achieved in linearity calibration using the superposition method are $\leq \pm 0.1\%$ for a 10 dB power range.

2.7 SUMMARY

This is a chapter on optical power meters. The range of topics includes all aspects of this instrument: construction, absolute power measurement, and calibration. In most cases, the potential uncertainties are also discussed, with the aim of improving the accuracy of optical-power measurement. The characteristics of state-of-the-art optical-power meters can be summarized as follows:

$\pm 2\%$ uncertainty at calibration conditions,
$\pm 3\%$ to 5% uncertainty at operating conditions,
$\pm 0.5\%$ nonlinearity for a power range of 50 dB or more,
an approximate power range -90 to 0 dBm,
(attenuation needed for higher power measurement).

ACKNOWLEDGMENTS

The author wishes to thank his colleagues Andreas Gerster, Siegmar Schmidt, and Dennis Derrickson for fruitful discussions and suggestions.

REFERENCES

1. Bischoff, K. 1968/69. *Ein einfacher Absolutempfänger hoher Genauigkeit,* Optik, 28. Band: 183–189.
2. Haars, H. and K. Möstl. 1997. *Dünnschicht-Thermosäule mit Online-Kalibrierung,* PTB Jahresberichte 1996. Physikalisch-Technische Bundesanstalt, Braunschweig, Germany.
3. Stock, K.D. and H. Hofer. 1993. Present state of the PTB primary standard for radiant power based on cryogenic radiometry. *Metrologia* 30: 291–296.
4. Zalewski, E.F. and J. Geist. 1980. *Silicon photodiode absolute spectral response self-calibration. Applied Optics* 19, No. 8: 1214–1216.
5. Hentschel, C. *Fiber Optics Handbook,* 1989. Böblinger, Germany: Hewlett Packard, P/N 5952–9654.
6. Stock, K.D. *Si-photodiode spectral nonlinearity in the infrared. Applied Optics* 25, No. 6, 830–832.
7. Gallawa, R.L. and X. Li. 1987. *Calibration of optical fiber power meters: the effect of connectors. Applied Optics* 26, No. 7: 1170–1174.
8. Gardner, J.L., et al. 1992. *International intercomparison of detector responsivity at 1300 and 1550 nm. Applied Optics* 31, No. 34: 7226–7231.
9. IEC Standard 1315, 1995. *Calibration of fibre-optic power meters,* International Electrotechnical Commission.
10. Hentschel, C. *Setting up a calibration system for fiber optic power meters,* Böblinger, Germany. Hewlett Packard, P/N 5964–9638E.
11. Yan, S., I. Vayshenker, et al. 1994. *Optical detector nonlinearity: a comparison of five methods,* Conference on Precision Electromagnetic Measurements, 455–456.
12. Sanders, C.L. 1962. *A photocell linearity tester, Applied Optics* 1, No. 3: 207–211.

CHAPTER

3

Optical Spectrum Analysis

Joachim Vobis, Dennis Derickson

3.1 INTRODUCTION TO OPTICAL SPECTRUM ANALYSIS

Optical spectrum analysis is the measurement of optical power as a function of wavelength. The spectrum of a light source is an important parameter in fiber-optic communication systems. For example, chromatic dispersion can occur in the fiber and limit the achievable modulation bandwidth of the system. The effect of chromatic dispersion can be seen in the time domain as pulse broadening of a digital waveform. Since chromatic dispersion is a function of the spectral width of the light source, narrow spectral widths are desirable for high-speed communication systems.

The prevalence of wavelength division multiplexed (WDM) systems has stimulated significant activity in the measurement of optical spectra. WDM has also made optical spectrum analysis a key measurement capability that must be embedded inside telecommunication network elements.

Figure 3.1 shows an example measurement made by an optical spectrum analyzer (OSA). It shows the power versus wavelength for a Fabry-Perot (FP) laser. The FP laser shows a series of longitudinal modes that have significant energy over a 20 nm span. The plot shows that the measurement has been made using an instrument filter bandwidth of 0.2 nm with an instrument sensitivity setting of −55 dBm. From the spacing of the modes and power distribution, the laser length and coherence properties of the laser can be determined.

This chapter is the first of three chapters covering the area of optical spectrum analysis. Chapter 3 covers the most common implementation using a diffraction-grating based optical filter. Chapter 4 covers wavelength meters based on Michelson interferometry. Wavelength meters offer high wavelength accuracy. Chapter 5 covers methods of

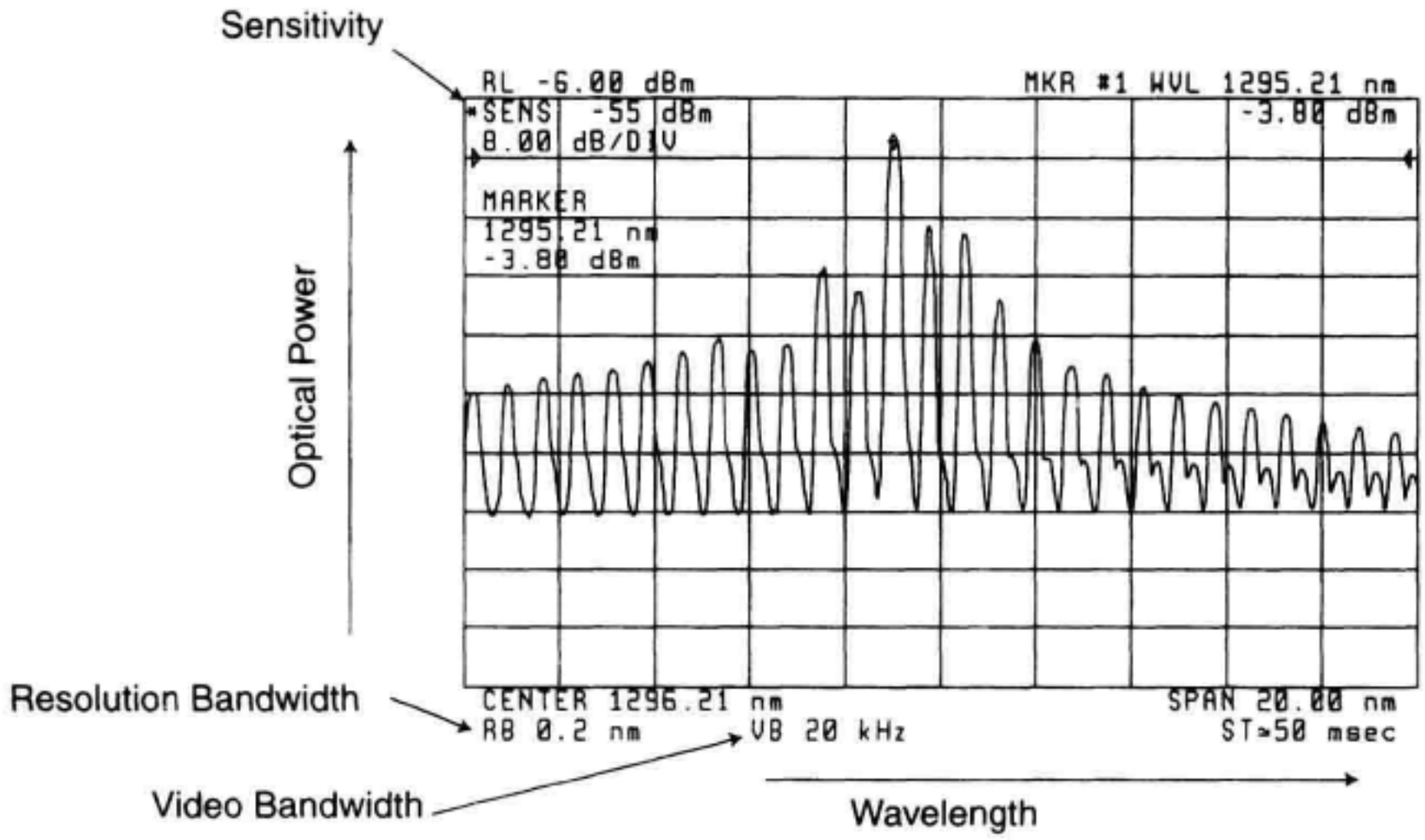

Figure 3.1 Optical spectrum analyzer measurement of a Fabry-Perot laser.

very-high wavelength resolution optical spectrum analysis using homodyne and heterodyne techniques.

3.2 TYPES OF OPTICAL SPECTRUM ANALYZERS

3.2.1 Basic Block Diagram

A simplified OSA block diagram is shown in Figure 3.2. The incoming light passes through a wavelength-tunable optical filter which resolves the individual spectral components. The photodetector then converts the optical signal to an electrical current proportional to the incident optical power.

The current from the photodetector is converted to a voltage by the transimpedance amplifier and is then digitized. Any remaining signal processing, such as applying correction factors, is performed digitally. The signal is then applied to the display as the vertical or power axis. A ramp generator determines the horizontal location of the trace as it sweeps from left to right. The ramp also tunes the optical filter so that its center wavelength is proportional to the horizontal position. A trace of optical power versus wavelength results. The displayed width of each mode of the laser is a function of the spectral resolution of the wavelength-tunable optical filter.

3.2.2 Fabry-Perot Interferometers

The FP interferometer, shown in Figure 3.3, consists of two highly reflective, parallel mirrors that act as a resonant cavity which filters the incoming light. The resolution of FP-interferometer-based OSAs depends on the reflection coefficient of the mirrors and

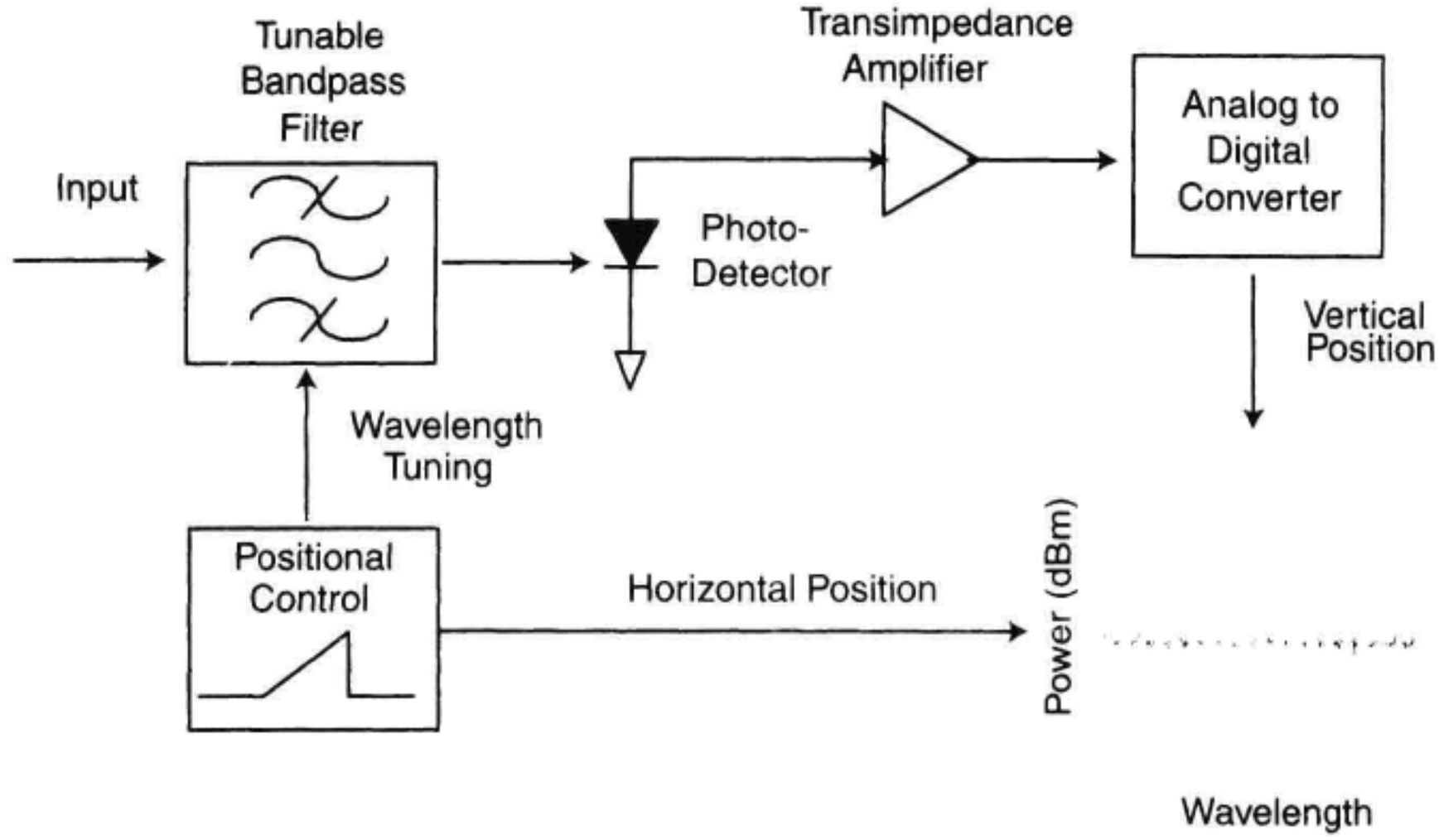

Figure 3.2 Simplified OSA block diagram.

the mirror spacing. Wavelength tuning of the FP interferometer is accomplished by adjusting the mirror spacing or by rotating the interferometer with respect to the input beam.

The advantage of the FP interferometer is its potential for very narrow spectral resolution and its simplicity of construction. The added resolution allows measurements such as laser chirp to be performed. The major disadvantage is that the filters have repeated passbands. The spacing between these passbands is called the free spectral range. If the mirrors are spaced very widely apart, very high resolution can be obtained, but the free spectral range is small. This problem can be solved by placing a second filter in cascade with the FP interferometer to filter out power outside the interferometer's free spectral range. Section 6.1 in Chapter 4 gives a more detailed description of FP-based OSAs.

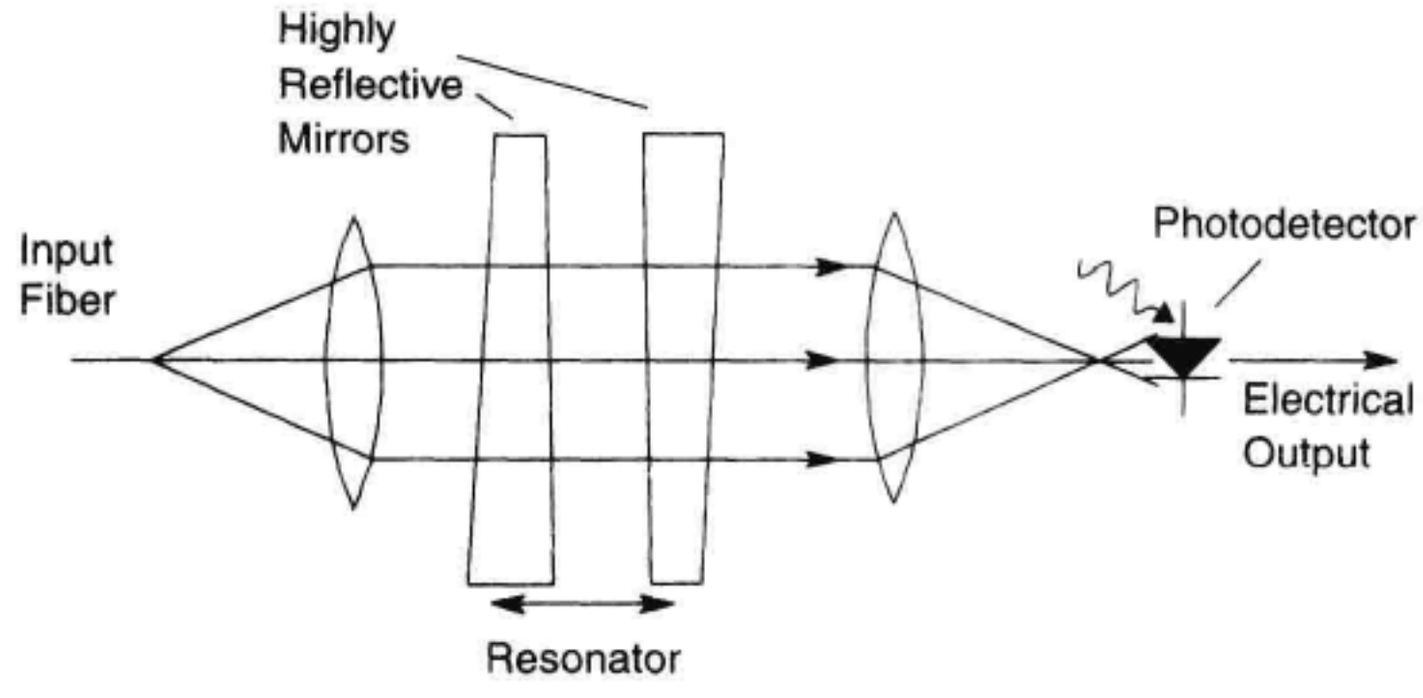

Figure 3.3 FP-interferometer-based OSA.

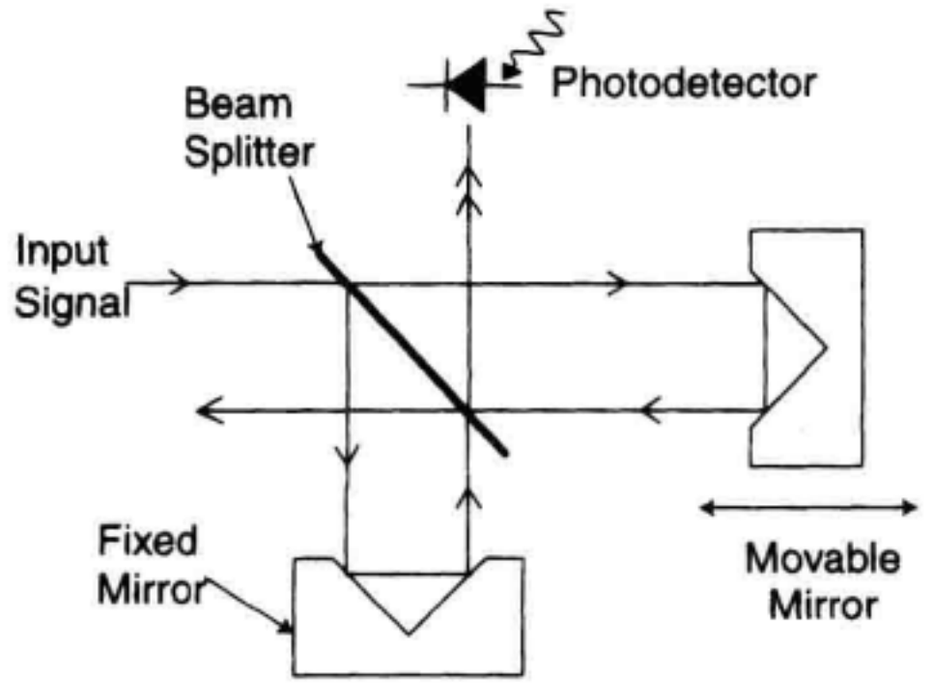

Figure 3.4 Michelson-interferometer-based OSA.

3.2.3 Interferometer-Based Optical Spectrum Analyzers

Another type of spectrum analyzer is based on the Michelson interferometer as shown in Figure 3.4. The input signal is split into two paths. One path is fixed in length and one is variable. The Michelson interferometer creates an interference pattern between the signal and a delayed version of itself at the detector. The resulting waveform is the autocorrelation function of the input signal and is often referred to as an interferogram. Michelson-interferometer-based spectrum analyzers make direct measurements of coherence length. Other types of OSAs cannot make direct coherence-length measurements. If the period of the zero crossings in the interferogram are accurately measured by comparison to a wavelength standard, the wavelength of the unknown signal can be determined with high accuracy. It is the potential for high wavelength accuracy that distinguishes this instrument. A state of the art wavelength meter can measure wavelength to less than 1 part per million. A 1550 nm laser could be measured to ±0.0015 nm.

The Michelson interferometer can also provide displays of power versus wavelength. To determine the power spectra of the input signal, a Fourier transform is performed on the interferogram. The resolution of the instrument is determined by the path-length delay that is used to create the interferogram. Because this instrument does not depend on a tunable bandpass filter for wavelength identification, Michelson-interferometer-based designs cannot be used in applications where a true bandpass filter is required. This type of analyzer also tends to have less dynamic range than diffraction-grating-based OSAs due to the shot noise that is always present in the optical receiver for large input signals. Chapter 4 discusses instruments based on the Michelson-interferometer in more detail.

3.2.4 Diffraction-Grating-Based Optical Spectrum Analyzers

The most common OSAs for fiber optic applications use diffraction gratings as the basis for a tunable optical filter. Figure 3.5 shows what a diffraction-grafting-based OSA might look like. In the monochromator, a diffraction grating (a mirror with finely spaced corrugated lines on the surface) separates the different wavelengths of light. The diffracted light comes off at an angle proportional to wavelength. The result is similar to the rainbow produced by visible light passing through a prism. In the infrared, prisms do not

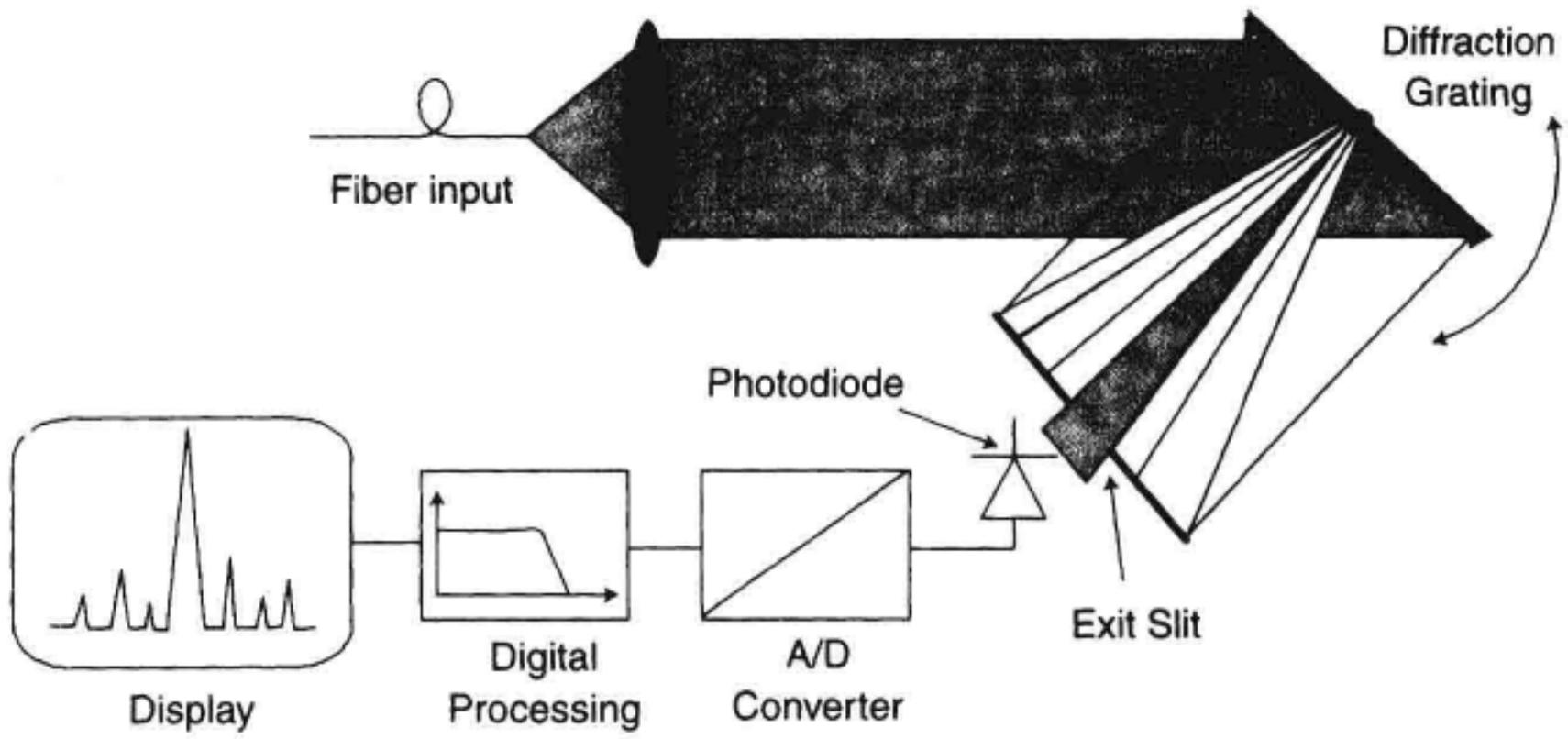

Figure 3.5 Concept of diffraction-grating-based OSA.

work very well because the dispersion (in other words, change of refractive index versus wavelength) of glass in the 1 to 2 μm wavelength range is small. Diffraction gratings are used instead. They provide a greater separation of wavelengths allowing for better wavelength resolution. A diffraction grating is made up of an array of equidistant parallel slits (in the case of a transmissive grating) or reflectors (in the case of a reflective grating). The spacing of the slits or reflectors is on the order of the wavelength of the light for which the grating is intended to be used. The grating separates the different wavelengths of light because the grating lines cause the reflected rays to undergo constructive interference only in very specific directions. Only the wavelength that passes through the aperture reaches the photodetector to be measured. The angle of the grating determines the wavelength to which the OSA is tuned. The size of the input and output apertures together with the size of the beam on the diffraction grating determines the spectral width of the optical filter.

3.3 ANATOMY OF A DIFFRACTION-GRATING-BASED OPTICAL SPECTRUM ANALYZER

In this section, the optical portion of a grating-based OSA will be dissected and an introduction to the function of each of the components will be given. This section will be useful to the reader unfamiliar with the internal workings of monochromators and spectrometers and the terms describing each of the components involved. Section 3.4 will describe some of the parameters that are important in a spectral measurement and relate them back to the workings of the monochromator.

3.3.1 Basic OSA Block Diagram

Figure 3.6 shows the various optical components in a basic OSA.[1] Here one can see that an OSA contains (in the order of the light propagating through the system) an entrance (or input) slit, collimating optics, a diffraction grating, focusing optics, an exit (or output) slit,

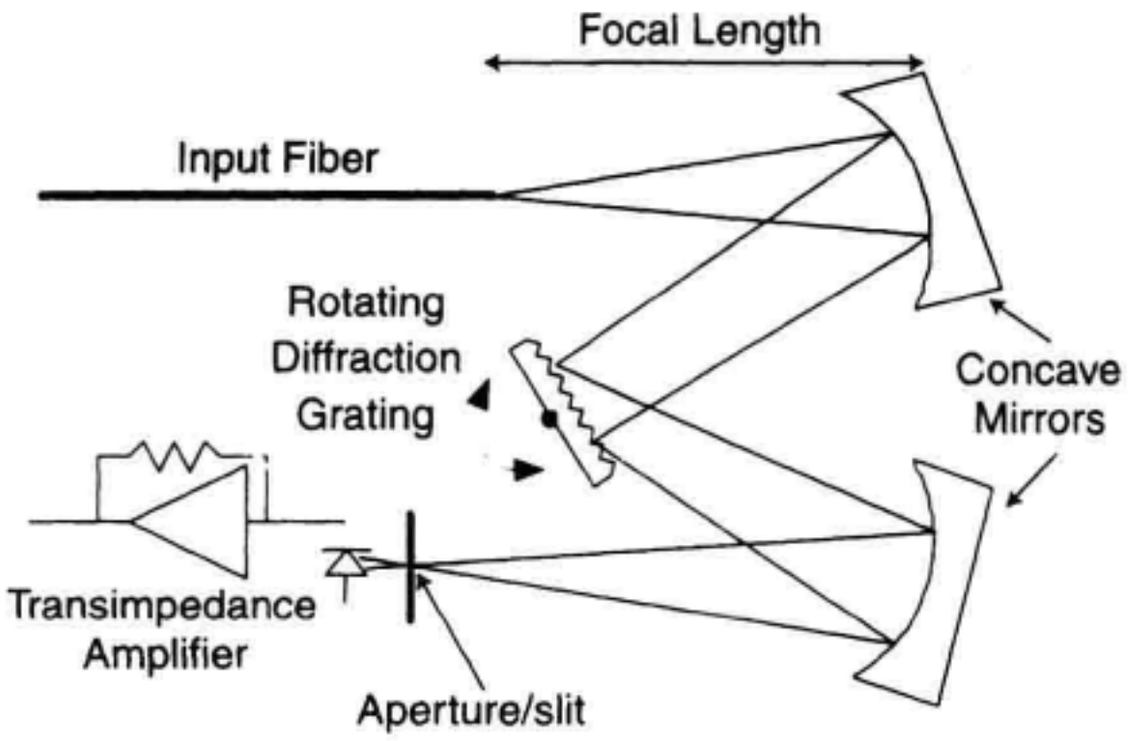

Figure 3.6 Optics of a single pass diffraction-grating based OSA.

and a detector. This optical portion of the OSA is usually referred to as a monochromator or as a spectrometer. Historically, a spectrometer usually refers to an instrument that has some means of separating the input light (for example, the input slit, the diffraction grating, and the output slit) to its various spectral components and a detector so that the spectrum can be recorded. This same instrument without the detector (in other words, having an optical output only), would be called a monochromator. A monochromator can be thought of as a tunable optical filter. One couples light from a source to the monochromator and at the output one has light consisting of a selected portion of the spectrum of that coupled source. Throughout the rest of this chapter, the word monochromator will be used to describe the optical portion of the OSA up to, but not including, the detector.

3.3.2 The Entrance or Input Slit

The light first enters the monochromator through the entrance or input slit. The input slit defines the spatial width of the input image. This input aperture, along with other components in the system, defines the wavelength resolution of the system. The narrower the input slit, the better the possible wavelength resolution. Narrower slits also reduce the optical throughput (number of photons) that the detector sees. In a modern fiber-optic input OSA, the input slit is often a singlemode or multimode fiber. This fiber defines the input image. For the case of a singlemode step-index fiber, the image will approximate a Gaussian amplitude distribution. It is more accurately described by the J_0 Bessel function in the core and the K_0 Bessel function in the cladding.

There are two methods often used to connect the input fiber to the monochromator in fiber-optic input spectrometers. These methods are shown in Figure 3.7.

In Figure 3.7a, the user's fiber directly defines the input aperture. OSAs with an input connection directly to the OSA allow you to connect fibers with different core diameters, and in some cases to apply open beams from optical benches as well. There is no insertion loss and no risk of scratching any internal fiber. This design has several disadvantages. Small particles can fall into the input hole and possibly harm the monochromator. The position of the input spot strongly depends on how an input signal is brought to the OSA. The image quality is defined by the shape of the fiber-end face polish. Scratches

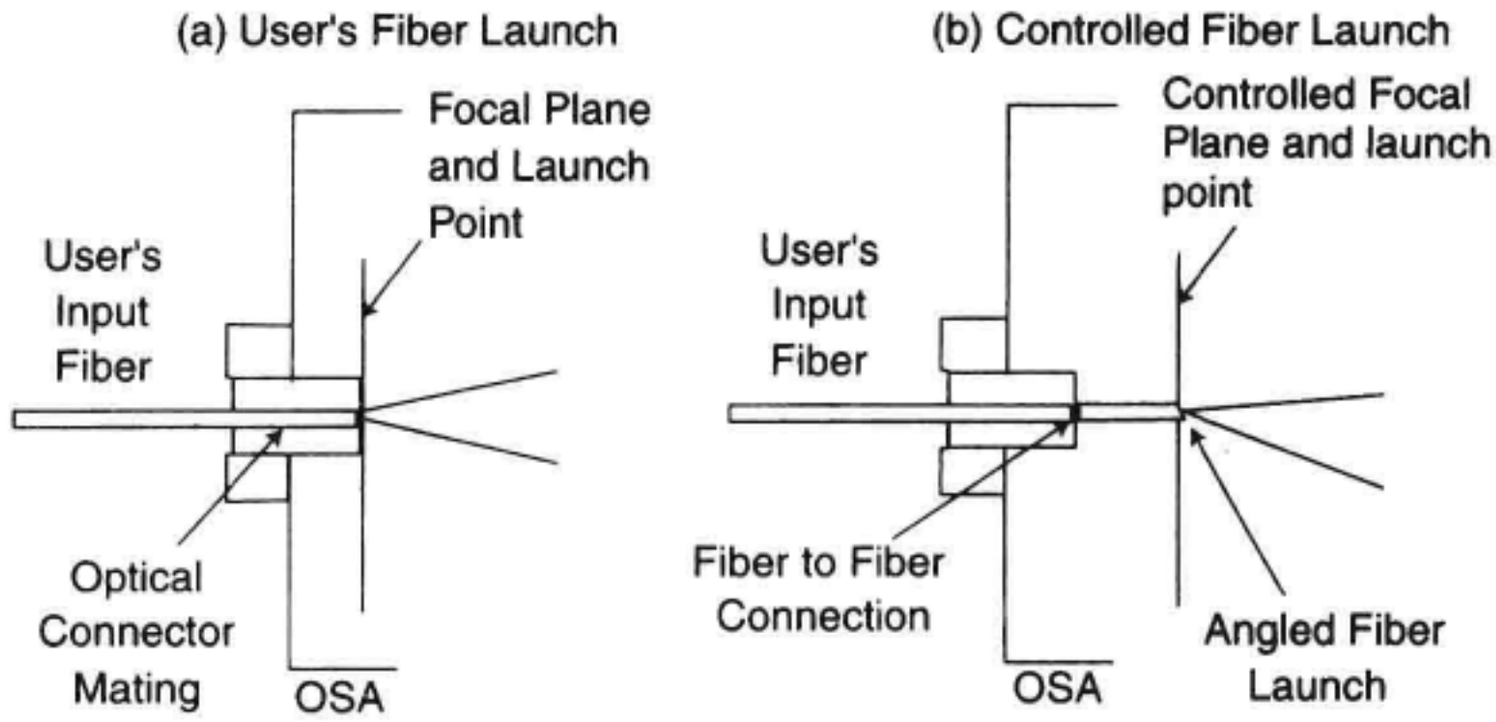

Figure 3.7 (a) Input slit with user's fiber. (b) Input slit using a short connector fiber.

and chips on the fiber core can affect the OSA filter response. Furthermore, a typical connector at the OSA input causes a 14 dB return loss (RL) due to the glass-to-air transition. Such a low RL can have an impact on measurement results. Many semiconductor lasers are sensitive to back reflections.

Figure 3.7b shows the user's fiber coupled to a captive length of fiber that is then used to form the entrance slit to the monochromator. This design has the advantage that the quality of the input image is well defined. The disadvantage of this approach is the insertion loss magnitude and insertion loss uncertainty found when mating together fibers. The use of a captive fiber allows the use of an angled fiber tip launch. The reflectivity of an 8 degree polished singlemode fiber can be greater than 70 dB in return loss. In this case the input reflectivity to the monochromator will be limited by the reflection from the fiber-to-fiber mating at the instrument front panel. The return loss from fiber mating typically exceeds 28 dB depending on the connector style (see Appendix C).

Singlemode versus Multimode Input. Either singlemode or multimode fibers can be used in the captive fiber design. It is possible to connect singlemode fibers to multimode fiber inputs (typically 50 or 62.5 μm) with very little insertion-loss uncertainty. If the multimode section is very short, the spot size will still be small where the light leaves the multimode fiber. The smaller spot size (9 μm) and the smaller numerical aperture of a singlemode fiber further improves the image quality, allowing tight specifications. However, the absolute power accuracy is affected by the insertion-loss uncertainty of a singlemode to singlemode connection at the instrument's input.

3.3.3 The Collimating Optics

The purpose of the collimating optics is to take the diverging beam from the input slit and collimate this beam to form a plane wave to illuminate the diffraction grating. In Figure 3.6, the collimation is accomplished using a concave mirror. In a reflective system, the collimating optics will be some form of a curved mirror, typically a section of an asphere

to minimize the introduction of optical aberrations in the monochromator. The collimating function can also be accomplished with a lens. In either case, the input slit is located at the focal point of the lens or concave mirror. It is important that the collimating optics perform well over the desired wavelength range of the instrument. Here are some of the important parameters for the collimating elements:

1. The reflectivity (mirror) or transmission (lens) should be as high as possible. Both lenses and mirrors are capable of high performance.
2. The focal length should be independent of wavelength. This parameter is also called chromatic aberration. A mirror's focal point will be quite independent of wavelength making this a very good choice. Single-element lenses have significant chromatic aberration. For a wide-wavelength range of operation, a multielement lens would be required to adequately compensate for the dispersion of the glasses used in the lens as well as to minimize the aberrations introduced by the spherical shape of the lens.
3. The size of the collimated beam should be as large as possible to achieve high wavelength resolution. Since the input fiber determines the divergence angle of the light reaching the collimating lens, a long focal length lens will be needed to get a large collimated beam size. It is more economical to make large mirrors as compared to large lenses.
4. Optics should be diffraction limited in their performance. The idea of diffraction-limited optics is illustrated in Figure 3.8. If a collimated beam is incident on a lens, the light will be focused to a small spot. If one thinks of the propagation of light in terms of rays passing through the lens and coming to a spot, one would think that the diameter of the light beam goes to zero at the focal point. In actuality, the beam goes to a minimum beam waist at the focal point of the system. This minimum beam waist is called the diffraction-limited spot size of a lens. Mathematically, the diffraction limited spot size is:[2]

$$w_0 \equiv \frac{2\lambda(fl)}{\pi(\text{diameter})} \tag{3.1}$$

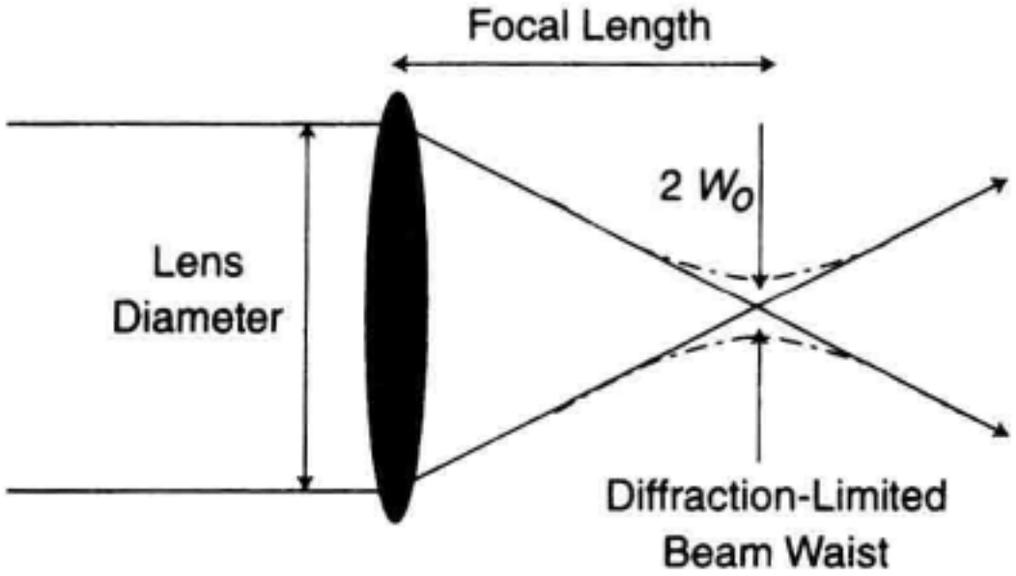

Figure 3.8 Diffraction-limited beam waist for a lens or for a concave mirror.

where w_0 is the spot radius at the $1/e$ power points, λ is the wavelength, *fl* is the focal length of the lens and *diameter* is the lens diameter. This is the minimum achievable spot size if the entire lens is illuminated by a plane wave. Aberrations in a lens can cause the minimum spot size to be degraded. Let's use this formula to calculate the diffraction-limited spot size of a lens that might be used in a fiber-optic input monochromator. Assume that the lens has a diameter of 5 cm and a focal length of 30 cm. At a wavelength of 1550 nm, the diffraction-limited spot radius would be 6 μm. If the shape of the lens or mirror is not correct, the actual minimum spot size for this lensing system could be significantly larger than 6 μm. It is the quality of this collimating system along with diffraction-grating performance that determines the filter response of the monochromator.

3.3.4 The Diffraction Grating

The diffraction grating is at the heart of the monochromator. The diffraction grating functions to "reflect" light at an angle proportional to wavelength.[3] This is the diffractive element in the system, that is, the light is diffracted according to wavelength. The monochromator can be tuned by changing the angle at which the light is incident on the grating. The diffraction grating is typically a reflective element consisting of a substrate and a reflective coating with periodic perturbations (typically referred to as lines or grooves) that form the grating.

The operation of a diffraction grating begins when light strikes the reflective lines of the grating. Each line of the grating diffracts the light off into a range of wavelet angles. For a given wavelength there will be a certain angle at which the diffracted wavelets will be exactly one wavelength out of phase with one another and will add constructively in a parallel wavefront (see Figure 3.9). The light of a given wavelength leaves the grating at a specific angle. Light of other wavelengths leaves the grating at slightly lower or higher angles. The shape or blaze of each grating line determines the overall efficiency of the diffracted beam with respect to the incident beam power.

The general equation for a diffraction grating is:[1]

$$n\lambda = d(\sin\beta - \sin\alpha) \tag{3.2}$$

where λ is the wavelength of the light (in air for most OSAs), d is the spacing of the lines on the grating, α is the angle of the incident light relative to the grating normal, β is the angle at which light leaves the grating, and n is an integer that is called the order of the spectrum. Here the two angles are defined as being on opposite sides of the grating normal as shown in Figure 3.9. The circled area of the figure illustrates the geometry that defines the grating equation.

When the diffracted rays are one wavelength out of phase with respect to each other, the diffracted beam is called first-order. At another angle where the wavelets are all exactly two wavelengths out of phase and will also add constructively, the spectrum is called a second-order spectrum. Even higher-order diffraction may also be present. Figure 3.10 illustrates diffracted orders. The first reflection is called the zero-order beam ($n = 0$)

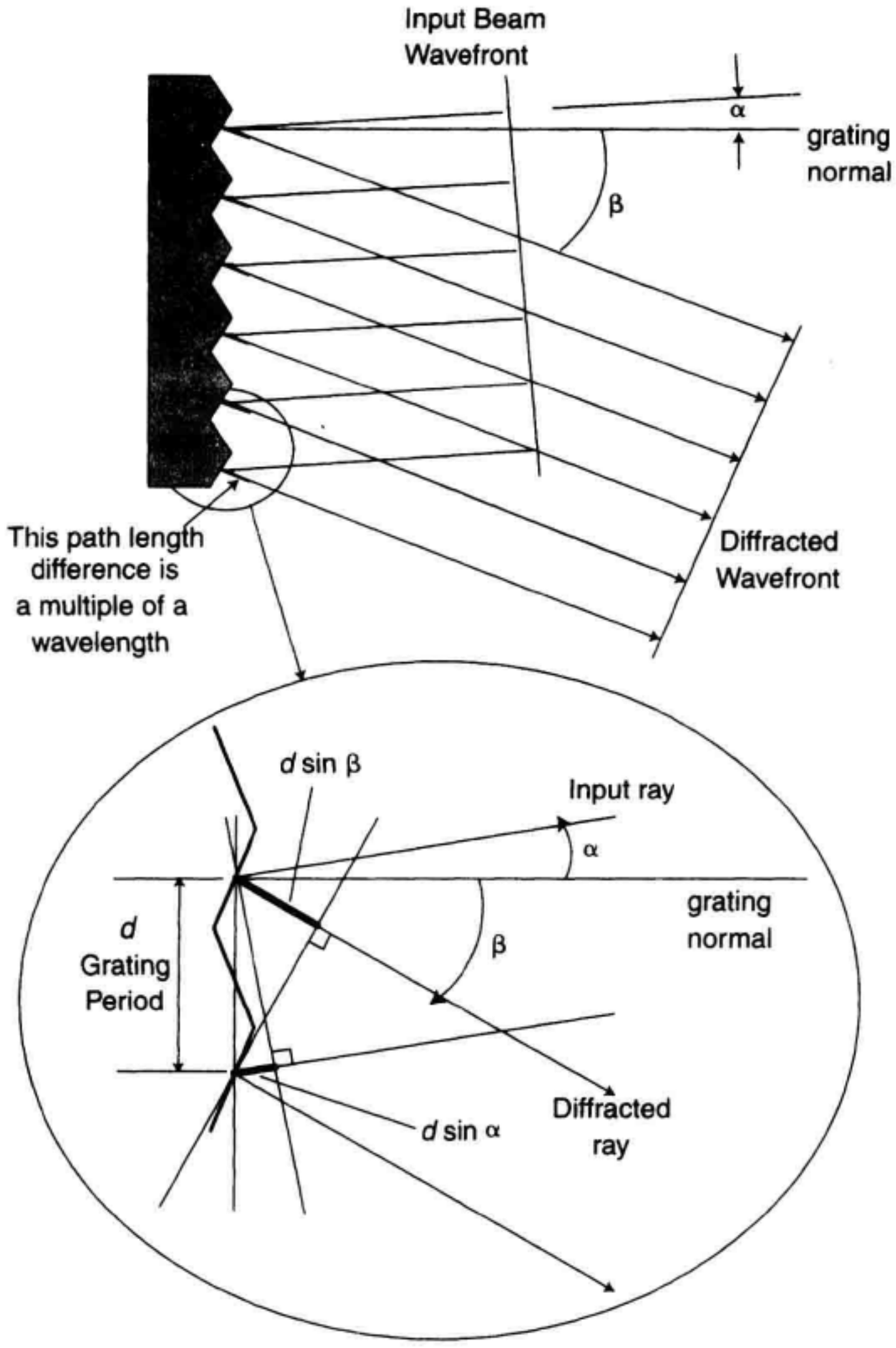

Figure 3.9 Diffraction-grating operation.

where the angle of incidence is equal to the angle of reflection. This zero-order reflected beam is not separated into different wavelengths and is not used by an OSA.

OSAs often use a diffraction grating in a special orientation called the Littrow condition. In this arrangement, the wavelength of interest leaves the diffraction grating and goes directly back along the path of the incident beam as shown in Figure 3.11. For the Littrow condition, the grating equation simplifies to:

$$n\lambda = 2\,d\sin\theta \tag{3.3}$$

where $\theta = \alpha - \beta$.

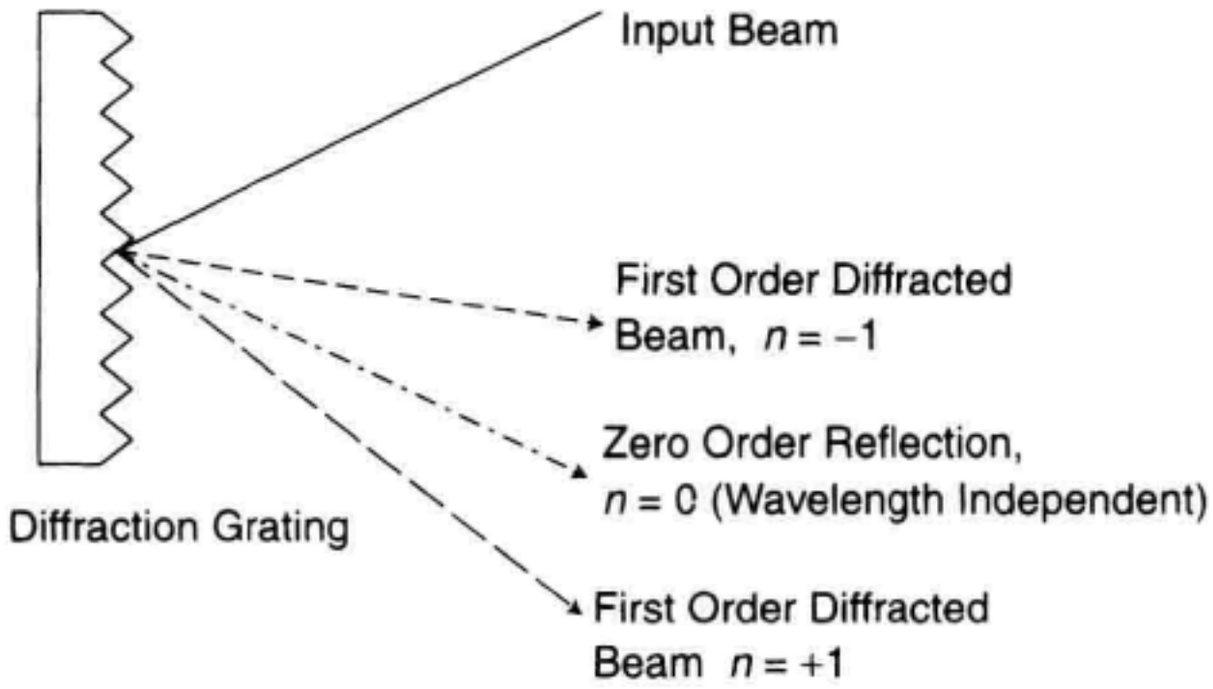

Figure 3.10 Diffracted beam orders.

Figure 3.9 shows that a diffracted plane wave is formed at a single angle where constructive interference is occurring between adjacent grooves of the grating. The diffracted beam actually occupies a narrow range of angles. Even for a single-wavelength input beam, this new diffracted wavefront will be slightly diverging. The divergence angle for this diffracted beam is given as:[2]

$$\Delta\beta_{min} = \frac{\lambda}{Nd\cos\beta} \tag{3.4}$$

where $\Delta\beta_{min}$ is the divergence angle of the diffracted beam for monochromatic light and N is the number of illuminated lines on the grating. This equation highlights a fundamental limitation on the filter width of a grating-based OSA. The resolution is limited by the diameter of the illuminated grating compared to the wavelength. This is analogous to a phased-array antenna. The more elements in the array, the narrower the beam width of the radiation pattern. The resolution of the overall instrument can be worse than this depending on the size of the input and output apertures and the performance of the collimating optics.

Another important property of the grating is its dispersion. Dispersion is a measure of how many degrees the diffracted beam rotates for a given input wavelength change.

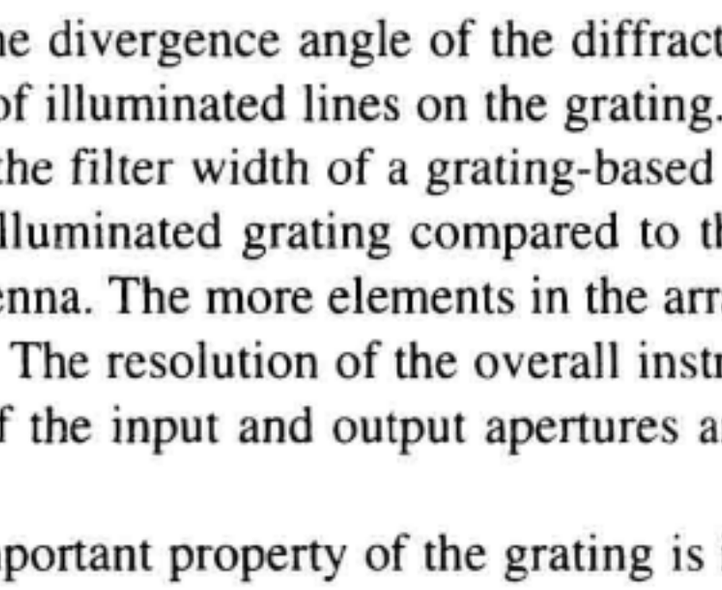

Figure 3.11 The Littrow condition.

The dispersion of a grating can be obtained by taking the derivative of Equation 3.2 with respect to wavelength. The dispersion of a diffraction grating is given as:

$$D = \frac{\Delta\beta}{\Delta\lambda} = \frac{n}{d\cos\beta} \tag{3.5}$$

where D is the dispersion coefficient in *radians/m.* The amount of dispersion of a diffraction grating changes with wavelength. This will cause the optical resolution of the monochromator to change with wavelength. Some OSAs have corrections for this.

In order to understand the limits on grating resolution, both Equations 3.4 and 3.5 must be utilized. Equation 3.4 shows the angular extent of a diffracted beam for a monochromatic input source. Equation 3.4 shows how fast the input angle changes with wavelength. If Equation 3.5 is solved for $\Delta\beta$, it can be equated to 3.4. The minimum achievable wavelength resolution can then be found by solving for $\Delta\lambda$. The resulting equation for minimum resolution is given as:[2]

$$\Delta\lambda_{min} = \frac{\lambda}{Nn} \tag{3.6}$$

where $\Delta\lambda_{min}$ is the minimum-wavelength resolution available from the diffraction grating. This is a very simple result involving only the wavelength, the number of lines illuminated on the grating, N, and the diffracted order, n.

The efficiency of a grating depends on the diffracted angles, the blaze of the grating lines, and the coatings on the grating. For a treatment of this topic, readers are referred to Hutley.[3] An important item to note is that the efficiency of a diffraction grating is polarization dependent. Methods to minimize polarization dependence are shown later in Section 3.4.4.

3.3.5 The Focusing Optics

The purpose of the focusing optics is to take the diffracted light from the grating and image it on the exit or output slit. The focusing optics in a monochromator essentially do in reverse what the collimating optics do. That is, the optics take the diffracted collimated light from the diffraction grating and focus the light on the exit or output slit. In the simplest implementation, these focusing optics could be of the exact same type as the collimating optics, just operated in the reverse direction. The diffraction grating produces a diffracted beam that has an angle proportional to wavelength. Let us consider what would happen if two monochromatic sources were present at the input to the monochromator. The focusing lens converts these input angles to a set of spots at the focal distance from the lens. This line is called the focal plane of the monochromator. The focal plane of the monochromator for this situation is illustrated in Figure 3.12.

The focusing lens functions to convert different diffracted angles from the diffraction grating to a position on the focal plane of the lens. Longer focal-length lenses will cause the spacing between the two signals at the focal plane to be separated by a larger distance. This in itself does not increase resolution since the image size of the DFB laser will be magnified. If the focal lengths of the input and the output collimators are equal,

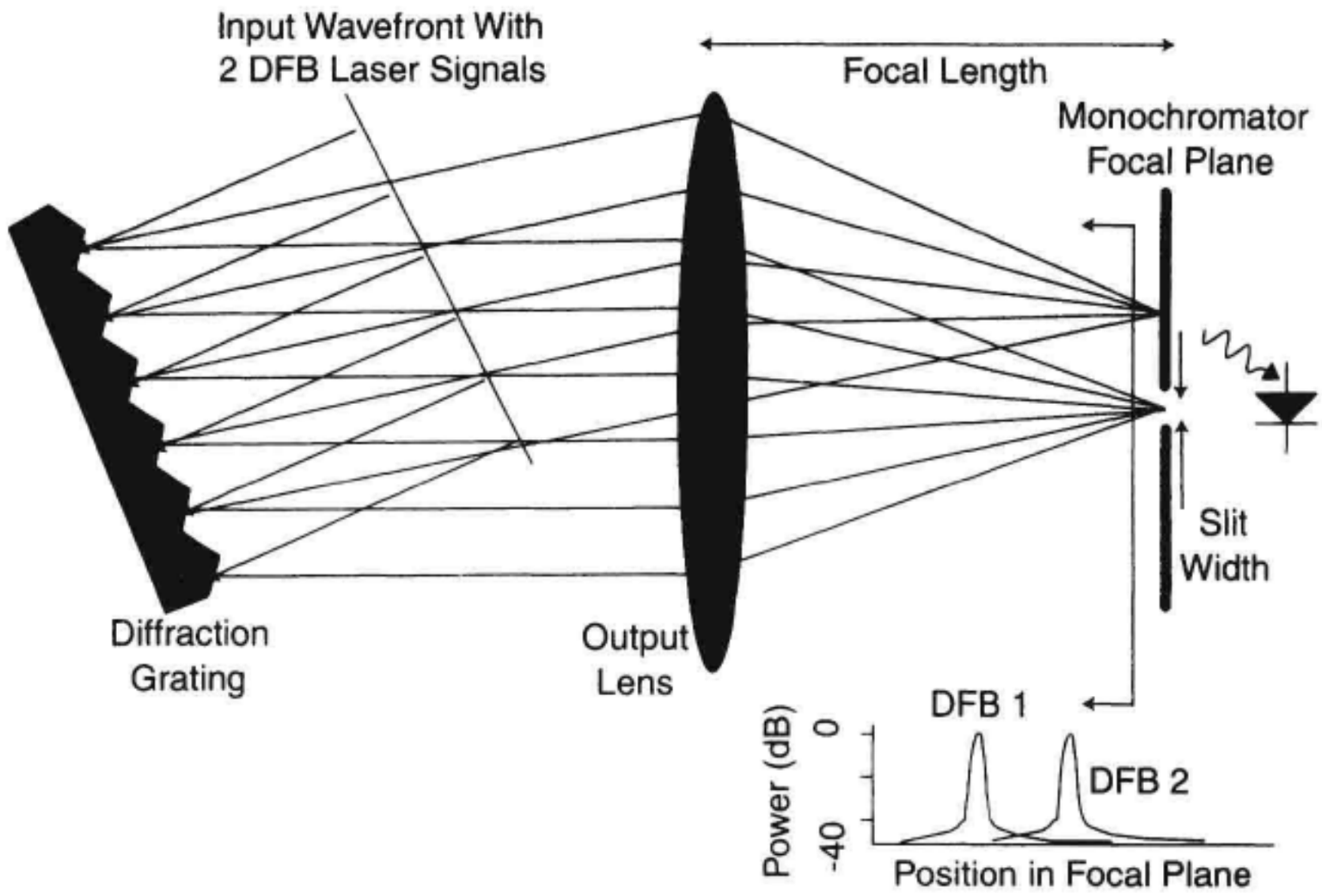

Figure 3.12 The focal plane of the monochromator.

the size of the spot at the output would be equal to the size of the spot at the input. The spot size can be magnified by the ratio of the output lens focal length to the input lens focal length. Notice that in the drawing, the DFB laser images show that the intensity of light away from the peak is greatly attenuated but does not go to zero. This is due to practical issues in a monochromator. Imperfections in the grating can cause light from a DFB laser to be scattered over a wide range of angles. This light will contribute to a low level distribution of light over the entire focal plane. It presents a fundamental limit to the rejection of the optical filter.

3.3.6 The Exit or Output Slit

The exit or output slit along with the entrance or input slit and the diffraction grating affect the resolution of the system. The purpose of the output slit is to spatially filter the light from the diffraction grating. The output slit is put into the focal plane of the monochromator. Because at this point the light is spatially dispersed according to wavelength, any spatial "selection" or filtering of the light will select or filter the spectrum of the light. This is a good place to adjust the optical resolution (in other words, how much of the spectrum of the light to pass) of the instrument. Typically, this slit is realized by an adjustable slit or a series of slits for the desired optical resolutions. A narrow slit will select only a very small portion of the spectrum and thus give high optical resolution. A wider slit will let more of the spectrum through and thus give poorer optical resolution. Typical numbers for optical resolution for a fiber-optic OSA are tenths of nanometers to nanometers of wavelength. One cannot just arbitrarily narrow the slit to give finer and finer opti-

cal resolution. Once the resolution limit presented by the diffraction grating in Equation 3.6 have been reached, any further narrowing of the slit only increases the insertion loss of the monochromator without an increase in the resolution.

The exit slit can be a simple aperture or a receiving optical fiber. An exit slit will pass light that is incident at any angle. Imperfections in the optical system may cause some stray light to be incident from large angles. Slits will not reject this high-angle light. If an optical fiber is used at the exit slit, the acceptance angle will limit high-angle stray light and improve the filter shape and stopband performance of the OSA.

3.3.7 The Detector

The purpose of the detector is to convert the selected light energy into electrical energy for either further processing or display/recording. Photomultiplier tubes are often used at wavelengths shorter than 1 μm resulting in very sensitive detection. The detector in an OSA typically is a semiconductor photodetector. The photodetector (and any associated optics) needs to work over the wavelength range of interest. InGaAs detectors (see Chapter 2) are commonly used for coverage of the long-wavelength fiber-optic communication bands at 1300 and 1550 nm. The bandwidth of the amplifier following the detector is a major factor affecting the sensitivity and sweep time of the instrument. Appendix A covers the noise issues of optical detection in detail.

3.3.8 Single Monochromator Summary

A brief overview of a single-pass grating-based monochromator was given in sections 3.3.1 to 3.3.7. The monochromator consists of an entrance (or input) slit, focusing optics, a diffracting element to angularly separate the wavelengths, collimating optics, and an exit (or output) slit. The input slit, the output slit, and the number of illuminated lines on the diffraction grating are the key elements that constrain the achievable width of the monochromater bandpass function. The input slit is a single or multimode fiber for fiber optic applications. The input slit image is then refocussed at the output focal plane. It is important to have a high-quality optical imaging system so that the output spot is as small and aberration-free as possible. The final filter function is a convolution of the output image with the shape of the output slit function. Filter bandwidths of near 0.1 nm at 1550 nm are achievable in monochromaters that will fit into benchtop packages. This filter width is much wider than the linewidth of a typical singlemode laser. The OSA typically traces out the filter shape of the instrument when measuring a DFB-laser mode for example. The high-resolution spectrum analysis techniques of Chapter 5 are needed to resolve the details of a laser-line shape.

Example Calculation of Monochromator Resolution. To illustrate the resolution capabilities of a single-pass monochromator that might be used for fiber optic applications, consider a monochromator with a singlemode fiber optic input, 5 cm diameter collimating lens with 20 cm long focal length and a diffraction grating with 1000 lines/mm at Littrow angle operating in first order. The wavelength for this example is 1550 nm.

For the Littrow condition, the angle of the input beam with respect to the grating normal would be 51 degrees (from Equation 3.3). The divergence angle for a singlemode fiber is 12 degrees. At 20 cm, the collimated beam diameter would be 4.2 cm. The lenses are just large enough to accommodate the input beam diameter. From Equation 3.6, the minimum available resolution from this system would be 0.037 nm. Using Equation 3.4, the divergence angle for a monochromatic input signal to the monochromator would be 0.00012 rad. A 20 cm long focal-length lens converts this angular change to a 2.4 μm positional change in the focal plane. This means that an aperture of 2.4 μm or slightly larger would be needed to obtain the narrowest instrument resolution. The actual filter shape of the instrument is the convolution of the rectangular slit aperture and the shape of the image in the focal plane.

3.3.9 Single Monochromator Versus Double Monochromator

The monochromator described in the previous section used a single pass off of the diffraction grating to achieve wavelength filtering. The selectivity for this configuration is often not sufficient for measuring side-mode suppression ratio in DFB lasers for telecommunications. One could increase the size of the diffraction grating and the collimated beam size to improve selectivity. The collimated beam size would get too large to be contained in a small benchtop package. In most cases, it is more efficient to cascade two monochromators in series to obtain adequate selectivity. Single monochromators also have a limited stopband performance due to imperfections in the diffraction grating and due to scattered light within the monochromator. Improved stopband performance is obtained with cascaded filters.

3.3.10 Double Monochromator

Double monochromators, such as shown in Figure 3.13, are equivalent to a pair of sweeping filters. While this technique improves dynamic range, double monochromators typically have reduced span widths due to the limitations of monochromator-to-monochromator tuning match; double monochromators also have degraded sensitivity due to losses in the monochromators.

3.3.11 Double-Pass Monochromator

An alternative to the double monochromator is the double-pass monochromator design.[4] The double-pass monochromator provides the dynamic-range advantage of the double monochromator and the sensitivity and size advantages of the single monochromator. Figure 3.14 shows an example double-pass monochromator. It uses the same diffracting grating and collimating optics twice. The grating is used in the Littrow configuration.

The first pass through the double-pass monochromator is similar to conventional single-monochromator systems. The input beam (1) is collimated by the optical element and dispersed by the diffraction grating. This results in an angular distribution of the light, based on wavelength. The diffraction grating is positioned such that the desired wavelength (2) passes through the aperture. The width of the aperture determines the band-

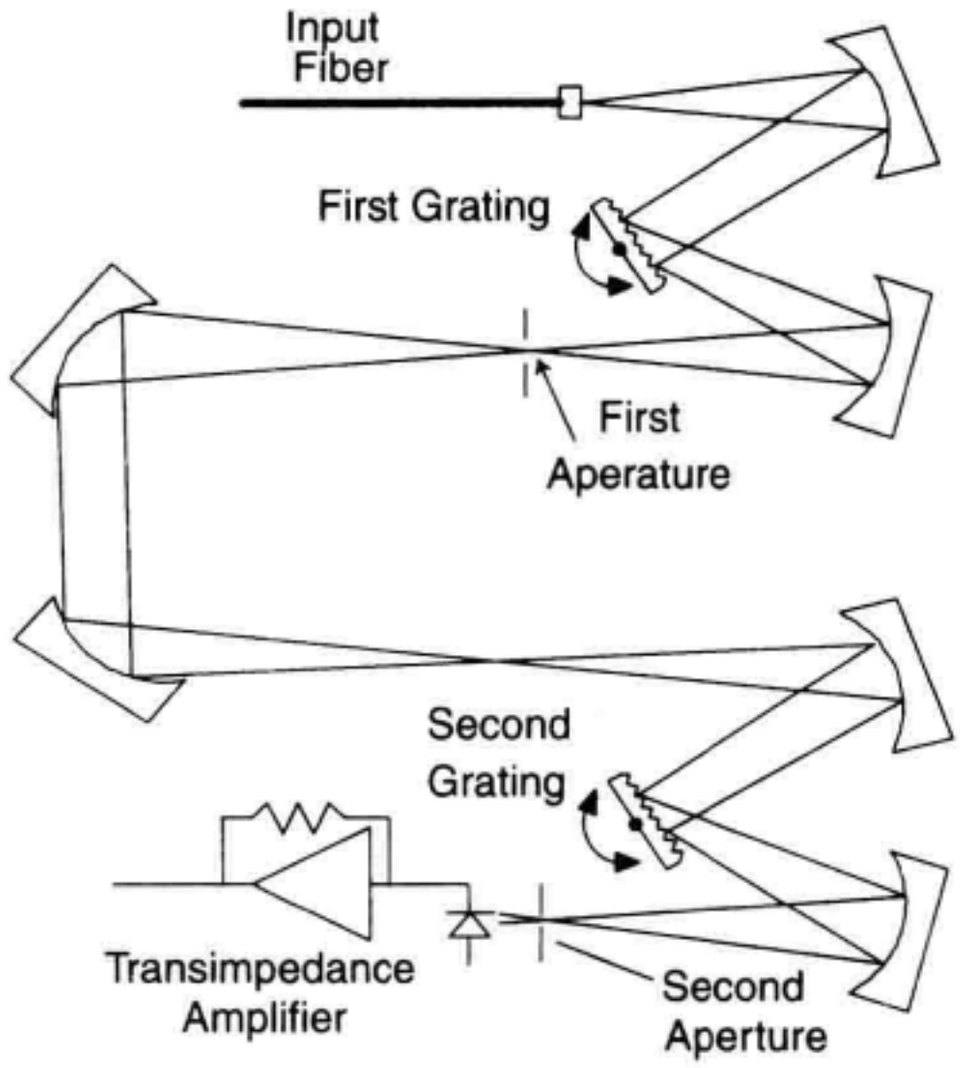

Figure 3.13 Double-monochromator-based OSA.

width of wavelengths allowed to pass to the detector. Various apertures are available to provide a range of resolution bandwidths. The minimum useful aperture size is limited by the diffraction-limited spot size of the optics.

This system shown in Figure 3.14 is unique in that the filtered light (3) is sent through the collimating element and diffraction grating for a second time. During this second pass through the monochromator, the temporal dispersion process is reversed. This means that all of the rays take the same total path length through the monochromator. The small resultant image (4) allows the light to be focused onto a fiber which carries the signal to the detector. This fiber acts as a second aperture in the system. The implementation of this second pass results in the high sensitivity of a single monochromator and the high dynamic range of a double monochromator. The size of the spot at the output of this monochromator is independent of the size of the resolution-determining slit. This allows the use of a small detector for all bandwidth settings. Since the dark current of a detector is proportional to the detector size, better detector sensitivity can be obtained with this double-pass configuration.

3.3.12 Littman Double-Pass Monochromator

In the Littman design (Figure 3.15), the diffraction grating is illuminated at a very shallow angle. The diffraction grating provides a large angular dispersion of wavelengths at shallow angles. The dispersion Equation 3.5 shows that the dispersion increases to a maximum value as β approaches 90 degrees. The diffracted light is retroreflected back to the grating for a second pass in this design. The light is then focused to an exit slit. A major advantage of the Littman configuration is the small size of the monochromator for its resolution. Normally a long focal length lens is required to illuminate a large number of lines

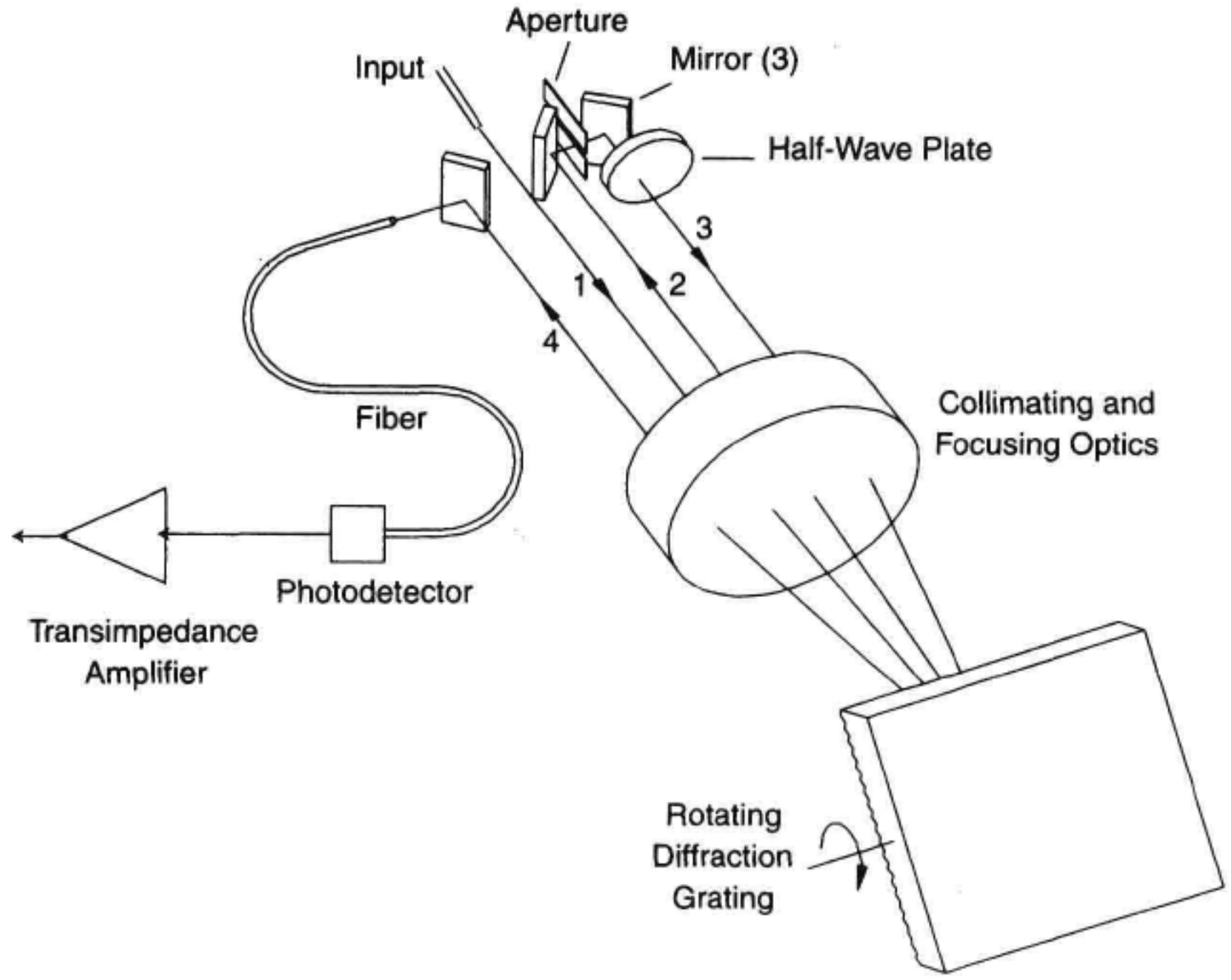

Figure 3.14 Block diagram of double-pass-monochromator OSA.

on the grating. Because the diffraction grating is placed at a shallow angle, only a small collimated beam size is needed for full illumination. If a two-dimensional retroreflector mirror is rotated for wavelength selection, the optical system is very forgiving in terms of optical alignment. A disadvantage of the double-pass Littman monochromator approach is the large amount of polarization sensitivity that is found for a shallow angle grating. The s-polarization (perpendicular to grating lines) is much more efficient than the p-polarization (parallel to grating lines).

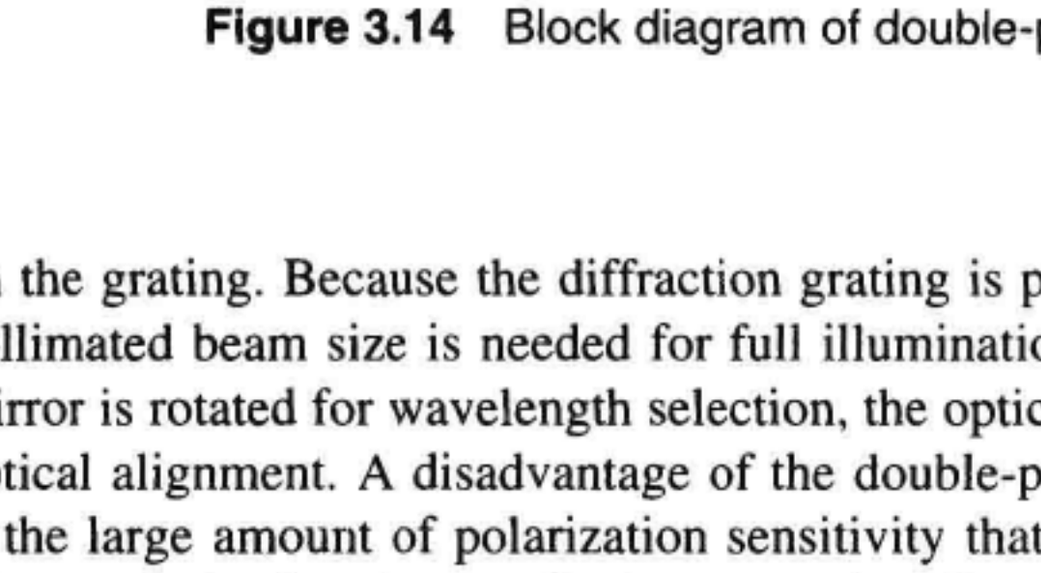

Figure 3.15 Configuration of a double-pass Littman monochromator.

3.4 OPERATION AND KEY SPECIFICATIONS OF DIFFRACTION-GRATING-BASED OPTICAL SPECTRUM ANALYZERS

3.4.1 Wavelength Accuracy

Wavelength-tuning Mechanism. The wavelength tuning of an OSA is controlled by the rotation of the diffraction grating. Each angle of the diffraction grating causes a corresponding wavelength of light to be focused directly at the center of the output slit. In order to sweep across a given span of wavelengths, the diffraction grating is rotated, with the initial and final wavelengths of the sweep determined by the initial and final angles. To provide accurate tuning, the diffraction-grating angle must be precisely controlled and very repeatable over time.

Grating-Motion Techniques. OSAs often use gear-reduction systems to obtain the required angular resolution of the diffraction grating. Gear-reduction systems offer very fine motion control but it is difficult to move the grating quickly. To overcome problems associated with gear-driven systems, some OSAs have implemented a direct-drive motor system. Optical encoder technology with interpolation techniques allow very fine motion control (4 million positions over a 360 degree rotation) and the ability to quickly move the grating to a desired starting position.

3.4.2 Wavelength-Calibration Techniques

The OSA determines the wavelength of any data point from the position of the grating. Therefore, any mechanical tolerance has a direct affect on the wavelength accuracy. To compensate for component variations, manufacturers calibrate the wavelength axis. However, shock and vibration as well as temperature changes can cause wavelength shifts on the order of ±1 nm. Compared to the full wavelength range, this is less than 0.1%—an excellent stability for bearings that have to hold the mass of the grating, position encoder, etc., while still performing many years without noticeable wear.

Calibration with a Well-Known Laser Wavelength. An OSA can be calibrated by measuring a source with a well-known wavelength.[5] A user calibration is only as accurate as the reference signal. Single-wavelength calibrations can be made at the accurate helium-neon laser wavelengths listed in Table 4.1 in the next chapter. Single-point calibrations allow very accurate measurements near the calibration wavelength but errors start to accumulate away from this calibration point. Alternately, a stable wavelength tunable laser can be calibrated with a wavelength meter and swept over a range of frequencies.

Figure 3.16 illustrates the measurement procedure to transfer the accuracy of a wavelength meter to an OSA. The power from the tunable laser is coupled to both the wavelength meter and the OSA. The OSA is then forced to read the same wavelength value as the wavelength meter. Wavelength meters can determine the source wavelength to 1 part per million accuracy (see chapter 4). As can be seen from the measurement set-up, this calibration method is rather expensive.

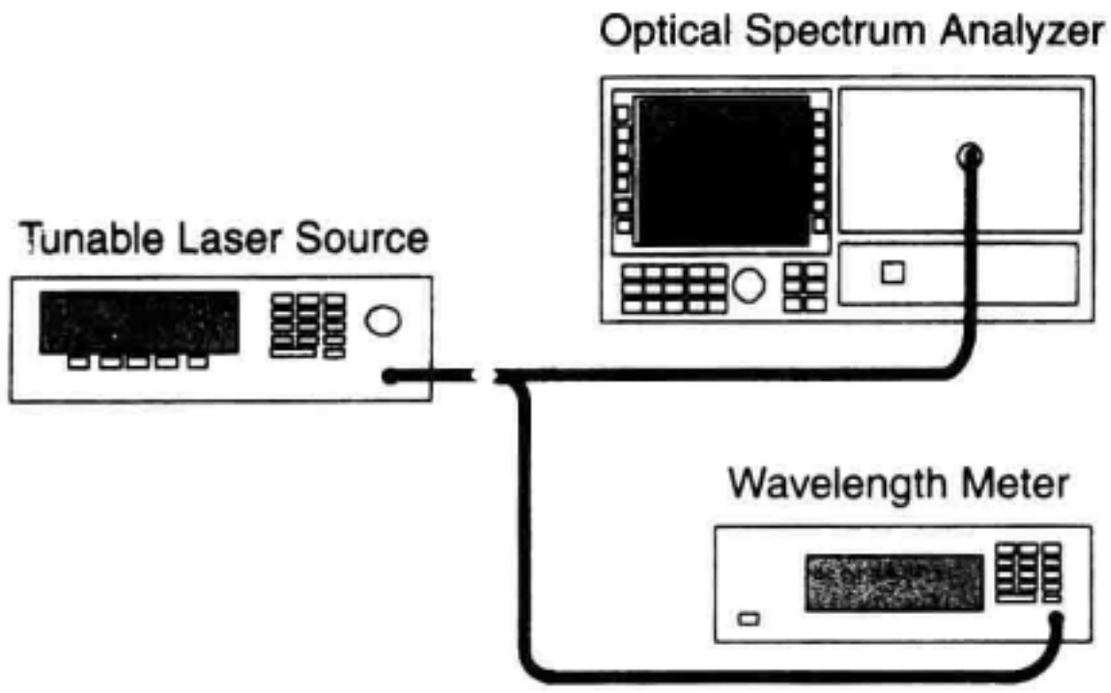

Figure 3.16 Wavelength calibration using a laser signal.

Calibration with Absorption Cells. Calibrating with gas absorption lines (Figure 3.17) has the advantage that such lines are natural constants.[6–12] The light from a broadband source such as an edge-emitting LED (see Chapter 9) is passed through a glass tube containing a molecular gas. Gas cells absorb radiation near the vibrational and rotational resonances of molecules. The resulting light is collected and passed on to an OSA. The strongest absorption occurs at the fundamental resonance frequency for gas molecules which most often occurs at wavelengths longer than 2 μm. The available absorption lines for the important 1550 nm fiber optic band are limited. The two most promising candidates are acetylene and hydrogen cyanide. The resonances for both of the molecules are overtones of the fundamental vibrational frequencies. Figure 3.18 shows the absorption spectrum for acetylene.[6] There is a set of absorption spikes that are nearly uniformly spaced over the 1510 to 1545 nm range. The length of the evacuated tube for this measurement is 5 cm and the gas pressure is 400 Torr. The magnitude of the absorption lines is less than 3 dB for these conditions. Tables 3.1 and 3.2 list the designations and wavelengths for the absorption lines in acetylene and some of its carbon isotopes.[7] The vacuum wavelengths of these absorption lines in the table have been measured to an accuracy of 0.001 nm. The R prefix in the tables designates resonances in the shorter wavelength lobe and the P prefix is for the longer wavelength absorption lobe. Saka, Sudo, and Ikegami[8] have studied the effect of temperature and pressure for the acetylene absorption band. They concluded that the temperature sensitivity is less than 100 kHz/K and the pressure

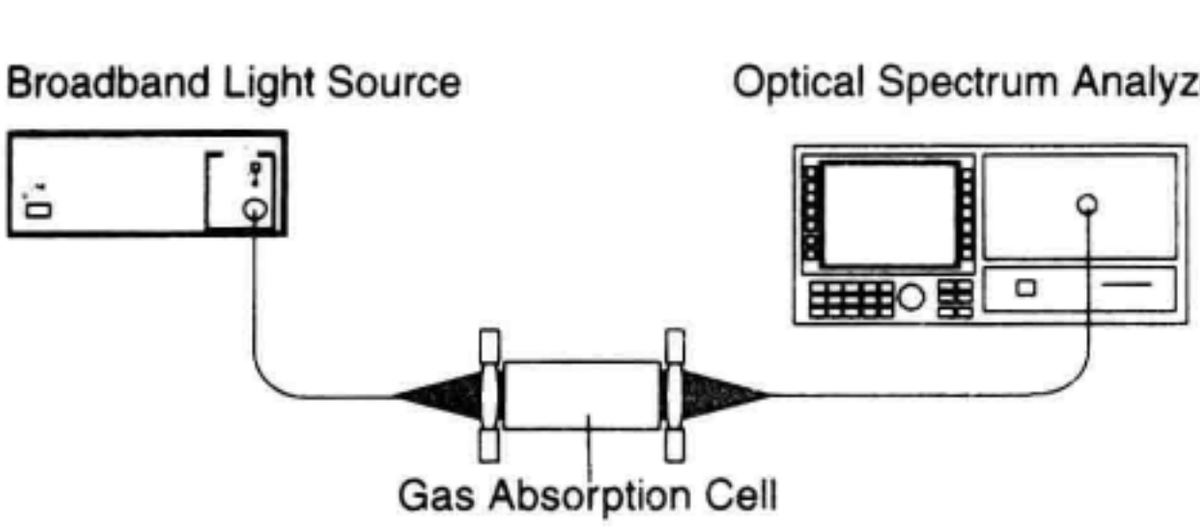

Figure 3.17 Wavelength calibration using natural absorption lines.

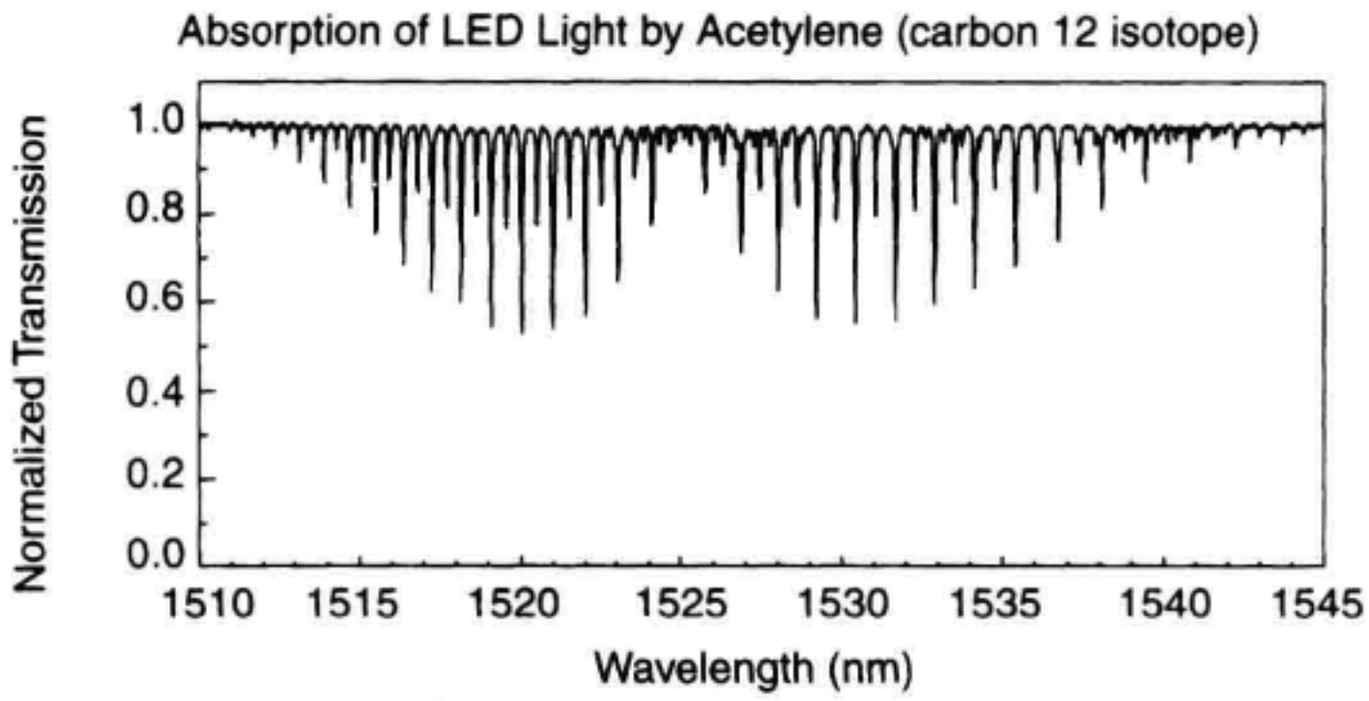

Figure 3.18 Absorption of LED light by acetylene $^{12}C_2H_2$ (source: Sarah Gilbert at NIST).

sensitivity is less than 1.5 kHz/Pascal. An extreme temperature variation would be 100 K resulting in a 1 MHz shift. This corresponds to a 0.000008 nm wavelength shift at 1550 nm and would therefore be unimportant. The absorption level per unit length in the cell can be increased by increasing the gas pressure inside the tube. At higher pressures, the width of the absorption lines will start to broaden as the individual molecules in the gas start interacting with each other.

An alternate absorption cell gas is hydrogen cyanide.[12] The absorption characteristics for a 15 cm long tube at 150 Torr is shown in Figure 3.19. Table 3.3 lists the absorption lines for hydrogen cyanide. Hydrogen cyanide absorption is well centered on the EDFA gain band around 1545 to 1560 nm. For this reason, it is a desirable absorption cell for WDM applications. The only drawback to hydrogen cyanide is its toxicity. Hydrogen cyanide attaches to hemoglobin molecules in the blood rendering them useless to carry oxygen. The amount of gas present in an absorption cell can be made small enough so that calibrations can be accomplished without hazard. DWDM system measurements require high wavelength accuracy giving absorption cell technology significant commercial interest.

Table 3.1 Vacuum wavelengths (nm) of selected acetylene ($^{12}C_2H_2$) absorption lines.

R27	1512.45	R13	1518.21	P1	1525.76	P15	1534.10
R25	1513.20	R11	1519.14	P3	1526.87	P17	1535.39
R23	1513.97	R9	1520.09	P5	1528.01	P19	1536.71
R21	1514.77	R7	1521.06	P7	1529.18	P21	1538.06
R19	1515.59	R5	1522.06	P9	1530.37	P23	1539.43
R17	1516.44	R3	1523.09	P11	1531.59	P25	1540.83
R15	1517.31	R1	1524.14	P13	1532.83	P27	1542.25

Table 3.2 Vacuum wavelengths (nm) of selected acetylene ($^{13}C_2H_2$) absorption lines

R26	1521.20	R12	1526.95	P2	1534.35	P16	1542.39
R24	1521.95	R10	1527.86	P4	1535.43	P18	1543.63
R22	1522.72	R8	1528.80	P6	1536.53	P20	1544.89
R20	1523.52	R6	1529.76	P8	1537.66	P22	1546.18
R18	1524.35	R4	1530.74	P10	1538.81	P24	1547.49
R16	1525.19	R2	1531.75	P12	1539.98	P26	1548.82
R14	1526.06	R0	1533.41	P14	1541.17	P28	1550.18

Air versus Vacuum Wavelengths. All fiber-optic input spectrum analyzers directly measure the wavelength of light in an air environment. No one has undertaken the challenge of building a vacuum chamber into an OSA. Most wavelength measurements are quoted in terms of vacuum wavelengths or optical frequency. This means that the OSA must convert between these display options. The relationships between these variables are:

$$c = f\lambda_{vac} \tag{3.7}$$

where $\lambda_{vac} = \lambda_m n_m$ is the wavelength of light in a vacuum, c = speed of light in vacuum (2.99792458E+8 m/s), f = optical frequency, λ_m = wavelength in medium (for example, air), and n_m = refractive index of the medium.

OSAs directly measure λ_m. The main issue is that the index of refraction depends on temperature, pressure, and humidity. To do a perfect conversion between the vacuum wavelength and air wavelength would require an accurate knowledge of the refractive index. The refractive index of air at sea level for a 15 C temperature and no humidity is 1.000273 (at 1550 nm). Chapter 4 has a section that describes how the index of refraction changes with environmental variables. It is necessary for the user to enter a value of the index of refraction in order to get accurate vacuum wavelength on frequency displays. Before the introduction of DWDM systems, the small errors introduced by uncertainty in the index of refraction were not significant for most measurements. An error of 0.4 nm is made if the index of refraction of air is ignored at a wavelength of 1550 nm. With 0.8 nm-spaced DWDM channels, this is a significant error.

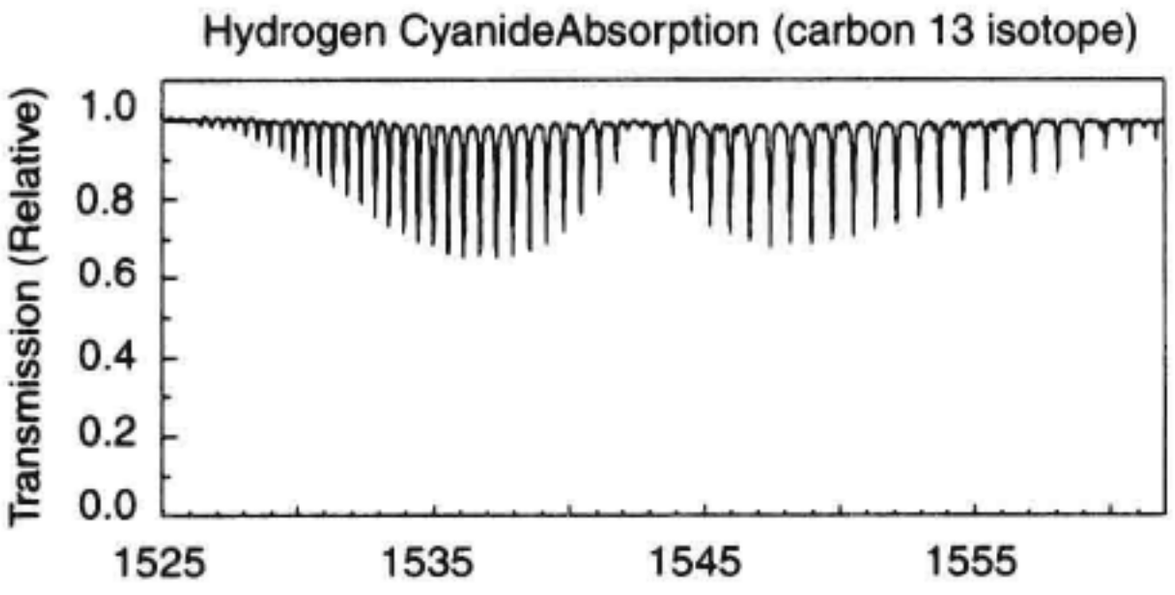

Figure 3.19 Absorption of LED light by hydrogen cyanide ($H^{13}CN$) (source: Sarah Gilbert at NIST).

Table 3.3 Vacuum wavelengths (nm) of selected hydrogen cyanide ($H^{13}CN$) absorption lines.

R25	1528.05	R12	1534.42	P1	1543.11	P14	1552.93
R24	1528.49	R11	1534.97	P2	1543.81	P15	1553.76
R23	1528.93	R10	1535.54	P3	1544.52	P16	1554.59
R22	1529.38	R9	1536.12	P4	1545.23	P17	1555.44
R21	1529.84	R8	1536.7	P5	1545.96	P18	1556.29
R20	1530.31	R7	1537.3	P6	1546.69	P19	1557.16
R19	1530.79	R6	1537.91	P7	1547.44	P20	1558.03
R18	1531.28	R5	1538.52	P8	1548.19	P21	1558.92
R17	1531.77	R4	1539.15	P9	1548.96	P22	1559.81
R16	1532.28	R3	1539.79	P10	1549.73	P23	1560.72
R15	1532.80	R2	1540.43	P11	1550.52	P24	1561.64
R14	1533.33	R1	1541.09	P12	1551.31	P25	1562.56
R13	1533.87	R0	1541.75	P13	1552.12	P26	1563.50

Let us assume that an OSA is calibrated with an acetylene absorption cell so that a 1550 nm laser reads exactly 1550 nm at sea level. What type of wavelength error would be introduced by a climb into the mountains with this OSA? Figure 3.20 shows how an OSA calibrated at sea level would change its displayed reading as a function of elevation. For a very tall mountain, 5000 m, the instrument would be in error by 0.2 nm. This would not be sufficiently accurate for many applications.

Accuracy After User Calibration. Wavelength reproducibility, as defined for most OSAs, specifies wavelength tuning drift in a 1 min period. This is specified with the OSA in a continuous sweep mode and with no changes made to the tuning. In addition to

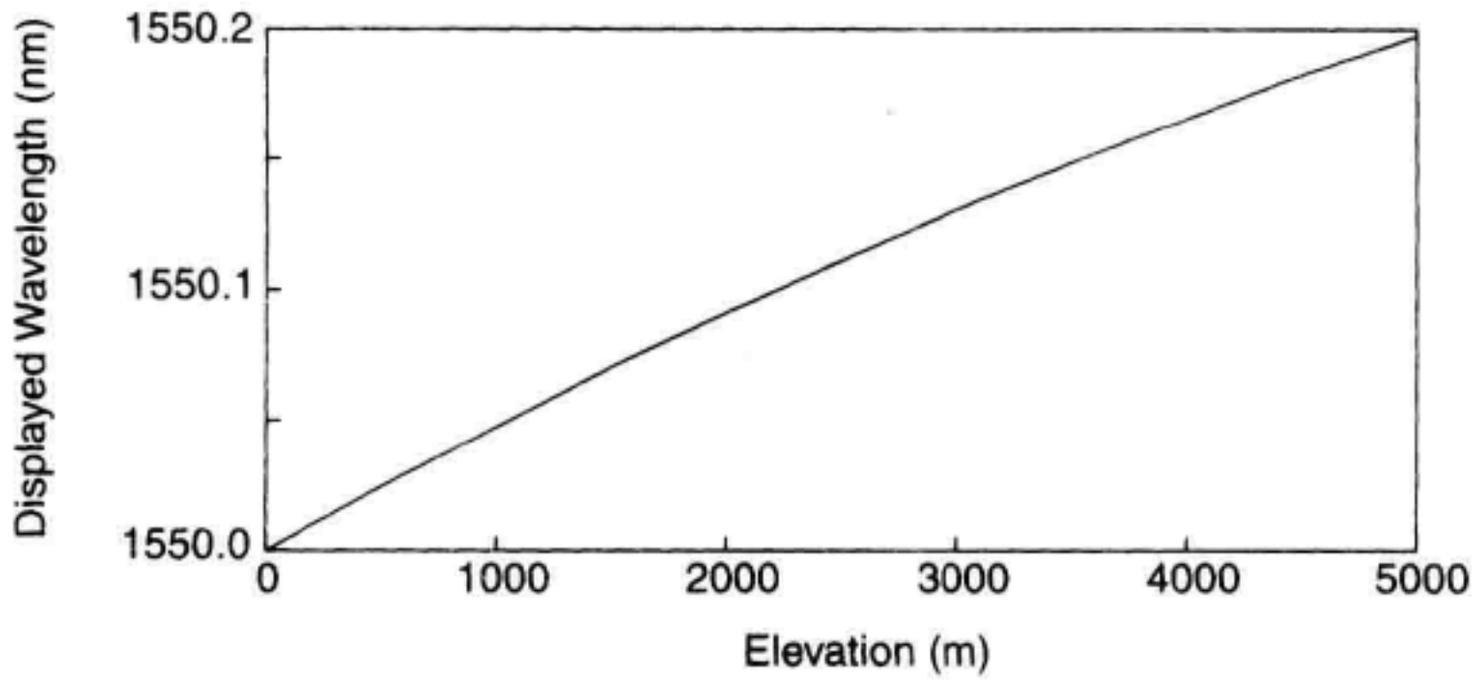

Figure 3.20 Measured wavelength as a function of elevation.

wavelength reproducibility, wavelength repeatability specifies the accuracy to which the OSA can be retuned to a given wavelength after a change in tuning. If a user calibrates the wavelength of the OSA making measurements, then the errors are greatly reduced. The tolerances due to shock and vibrations are compensated, and temperature changes during the measurement usually are less than a few degrees (we assume that the user calibrates the OSA after it has been warmed up). The remaining uncertainties stem from the image quality, the mechanical repeatability, residual nonlinearities, and the limitations of the encoder that determines the grating angle. For further details on OSA calibration, see Reference 5.

3.4.3 Wavelength Resolution and Dynamic Range

Resolution Bandwidth. The ability of an OSA to display two signals closely spaced in wavelength as two distinct responses is determined by the wavelength resolution. Wavelength resolution is, in turn, determined by the bandwidth of the optical filter. The term resolution bandwidth is often used to describe the width of the optical filter in an OSA. The filter bandwidth is limited by the grating resolution (Equation 3.6) together with the input and output aperture sizes and the quality of the optical components. An example calculation for a single-pass monochromator was given in section 3.3.8. The resolution is also influenced by the number of times that the optical signal impinges upon the diffraction grating. Double monochromators have significantly sharper filter skirts than single monochromators. OSAs have selectable filters of 10 nm down to less than 0.1 nm, that make it possible to select the appropriate resolution for most measurements.

Figure 3.21 shows the filter shape typical for a double-pass monochromator with singlemode fiber at its input for several values of resolution bandwidth. The collimated beam diameter in this example is 2 cm using a 1000 lines/mm diffraction grating in the Littrow configuration. The shape of the filter is important for measuring parameters such as the side-mode suppression ratio in DFB lasers or for measuring the signal-to-noise ratio in amplified DWDM systems. The filter shape also affects noise-level measurements. This figure illustrates graphically how the width of the exit slit and the size of the image in the focal plane combine to determine the filter shape of the instrument. The size

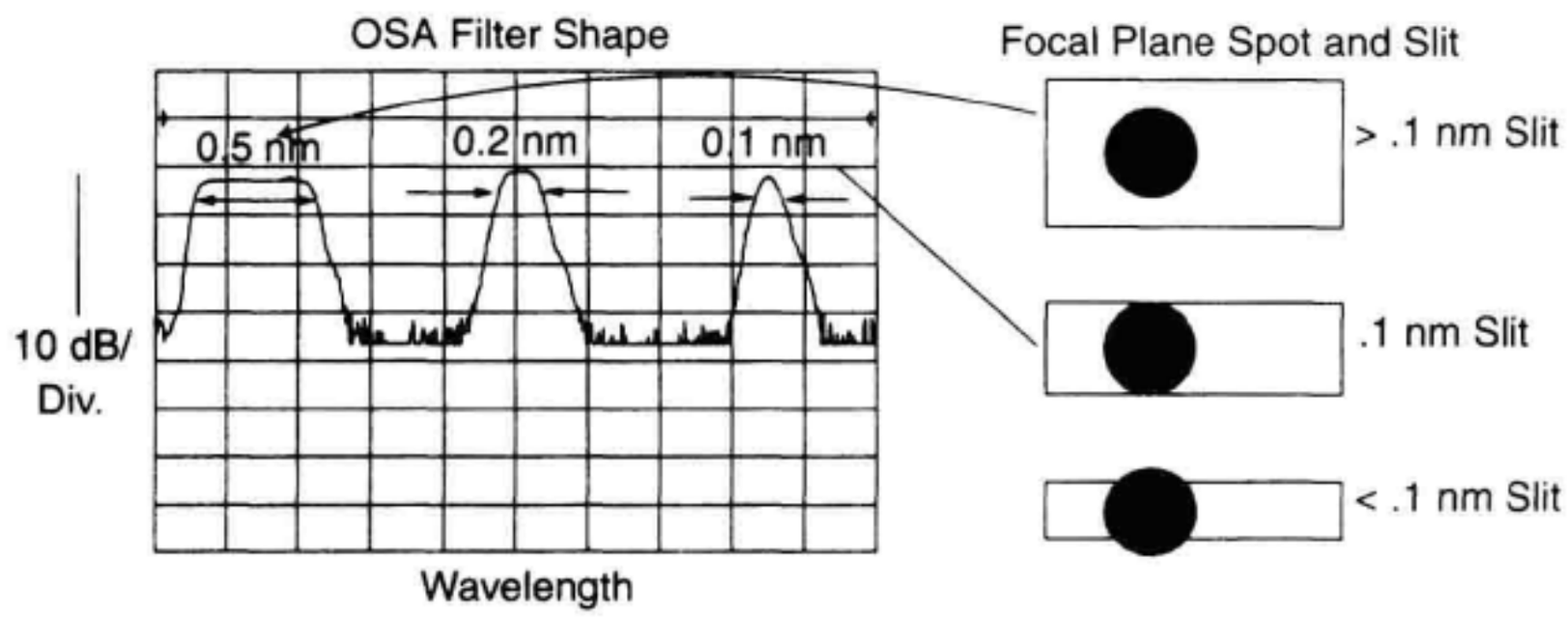

Figure 3.21 Typical filter shape.

of the imaged spot is determined by the number of illuminated lines on the grating and the number of passes off of the grating. The shape of the image can also be influenced by the quality of the collimating optics and the input-image quality. The filter shape of the instrument is the convolution of the image shape and the slit shape. If the exit slit is wider than the image size, the passband is dominated by the slit width. The minimum resolution is obtained when the slit and image size are approximately the same size. If the slit width is decreased further, the insertion loss of the filter will increase for a small narrowing of the filter width.

Noise Bandwidth. An OSA reads out a nominal resolution bandwidth setting from its front panel control. Most noise measurements are defined for a filter shape with a flat-topped passband and infinitely steep filter skirts. Since OSAs do not achieve this perfect filter shape, an effective noise bandwidth of the filter must be measured and calculated. The effective noise bandwidth of a filter is such that it would pass the same total noise power as a flat-topped filter of the same bandwidth. OSAs have a noise marker function that uses stored filter shape data so that the effective noise bandwidth can be directly read out without the need for the user to measure the filter shape.

Dynamic Range. Dynamic range refers to the ability of a spectrum analyzer to simultaneously look at large and small signals in the same sweep. The dynamic range of an OSA is primarily determined by the filter shape and stopband performance of the tunable filter. Very sharp filter skirts and deep stopbands in the filter response are desired. Figure 3.22 shows the filter shape of a single monochromator versus a double-pass monochromator instrument. The advantage of double monochromators over single monochromators is that double-monochromator filter skirts are much steeper, and they allow greater dynamic range for the measurement of weak spectral components located very close to a large spectral component. The monochromator parameters for the double-pass case are the same as that for Figure 3.21.

Scattered light within a monochromator limits the ultimate stopband performance of a monochromator. Imperfections in the grating lines are an example mechanism for scat-

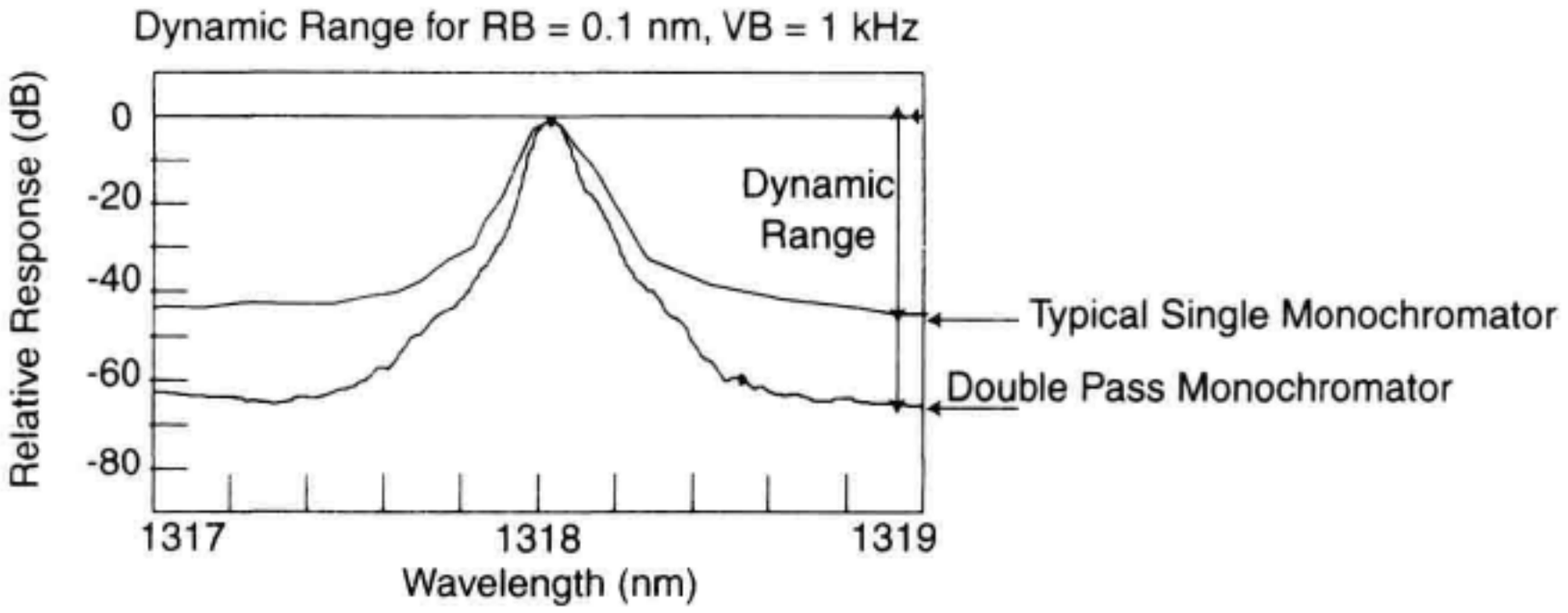

Figure 3.22 Example filter shapes, of a single- and double-monochromator OSA.

tered light. Dynamic range is commonly specified at 0.5 nm and 1.0 nm offsets from the main response. Specifying dynamic range at these offsets is driven by the mode spacings of typical DFB lasers. A –60 dB dynamic-range specification at 1.0 nm and greater indicates that the OSA's response to a purely monochromatic signal will be –60 dBc or less at offsets of 1.0 nm and greater.

Stray-light Limitations on Dynamic Range. The stopband performance of a monochromator is often limited by stray light. The stray light is caused by scattering of light within the optical system. The stopband performance of the filter can be improved if the detector can distinguish between the stray light and the desired light from the monochromator. Improvements in performance can be obtained in several ways. The scattered light in the focal plane of the monochromator can be sensed and the OSA can measure the difference between the received light and the background light level. The improvement in dynamic range performance for such a subtraction scheme is illustrated in Figure 3.23. The main purpose of this chopper mode is to provide stable sensitivity levels for long sweep times, which could otherwise be affected by drift of the electronic circuitry. The desired stability is achieved by automatically chopping the light to stabilize electronic drift in long sweeps. The procedure samples the noise and stray light before each trace point and subtracts them from the trace point reading. Another method to reject stray light is to chop the light in the signal path. The detector can have a bandpass filter at the chop frequency to distinguish stray light from that coming from the desired optical path.

Figure 3.24 shows a DFB laser measured using a single and double-pass monochromator. It illustrates the importance of the resolution bandwidth, the filter shape, and dynamic range of OSAs for DFB laser measurements. Single monochromators often do not have steep enough filter skirts to see the low-level longitudinal modes adjacent to the main peak.

Dense wavelength division multiplexing (DWDM) systems are pushing dynamic range requirements. To characterize channels with 100 GHz (0.8 nm) spacing, the mono-

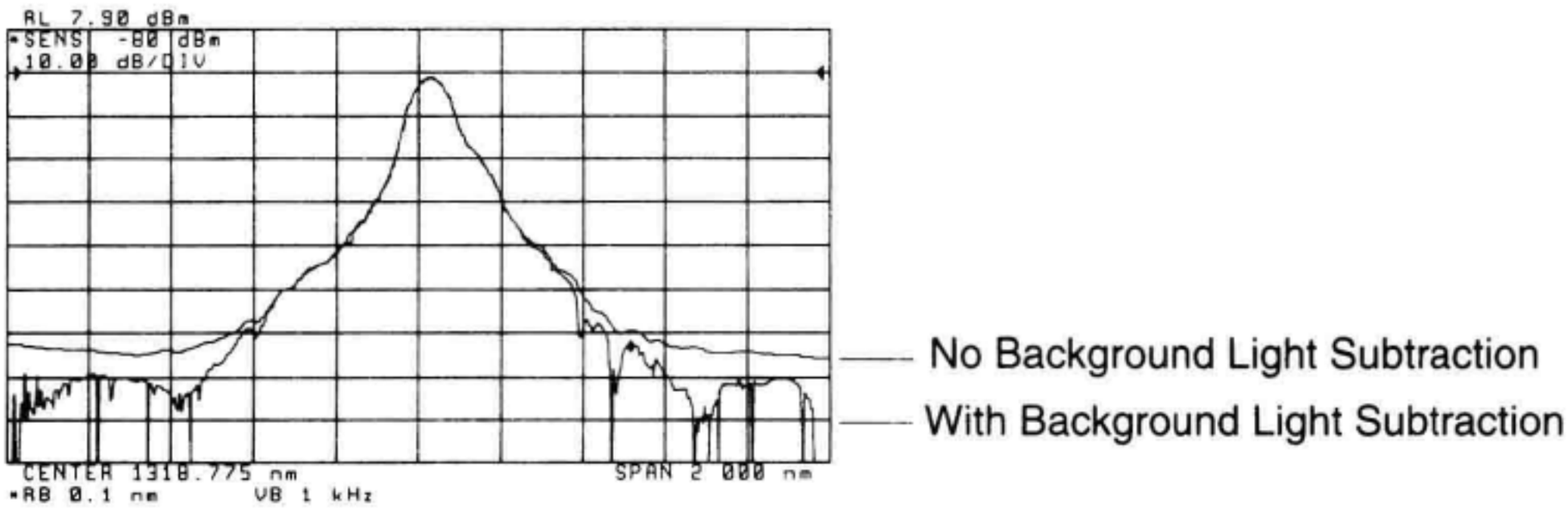

Figure 3.23 Dynamic-range improvement from the background subtraction (chopper) mode.

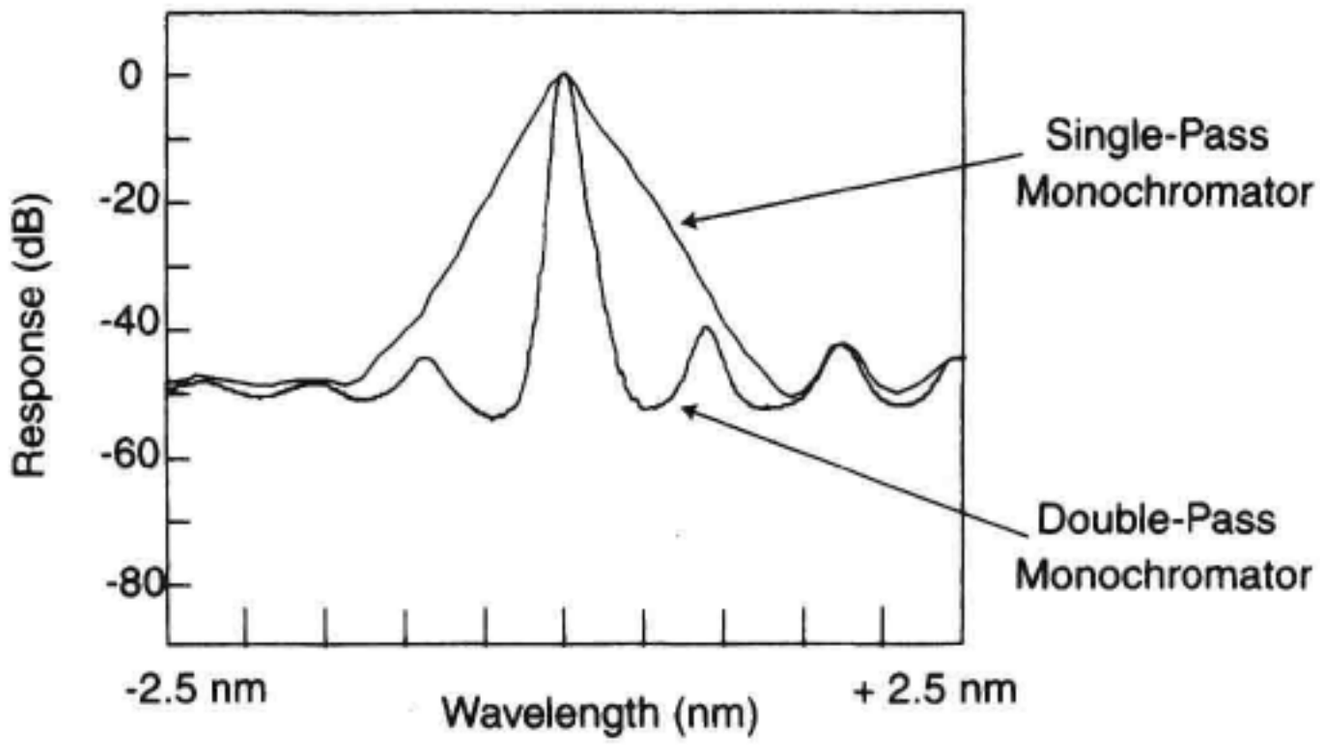

Figure 3.24 Typical dynamic-range limits for single, double, and double-pass monochromators.

chromator must have good stopband performance and steep skirts. Figure 3.25 shows a single-to-noise ratio (SNR) measurement on a four channel DWDM system with 200 GHz (1.6 nm) channel spacing. For signal-to-noise ratio measurements in 0.8 nm spaced channels, the desired dynamic range is at least 40 dB at a 0.4 nm offset.

3.4.4 Sensitivity and Sweep Time

Sensitivity is defined as the minimum detectable signal and is often defined as six times the root-mean-square (rms) noise level of the instrument. The sensitivity of an instrument is determined by the loss in the monochromator, and the sensitivity of the optical detector following the monochromator. The resolution bandwidth of the instrument does not affect the sensitivity as it does in electrical spectrum analyzers.

The dominant loss mechanism for the monochromator is the diffraction-grating efficiency. The blaze (the shape of the lines in the grating) of the diffraction grating can be optimized for the wavelength at which the OSA is intended to operate. For the fiber-optic telecommunications bands at 1300 nm and 1550 nm, the diffraction grating is gold-coated

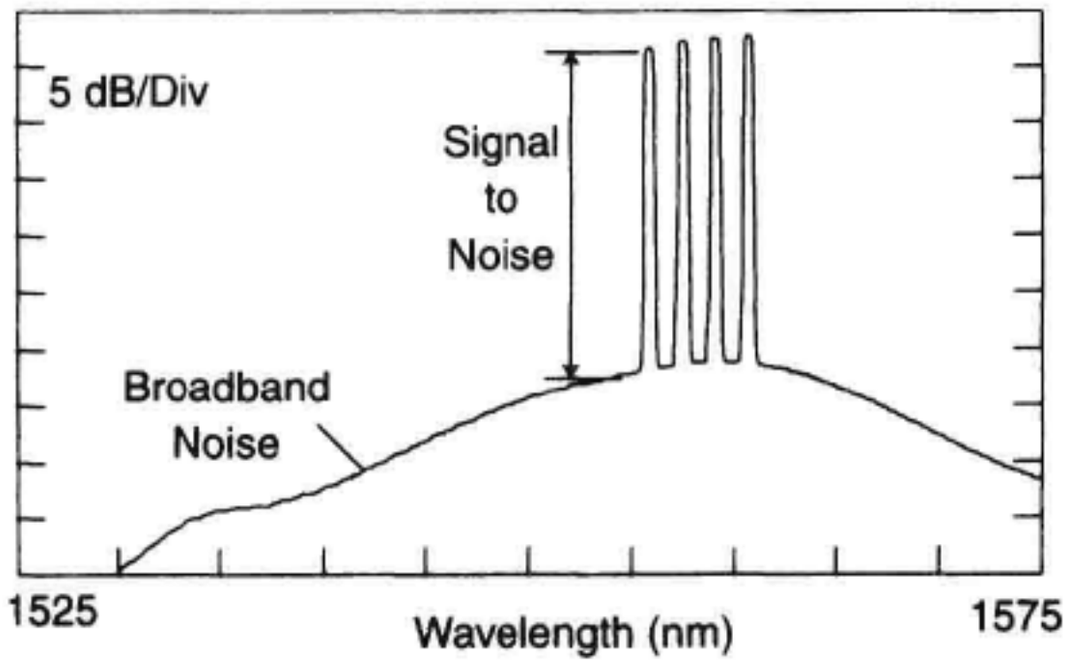

Figure 3.25 Signal-to-noise ratio measurements in optically amplified DWDM systems.

to increase diffraction efficiency. The loss of a single pass through a monochromator is in the 3 to 8 dB range.

Sensitivity is coupled directly to video bandwidth, as illustrated in Figure 3.26. The video bandwidth controls the amount of noise present in the receiving electronics. The sensitivity of the optical receivers is covered in detail in Appendix A. The major considerations are the dark current of the detector and the bandwidth and noise contribution of the amplifying electronics. The dark current of a detector scales with the area of the detector. The minimum size for the detector is determined by the slit widths that are chosen in the image plane. For the special case of the double-pass monochromator shown in Figure 3.14, the detector size can be made very small, independent of the size of the slit width. It is surprising to note that the filter bandwidth does not affect OSA sensitivity. This is in contrast to electrical spectrum analyzers which have a sensitivity proportional to the filter bandwidth.

Sweep-Time Limits. For fast sweeps and low sensitivity settings, sweep time is limited by the maximum tuning rate of the monochromator. A direct-drive-motor system allows for faster sweep rates when compared with OSAs that use gear-reduction systems to rotate the diffraction grating. As the sensitivity level increases, the video detector bandwidth decreases (the transimpedance amplifier gain increases), resulting in a longer sweep time, since the sweep time is inversely proportional to the video bandwidth.

Continuously variable digital video bandwidths improve the sweep time for high-sensitivity sweeps in two ways. First, the implementation of digital video filtering is faster than the response time required by narrow analog filters during autoranging of amplifier gains. Second, since the video bandwidth can be selected with great resolution, just enough video filtering can be employed, resulting in no unnecessary sweep-time penalty caused by using a narrower video bandwidth than required.

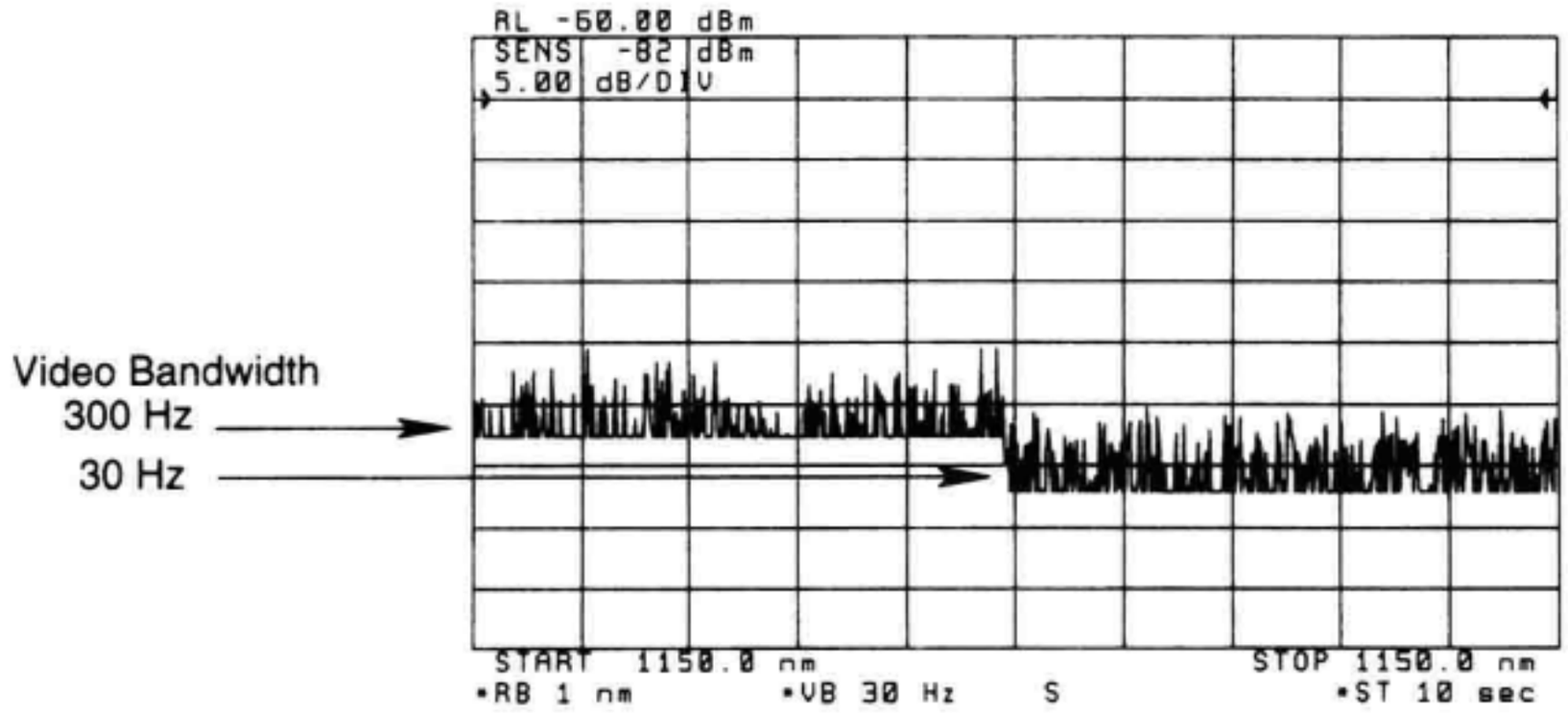

Figure 3.26 Video bandwidth directly affects sensitivity.

3.4.5 Input Polarization Sensitivity

Cause of Polarization Sensitivity. Polarization sensitivity results from the insertion loss of the diffraction grating being a function of the polarization angle of the light that strikes it. Polarized light can be divided into two components. The component parallel to the direction of the lines on the diffraction grating is labeled p-polarization and the component perpendicular to the direction of the lines on the diffraction grating is labeled s-polarization. The loss of the diffraction grating differs for the two different polarizations, and each loss varies with wavelength. At each wavelength, the loss of p-polarized light and the loss of s-polarized light represent the minimum and maximum losses possible for linearly polarized light. At some wavelengths, the loss experienced by p-polarized light is greater than that of s-polarized light, while at other wavelengths, the situation is reversed. This polarization sensitivity results in an amplitude uncertainty for measurements of polarized light and is specified as polarization dependence.

Solutions to Polarization Sensitivity Problem. Two solutions for reducing polarization sensitivity in monochromators are shown in Figure 3.27.[4,13,14] In Figure 3.27a, a half-wave plate has been placed in the path of the optical signal between the first and second pass in the double-pass monochromator. A half-wave plate rotates the polarization of an s-polarized input component to a p-polarized component. Similarly a p-polarized component is transformed into an s-polarized component. In this implementation, the total loss of any input polarization receives the same total loss on two passes through the grating. This forms a monochromator that is independent of polarization. The difficulty in this design is finding a waveplate with adequate wavelength coverage.

In Figure 3.27b, the light to the monochromator is separated into separate paths for each polarization with a polarization walk-off crystal. Separate detectors are used at the output to measure the transmitted power in each polarization. If the loss for the monochromator in both polarizations is characterized and stored in the instrument, the dis-

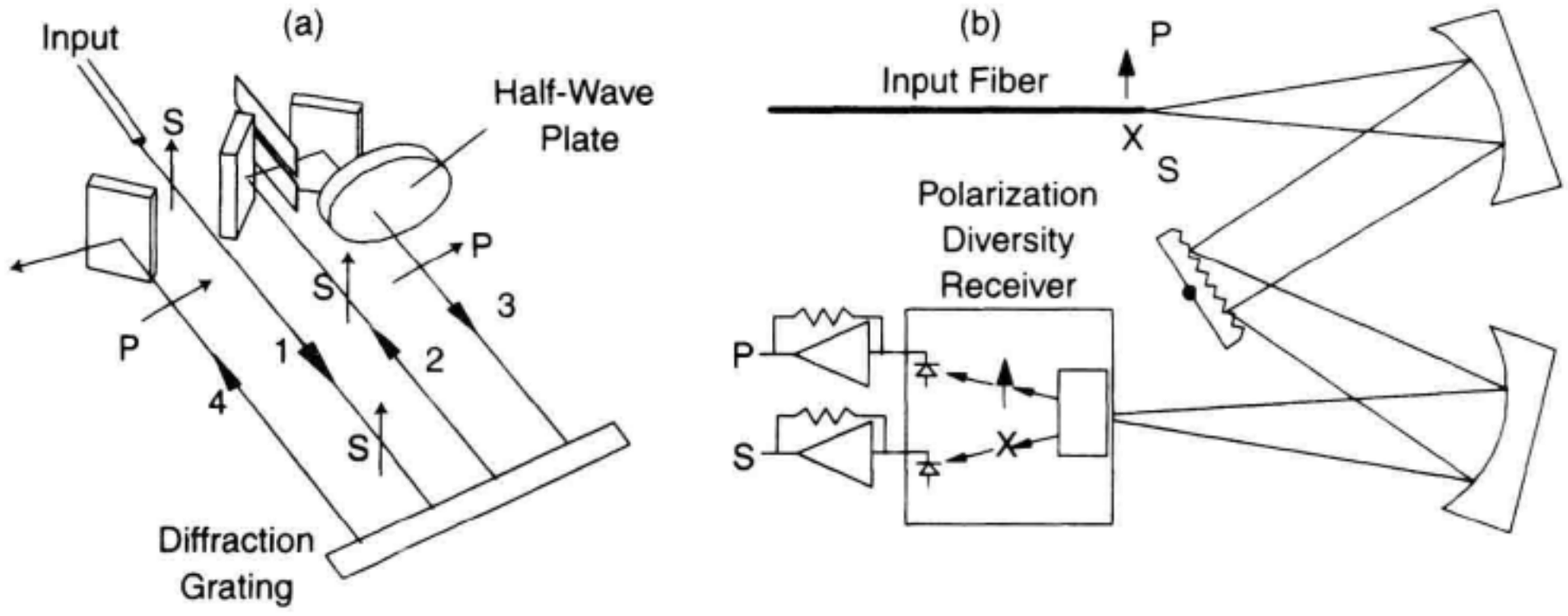

Figure 3.27 (a) A half-wave plate used to reduce polarization sensitivity. (b) Polarization-diversity receiver method to reduce polarization sensitivity.

played results can be made independent of polarization. A disadvantage of this technique is that the instrument sensitivity depends on the input light polarization. This technique does not permit a monochromator fiber output that is polarization insensitive.

3.5 SPECTRAL MEASUREMENTS ON MODULATED SIGNALS

3.5.1 Signal Processing in an OSA

If the light at the OSA input changes with time, then the signal to be measured must be described as a function of wavelength and time. However, the operation of the instrument also depends on time. In order to measure all spectral components, the grating rotates so that different wavelengths pass through the slit. If the modulation rate of the incoming light is very much higher than the rotation rate of the OSA, the correct time averaged spectrum will be measured. If the modulation rate is comparable to the speed of the grating rotation or the speed of the detection electronics, then care must be taken to get correct spectral measurements. Special triggering modes are available in OSAs to facilitate measurements of sources modulated at low repetition rates (for example, <250 kHz).

To understand triggering modes, it is useful to review the data acquisition procedure for an OSA. Figure 3.28 illustrates the standard free-run mode of operation. Refer to Figure 3.2 for the block diagram of an OSA. The instrument initiates a sweep of the diffraction grating. The signal from the photodetector is amplified and applied to the analog-to-digital converter (ADC) for data acquisition samples. The analog-to-digital conversion occurs at a fixed rate (for example, 37.5 μs). In the best case, it takes the trace length (for example, 800 points) times the ADC conversion time to scan a given wavelength range (for example, 30 ms/trace). After the ADC, a digital signal processor (DSP) further processes the data. For example, the video bandwidth function is often implemented in the digital processor. Finally, the data is log-converted and transferred to a display unit. When the sweep has been completed, the grating moves back into the start position. This cycle repeats itself as long as continuous sweep is active.

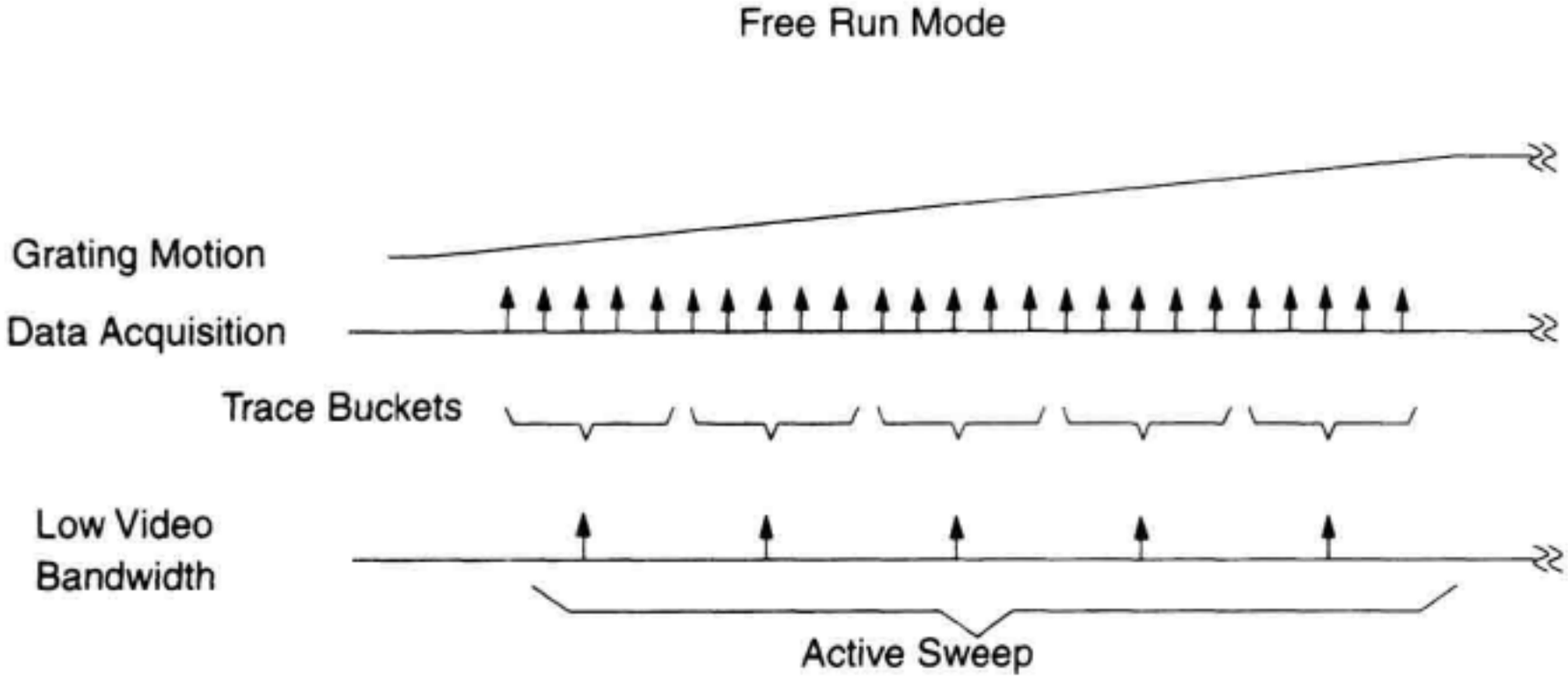

Figure 3.28 Free-run mode.

If the input power and spectrum are constant over time, then only the grating motion and the digital filters in the DSP must be synchronized to generate an accurate trace on the screen. In this case, the grating speed mainly depends on the wavelength range to be covered and the required sensitivity: the slower the grating rotates, the more samples from the ADC can be averaged by the video bandwidth (VBW) function into one trace point on the screen. Sometimes such a trace point is called a "trace bucket" because it actually combines several ADC values.

If the signal is modulated at a high enough frequency, the OSA still can measure the average spectrum without any external synchronization. The VBW must be significantly smaller than the lowest modulation frequency component, otherwise the signal can look very distorted (Figure 3.29).

In many cases the spectrum at a given point within the modulation period is more meaningful than the average spectrum. Some OSAs offer a great variety of triggering modes to characterize test signals from components, sensors, subsystems, or other light sources modulated in the frequency range approximately between 10 Hz and 250 kHz. Again, it is possible to measure only the average spectrum by choosing a low VBW. Even if the analog bandwidth is higher than the modulation of the signal, the VBW function will low-pass filter the samples. A signal at the trigger input of the OSA can synchronize a variety of functions. For example, the trigger signal can (mutually exclusive):

- Initiate measurements with the grating remaining fixed at a specific wavelength (zero span mode)
- Start the grating motion on a trigger signal *(triggered sweep)*

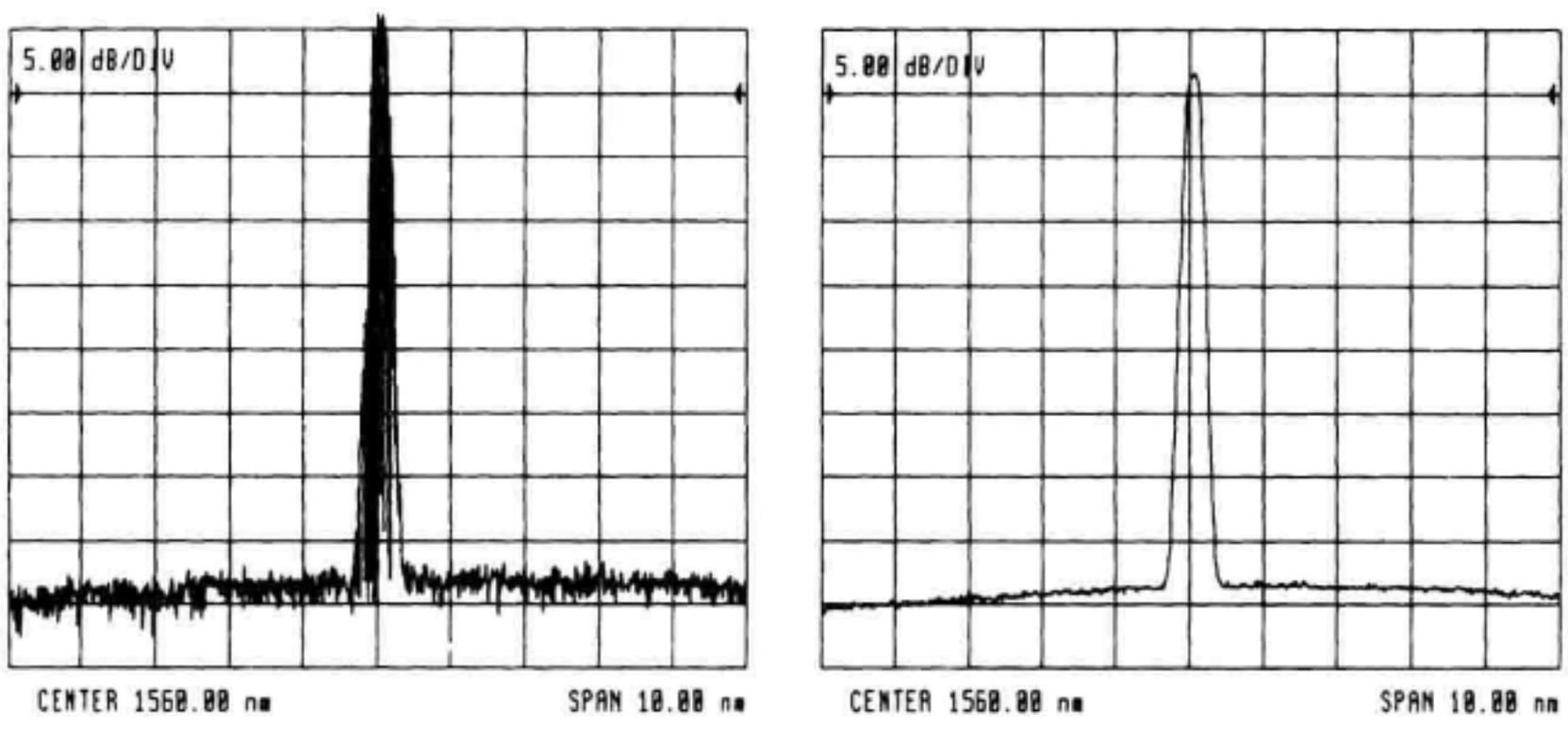

Figure 3.29 Video-bandwidth effects for modulated signals. (a) The low frequency modulation occurs at a rate lower than the video bandwidth. (b) The modulation frequency is above the video bandwidth.

- Sample and A/D convert a data point a specified time after the trigger signal *(ADC trigger mode)*
- Tell the DSP when the optical spectrum is valid *(gated sweep)*

The following sections will describe these methods in more detail.

3.5.2 Zero-Span Mode

If the span is zero (in other words, start wavelength = stop wavelength), then the grating remains at the angular position representing the center wavelength. The optical filter is fixed in wavelength. This measurement will record the power at any particular time after the trigger event that started the measurement. If the time response is successively recorded at many different wavelengths, the spectrum versus time of a pulse signal can be recorded.

Besides looking at a low frequency (< 10 kHz) modulation, this mode has a major speed benefit for an accurate power measurement at one wavelength. Instead of placing a marker at a desired wavelength and then reading its power level, the OSA can be placed in zero span at that wavelength and then *the average power of the whole trace can be read.* Because a trace consists of many points, the values for all of these points can be averaged. To achieve the same noise or modulation suppression for a sweep with span greater than zero, the VBW must be very low, and therefore the sweep time becomes very long.

3.5.3 Triggered Sweep Mode

In this mode, the grating waits in a position according to the start wavelength until it receives a trigger pulse (Figure 3.30). Then the grating starts to move in the same way as in the free-run mode. There is no difference in building trace buckets or averaging the signal by a low VBW. After the sweep, the grating stops at the start position and waits for the next trigger event.

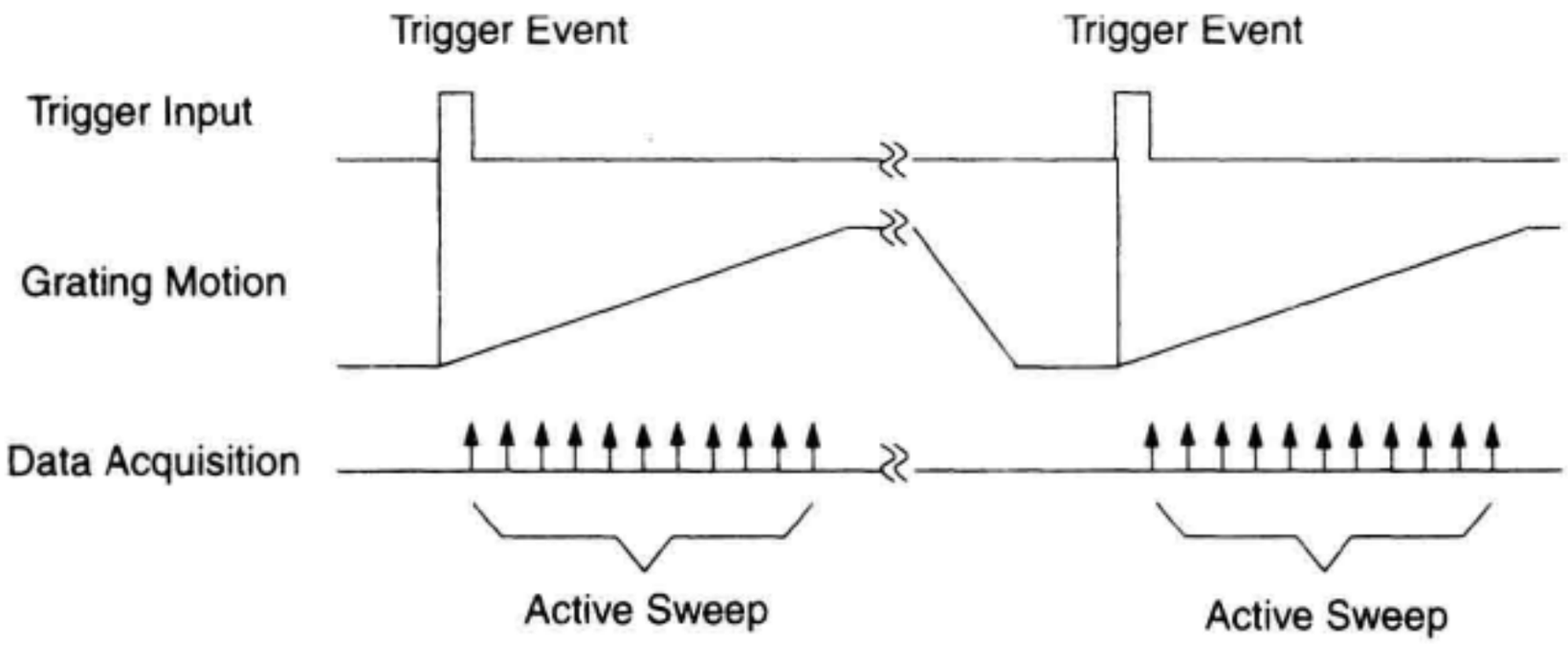

Figure 3.30 Triggered-sweep mode.

Each sweep results in a trace which can be processed further. For example, the max. hold function will take the trace displayed before, compare each trace point with the new data, and then display only the greater value of each point. Often, a swept source, such as a tunable laser, triggers a sweep after each wavelength step. Triggered sweep also works in zero-span mode. In this case, a trigger edge causes the start of the data acquisition for an entire trace.

3.5.4 ADC-Trigger Mode

The ADC-trigger mode samples the raw data at a specified time after a positive or negative edge of the signal is at the trigger input (Figure 3.31). The grating runs continuously but the data acquisition is synchronized. If there is a trigger event, then the OSA will sample the data after the specified delay and digitize it.

Testing an unpackaged source component, such as a laser or LED on a chip, is a common OSA application of this trigger mode. Pulse current to the laser is used to avoid heating effects which alter the spectral shape. Figure 3.31 shows the current versus time and power versus time for a pulsed laser. The ADC-trigger mode allows the spectrum to be sampled during the "on" time of the laser.

3.5.5 ADC-AC Mode

Similar to the ADC-trigger mode, ADC-AC samples the data delayed after a trigger event. While the first event triggers on either a positive or a negative edge, the ADC-AC mode alternates between positive and negative edges (Figure 3.32). In addition, the DSP processes the data differently: It calculates the absolute difference between the samples acquired after the positive trigger edge and the ones acquired after the negative edge. The resulting trace point represents only the modulation amplitude, so that any constant light or light modulated at a different frequency cancels out.

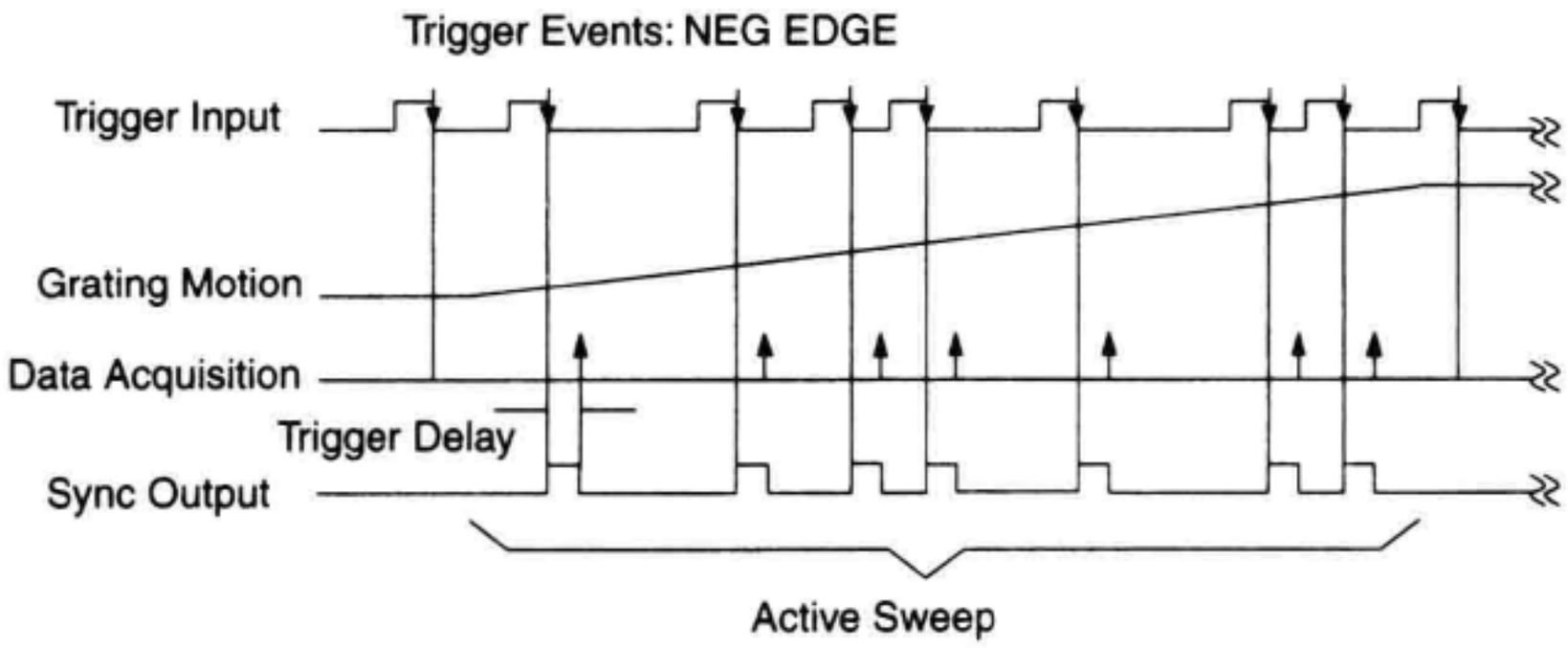

Figure 3.31 Pulsed-light signal synchronization using the ADC-trigger mode.

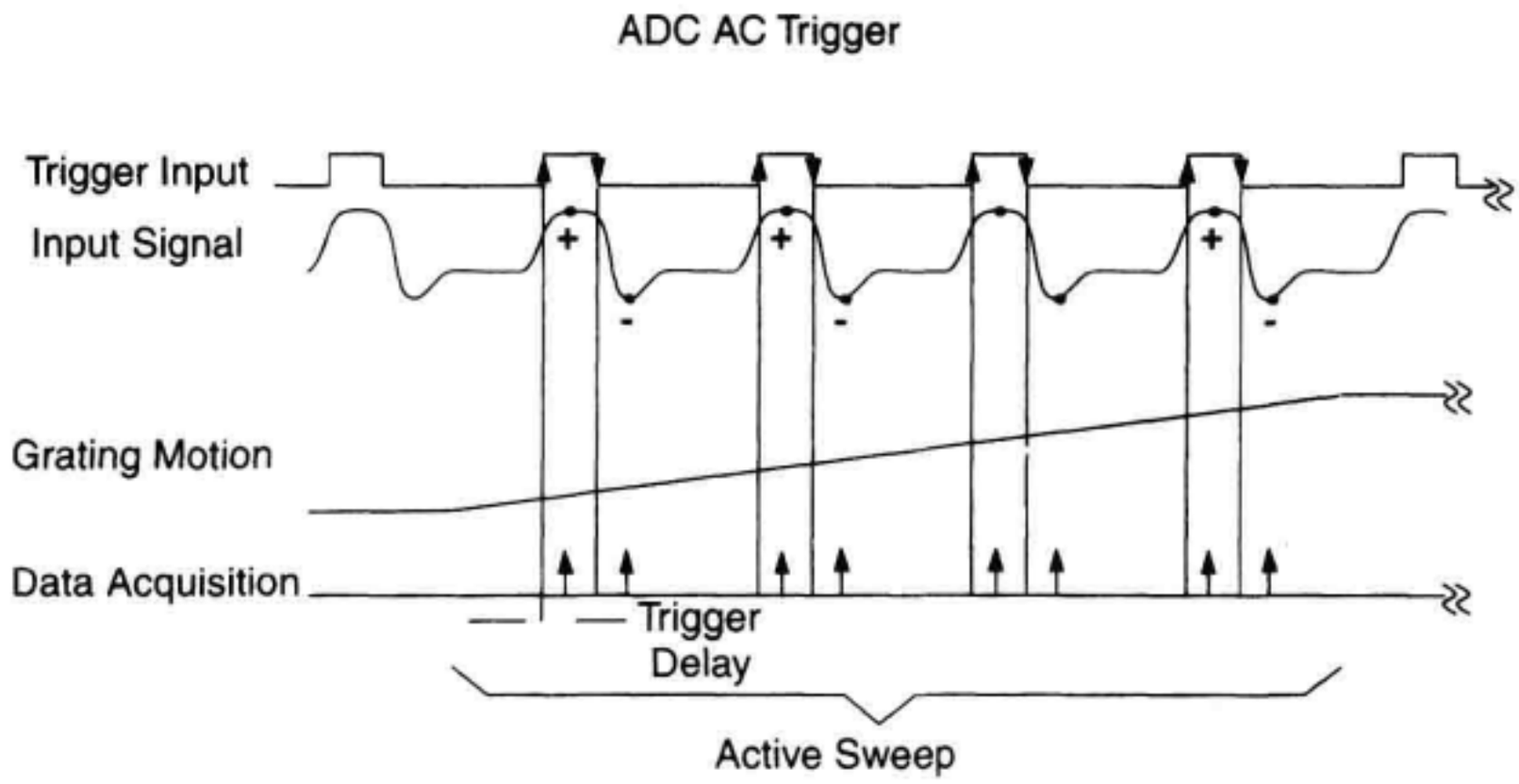

Figure 3.32 ADC-AC trigger.

In this mode, the DSP runs two VBW filters on the raw data from the ADC (one for the positive and one for the negative samples). Therefore, it reduces random noise without affecting the true amplitude of the signal.

The ADC-AC mode is similar to lock-in techniques. It measures the modulation portion of the light only, and it suppresses light that is not modulated. The impact on the effective VBW and the amplitude-range-setting considerations discussed above apply to the ADC-AC mode as well.

Applications for this mode include tests for systems incorporating EDFAs, or open-beam setups which use a 270 Hz modulation in order to suppress ambient light.

3.5.6 Gated-Sweep Mode

The gated-sweep mode tells the DSP when to retain or ignore the data coming from the ADC. Both the grating and the ADC run without synchronization to any external signal. If the trigger input is high, then the DSP takes the ADC value as a valid data point. Otherwise, it replaces the sample by a small value (for example, –200 dBm). In both cases it continues processing according to the functions selected (for example, VBW, max. hold, etc.).

If the time of the low level is longer than the time needed for the grating to move from one trace point to the next one, then the trace will have gaps (Figure 3.33). There are two alternatives to close the gaps: either increase the sweep time to at least 1.2 to 2 times the longest "low-level" period, or activate the max. hold function and let the OSA sweep several times. In the first case, the DSP will have at least one data sample marked valid (high level) per trace point. In the second case, multiple sweeps fill the gaps because the high and low levels of the gating signal occur independently of the grating position.

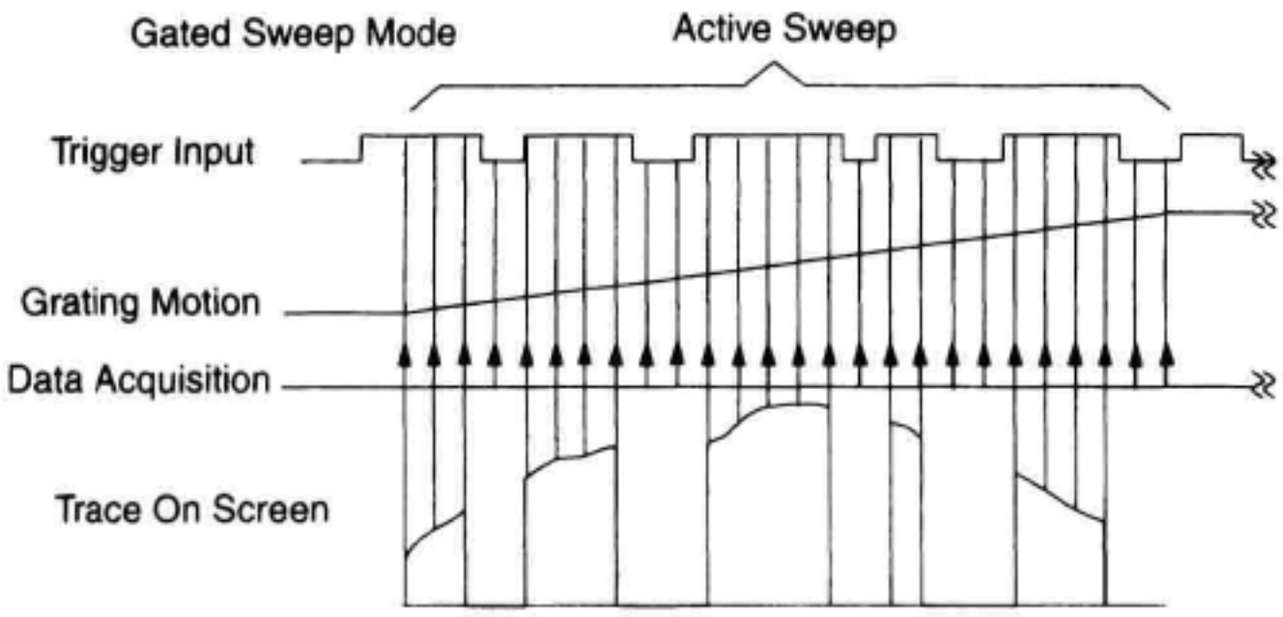

Figure 3.33 Gated-sweep mode.

3.6 OSA APPLICATION EXAMPLES

3.6.1 Light-Emitting Diodes (LEDs)

Light-emitting diodes (LEDs) produce light with a broad spectral width. They can be modulated at frequencies up to about 200 MHz. Figure 3.34 shows the spectrum of an LED. The broad spectral width of the source is often specified by the full-width at half-maximum (half-power points of the spectrum). Typical values for full-width at half-maximum (FWHM) range from 20 nm to 80 nm for LEDs.

There are many parameters of LEDs that are commonly measured. These parameters can be automatically measured as shown in Figure 3.34. Some parameters (such as mean wavelength and spectral width) have two methods by which they can be measured. One method takes into account the entire spectrum, while the other takes into account only a few points of the spectrum. The definition of each parameter is described below.

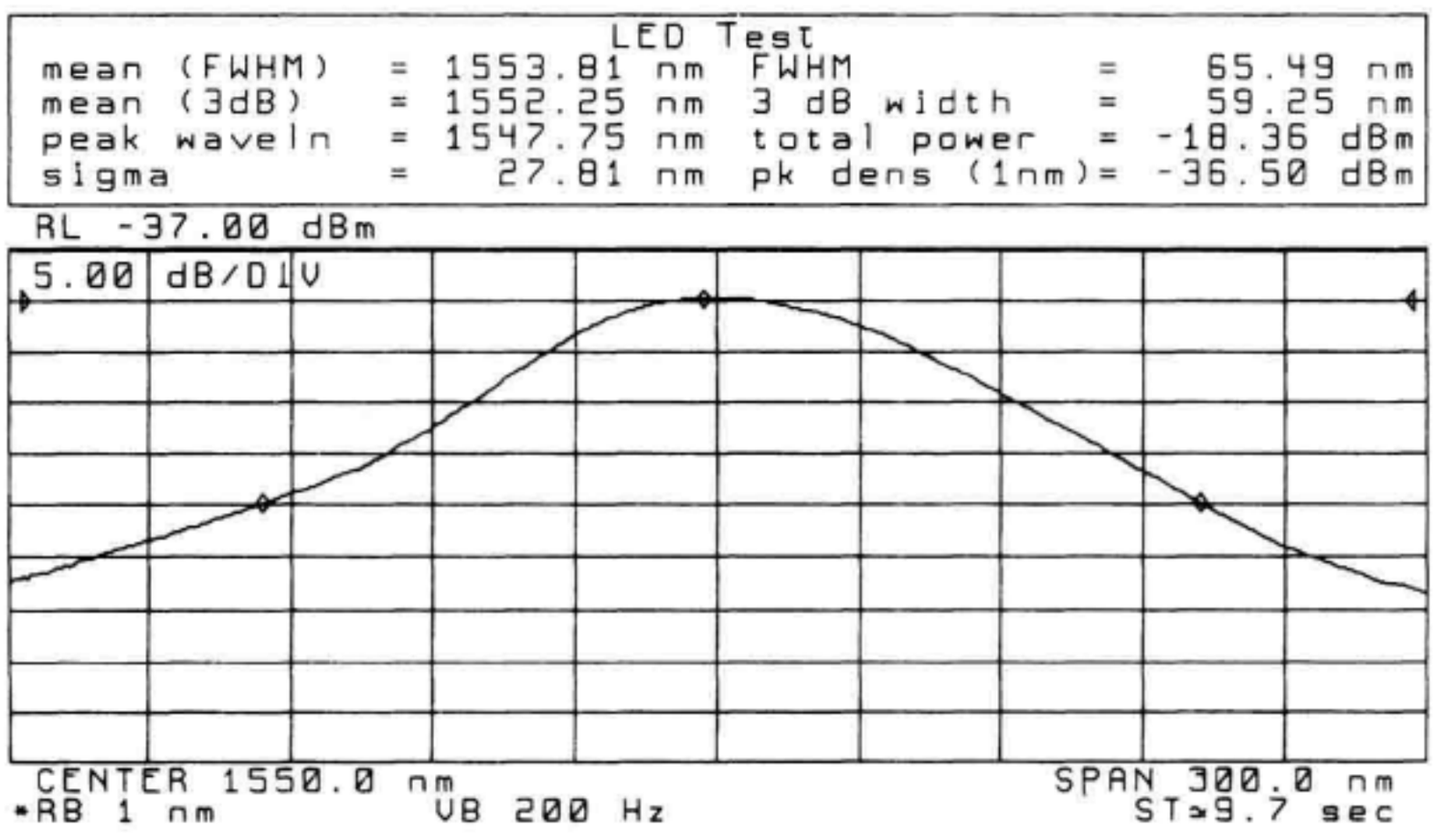

Figure 3.34 Spectrum of a light-emitting diode.

Total Power. The summation of the power at each trace point, normalized by the ratio of the trace-point spacing/resolution bandwidth. This normalization is required because the spectrum of the LED is continuous, rather than containing discrete spectral components (as a laser does).

$$P_{\text{Total}} = \sum_{i=1}^{N}\left(P_i \frac{\text{trace point spacing}}{\text{resolution bandwidth}}\right) \tag{3.8}$$

Mean (FWHM). This wavelength represents the center of mass of the trace points. The power and wavelength of each trace point are used to calculate the mean (FWHM) wavelength.

$$\lambda_{\text{Mean}} = \sum_{i=1}^{N}\left(\frac{\lambda_i P_i}{P_{\text{Total}}} \frac{\text{trace point spacing}}{\text{resolution bandwidth}}\right) \tag{3.9}$$

Sigma. An rms calculation of the spectral width of the LED based on a Gaussian distribution. The power and wavelength of each trace point are used to calculate sigma.

$$\sigma = \sum_{i=1}^{N}\left[(\lambda_i - \lambda_{\text{Mean}})^2 \frac{P_i}{P_{\text{Total}}} \frac{\text{trace point spacing}}{\text{resolution bandwidth}}\right] \tag{3.10}$$

FWHM (Full-Width at Half-Maximum). Describes the spectral width of the half-power points of the LED, assuming a continuous, Gaussian power distribution. The half-power points are those where the power-spectral density is one-half that of the peak amplitude.

$$FWHM = 2.355\sigma \tag{3.11}$$

3 dB Width. Used to describe the spectral width of the LED based on the separation of the two wavelengths that each have a spectral density equal to one-half the peak power-spectral density. The 3 dB width is determined by finding the peak of the LED spectrum, and dropping down 3 dB on each side.

Mean (3 dB). The wavelength that is the average of the two wavelengths determined in the 3 dB width measurement.

Peak Wavelength. The wavelength at which the peak of the LED's spectrum occurs.

Density (1 nm). The power-spectral density (normalized to a 1 nm bandwidth) of the LED at the peak wavelength.

Distribution Trace. A trace can be displayed that is based on the total power, power distribution, and mean wavelength of the LED. This trace has a Gaussian spectral distribution and represents a Gaussian approximation to the measured spectrum.

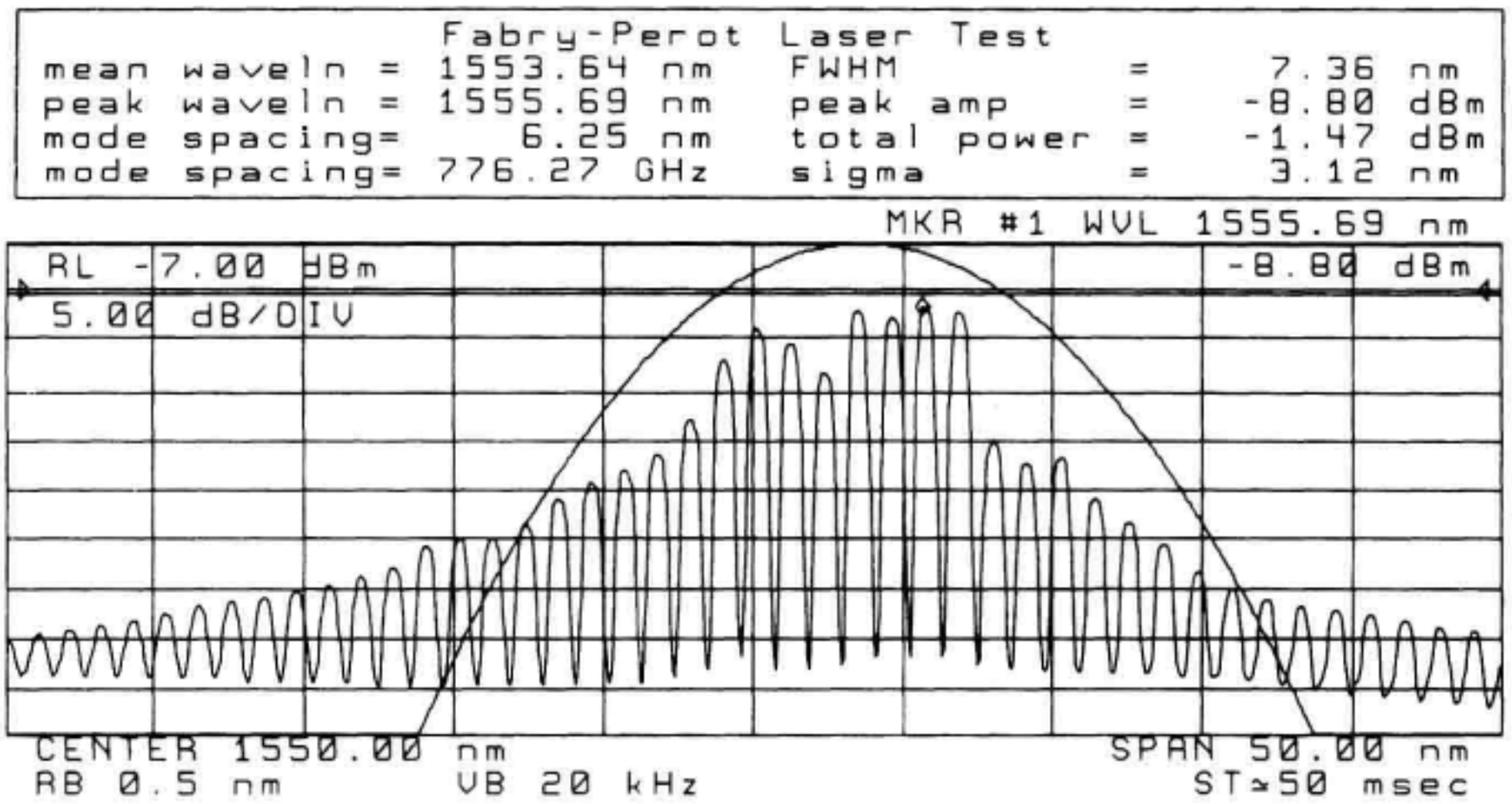

Figure 3.35 Results of an automatic Fabry-Perot laser measurement routine.

3.6.2 Fabry-Perot Lasers

As with the LED, many OSAs have an automatic measurement routine for FP lasers. The results from an FP laser measurement routine are shown in Figure 3.35. The following parameters are of interest.

Total Power. The summation of the power in each of the displayed spectral components, or modes, that satisfy the peak-excursion criteria. (See below for discussion of peak-excursion criteria.)

$$P_{\text{Total}} = \sum_{i=1}^{N} P_i \tag{3.12}$$

Mean Wavelength. Represents the center of mass of the spectral components on screen. The power and wavelength of each spectral component is used to calculate the mean wavelength.

$$\lambda_{\text{Mean}} = \sum_{i=1}^{N} P_i \lambda_i \tag{3.13}$$

Sigma. An rms calculation of the spectral width of the FP laser based on a Gaussian distribution. The power and wavelength of each spectral component is used to calculate the mean wavelength.

$$\sigma = \sqrt{\frac{1}{P_{\text{total}}} \sum_{i=1}^{N} P_i (\lambda_i - \lambda_{\text{Mean}})^2} \tag{3.14}$$

FWHM (Full-Width at Half-Maximum). Describes the spectral width of the half-power points of the FP laser, assuming a continuous, Gaussian power distribution. The half-power points are those where the power-spectral density is one-half that of the peak amplitude.

$$FWHM = 2.355\sigma \tag{3.15}$$

Mode Spacing. The average wavelength spacing between the individual spectral components of the FP laser.

Peak Amplitude. The power level of the peak spectral component of the FP laser.

Peak Wavelength. This is the wavelength at which the peak spectral component of the FP laser occurs.

Peak Excursion. The peak excursion value (in dB) can be set by the user and is used to determine which on screen responses are accepted as discrete spectral responses. To be accepted, each trace peak must rise, and then fall, by at least the peak excursion value about a given spectral component. Setting the value too high will result in failure to include the smaller responses near the noise floor. Setting the value too low will cause all spectral components to be accepted, but unwanted responses, including noise spikes and the second peak of a response with a slight dip, could be erroneously included.

Peaks Function. The peaks function displays a vertical line from the bottom of the grid to each counted spectral component of the signal. This function is useful to determine if an adjustment of the peak excursion value is required.

Distribution Trace. A trace is displayed that is based on the total power, individual wavelengths, mean wavelength, and mode spacing of the laser. This trace has a Gaussian spectral distribution and represents a continuous approximation to the actual, discrete spectrum.

3.6.3 Distributed Feedback (DFB) Lasers

Distributed feedback lasers are similar to FP lasers, except that all but one of their spectral components are significantly reduced as shown in Figure 3.36. Because its spectrum has only one line, the spectral width of a distributed feedback laser is much less than that of an FP laser. This greatly reduces the effect of chromatic dispersion in fiber optic systems, allowing for greater transmission bandwidths.

Most OSAs have an automatic measurement routine for distributed feedback lasers. The results from a DFB-laser measurement routine are shown in Figure 3.36. The following parameters are often of interest and are measured by the automatic routine.

Peak Wavelength. The wavelength at which the main spectral component of the DFB laser occurs.

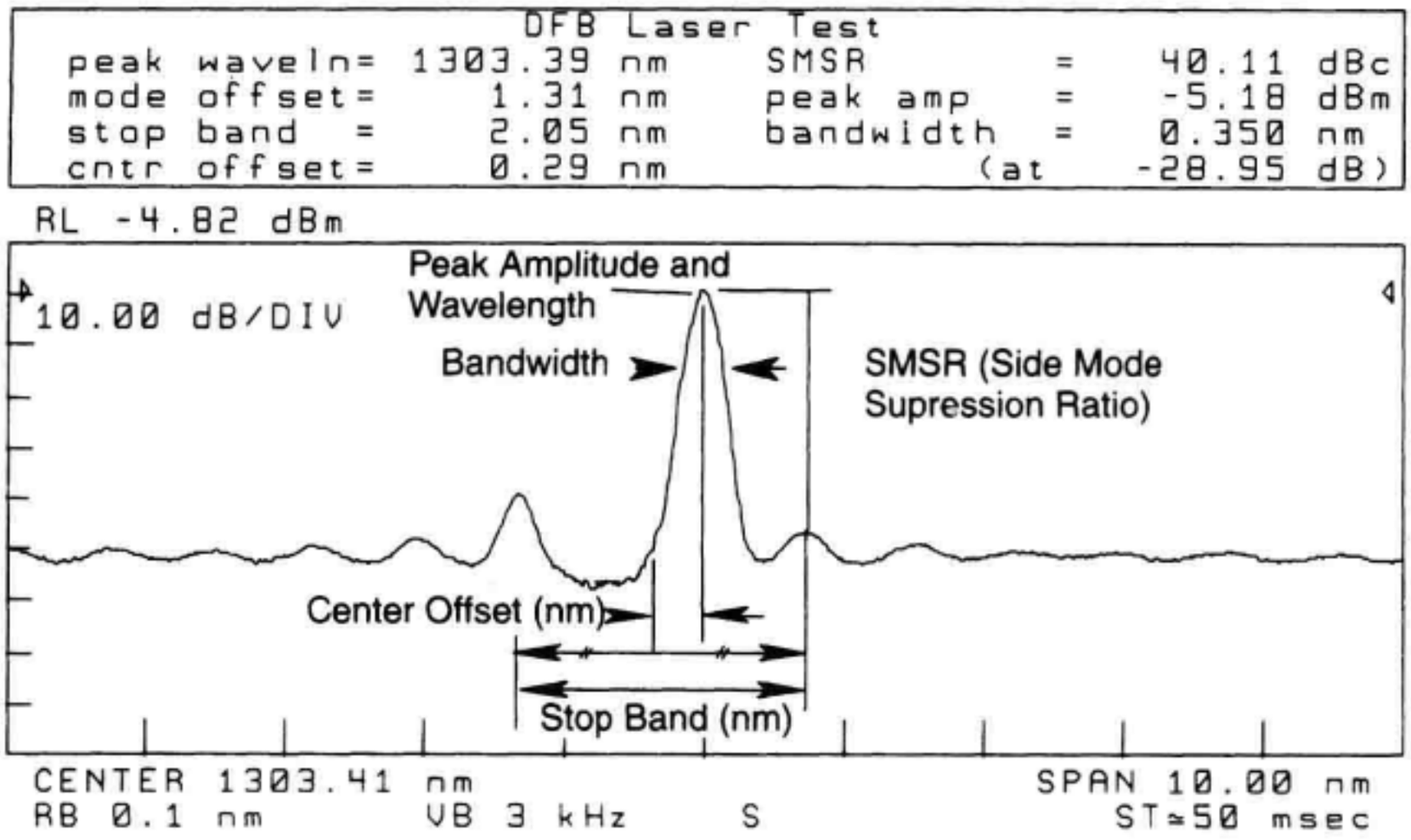

Figure 3.36 Results of automatic DFB-laser measurement routine.

Side Mode Suppression Ratio (SMSR). The amplitude difference between the main spectral component and the largest side mode.

Mode Offset. Wavelength separation (in nanometers) between the main spectral component and the SMSR mode.

Peak Amplitude. The power level of the main spectral component of the DFB laser.

Stopband. Wavelength spacing between the upper and lower side modes adjacent to the main mode.

Center Offset. Indicates how well the main mode is centered in the stopband. This value equals the wavelength of the main spectral component minus the mean of the upper and lower stopband-component wavelengths.

Bandwidth. Measures the displayed bandwidth of the main spectral component of the DFB laser. The amplitude level, relative to the peak, that is used to measure the bandwidth can be set by the user. In Figure 3.36, the amplitude level used is –20 dBc. Due to the narrow line width of lasers, the result of this measurement for an unmodulated laser is strictly dependent upon the resolution-bandwidth filter of the OSA. With modulation applied, the resultant waveform is a convolution of the analyzers filter and the modulated laser's spectrum, causing the measured bandwidth to increase. The combination of the modulated reading and unmodulated reading can be used to determine the bandwidth of the modulated laser and the presence of chirp.

Peak Excursion. The peak excursion value (in dB) can be set by the user and is used to determine which three on-screen responses will be accepted as discrete spectral responses. To be counted, the trace must rise, and then fall, by at least the peak ex-

cursion value about a given spectral component. Setting the value too high will result in failure to count small responses near the noise floor.

Peaks Function. The peaks function displays a vertical line from the bottom of the grid to each counted spectral component of the signal. This function is useful to determine if an adjustment of the peak excursion value is required.

3.6.4 Optical Amplifier Measurements

Chapter 13 discusses optical amplifiers and how to characterize them. Therefore, we give here only a quick overview of the most common measurement setup and procedure.[15–17]

Most test setups contain a tunable laser with adjustable output-power level and an OSA (Figure 3.37). The laser drives the amplifier into its saturated gain operating point. The OSA characterizes the signal and noise spectrum before and after amplification. From these two measurements, the gain and noise figure of the optical amplifier can be determined.

The measurement of signal power at the input and output is straightforward. The measurement of the amplifier output noise is more difficult. First, the signal is covering up the noise level at the wavelength of interest. The second consideration is that broadband noise present at the input signal may be amplified and add to the noise output of the optical amplifier. Because the amplified laser signal hides the noise level at the wavelength of interest, the most common measurement technique uses interpolation (Figure 3.38). Markers on either side of the signal are averaged to infer the noise level at the signal wavelength. The accuracy of the noise measurement is very important. The amplitude accuracy of the instrument may need to be compared to a power meter. It is also important that the noise bandwidth marker function be used to measure the noise level. The noise marker takes into account the optical filter shape of the monochromator to define the effective noise bandwidth of the filter. If the noise marker function is not available, it will be necessary to characterize the filter shape of the monochromator as an additional measurement step. To account for the amplified broadband noise of the source, noise subtraction algorithms have been used and are described well in Chapter 13.

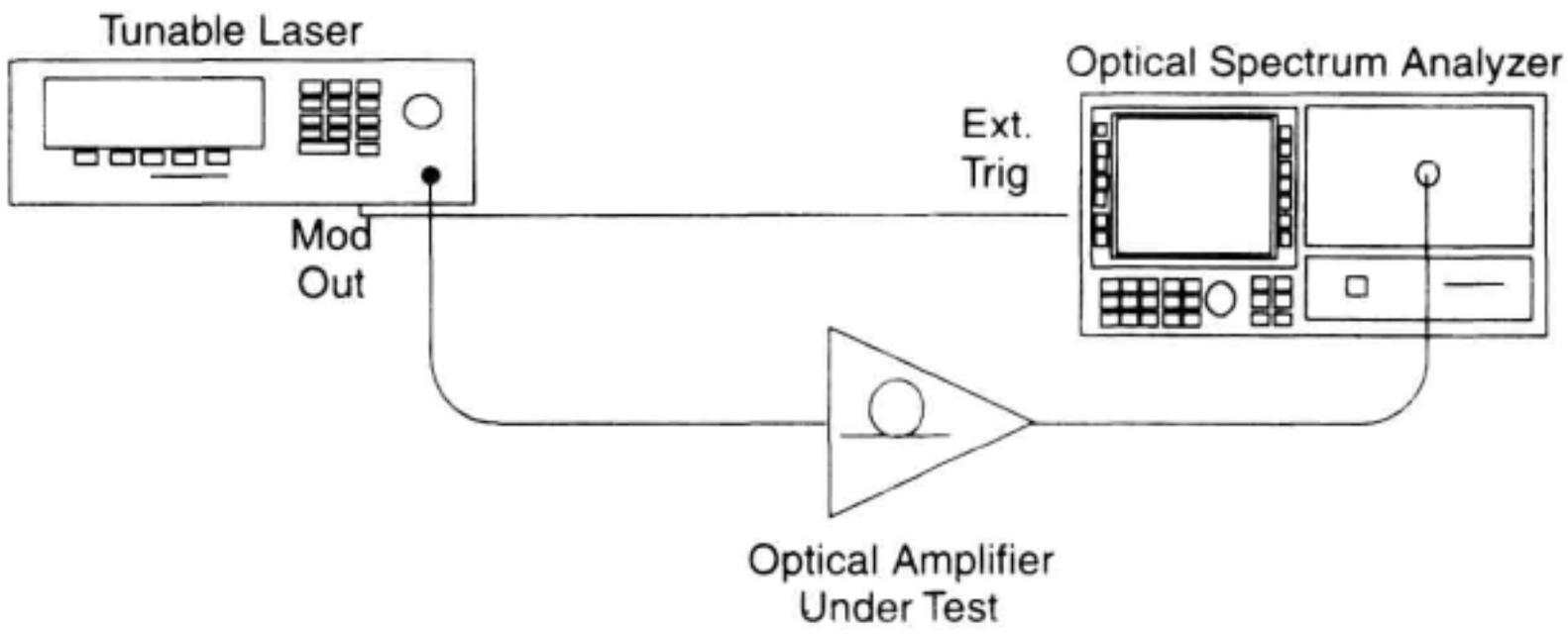

Figure 3.37 Basic optical-amplifier test setup.

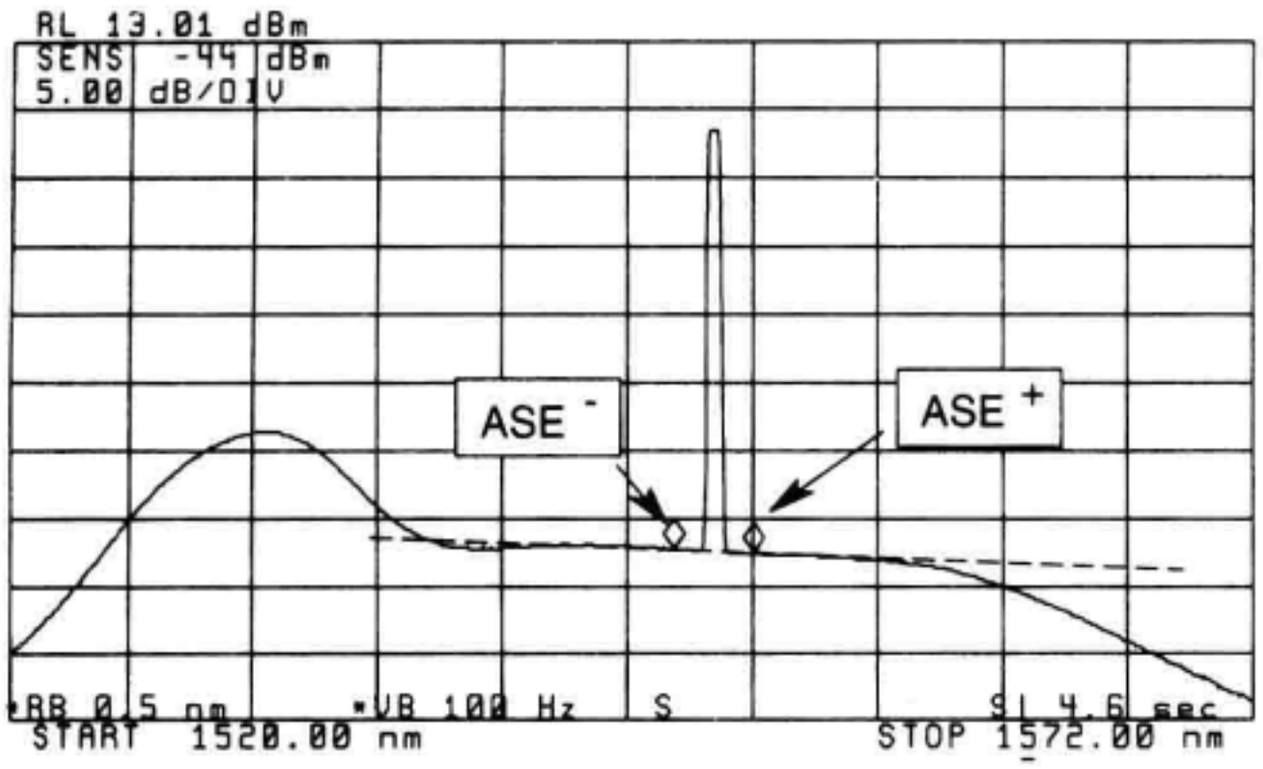

Figure 3.38 Interpolation of the amplified spontaneous emission.

3.6.5 Recirculating Loop

Researchers desire to measure how an optical spectrum shape can change when traveling along thousands of kilometers of fiber and through many optical amplifiers. Since it is impractical and expensive to build very long link lengths, researchers have resorted to methods involving recirculating loops. The setup in Figure 3.39 uses a loop technique. Typically, the loop consists of only a few EDFAs with 30 to 70 km long fibers between them, and one circulation lasts about 0.2 to 2 ms. Several circulations of a signal then simulate how that signal would behave on a very long link. This experimental setup presents significant measurement challenges for OSAs. The spectrum needs to be measured once for each circulation around the loop.

Let us examine how the spectrum can be resolved for each circulation. A pulse generator controls the timing. First, the acousto-optic modulator (AOM) 1 is open and AOM

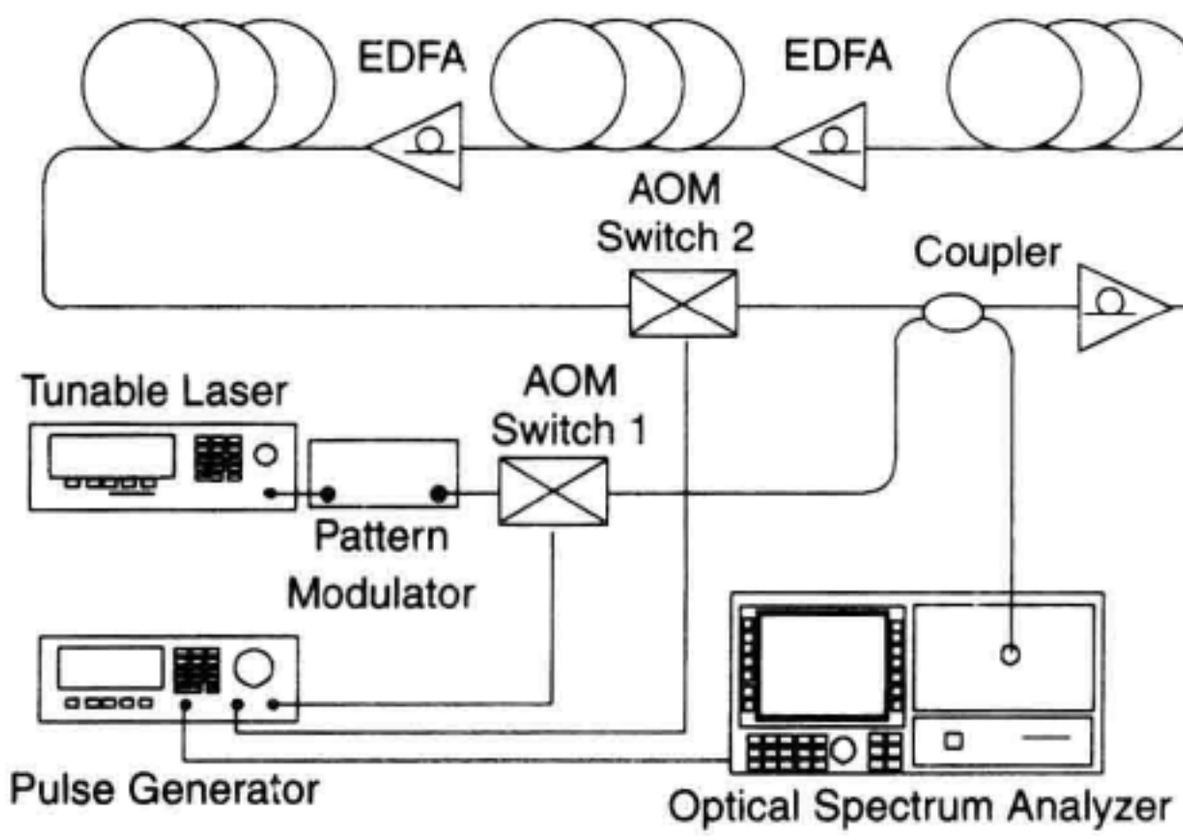

Figure 3.39 Recirculating loop setup.

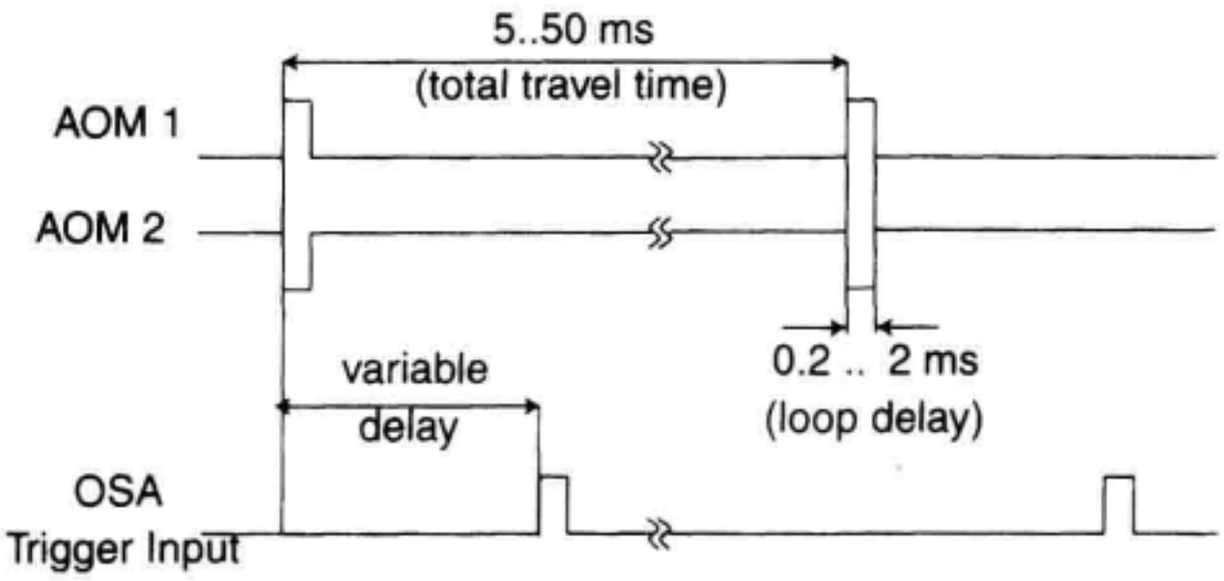

Figure 3.40 Recirculating loop timing.

2 is closed (Figure 3.40). At this time, the TLS in conjunction with an external modulator fills the loop with a pseudorandom modulated bit pattern (see Chapter 8). Second, switch 1 closes and switch 2 opens, allowing the pattern to circulate adequately (about 5 ms per 1000 simulated kilometers). Third, the OSA measures the spectrum at a variable delay (in other words, at a variable simulated distance). The three steps are repeated until the OSA has built a complete trace.

To measure the spectrum at a given distance, two trigger techniques may be used: ADC trigger or gated sweep. When using ADC trigger, the OSA samples only one data point per trigger but the time of the sampling is very well known. The OSA sweep time must exceed the total travel time multiplied by the number of trace points (for example, 50 ms × 800 = 40 s. To allow for processing overhead, choose 50 to 80 s).

When using gated sweep, the OSA keeps data samples as long as the OSA trigger is high. If the sweep time is as long as above, then the trace will be completed within one sweep. Otherwise, use max. hold, so that several sweeps can close the gaps caused during the time the ADC trigger input is low. Gated sweep also provides the advantage that the OSA measures the spectrum of a longer piece of the bit pattern (in other words, over the width of the gating pulse).

Under control of a remote program and by using a spreadsheet or math program, it is possible to create a three-dimensional (3-D) graph showing the signal and ASE amplitude as a function of wavelength and distance. There are two basic methods, each having their own advantages and disadvantages: scanning along the wavelength axis or scanning along the time axis.

Wavelength Scan. The OSA repetitively measures the spectrum for subsequent variable delays. Each time the trace data is transferred to a computer which finally creates the 3-D plot (Figure 3.41). Because it typically takes about a minute to acquire one trace (see above), the total measurement time is in the order of M minutes (M = number of different delays, typically 10 to 30). The default trace length is 800, so this method provides good wavelength resolution. However, a fine-distance resolution requires a large M and therefore a long total time.

Time-Domain Scan. When the OSA is set to zero span, the grating behaves as a filter with fixed-center wavelength. If the signal going to AOM 1 triggers a sweep, then

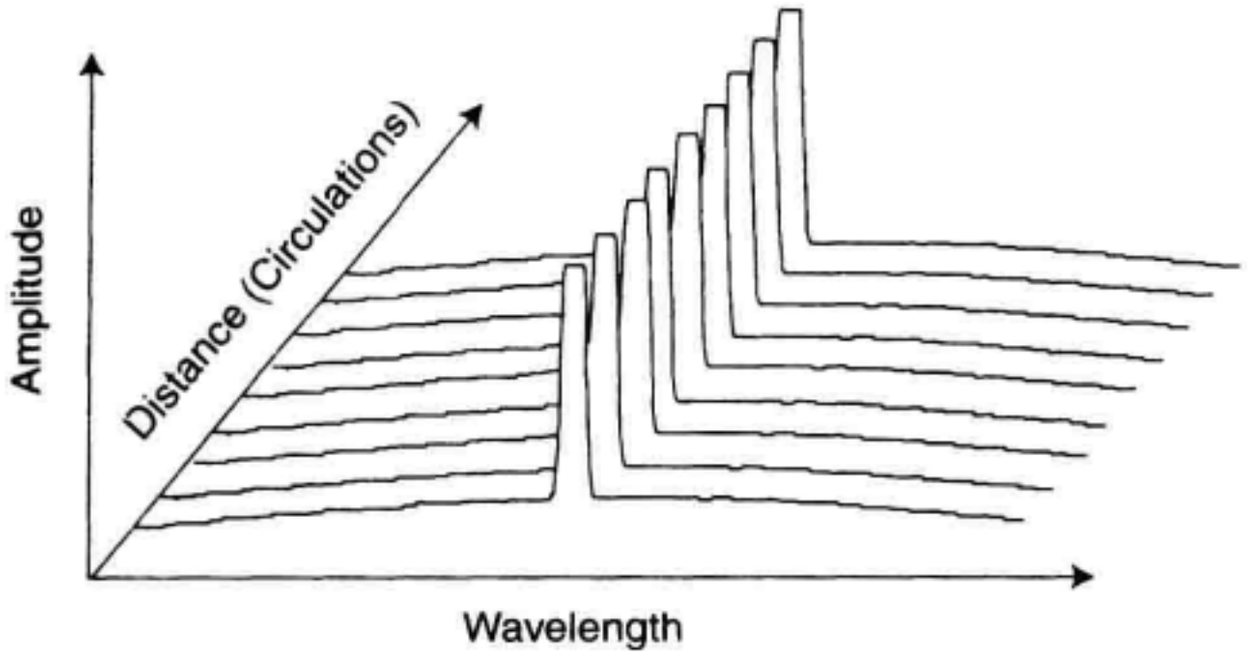

Figure 3.41 Three-dimensional loop spectrum.

subsequent ADC values represent the power versus time of the center wavelength of the OSA. With 50 ms sweep time and 800 points/trace, the distance resolution is about 7.5 km. This measurement has to be repeated for N wavelengths (typically 50 to 200) in order to create the 3-D plot (Figure 3.42). N and the span to be covered determine the wavelength accuracy. Assuming that a trace transfer to a computer lasts only few seconds, the data acquisition for this 3-D plot takes several minutes.

3.7 SUMMARY

The operation of a diffraction-grating based optical spectrum analyzer was described and example measurements were shown. The resolution and dynamic range of the monochromator filter was found to be determined by the number of illuminated lines on the grating, the input and output slit widths, and the quality of the collimating optics and the number of passes off of the diffraction grating. The wavelength accuracy of a monochromator is very important due to the demands of DWDM telecommunications systems. Absolute

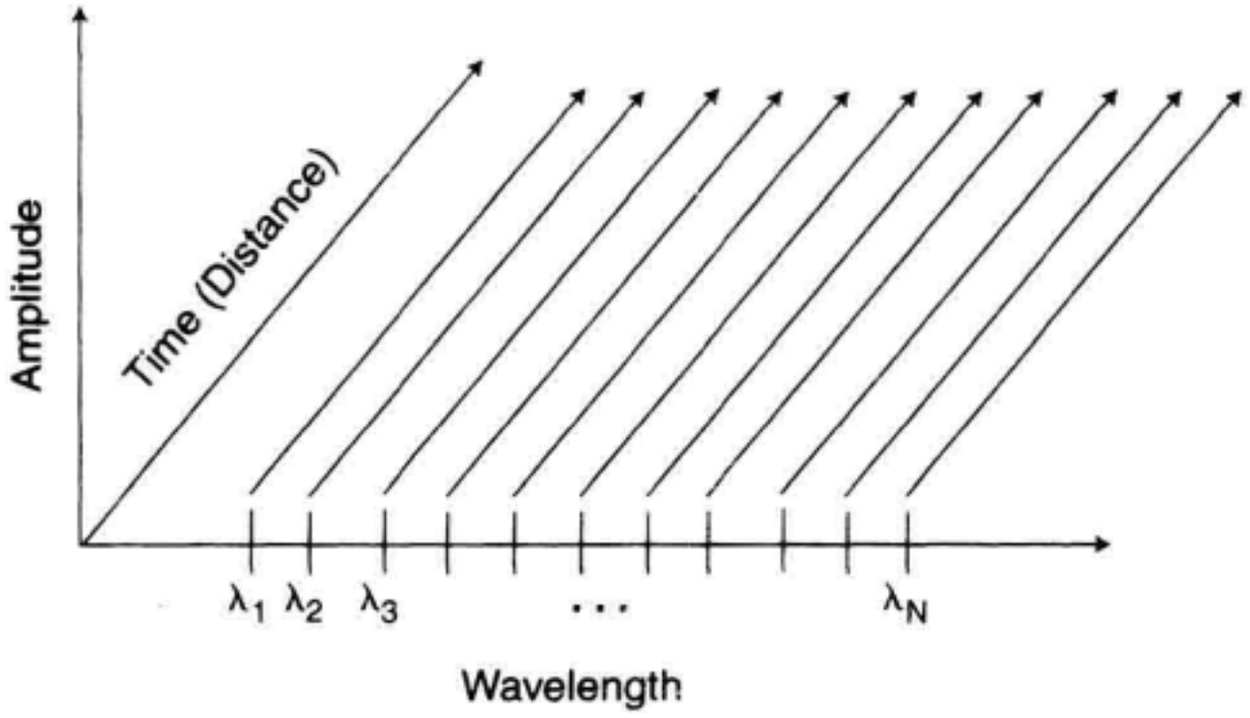

Figure 3.42 3-D scan using the zero span method.

wavelength calibration can be obtained by comparison to a laser wavelength standard, a wavelength meter (Chapter 4) or a gas absorption cell. Care must be taken in OSA design to minimize the polarization dependence of the monochromator design. The measurement of signals with low frequency modulation requires a set of triggering features to be present in the optical spectrum analyzer. Applications for OSAs including measurements of LEDs, FP lasers, DFB lasers, EDFAs, and recirculating loop experiments were given.

ACKNOWLEDGMENTS

The author would like to thank Val Mcomber, Mike LeVernier, Jim Stimple, Kenn Wildnauer and many other colleagues for their excellent material that has been the basis to write this section. Furthermore, many thanks to Anneliese, Kay-Mario, Vanessa and Yasmin for their support and patience while the author was working on his part of the book in his spare time.

REFERENCES

1. *Optical spectrum analysis basics, application note 1550–4.* 1992. HP literature number 5963-7145E. Santa Rosa, CA: Hewlett Packard Lightwave Division.
2. Hecht, E. and A. Zajag. 1979. *Optics.* Reading, MA: Addison-Wesley.
3. Hutley, M.C. 1982. *Diffraction Gratings.* London: Academic Press.
4. Wildnauer, K.R. and Z. Azary. 1993. A double-pass monochromator for wavelength selection in an optical spectrum analyzer. Hewlett Packard Journal, 44, No. 6, pp. 68–74.
5. *Calibration of Optical Spectrum Analyzers.* Geneva, Switzerland IEC Technical Committee No. 86: Fiber Optics, Working Group 4, Subgroup 5.
6. Gilbert, S.L., T.J. Drapela, and D.L. Franzen, 1992. Moderate-accuracy wavelength standards for optical communications, in *Technical Digest—Symposium on Optical Fiber Measurements.* Boulder, CO: NIST Spec. Publ. 839: pp. 191–194.
7. Varanasi, P. and B.R.P. Bangaru. 1975. Intensity and half-width measurements in the 1.525 μm band of acetylene. *J. Quant. Spectrosc. Radiat. Transfer* 15, 267.
8. Sakai, Y., S. Sudo, and T. Ikegami. 1992. Frequency stabilization of laser diodes using 1.51–1.55 μm lines of $^{12}C_2H_2$ and $^{13}C_2H_2$. *IEEE J. Quantum Electron.* 28: 75.
9. Baldacci, A., S. Ghersetti, and K.N. Rao. 1977. Interpretation of the acetylene spectrum at 1.5 μm, *J. Mol. Spectrosc.* 68:183.
10. Chanm, K., H. Ito, and H. Inaba. 1983. Optical remote monitoring of CH_4 gas using low-loss optical fiber link and InGaAsP light-emitting diode in the 1.33 μm region. *Appl. Phys. Lett.* 43: 634.
11. Nakagawa, K. Labachelerie, M. Awaji, Y. Kourogi, M. 1996. Accurate Optical Frequency Atlas of the 1.5 μm bands of acetylene. Journal of the Optical Society of America B, 13, No. 12, pp. 2708–2714.
12. Sasada, H. Yamada, K. Calibration lines of HCN in the 1.5 μm region. Applied Optics, Vol. 29, (1990) pages 3535–3547.

13. Sonobe, Y., S. Ishigaki, T. Kikugawa. Apparatus for measuring spectral power of a light beam. U.S. patent number 4,758,086.
14. Shirasaki, M., R. Yamamoto, Y. Watanabe, and S. Nishina. 1991. Polarization independent grating-type optical spectrum analyzer with fiber interface. San Diego, CA: Optical Fiber Conference, Optical Society of America, Paper WNS, pp. 130.
15. *EDFA testing with the time domain extinction technique.* 1995. HP literature number 5963-7147E. Santa Rosa, CA: Hewlett-Packard Lightwave Division.
16. *EDFA noise gain profile and noise gain peak measurements.* 1995. HP literature number 5963-7148E. Santa Rosa, CA: Hewlett-Packard Lightwave Division.
17. *WDM passive components test guide.* 1996. HP literature number 5965-3124E. Santa Rosa, CA: Hewlett-Packard Lightwave Division.

CHAPTER

4

Wavelength Meters

Dennis Derickson, Loren Stokes

4.1 INTRODUCTION

Chapter 3 covered optical spectrum analysis in general, and then went on to explain the operation of grating-based optical spectrum analyzers (OSAs) in detail. This chapter concentrates on another topic in optical spectrum analysis—wavelength meters. Wavelength meters can measure amplitude versus wavelength, as do grating-based OSAs. Wavelength meters distinguish themselves by making very accurate measurements of wavelength. A grating-based OSA can measure a 1550 nm signal with ±0.1 nm absolute-wavelength accuracy, assuming that the instrument has had a recent user calibration. A wavelength meter can make this measurement with better than ±0.001 nm accuracy. This represents a 100 times improvement.

One could ask why it is important to measure a 1550 nm signal to ± 0.001 nm accuracy. Here are four examples of fiber optic measurements that require very accurate measurement of wavelength.

1. A researcher may want to study long-term wavelength drift of a distributed feedback (DFB) laser for use in a wavelength division multiplexed (WDM) communication system. WDM lasers must be proven to drift less than 0.1 nm over a 25 year lifetime with accelerated aging studies.
2. A wavelength tunable laser is used for wavelength-resolved insertion loss measurements on a fiber-Bragg grating filter (see Chapter 9). Fiber-Bragg gratings have insertion-loss features that can change very rapidly with wavelength on the filter skirts. Tunable lasers have frequency steps of less than 0.001 nm but the step size may not always be linear. One picometer out of a wavelength of 1550 nm requires a

wavelength accuracy of 0.64 parts per million (ppm). Thus the wavelength meter can be used to calibrate the wavelength steps of the tunable laser so that the insertion loss plot has a sufficiently accurate wavelength axis.

3. When making chromatic dispersion measurements (see Chapter 12), it is necessary to measure the slope of the group delay versus wavelength function. Manufacturers need to know the zero-dispersion wavelength for components like dispersion compensators to tenths of a nanometer. Dispersion measurement algorithms require a derivative of the group delay with respect to wavelength. In order to get accurate dispersion values, the relative wavelength steps must be measured very accurately.
4. Accurate measurement of wavelength, power, and signal-to-noise ratio is very important for telecommunications systems using wavelength division multiplexing. A common WDM channel spacing is 100 GHz (0.8 nm at 1550 nm). The laser must be tuned to the precise center of each channel by temperature adjustment. This requires a wavelength settability of less than 0.05 nm. The measured data from the wavelength meter can be used to wavelength and amplitude stabilize the signals in the WDM system.

4.1.1 Wavelength Definition

For accurate measurement of wavelength in instrumentation, it is important to be clear on the medium that the wavelength is measured in. Some OSAs display the wavelength as measured in air. Other sources quote the vacuum wavelength of a signal. The relationship between the wavelength in air and vacuum is the well-known relationship:

$$\lambda_{vac} = n_{air}\lambda_{air} \tag{4.1}$$

where λ_{vac} is the vacuum wavelength, λ_{air} is the air wavelength, and n_{air} is the index of refraction of air. Although the wavelength in air and vacuum are close ($n_{air} \approx 1.00027$), this difference is 270 ppm. A 1550 nm vacuum wavelength source would have a wavelength of 1549.58 nm in standard dry air (15C temperature and 760 Torr pressure). Grating-based OSAs directly measure the wavelength in air. The instrument then calculates the vacuum wavelength based on an assumption for the index of refraction. With WDM channels spacings of 100 GHz, one can no longer ignore the difference between vacuum and air wavelengths. Section 4.4.2 describes models for the index of refraction in air as a function of temperature, pressure, and humidity. With proper attention to environmental variables, the vacuum wavelength to air wavelength conversion can be resolved to better than 1 ppm accuracy.

4.1.2 Methods of Accurate Wavelength Measurement

There are several approaches that are used to accurately measure wavelength.

1. Optical bandpass filter techniques. Chapter 3 has already covered optical spectrum analysis using a grating-based filter. Fabry-Perot (FP) filters are discussed in Section 4.6.1. Wavelength calibrator cells (see Chapter 3) are used to improve the accuracy of these measurements.

2. Interferometric fringe-counting techniques are commonly used for high accuracy applications. This chapter will concentrate on describing this method.
3. Wavelength discriminator techniques. A sloping insertion loss versus wavelength function can be used to determine optical wavelength. Section 4.6.4 will describe one implementation of this technique.

This chapter starts with a description of wavelength meters based on the Michelson interferometer. The principles of operation will be discussed in Section 4.2. The Michelson interferometer measurement technique will be generalized to multiple signal environments using Fourier transform techniques in Section 4.3. Then a discussion of wavelength accuracy considerations will be made in Section 4.4. Section 4.5 discusses other measurement considerations for Michelson interferometer instruments. Section 4.6 will discuss some alternate wavelength meter and spectrum analysis techniques that fall into the general class of wavelength meters. Finally, a comparison of all wavelength meters types will be made in Section 4.7 to show the strengths and weaknesses of each approach.

As a last note before starting wavelength meter discussion, it is appropriate to mention that there are several popular ways to display the results of a laser wavelength measurement.

vacuum wavelength, λ_{vac}
standard dry air wavelength (see section 4.4), λ_{air}
frequency = speed of light/$\lambda_{vac} = f$ or ν
wavenumber or spatial frequency = $1/\lambda_{vac} = \sigma$

Vacuum wavelength is the most often used measure in fiber optic measurements. The frequency of a laser is coming into more common usage because the WDM-wavelength grid is established in THz.

4.2 THE MICHELSON INTERFEROMETER WAVELENGTH METER

Figure 4.1 shows a block diagram of a Michelson interferometer.[1–4] Light from a fiber optic input is collimated and directed to the input of the interferometer. Singlemode fibers are most commonly used for fiber optic applications. The input signal is split into two paths with a beamsplitter. Both beams are then incident on 100%-reflecting mirrors that bounce the light back toward the beamsplitter. These mirrors are most often constructed as retroreflectors so that the beams are reflected back at nearly the same angle as they are sent into the mirror. Part of the light reflected from the two arms of the interferometer goes back toward the input beam. The other portion of the light is incident on a photodetector. Since there is no loss assumed in the interferometer, all of the light is directed to either the photodetector or the input port.

If the variable length interferometer mirror is moved, the amount of light reaching the photodetector will oscillate up and down because of constructive and destructive in-